Human periodontal ligament stromal cells and three-dimensional Bombyx mori fibroin silk scaffold for periodontal tissue regeneration

Fahad Maizar Al-Dabbagh

BDS, MSc (Clin) Periodontology, LDS RCS (Eng)

Submitted in accordance with the requirements for the degree of Doctor of Philosophy

The University of Leeds
School of Dentistry

July 2020

The candidate confirms that the work submitted is his own and that appropriate credit has been given where reference has been made to the work of others.

Acknowledgements

﴿ وَلَقَدْ خَلَقْنَا الْإِنسَانَ مِن سُلَالَةٍ مِّن طِينٍ ﴿12﴾ ثُمَّ جَعَلْنَاهُ نُطْفَةً فِي قَرَارٍ مَّكِينٍ ﴿13﴾

ثُمَّ خَلَقْنَا النُّطْفَةَ عَلَقَةً فَخَلَقْنَا الْعَلَقَةَ مُضْغَةً فَخَلَقْنَا الْمُضْغَةَ عِظَامًا فَكَسَوْنَا الْعِظَامَ لَحْمًا ثُمَّ أَنشَأْنَاهُ خَلْقًا آخَرَ

فَتَبَارَكَ اللَّهُ أَحْسَنُ الْخَالِقِينَ ﴿14﴾ ﴾

سورة المؤمنون

"Verily We created man from a product of wet earth; then placed him as a drop (of seed) in a safe lodging; then We fashioned the drop into a clot, then We fashioned the clot into a little lump, then We fashioned the little lump into bones, then clothed the bones with flesh, and then produced it another creation. So blessed be Allah, the Best of Creators!"

The Quran (Chapter 23)

First and foremost, I am most grateful to Almighty Allah to inspire me the knowledge and grant me the opportunity, determination and strength to be in the learning path.

Dear Mom and Dad, this achievement could not see the light without your efforts and prayers for us. I realised how much you suffered to provide the best for my brothers and me. You were like a candle that burns up to light the path up for us, heartfelt gratitude for both of you.

Dear Rasha, words are never enough to tell how fortune I am to have you beside me as a wife and friend. I am praying every day for this blessing to last forever, for you to stay my companion in this life and then after.

I would like to express my appreciation and sincere gratitude to my country, IRAQ, represented by the Higher Committee of Education Development in Iraq (HCED), for offering me the opportunity to complete the PhD degree at one of the world's top-ranked universities.

I am indebted towards *Dr Xuebin Yang* for his academic supervision and support throughout the last years. Thank you, Sir, for your patience and support, which set this work possible as it is till the end. Also, I would like to take this opportunity to express my appreciation to *Professor Val Clerehugh* for her feedback and constructive comments. Furthermore, my thanks go to *Dr Margaret Kellett* for her contributions.

My sincere thanks go to Mrs Jackie Hudson, Dr Ali Marie, Dr Liam Lawlor and Dr Hasanain Al-Khafaji for the help and support they generously

offered, while introducing me to many laboratory techniques, e.g. histology, immunohistochemistry, biochemical assays, in addition to *In vitro* imaging.

Also, I would like to thank all the staff at the Department of Oral Biology for the support and help during these years, especially *Mr Gregory Baugh, Ms Ruth Kayman* and *Ms Julie McDermott and Ms Sarah Myers*

It is impossible to forget the enjoying and rich experience I had with *Professor Jillian Cornish's* group of the *Cell and Molecular Biology Bone* at the Joint Research Department of Medicine, the University of Auckland, New Zealand. You are the most friendly and helpful people I ever met during this journey. Thanks for your generous hospitality.

I would also like to express my appreciation to my friends in Iraq; this opportunity would not have been possible without their generous support. *Dr Abdulsattar Salim, Dr Saif Saad, Mr Manaf Basil, Dr Raafat Tariq, Mr Zaid Abdulaziz and Dr Sufian Hamadi*; thank you all.

My wonderful brother, *Fanar*, I am grateful for you for taking care of our parent and younger brothers during the most challenging times!

My beloved angels, *junior Rasha* and *Yusuf*, you are the hope and the joy of my life. You were our companions during this challenging journey, and you were patient enough while your dad and mum being busy with their PhDs. I want you to know that we did our best not to let you down or to make you feel lonely.

Being in a place thousands of miles away from your home, put extra stress on my family and me. Fortunately, this dissipated by the help of those wonderful people who become our family here in the United Kingdom. Thanks for you all.

Last but not least, thanks for everyone I learned from, even in a painful way! For anyone who was the motive for me to set new goals and chase them up.

Abstract

Restoring the structure and function of damaged periodontal tissues remains one of the clinical challenges in dentistry. The reason behind that could be attributed to the complex biology of the periodontium. Cellular therapy and tissue engineering were introduced as possible alternatives to overcome the limitations of current treatment modalities. Accordingly, this study aimed to investigate the potential of using primary human periodontal ligament stromal cells (hPDLSCs) with Bombyx mori fibroin (Bmf) silk scaffold for enhancing periodontal regeneration *in vitro.* The project also aimed to develop a novel mechanical stimulation bioreactor that can be a useful tool to study the effect of cyclic compressive/tensile stimulation on the behaviour of hPDLSCs in a 3D, *in vitro* environment.

Human periodontal ligament cells (hPDLCs) were isolated from extracted healthy third molar teeth of three donors. The hPDLCs (passage two) were characterised using Colony-forming unit-fibroblast (CFU-F) assay, multicolour flow cytometry to measure the expression of mesenchymal (CD29, CD73 and STRO-1) and haemopoietic (CD34 and CD45) stem cells markers, as well as trilineage (osteogenic, adipogenic and chondrogenic) differentiation.

The immunogenicity of Bmf silk scaffold was investigated by measuring the release of inflammatory cytokines (TNF-α and IL-1β) of THP-1 cell in response to their exposure to the scaffold. The scaffold cytocompatibility was then evaluated by culturing hPDLSCs with the scaffold for four weeks in basal/osteogenic media. The *in vivo* behaviour of hPDLSCs-Bmf silk construct was examined following seven weeks of intraperitoneal implantation (diffusion chamber model) in CD-1 nude mice.

A novel mechanical stimulation bioreactor was designed and manufactured in house. The bioreactor was used to apply a cyclic compressive loading on hPDLSCs-Bmf silk constructs for fourteen days at a 30 cycle/min for 15 min, twice daily. The proliferation and differentiation (osteogenic and cementogenic) of the control and experimental groups were compared.

Throughout the project, various techniques were used to evaluate cellular activities (viability, proliferation and differentiation), including biochemical assays, fluorescent cell labelling, histological and immunohistochemical examination.

The CFU-F assay revealed a significant difference among donors. Moreover, hPDLCs expressed high CD29 and CD73 (99.95% and 100%, respectively), while the level of STRO-1 was 1.05%. In contrast, the expression of CD34 was limited (0.73%). However, the expression of CD45 showed a remarkable variation among donors (28.73%). Cells of all donors had the capacity to differentiate into osteogenic, chondrogenic and adipogenic cues.

The Bmf silk scaffold induced low levels of inflammatory cytokines, which were comparable to those induced by 3D collagen-type 1 (COL-1) scaffold. Also, Bmf scaffold supported the proliferation and differentiation of hPDLSCs *in vitro* and *in vivo*.

With the novel bioreactor, it was possible to apply static/cyclic mechanical stimulation on eight samples simultaneously using different loading frequencies. Also, the results showed that compression stimulation enhanced the proliferation and differentiation of hPDLSCs *in vitro.*

In conclusion, the current findings confirm the presence of multipotent mesenchymal stromal cells MSCs within primary hPDLCs. However, it is crucial to evaluate the cells' characteristics before their implication for research/therapeutic purpose due to donor dependency. Additionally, Bmf silk material is a potential biocompatible scaffold that could support periodontal tissue regeneration *in vitro* and *in vivo.* Enrolling mechanical stimulation is crucial as it affects the behaviour of hPDLSCs. The manufactured bioreactor could be a feasible tool for studying cyclic compression on cellular activity *in vitro.* However, several parameters (e.g. type of stimulation, load, frequency, and mode of application) need to be further optimised to support the regeneration process positively.

Table of Contents

List of Tables

List of Figures

List of Abbreviations

2D	Two dimensional
3D	Three dimensional
A	Ampere
ALP	Alkaline phosphatase
ANOVA	Analysis of variance
Bmf	Bombyx mori fibroin
BMP	Bone morphogenic protein
Ca^{2+}	Calcium ion
CD	Cluster of differentiation
cDNA	Complementary deoxyribonucleic acid
CEMP1	Cementoblastoma-derived protein 1
CFU-F	Colony-forming units- fibroblast
CMFDA	5-chloromethylfluorescein diacetate
CO_2	Carbon dioxide
COL-1	Collage type 1
CP-23	Cementum protein-23
dH_2O	Distilled water
DMSO	Dimethylsulfoxide
DNA	Deoxy ribonucleic acid
DPX	Dibutyl phthalate, polystyrene, xylene
ECM	Extracellular matrix
EDTA	Ethylene diamine tetraacetic acid
ETH-1	Ethidium Homodimer-1
FBS	Foetal bovine serum
Fc	Fragment crystallisable
FGF	Fibroblast growth factor
FITC	Fluorescein isothiocyanate

FMO	Fluorescence minus one
GAPDH	Glyceraldehyde 3-phosphate dehydrogenase
H&E	Hematoxylin and Eosin
hBMSCs	Bone marrow stem cells
HCL	Hydrochloric acid
hDPSCs	Human dental pulp stromal cells
hPDLSCs	Human periodontal ligament stromal cells
Hr	Hour
IL-1β	Interleukin-1 beta
ISCT	International Society for Cellular Therapy
KV	Kilovolt
LiBr	Lithium bromide
M	Molarity
Min	Minute
MSCs	Mesenchymal stromal cells
MSCs	Mesenchymal stromal cells
N	Number of samples
Na_2CO_3	Sodium carbonate
NaCl	Sodium chloride
NBF	Neutral buffer formalin
^oC	Degree centigrade
OCN	Osteocalcin
OPN	Osteopontin
P	Passage
P/S	Penicillin/Streptomycin
Pa	Pascal
PBS	Phosphate buffer saline
PDGF	Platelet-derived growth factor

PDLCs	Periodontal ligament cells
PMA	Phorbol 12-myristate 13-acetate
PMMA	Polymethyl methacrylate
p-value	Probability value
qRT-PCR	Quantitative real-time polymerase chain reaction
Rcf	Relative centrifugal force
RNA	Ribonucleic acid
Rpm	Round per minute
RT	Room temperature
RUNX	Runt-related transcription factor
SD	Standard deviation
SEM	Scanning electron microscopy
TGF-β	Transforming growth factor-beta
THP-1	Human acute monocytic leukaemia cell line
TNF-α	Tumour necrosis factor-alpha
UV	Ultraviolet
v/v	Volume per volume
VG	Van Gieson
VK	Von Kossa
w/v	Weight per volume
α-MEM	Alpha-minimum essential medium
β-ME	β-Mercaptoethanol

Chapter One: Literature review

1.1 Introduction

Despite many decades of research, periodontal tissue regeneration is still one of the challenging dentistry topics (Rylev and Kilian, 2008). The reason behind this could be the fascinating biological architecture of the periodontium, which enables this unique joint to serve its crucial role in maintaining the integrity of oral and dental tissues (Beertsen *et al.*, 1997). Understanding this unique joint's anatomy and biology that connects two different types of hard tissue with fibrous connective tissue is a demand that helps in the alternative approach to overcome current treatment limitations.

This chapter presents a picture of the development of the periodontium and describes its anatomical components. The chapter then moves on to discuss the periodontal diseases and to demonstrate the outcomes alongside the limitations of the current treatment modalities. In the 1970s, tissue engineering was introduced as an alternative that could help the regeneration of damaged tissues (Friedenstein *et al.*, 1976; Kumar *et al.*, 2011). Basically, tissue engineering is dependent on precise synchronisation between the central pillars; cells, scaffold and chemical/ mechanical modulating factors. The role of these factors in periodontal regeneration will be reviewed in-depth in this chapter. As a final point, periodontal regeneration challenges are addressed based on the existing body of literature and scientific evidence.

1.2 An overview of the periodontal tissue

The periodontal tissue, which is also referred to as periodontium, represents a specialised tooth-supporting apparatus that consists of both hard and soft tissues of ectomesenchymal origin. These components are hidden under the gingival cover (Hassell, 1993; Cho and Garant, 2000).

Periodontium is a multifunctional organ that plays an essential role in maintaining teeth integrity and supporting bones. This organ's primary function is to connect teeth to cranial bones through its components; the PDL, cementum and alveolar bone. Also, it acts as a shock absorber that

prevents the masticatory forces from damaging other oral structures by the distribution of occlusal stress. Moreover, it has nutritional and proprioceptive functions by acting as a jaw positioning system (Nanci and Bosshardt, 2006; Trulsson, 2006; Kosaka *et al.*, 2014).

1.2.1 Embryology and development of periodontal tissue

Dental and periodontal tissues are derived from the ectomesenchymal tissue of tooth germ, which gives rise to three parts, the enamel organ, which is responsible for enamel and root formation; the dental papilla that leads to the development of dentine and tooth pulpal tissues; and the dental follicle, from which the periodontal attachment apparatus originates, e.g. cementum, periodontal ligament and the alveolar bone.

Periodontal tissue development begins during tooth root formation (Beertsen *et al.*, 1997; Cho and Garant, 2000). This stage occurs when Hertwig's epithelial sheath (HERS), a bilayer structure of odontogenic epithelium, sends inductive signals to the cells of dental papilla that leads to their differentiation into odontoblasts, which eventually form the root dentine; moreover, these changes cause disintegration of HERS, which makes dental follicle cells in direct contact with the newly formed dentine (Nanci, 2017). This contact induces differentiation of these cells into cementoblasts. Some evidence suggests that HERS transforms into cementoblast cells. After that, the mesenchymal cells differentiate into fibroblast cells that begin to produce collagen (mainly type-I) that arranges in a bundle-like pattern, extending between the newly formed cementum and the bone. The collagen bundles inserted in these two hard tissues are termed Sharpey's fibres, while the central core of the bundles that fill the periodontal space is called principle fibres (Wouter Beertsen, 1997).

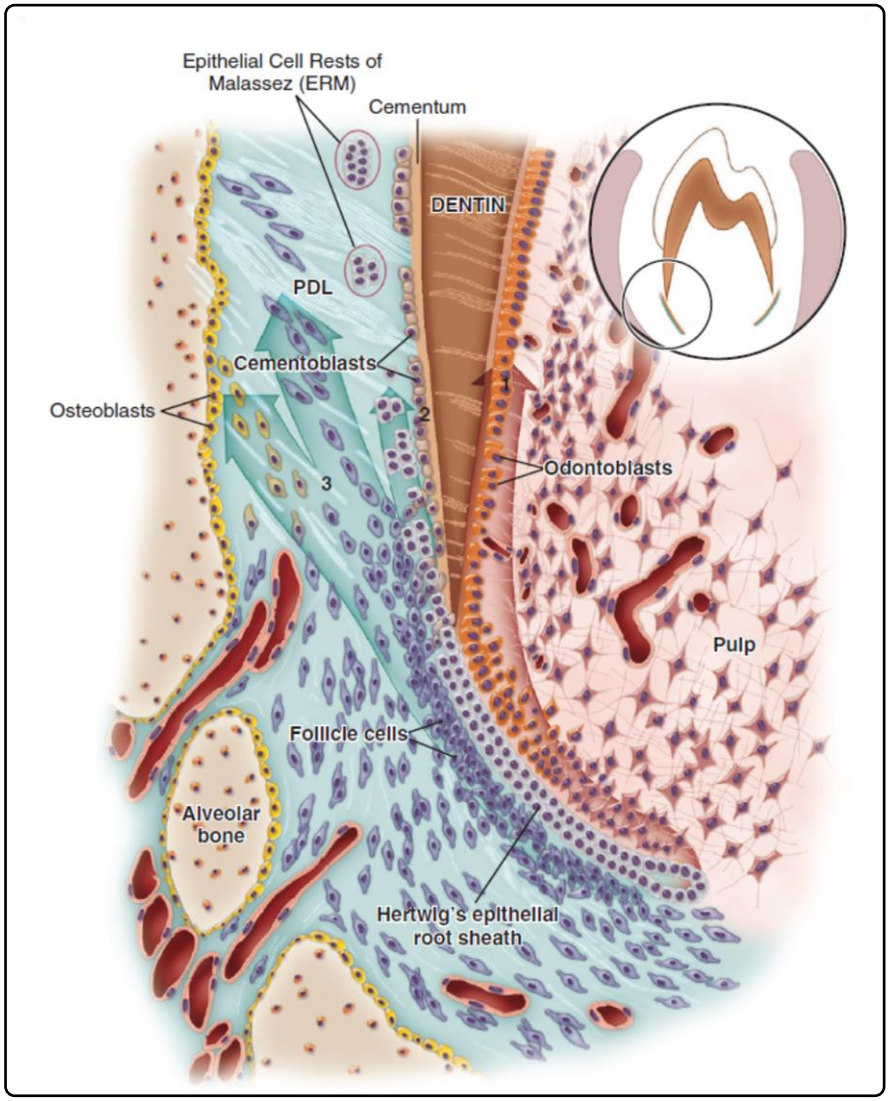

Figure 1-1: Summary of the differentiation of odontoblasts from ectomesenchymal cells in the radicular pulp. The fragmentation of Hertwig's epithelial root sheath with residual portions forming the epithelial rests of Malassez, and the ensuing differentiation of cementoblasts from Hertwig's epithelial root sheath cells of follicle cells, and the follicle contribution to the formation of the fibre bundles of the periodontal ligament (PDL) and, possibly, osteoblasts (Nanci, 2017).

1.2.2 Macro and microanatomy of periodontal tissues

The multifunctional feature of the periodontium is due to its components' diversity and unique arrangement. This section presents a general description of periodontal anatomy (Hassell, 1993; Nanci, 2017).

Periodontium is composed of different tissues: the cementum covering the teeth roots, the fibrous PDL that occupies the intermediate space, and the hard lining of alveolar bone that invests the teeth (Figure 1-1). Together, all these components form the tooth attachment apparatus that promotes tooth attachment to the surrounding bony structure and helps maintain their integrity. Gingiva is the fourth component, extending over the alveolar bone's outer surface and providing the attachment apparatus's coronal seal. Breaking of this seal results in bacterial invasion of underlying tissues and initiation of the destruction process.

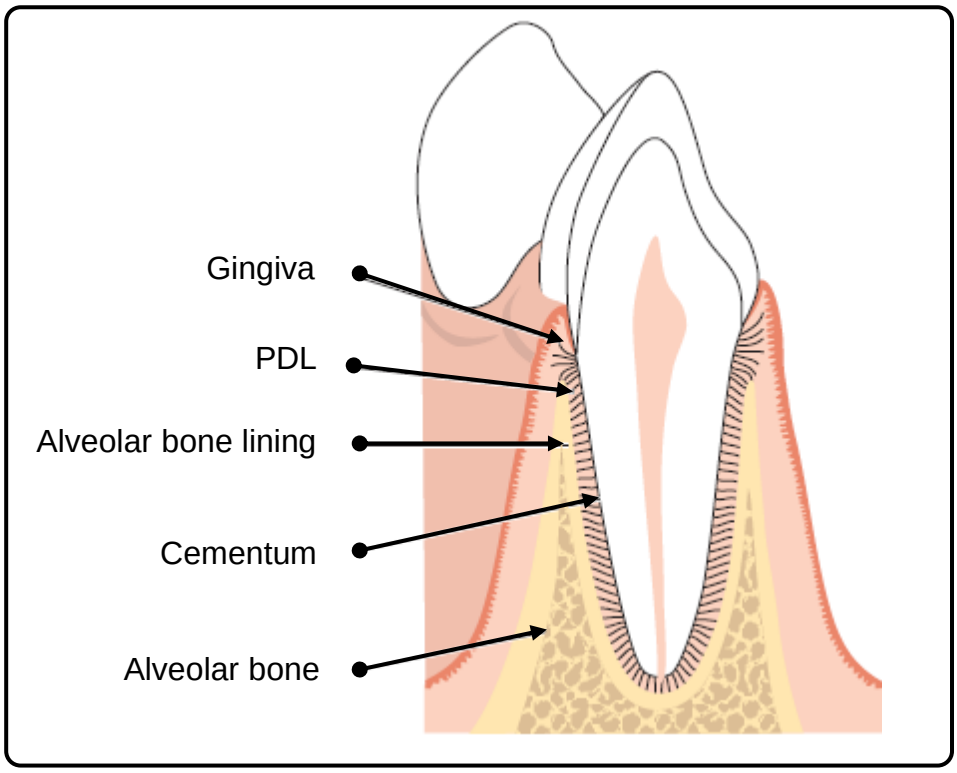

Figure 1-2: Anatomy of the periodontium. Modified from Lindha, *et al.* (2008).

1.2.2.1 Cementum

Cementum is a hard, avascular, non-innervated tissue that covers the surfaces of human teeth roots. This specialised tissue represents the site of insertion of the periodontal ligament's principle fibres, thus helping in the attachment of the tooth to the surrounding investing tissues. The thickness of cementum varies across different parts of the root. It ranges from 10-15 µM at the tooth cervix to 50-200 µM at the root apex. Furthermore, the

thickness of cementum depends on the tooth number and location within the jaw.

Cementum is composed of inorganic (45-50%), mainly needle-like hydroxyapatite crystals ($Ca_{10}(PO_4)_6(OH)_2$), and organic (55-50%) constituents, containing both collagenous and non-collagenous matrix proteins. Collagen type I dominates the organic component (up to 90%) and other collagen types, e.g. type III, XII and traces of V, VI, XIV. The non-collagenous proteins present in this tissue include alkaline phosphatase, osteocalcin, osteopontin, bone sialoprotein, dentin matrix protein 1 (DMP-1), dentin sialoprotein, fibronectin, osteonectin, tenascin. Furthermore, cementum has some specific proteins such as cementum attachment protein (CAP), cementum-derived growth factor (CDGF) and cementum protein 23 (CP-23)(Hassell, 1993; Nanci, 2017).

The presence of small leucine-rich proteoglycans (SLRPs), such as biglycan and decorin, play an important role in controlling cellular activity in addition to regulating the formation of hydroxyapatite crystals. This role could be attributed to these proteoglycans' binding capacity to the collagenous extracellular matrix (ECM) and growth factors.

Due to cementum's cellular contents and the source of its collagenous components, this hard tissue can be categorised into two types that have different structure and function. The acellular extrinsic fibre cementum (AEFC), also called primary cementum, overlays the dentine layer in the root's coronal and middle part. The collagenous fibrils of AEFC are produced by the adjacent PDL fibroblast cells, which form the required attachment between PDL and cementum. Thus, the teeth are maintained in their physiological position, and occlusal forces are distributed to the surrounding bone (Bosshardt and Selvig, 1997; Nanci, 2017).

The cellular intrinsic fibre cementum (CIFC), secondary cementum, contains cementoblasts enclosed by cementum deposits (cementoid) to become cementocytes. These cells are responsible for the deposition of new cementum throughout life. Secondary cementum is found mainly in the apical and inter-radicular regions. Its collagenous fibrils are produced by the

cementocytes themselves. This type of cementum's regenerative role helps in defect repair that could result from trauma or disease. Also, it helps in accommodating the changes that could result from tooth wear or movement (Lekic and McCulloch, 1996; Benatti *et al.*, 2007; Newman, 2012)

1.2.2.2 Periodontal ligament

The periodontal ligament is a soft fibrous connective tissue; it is the only human ligament that connects two different hard tissues (bone and cementum). These ligaments run in the space (0.15 - 0.38 mm) between the alveolar bone and root cementum providing teeth attachment. Like other connective tissues, PDL consists of different types of cells and fibres and amorphous intercellular substance. Fibroblasts are the predominant cell type and are characterised by an abundance of cytoplasm, rich with protein synthesis organelles. This attribute explains the extracellular components' high turnover capacity, specifically the collagen (Berkovitz, 1990; Nanci, 2017).

Furthermore, these cells have a prominent actin network that explains the well-developed cellular structure required to withstand these cells' functional demands. The periodontal ligament also contains other types of cells, including osteoblasts and cementoblasts, found adjacent to the surface of bone and cementum, respectively and contribute to the remodelling process in response to mechanical stimulation. Another essential cell type is mesenchymal stromal cells that differentiate into different cell types (Huang *et al.*, 2009; Zhu and Liang 2015).

The predominant collagen in PDL is type I, with other types such as type III and XII also present. Collagen fibrils are spliced together, forming larger fibres and bundles. Among those fibres, principle fibres are the most common. They are collagen bundles with a wavy orientation which run between alveolar bone and cementum. This orientation serves the periodontal function of anchoring teeth and withstanding the masticatory forces (Daniel, 2014; Nanci, 2017).

Gingiva is the oral mucosa surrounding teeth. It is composed of keratinised oral epithelial supported by connective tissue. The gingiva and tooth form a

V-shaped sulcus that is called the gingival sulcus. This anatomical site is regarded as the starting point for the aggregation of oral bacteria and PDD initiation (Lindha *et al.*, 2008; Newman, 2012).

1.2.2.3 Alveolar bone

Alveolar bone represents that part of the mandible and maxilla that invests and supports teeth. As with other bones, alveolar bone grossly includes a compact bone that forms the outer surface, the tooth socket's lining, and an inner cancellous bone. Histologically, it is composed of three types of lamella; circumferential that makes the compact bone volume, the concentric, which is composed of osteons and with a circular orientation around a central capillary, thus providing a highly vascularised network within the compact bone. These osteons are located parallel to each other and parallel to the long axis of the bone itself; lastly, the interstitial lamella is distributed between the osteons and is made up of concentric layers which have been produced during the remodelling stage and that have different shapes (Cho and Garant, 2000; Nanci, 2017;).

Moreover, the chemical composition of the bone can be categorised into inorganic and organic components. Sixty-seven percent of the bone is made up by the inorganic component that gives the bone its rigidity. It is mainly composed of needle-like crystals of hydroxyapatite that accumulate inside the gaps of collagen fibrils. The remaining 33% of bone volume represents the organic part, with collagen type I being the major ingredient (90%). A trace amount of both collagen types III and V are present too. Other non-collagenous components include matrix proteins such as osteocalcin, osteopontin, osteonectin, bone sialoprotein, as well as growth factors, e.g. Bone morphogenic proteins (BMPs), insulin-like growth factor (IGF-I and IGF II), transforming growth factor and platelet-derived growth factor. These proteins and factors help in controlling cell activity and bone formation.

Bone formation, maintenance and resorption are mediated by the action of different types of cells. According to their origin, these cells can be classified into two types: cells of ectomesenchymal origin (e.g. osteoblast and fibroblasts) and those of hemopoietic origin (e.g. osteocyte).

The osteoblast is a mononuclear, specialised fibroblast-like cell found on the external and internal bone surface and the lining of its Haversian canals. It is responsible for the formation of both collagenous and non-collagenous organic bone matrix. Active cells are characterised by a cuboidal shape with a prominent nucleus, an extensive amount of endoplasmic reticulum and spherical Golgi apparatus. Another characteristic feature is the cell-cell adherence that is mediated by microfilaments and helps in cell-cell communication. These cells secrete a thin layer of unmineralised organic material that is termed the osteoid. This layer is composed of parallel aligned COL- 1 fibrils.

Moreover, some proteins are found as osteocalcin and Cbfa-1 (Runx2), which are regarded as specific markers for osteoblasts. Another indicator of osteogenic differentiation is an alkaline phosphatase that has a role in mineralising the organic matrix. Mineralisation foci are formed inside the osteoids which contain other non-collagenous proteins, e.g. bone sialoprotein and osteopontin that contribute to the calcification process.

During deposition of organic and non-organic components, some of the osteoblast cells, about 30%, become trapped within a formed bone and are termed osteocytes at this stage. However, these cells maintain their connection with other osteocyte and osteoblast cells through their processes which extend within canaliculi. Due to the cells' communication network and widespread distribution of osteocytes within the bone, they can be regarded as mechano-sensors that control the bone response to the mechanical and biochemical stimulation. These cells share many markers with osteoblasts; this is evident because of their origin. Nevertheless, one of the distinguishing features is the absence of alkaline phosphatase activity.

Other important cells originating from the hemopoietic monocytes/macrophage cell lineage are the osteoclast cells. They are large, multinucleated cells, with prominent Golgi complex and less endoplasmic reticulum. These cells are responsible for bone resorption. Tartrate-resistant acid phosphate is an important marker for these cells; it

demineralises the inorganic bone component. Moreover, the organic deposit is destroyed by the action of lysosomal and non-lysosomal enzymes of these cells (matrix metalloproteinases and cathepsins, respectively).

To maintain the regeneration capacity throughout life, osteo-progenitor cells are distributed in many places, including in periosteum under the osteoblast cells, PDL and the bone marrow space. These cells originate from stem cells that possess the self-renewal ability. During cell division of stem cells, one of the daughter cells remains a stem cell, while the other differentiates into a different cell type. The differentiated cell passes through several divisions before becoming an osteoblast. This is accompanied by the expression of different genes during this journey. At an early stage, a high level of cell- growth genes are expressed, e.g. Runx2, c-*fos*. Then, some genes of osteoblast-related products are expressed, including collagen type I, fibronectin and alkaline phosphatase. Finally, bone mineralisation genes are expressed like osteocalcin, osteopontin and bone sialoprotein (Newman, 2012, Nanci, 2017).

1.3 Periodontal disease

Periodontal disease (PDD) is a widespread chronic oral disease that affects about half of the adult population (Petersen and Ogawa, 2012; Jeffcoat *et al.* 2014). This type of disease is due to the interaction between periodontal pathogens and the host immune response.

The primary causative factor of PDD is dental plaque, a biofilm of polysaccharide containing a mixture of host and bacterial components (Bascones and Figuero, 2005; Nair *et al.*, 2014).

The inflammatory process in periodontal disease is initially confined to the gingival part and is manifested as oedema, erythema and bleeding; this reversible stage can progress to a pathological deepening of gingival sulcus leading to the formation of a periodontal pocket. This significant consequence is due to the destruction of PDL attachment, alveolar bone resorption, and cementum necrosis that cause increased tooth mobility (Lindha *et al.*, 2008; Newman, 2012). Unfortunately, all these events lead

to tooth loss causing impairment of dental function and aesthetics. This necessitates early diagnosis and appropriate treatment approaches.

1.4 Periodontal treatment: current approaches

The ideal aim of any periodontal treatment is to stop disease progression and restore healthy structure and normal function. Treatment of PDD focuses on the elimination of periodontal pathogens found in dental plaque and calculus. This is usually accomplished using mechanical debridement that may be supported by antimicrobial agents to provide a healthy environment that favours the regeneration process (Jin, 2010; Vaquett*e et al.*, 2012; Iwata *et al.*, 2014).

1.4.1 Non-surgical and surgical debridement

Mechanical debridement is a crucial method for this type of treatment. This method involves debridement of bacterial aggregations from accessible tooth surfaces and pathological periodontal pockets. However, the pathological deposits in deeper areas may indicate making a surgical flap to provide access for thorough elimination of these deposits. (Reynolds *et at.*, 2010). However, healing following this type of therapy is neither absolute nor stable. It is characterised by forming fragile epithelial attachments instead of PDL (Nievers *et al.,* 1999; Shimono *et al.*, 2003; Requicha *et al.* 2014). Accordingly, advanced surgical techniques are recommended to overcome these issues (Bosshardt and Sculean, 2009).

1.4.2 Surgical regenerative therapy

Regenerative therapy is aimed to re-establish the function and structure of the diseased or traumatised tissue by the formation of new tissues (Polimeni *et al.,* 2006; Chen and Jin, 2010; Ramseier *et al.,* 2012). Achieving this goal necessitates using materials that initiate cell proliferation and differentiation and support tissue regeneration.

Grafting materials support tissue regeneration by serving as a framework that stabilises the clot and bridges the wound gap (osteoconductive); or via cells and growth factors within it, stimulating cell division (osteogenic, osteo-

inductive). According to their source, grafts can be categorised into different types. Autograft, which is harvested from the same individual, represents the gold standard as it contains all properties of graft: osteoconduction, osteoinduction and osteogenicity (Caton and Zander, 1976; Reynolds *et at.*, 2010); Allogeneic graft, here the graft is transferred between the same species; while the xenogeneic graft is used between different species, such as bovine bone; Another type is the alloplastic graft, which is made from biocompatible synthetic or inorganic materials like β-tricalcium phosphate (Caton and Zander, 1976; Reynolds *et at.*, 2010).

Many preclinical and clinical studies investigated the efficiency of using different grafting materials to enhance periodontal regeneration. Although the clinical outcomes reflected an improvement regarding the reduction of pocket depth and clinical attachment level, the histological examination demonstrated a limited amount of PDT formation. Additionally, the fast rate of epithelial cell growth resulted in occupying the periodontal space between cementum and newly formed bone (Caton and Greenstein, 1993; Trombelli *et al.*, 2002; Reynolds *et al.*, 2003).

Guided tissue regeneration is another technique that depends on applying a physical barrier (membrane) to preclude epithelial cells from dominating the wound gap, thus providing a space for PDT formation. The membranes are either degradable or non-degradable, characterised by superior mechanical properties (Karring *et al.* 1993; Ramseier *et al.,* 2012). Both types have been examined clinically in many periodontal defects with histological evidence of periodontal regeneration. Nevertheless, many drawbacks arise, including exposure of non-degradable membranes to the oral cavity with an increased possibility of infection and delayed healing. Conversely, absorbable membranes lack the necessary mechanical support to maintain enough space for the regeneration process (Karring *et al.*, 2003; Bornstein *et al.*2009).

It was found that using a grafting material with protective membranes can lead to superior outcomes, with most of the newly formed tissue being bony in nature (Cortellini and Bowers, 1995, Machtei and Schallhorn, 1995; Pini

et al., 1996). However, complications associated with these two approaches include a high risk of infection, morbidity at donor sites, graft rejection and resorption with unpredictable clinical outcomes. These factors limit their application to specific clinical situations (Needleman *et al.* 2006; Ivanovski, 2009; Iwata *et al.*, 2014).

1.5 Tissue engineering: an alternative approach for periodontal treatment

Tissue engineering (TE) emerged as a rapidly-progressed topic at the early 70s (Langer and Vacanti, 1993; Vacanti *et al.*, 2006). It aims to restore damaged tissues due to trauma or disease through a combination of primary tissue regeneration elements, including cells and skeletons as well as biochemical and physiological factors that control this process (Spector *et al.*1999; Vacanti *et al.*, 2006).

1.5.1 Cells

Cells are regarded as the basic unit for any tissue. During the regeneration process of damaged tissue, the organ's cells start proliferation and differentiation into specific types to rebuild organ structure. If an organ's cells failed to achieve this role, cells might derive from undifferentiated or progenitor cells isolated from the same organs or a different one (Thesleff and Tummers 2003; Atala and Yoo, 2009). In TE, stem cells are primary cell types with self-renewal capacity and can be differentiated into other specialised cells. Stem cells can be isolated from embryonic or adult tissues. The embryonic stem cells are totipotent that can differentiate to any other cell type. Adult stem cells are responsible for continuous renewal and maintenance of the human body throughout life. In contrast to embryonic stem cells, these cells can produce limited cell types (Thesleff and Tummers 2003; Lin 2008; Darby 2011).

Periodontal tissue development is initiated by dental cranial neural crest cells. Therefore mesenchymal or neural crest-derived stem cells are regarded as the most valuable cell type for periodontal TE. Different types

of human mesenchymal stem cells (MSCs) have been used for periodontal regeneration, and categorised according to their origin into non-oral and oral stem cells (Ishikawa *et al.*, 2009; Iwata, 2014).

Bone marrow-derived MSCs (BMSCs) is the first and most commonly investigated type of MSCs. Wei *et al.* (2010) reported the use of BMSCs to regenerate new cementum, bone, PDL and blood vessels *in vitro*. BMSCs can express typical surface markers of osteoblasts and fibroblasts. Similarly, Yang *et al.* (2010) observed the evidence of regeneration of bone, cementum and PDL using BMSCs transplanted in animal models. The newly formed PDLs appeared to have well-oriented ligament structures. Adipose-Derived Stem Cells (ADSCs) are another promising option for TE. Their availability, easy harvesting, high survival rate, and role in enhancing periodontal regeneration are among the essential characteristics of this type of stem cells, (Huang *et al.*,2009; Hung *et al.*, 2011).

Dental pulp stem cell (DPSCs) was the first type of dental MSCs used in tissue regeneration. They can be isolated from the dental pulp tissue of extracted teeth. This cell type has multilineage capacity and can be differentiated to odontoblasts, osteoblasts, neuron-like cells, chondrocytes and adipocytes. (Huang *et al.*, 2009; Volponi *et al.*, 2010; Zainal *et al.*, 2013).

Several studies have shown that PDL-derived stem cells (PDLSCs) can differentiate into fibroblasts, cementoblasts, osteoblasts progenitor cells, chondrocytes, and adipocytes (Huang *et al.*, 2009; Paula-Silva *et al.,* 2010; Zhu and Liang, 2015). According to Liu *et al.* (2008), these cells could achieve complete periodontal regeneration. Previous studies demonstrated that using these cells can lead to regeneration of well-oriented PDL. Also, teeth roots were found covered with cementum-like tissue with no evidence of ankylosis and root resorption (Boyko *et al.*,1981; Lang *et al.*,1995; Zhu and Liang 2015). PDLSCs can be isolated from the middle third of extracted teeth, i.e. teeth extracted for orthodontic purposes, impacted teeth, deciduous or supernumerary teeth. However, other studies found that PDLSCs that remain in the alveolar socket after extraction could have

higher osteogenic and adipogenic differentiation capacities (Wang *et al.*, 2011; Song *et al.*, 2012).

Other oral cell types were examined for their differentiation capacity into PDL cells. Cementum-derived cells have been used in combination with hydroxyapatite-tricalcium phosphate ceramics scaffold to form cementum-like tissue with a similar structure to normal cementum (Grzesik *et al.* 1998). Oral mucosa/gingiva-derived MSCs used as a potential candidate for periodontal regeneration. Also, they have immune-modulatory and anti-inflammatory characteristics. These cells could be used to increasing the keratinised gingival zone and treatment of chronic desquamative gingivitis (Okuda *et al.*, 2004; McGuire *et al.* 2011; Zhang *et al.* 2012). Nevertheless, using orally originated MSCs have a high rate of morbidity to the donor site in addition to the limited amount of harvested cells, which make it important to investigate the potential of using MSCs from other parts of the human body (Huang *et al.*, 2009; Requicha *et al.*, 2014).

1.5.2 Growth factors

Cellular metabolic activities are controlled by a bio-singling system that consists of particular biochemical molecules, including growth factors. Growth factors are polypeptides acting as biological mediators that interact with specific receptors on/within the cell to exert the required actions. They are responsible for regulating cells' biological process, including proliferation, differentiation, chemotaxis and matrix synthesis (Giannobile *et al.*, 1996; Atala and Yoo *et al.*, 2009). Many growth factors were investigated for their roles in periodontal TE. Lynch *et al.* (1989) reported that platelet-derived growth factor (PDGF) was the first factor for used for TE. This factor has roles in proliferation, migration and matrix synthesis of periodontal cells such as gingival fibroblasts, osteoblasts and cementoblasts. (Janssens *et al.,* 2005; Sood *et al.,* 2012).

Transforming Growth Factor-βs (TGF-βs) play a significant role in differentiating PDLSCs into fibroblasts, and maintaining PDL integrity under physiological stimulation (Tatakis *et al.*, 2000; Fujii *et al.*, 2010). Another group of TGFs is bone morphogenetic proteins (BMPs) that stimulate the

differentiation to osteoblasts and promote bone formation; Sood *et al.* (2012) and Iwata *et al.* (2014) reported that BMPs could be used to improve bone augmentation around the dental implant and sinus lifting procedure. BMP-7 and BMP-12 have a significant cementogenesis and periodontal repair roles, respectively (Wolfman *et al.*, 1997; Ripamonti *et al.*, 2001). Growth/differentiation factor-5, a type of bone morphogenetic proteins, was found to enhance ligament and bone formation in many musculoskeletal tissues, including the periodontium (Moore *et al.*, 2010). Many studies analysed the essential fibroblast growth factor (bFGF) effect and concluded that bFGF is effective and safe for PDT regeneration (Murakami *et al.*, 1993, 2003; Takayama *et al.*, 2001 and Kitamura *et al.*, 2008; 2011). Takeda *et al.* (2005) suggested that brain-derived neurotrophic (BNF) factor has numerous vital functions. BNF could stimulate new bone formation, cementum with newly formed fibres inserted between them, and stimulated new blood capillary formation.

1.5.3 Scaffolds materials in PDTE

Scaffold represents the platform from which tissue regeneration begins; it simulates the extracellular matrix (ECM) role in normal tissues, and act as a skeleton that enhances cells adhesion and proliferation. Also, It provides growth factors that control the regeneration process and tissue its mechanical properties/geometrical structure. (Hutmacher and Cool, 2007; Shimauchi *et al.*, 2013). Specific properties must characterise the scaffold to meet the required aim, such as biocompatibility, controllable biodegradability and optimum mechanical properties to achieve the required goal. The scaffold architectural characteristics can be modified based on the type of regenerated tissue, including shape pores size, and surface topography. Manufacturing feasibility and expenses are other factors that affect the selection of scaffold. (Chan and Leong, 2008; O'Brien, 2011).

Many types of the scaffold were utilised for periodontal regeneration, depending on specific properties of the regenerated part of the periodontium (bone, cementum or PDL). Table 2-1 shows some of the scaffolds used in periodontal TE.

Among different biomaterials used as scaffolds, both natural and synthetic polymers have attracted more attention due to their favourable properties, e.g. biocompatibility, biodegradability, and easy manipulation. However, there are still some limitations such as weak mechanical structure, mainly in natural polymers (Liu and Ma, 2004; Weigel *et al.* 2006).

Table 1-1: Scaffolds used in PDT regeneration

Scaffold	Cells	Outcomes	Reference
Doubled layer poly (ε-caprolactone)	Canine ADSCs	Osteogenic differentiation	Requicha *et al.,* 2014
Alginate	PDLSCs	Osteogenic differentiation	Moshaverinia *et al.,* 2014
Hydroxyapatite – collagen	PDLCs	Adhesion and proliferation	Guo *et al.,* 2013.
Strontium-containing mesoporous bioactive glass	PDLCs	Osteogenic/cementogenic differentiation	Wu *et al.,* 2012
Biphasic polycaprolactone containing β-TCP	PDLCs	Bone/PDL complex	Vaquette *et al.,* 2012.
alginate/nano bioactive glass-ceramic	PDLFs	Osteogenic differentiation	Srinivasan *et al.,* 2012
lithium-containing mesopore-bioglass (Li-MBG)	PDLCs	Cementogenic differentiation	Han *et al.,* 2012
β-TCP	PDLCs	Osteogenic differentiation	Xia *et al.,* 2011.
Enamel matrix derivatives	Induced Pluripotent Stem Cells	Osteogenic/cementogenic differentiation	Duan X. *et al.,* 2011
Calcium Hydroxide	PDLSCs	Cementogenic differentiation	Paula-Silva *et al.,* 2010

Silk is one of the natural polymers used for centuries for many medical applications, commonly as suturing material. In contrast to other polymers, silk is characterised by its superior mechanical properties and tunable degradation rate. Silk can be cast into different forms. It can also be combined with other materials to produce different scaffolds that support many tissues' regeneration (Kearns *et al.*, 2008).

Both spiders and silkworms produce silk. Silkworms are either domestic silkworm, e.g. Bombyx mori (mulberry), or wild silkworms (non-mulberry), e.g. Antheraea pernyi and Antheraea mylitta (Kim *et al.*, 2015; Bhattacharjee *et al.*, 2017). In contrast to silk obtained from silkworms, spiders silk has limited applications due to difficulties in breeding these species. Additionally, the amount of silk isolated from spider web (12 m) is limited compared to the amount isolated from silkworm cocoon (600-900 m) (Lewis, 1996).

Chemical composition and structure of silk determine its unique properties, specifically, its superior mechanical features (Liu and Zhang, 2014). Macroscopically, Bombyx mori silk's fibre is composed of two cores covered with a protein coat, see figure 1.3. This polymer (silk) contains two proteins, fibroin (70-75%) and Sericin (25-30%). Fibroin forms the silk core structure by light and heavy chains; these two chains are linked together with a single disulphide bond at one end. Sericin is a glycoprotein which encloses the fibroin core (Hardy *et al.* 2008; Zhang *et al.* 2009; Rajkhowa *et al.* 2010(Liu and Zhang, 2014). Both the light and heavy chains of fibroin are composed of standard amino acids. However, the sequence of these amino acids in the light chain is nonrepetitive compared to the high repetitive (Glycine-Alanine) sequence of the heavy chains with motif and tyrosine-rich domains (Zhou *et al.*, 2000). Fibroin fibres have a hydrophobic region at the central part of the protein. In contrast, the hydrophilic region is found at the light chain's amino and carboxy-terminal domains because of unrepetitive amino acid sequences (Bini *et al.*, 2004; Qi *et al.*, 2017).

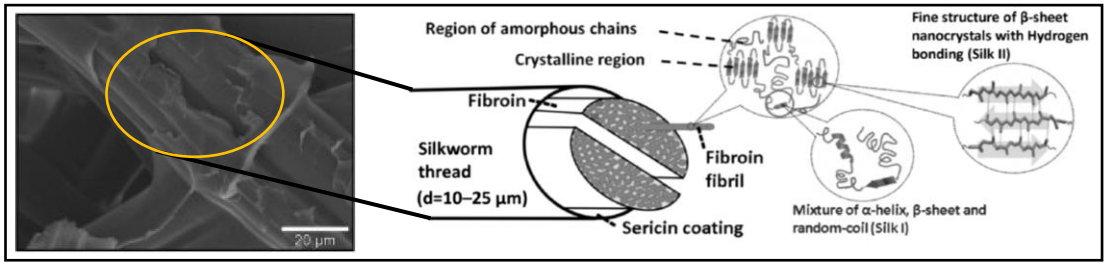

Figure 1-3: Silk fibroin structure of a single silkworm thread (Hardy *et al.*, 2008; Volkov *et al.*, 2015).

Silk is a fibrous protein composed of three structural parts, crystalline β-sheets rich in Alanine, elastic β-spirals, and tight amino acid repeats, forming α-helices and spacer regions. It is believed the mechanical properties of Bmf silk is due to the crystalline β-sheets, which represent 50% of silk fibre. These sheets are oriented in a parallel direction to the fibre long axis. The amorphous or non-crystalline region forms the remaining 50% of the fibre (Liu and Zhang, 2014). It has been suggested that elastic β-spirals and α-helices are responsible for the amorphous part.

Silk is subjected to specific processing before being used for biomedical applications, which is termed the degumming process. This process involves removing the sericin coating that is reported to induce immunological reactions (Kearns *et al.*, 2008).

The mammalian cells can adhere to biomaterials in several ways. Initially, cells can be attached to the substrate surface by the action of electrostatic force as these cells are negatively charged. Afterwards, cells recognise specific sites that mediate their chemical attachment to the substrate. In silk fibroin, the electrostatic force is the primary means for cellular attachment (Minoura *et al.*, 1995; Teuschl *et al.*, 2014). Furthermore, the amino acid sequence of silk fibroin presents a specific recognition site for cellular attachment (Ruoslahti and Pierschbacher, 1987). In contrast to chitosan that limits cellular spread and migration, Silk fibroin promotes cellular attachment and growth at a comparable level to collagen (Minoura *et al.*, 1995; Teuschl *et al.*, 2014).

Another important feature of silk fibroin is its controllable degradability. This property is a requirement for scaffold material to allow for gradual cell growth and tissue formation. During four weeks of *in vitro* culture, it has been reported that silk fibroin shows a slow rate of degradation by proteolysis (Taddei *et al.*, 2006; Kearns *et al.*, 2008). Similarly, silk fibroin demonstrated a slow rate of degradation following six weeks of *in vivo* culture (Meinel *et al.*, 2005). The rate of degradability of silk scaffold can be adjusted from a few weeks to a year by controlling β-sheet content (Wang *et al.*, 2008; Mieszawska *et al.*, 2011). Hu *et al.* (2012) found that slow degradation rate was associated with an increase in the contents of β-sheets. The degradation rate of silk fibroin was also linked to its form. Fibroin films showed a higher degradation rate than the fibroin fibres, attributed to an increased surface area and broad exposure to proteolytic enzymes. Interestingly, the silk fibroin's pre-treatment with methanol was found to decrease its degradability (Minoura *et al.*, 1990; Uebersax *et al.*, 2006).

Several studies investigated the capacity of using silk as a scaffold in TE, especially for ligament, tendon, and bone regeneration, with promising findings (Kuboyama *et al.* 2013; and Saha, *et al.*, 2013; Musson *et al.*, 2015). However, the application of Bombyx mori fibroin scaffold in periodontal regeneration is still limited. Most of the published work in this field involved using the Bmf either as a vehicle for delivering the antimicrobial agent clinically or as a composite scaffold in combination with other materials to enhance periodontal tissue regeneration (Vera-Sánchez, M *et al.*; Kim *et al.*, 2005; Hwang *et al.*, 2009; Yang *et al.*, 2013; Jin *et al.*, 2014; Vera-Sánchez, Mar *et al.*, 2016; Geão *et al.*, 2019).

Etienne *et al.* (2009) investigated cellular behaviour in response to silk fibroin gel. In this study, silk fibroin gel was seeded with human dermal fibroblasts and cultured *in vitro* and *in vivo.* This study concluded that this material could support cellular growth and initiate a limited adverse reaction. Furthermore, Woloszyk *et al.* (2016) found that silk fibroin in a 3D porous form supports vascularisation and homogeneous distribution of blood vessels. Here, silk scaffold was seeded with either human dental pulp stem

cells or human gingival fibroblasts, then implanted for seven days in a chick embryo.

Silk was also used in conjunction with other biomaterials in an attempt to develop scaffold that enhances the growth of hPDLCs. Rodríguez-Lozano *et al.* (2014) investigated the effect of using composite graphene oxide and silk fibroin films on the mesenchymal phenotyping, cellular activity and proliferation rate of hPDLSCs. The study concluded that combining these two materials in one scaffold affects cell proliferation rate, with cells seeded on graphene oxide film showing a higher proliferation rate. Also, there was no significant difference in the expression of mesenchymal cell markers (CD73, CD90 and CD105) between the composite scaffold and silk fibroin film groups. Accordingly, the current study tries to shed light on the feasibility of using Bmf as an individual scaffold material to support different periodontal tissue regeneration.

1.5.4 Mechanical stimulation and its role in periodontal tissue regeneration

Periodontium is a dynamic tissue, where mechanical stimulation plays a significant role in the regeneration and remodelling of its component tissues. Absence of regular occlusal stimulation seen in patients with dental malocclusion leads to atrophy of PDT and narrowing of PDL space in addition to a decrease in tooth movement (Cohn, 1965; Ohshima *et al.*, 1991; Usumi-Fujita *et al.*, 2013). Another representation for this role is teeth subjected to orthodontic forces, where they can be moved to a certain distance within intact alveolar bone and PDT. The tooth movement process is mediated by the formation of pressure and tension sites across the periodontium, which induces resorption and formation processes, respectively (Motokawa *et al.*, 2013 and Usumi-Fujita *et al.*, 2013).

One of the primary challenges in PDTE remains the regeneration of different types of tissues in one model; this is due to the complex architecture of periodontium and diversity in biological and mechanical characteristics of its component tissues. This tissue remodelling cannot be accomplished without considering the role of physiological mechanical stimulation, which

acts on the entire periodontium (Talal *et al.*, 2010). Garlet *et al.* (2007) reported expression of different pro-/anti-inflammatory cytokines at compression and tension sides of periodontium following one week of orthodontic forces application (7 N) on human teeth clinically. Thus, mechanical stimulation affects cellular growth and determines their differentiation path (Goetzke *et al.*, 2018).

Studying the periodontium mechanobiology remains a challenge due to the complex anatomical and biological nature of periodontium, where simulating mastication's biomechanics. Many studies tried to investigate the effect of applying different types of forces on periodontal cells. Table 1-2 briefly illustrates studies published in this area. Some studies investigated compression forces' effect by applying a continuous, static, unidirectional force on cells. This was accomplished by placing a sterile glass cylinder filled with metal beads of known weight (Figure 1-4). However, this approach could only simulate the static orthodontic forces rather than intermittent masticatory forces (Li, Y. *et al.*, 2013; Chen *et al.*, 2015). Another approach used in studying the role of compression force on cellular behaviour is using centrifuging forces (Wei *et al.*, 2008). Here, the cells are seeded in monolayer in microplates and centrifuged in a horizontal centrifuge. The amount of force applied in this method is higher than that of the weight one. Again, this approach helps study the orthodontic forces. Also, cells will be subjected to fluid shear stress in addition to the compression force (Figure 1-4).

Table 1-2: Some Studies that investigated the effect of mechanical loading on PDTE.

Cells	Type of stimulation	Loading system	Effect	Reference
PDLSCs	Stretch	Flexcell FX-5000 tension system (USA)	Osteogenic differentiation and alignment	Wei *et al.* 2015
PDLCs	Stretch (cyclic)	STB-140 (Japan)	Proliferation, osteoblastic and cementoblastic differentiation	Monnouchi *et al.* 2015
PDLCs	Ultrasonic pulses	LIPUS exposure device (China)	Osteogenic differentiation	Hu *et al.* 2014
PDLSCs	Tensile strain	Flexcell FX-4000T tension plus system (USA)	Osteogenic differentiation	Shen *et al.* 2014
PDLCs	Tensile strain (Cyclic)	Flexcell FX-5000 tension system (USA)	Osteogenic differentiation	Li *et al.* 2013
PDLF, HOB	Strain	Flexcell FX-5000tension system (USA)	Osteogenic differentiation	Jacobs *et al.* 2013
PDLCs	Stretch	Flexcell FX-4000 strain system (USA)	MMP2, collagen, lysyl oxidase (favour ECM stabilisation)	Chen, 2013
PDLSCs	Vibration	GJX-5 vibration sensor (China)	Osteogenic differentiation	Zhang *et al.* 2012
PDLSCs	Tensile strain (Cyclic)	Self-made four-point bending system (cyclic uniaxial tensile stress)	Osteogenic orientation	Tang *et al.*, 2012
PDLCs	Shear stress	Custom made shear stress system.	Cells and fibres alignment	Kim *et al.*, 2011
PDLF	Compression and tension	Membrane	ECM synthesis and degradation	He *et al.*, 2004

One of the most used models for studying PDLCs' biomechanics involves seeding cells on a 3D flexible scaffold, followed by applying tensile or compressive forces. Flexcell tension and compression systems have commonly used bioreactor for that purpose (Liu *et al.*, 2012; Yang *et al.*, 2015). This approach is more representative as it simulates the 3D tissue environment. Nevertheless, these systems can apply one mode of force to the samples. Furthermore, collagen gel is the scaffold of choice, which proved to have poor mechanical properties to support hard tissue regeneration. Despite being controlled by a computer-based system, which improves the adjustment of force parameters, Flexcell is a costly machine (Li, M. *et al.*, 2019). Berendsen *et al.* (2009) developed a unique bioreactor able to apply a force range between 67 N to 200 N on cells seeded on collagen gel, either in cyclic or static mode. This device requires careful handling during the scaffold-cells sample harvest, as the collagen gel is filling a tiny space of 200µm. Also, it mainly studies the effect of shear stress rather than compression force.

In contrast to compression force, the effect of tensile force on PDLCs' behaviour has been extensively investigated (Raif el, 2008; Huang *et al.*, 2009; Yu *et al.*, 2009; Tang *et al.*, 2012; Li, L. *et al.*, 2013; Li, L. *et al.*, 2014; Wada *et al.*, 2017).

Due to the reasons demonstrated before, recreating the typical masticatory force system becomes a requirement to simulate the type, magnitude, and direction of applied forces. Mastication initiates a series of compressive, shear and tensile forces across different areas of the periodontium. Several studies tried to investigate the effect of mechanical stimulation on the behaviour of periodontal cells *in vitro* by developing special bioreactors to simulate masticatory mechanism (He *et al.*, 2004; Kim, S.G. *et al.*, 2011; Chen, Y.J. *et al.*, 2013; Jacobs, Collin *et al.*, 2013; Monnouchi *et al.*, 2015).

However, the bioreactors used in these studies were basic and simulated limited aspects of the masticatory process. Some of these bioreactors were limited to applying static force, while others were applicable for monolayered cells rather than those in the 3D anatomical setting.

Due to previous studies' limitations, the present study is trying to bridge this gap by developing a novel bioreactor, that could apply more than one type of masticatory forces on 3D tissue-engineered construct. Also, to improve the researcher control over the essential parameters such as mode, magnitude, direction, and frequency applied forces.

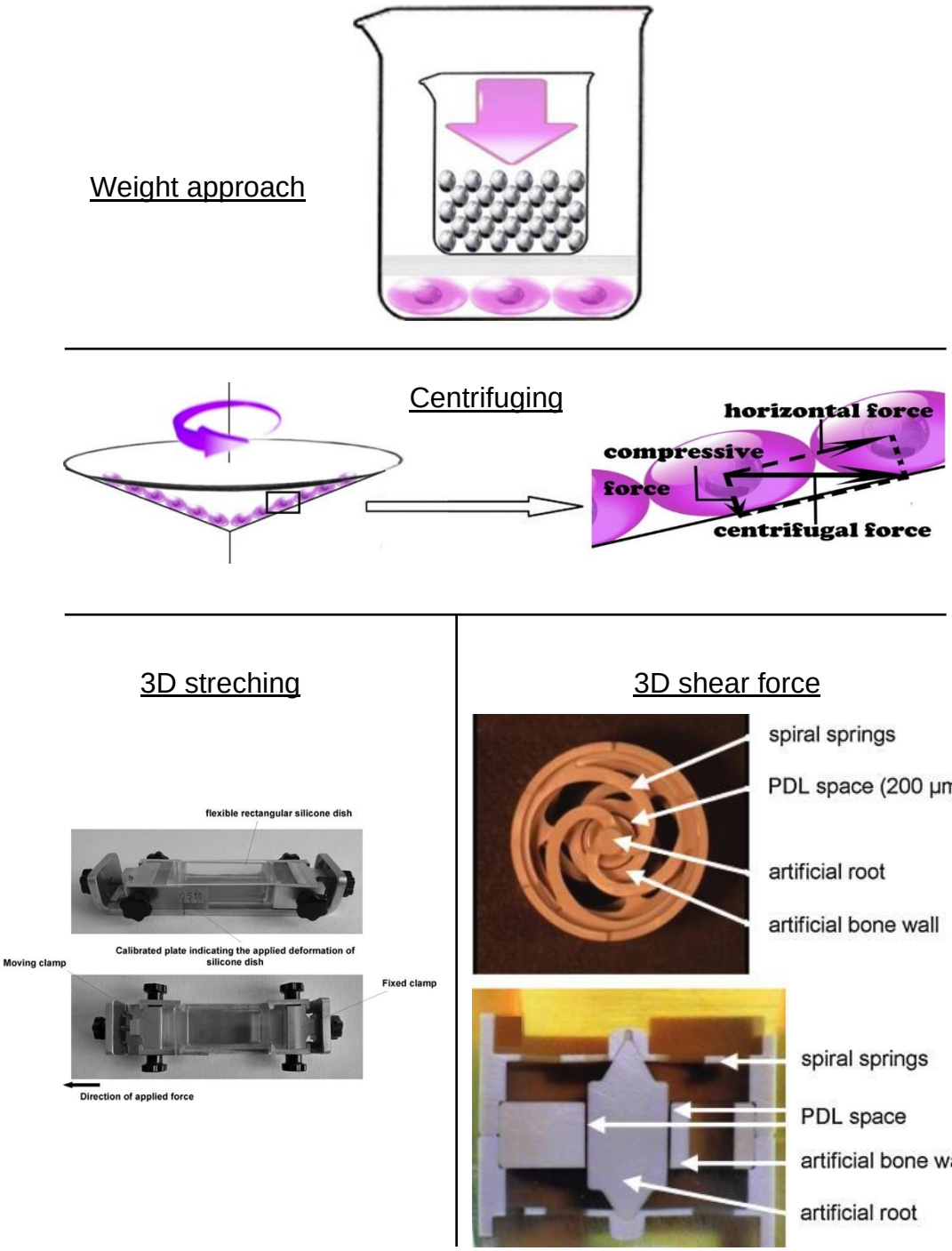

Figure 1-4: Bioreactors used for studying the effect of mechanical stimulation on cell behaviour (Berendsen *et al.*, 2009; Yang *et al.*, 2015; Papadopoulou *et al.*, 2016).

1.6 Aims and objectives

This project investigates the feasibility of using hPDLSCs and Bmf silk scaffold to enhance the regeneration of periodontal tissue *in vitro* and develop a novel bioreactor to apply and study the effect of cyclic compressive stimulation on the hPDLSCs in 3D, *in vitro* setting.

The objectives of the current project can be categorised into the following:

1. Isolation and *In vitro* characterisation of hPDLCs:

- To isolate hPDLCs from extracted, healthy third molar teeth of three donors.
- To examine the multipotent MSCs characteristics of the hPDLCs

2. Evaluation of biological efficacy of Bmf silk as a potential scaffold to support hPDLSCs proliferation and osteogenic differentiation:

- To determine the macroscopic and microscopic features of Bmf silk scaffold.
- To examine the immunogenicity of Bmf scaffold upon exposure to THP-1 cells.
- To investigate the cytocompatibility of Bmf scaffold upon culture with hPDLSCs *in vitro*.
- To investigate the behaviour of hPDLSCs-Bmf silk construct *in vivo*.

3. Developing a novel mechanical stimulation bioreactor to study the effect of cyclic compressive stimulation on the activity of hPDLSCs *in vitro*:

- To establish the bioreactor design and identify the required compartments for its manufacturing.
- To evaluate the biocompatibility of material used for the manufacturing of bioreactor cells' chambers unit.
- To investigate the effect of cyclic compressive stimulation on the proliferation and differentiation of hPDLSCs in 3D, *in vitro* setting

Table (1-3) presents an overview of the objectives of the current project.

Table 1-3: Overview of the project objectives

Isolation of hPDLCs	***In vitro* characterisation of hPDLCs**	**Evaluation of biological efficacy of Bmf silk as a potential scaffold to support hPDLSCs proliferation and osteogenic differentiation**	**Developing a novel mechanical stimulation bioreactor to study the effect of cyclic compressive on the activity of hPDLSCs *in vitro***
Chapter two	**Chapter three**	**Chapter four**	**Chapter five**
Isolation of hPDLCs from extracted, healthy third molars of three donors	**CFU-F assay** Investigating the cellular clonogenicity and proliferative potencies	**Immunogenicity assay** Determining the expression level of inflammatory cytokines (TNF-α, IL-1β) of THP-1 cells upon exposure to Bmf silk scaffold	Establishing the design of the bioreactor using designing software. Also, identifying the required material and compartments for its manufacturing
Examining cellular morphology	**Multi-colour flow cytometry** Determining the expression level of MSCs (CD29, CD73, STRO-1) and HSCs (CD34, CD45) markers	**Optimisation of cells seeding technique**	**Immunogenicity assay** Determining the expression level of inflammatory cytokines (TNF-α, IL-1β) of THP-1 cells upon exposure to PMMA, which is proposed for the fabrication of bioreactor cells' chambers unit
	***In vitro* induced trilineage differentiation** (Osteogenic, chondrogenic and adipogenic)	**Cytocompatibility** Investigating the viability, metabolic activity and osteogenic differentiation capacity of hPDLSCs seeded on Bmf scaffold *in vitro*	**Cytocompatibility** Investigating the viability and metabolic activity of hPDLSCs seeded on PMMA *in vitro*
		***In vivo* animal model** Evaluating the behaviour of hPDLSCs-Bmf silk construct implanted within DCs, in CD-1 nude mice	Investigating the effect of cyclic compressive stimulation on the proliferation and differentiation of hPDLSCs in 3D, *in vitro* setting

Chapter Two: General materials and methods

2.1 Introduction

This chapter describes the general materials and methods used for the experiments of this project. However, certain materials and more specific methods will be referred to in the relevant chapters.

Unless otherwise stated, all tissue culture vessels (surface treated flasks, culture dishes, tubes and flat-bottom well plates) were supplied from Corning Life Sciences (Flintshire, UK). Essential reagents, including calcium and magnesium-free 1× phosphate buffer saline (PBS) (pH 7.4), culture medium, e.g. alpha-minimum essential medium (α-MEM), and foetal calf serum (FBS) were purchased from Lonza Bioscience (Slough, UK). Other medium supplements, e.g. L-glutamine, penicillin/streptomycin antibiotic mix, Amphotericin-B (Antifungal) and trypsin-EDTA were from Sigma-Aldrich (Missouri, USA). Several types of medium were used during the current project. Full description of these media with their components are listed in Table 2-1.

Different types of cells were used for the experiments of the current project. hPDLCs were used to perform formal experiments in 2D and 3D culture. The experiments of this project were conducted following the ethical approval granted by the Dental Research Ethics Committee (DREC) of Leeds Dental School (Tissue Bank application number 031114/FA/148) to use tissues of the donors (extracted teeth) for research purposes only. Table (2-2) summarise the details of donors from whom teeth were obtained.

Human THP-1 cell line, supplied in a frozen ampoule, was purchased from Sigma-Aldrich (Missouri, USA). These cells were isolated from the peripheral blood of a one-year-old male with an acute monocytic leukaemia, and they have the morphology of monocytes.

Table 2-1: Main types of culture medium used throughout the project with their components

Medium	Components
Plain	• α-MEM medium without any supplements
Basal	• α-MEM medium. • 10% FCS • 1% L-glutamine • 100 unit/mL Penicillin/ Streptomycin • 100 unit/mL Amphotericin-B
Digestive	• Plain medium • 100 unit/mL Penicillin/ Streptomycin • 100 unit/mL Amphotericin-B • 3 mg/mL of Collagenase- I • 4 mg/mL of Dispase (the last two items were supplied from Gibco Life Technologies, Loughborough, UK)
Cryopreservation	• 50% FCS • 40% basal medium • 10% dimethyl sulfoxide (DMSO) (Sigma-Aldrich, Missouri, USA)

Table 2-2: Details of donors and types of teeth.

Donor	Gender	Age (Year)	Tooth type
1st	Male	25	Third molar
2nd	Female	22	Third molar
3rd	Female	19	Third molar

2.2 Cells' isolation, passage, monolayer culture, and cryopreservation procedures:

2.2.1 Isolation procedure of hPDLCs

Human PDLCs were isolated from extracted human healthy teeth as described previously (Seo, B.-M. *et al.*, 2004a; Gay, I.C. *et al.*, 2007; Mrozik *et al.*, 2010). Following the extraction, the tooth was held from its crown to minimise the damage to the periodontal tissues. The tooth was then stored immediately in a sterile tube at 4^{o}C to minimise the risk of tissue dehydration and cell lysis. The extracted tooth was washed thoroughly and gently twice with sterile 1× PBS. Only the tissues attached to the root middle part were scraped using a sterile scalpel and surgical blade size 11. This step was performed to prevent the contamination of the PDLCs with other cells, e.g. cervical gingival or periapical cells. The extracted tissue was transferred into a sterile Petri dish, kept moisturised in 2 mL of plain medium (Table 2-1) and stored at low temperature (4^{o}C) to be ready for the next step.

The extracted periodontal tissue was subjected to mechanical dissection, followed by enzymatic digestion. The extracted tissue was minced into small pieces of (1-2 mm^3), using a sterile surgical blade size 11, to enhance the digestion efficiency. For enzymatic digestion, the minced tissue was immersed in digestive medium and cultured at 37^{o}C, 5% CO_2 and ≥ 90% humidity for 45 min under continuous slow-speed rotation to ensure even tissue exposure to the digestive enzyme. MACSmix™ Tube Rotator (Miltenyi Biotec, Bergisch Gladbach, Germany) was used for this purpose. When the gross tissue pieces disappeared, the process stopped, where the action of the collagenase action and dispase was neutralised by adding basal medium. The formed cell suspension was centrifuged in Eppendorf centrifuge 5702 (Hamburg, Germany) at 200 rcf for 5 min, followed by supernatant aspiration. The collected pellet was re-suspended in plain medium and filtered through 70 µm cells strainer (BD Falcon, Schaffhausen, Switzerland) to obtain the single-cell suspension. The collected cells were then cultured in basal medium (Table 2-1) in a T25 flask at specific culture conditions (37^{o}C, 5% CO_2 and ≥ 90% humidity).

2.2.2 Cells passage and monolayer culture at different densities

When cells reached a confluency level of ~ 80%, based on cells distribution over the flask surface area, the medium was removed. Then, the monolayered cells were washed gently twice with 4 mL of 1× PBS. Cells

were detached from the vessel surface by adding 4 mL of trypsin/EDTA and incubated for 5-10 min at 37ºC, 5% CO_2 and ≥ 90% humidity. When all cells were seen floating, using Olympus-CKX41 bright field microscope (Tokyo, Japan), the reaction was stopped by adding 8 mL of basal medium. The cell suspension was then centrifuged at 200 rcf for 5 min, with the collected pellet re-suspended in 5 mL of the basal medium (Table 2-1).

For cell counting, 10 µl of cell suspension was mixed with the same volume of Trypan blue (Sigma-Ald1`rich, Missouri, USA) and introduced into a two-chamber haemocytometer (Boeco, Hamburg, Germany). Using the Olympus-CKX41 bright field microscope, the viable cells, which appeared round in shape with bright contents, were counted manually. The total number of cells was calculated as follow:

$$(1)\ Number\ of\ cells\ in\ each\ ml\ of\ suspension\ (cell/ml) = \left(\frac{number\ of\ counted\ cells\ in\ 4\ squares}{number\ of\ haemocytometer\ squares\ (4)}\right) \times dilution\ factor \times 10000$$

The required cells suspension of specific seeding density determined as follow:

$$(2)\ Volume\ of\ cells'\ suspnsion\ needed\ for\ a\ specific\ cell\ dencity\ (\mathrm{mL}) = \left(\frac{vessel\ surface\ area \times required\ density}{Number\ of\ cells\ in\ each\ ml\ of\ suspension\ (equation\ no.1)}\right)$$

According to each experiment, calculated volumes of the required cells density were added to the vessel and incubated at the specific culture condition. Cells passage was performed every 48-72 hr depending on the confluency level of the cells. The medium was replaced every 3-4 days.

2.2.3 Cryopreservation of cells

Where cells were not required for the immediate experiment, the cells were detached and pelleted as described previously in **2.2.2.** to be cryopreserved as described by (Seo, B.M. *et al.*, 2005). The pellet was re-suspended in 1.5 mL of cryopreservation medium (Table 2-1). Cell suspension was transferred into a 2 mL cryovial (Star Lab, Blake lands, UK), and kept within a freezing container, Mr Frosty (Nalgene ®, Neots, UK) before being transferred into a -80ºC freezer. This freezing container contains 250 mL of 100% isopropyl alcohol, which allows for a gradual decrease in the temperature at a rate of -1ºC/min. This step prevents the formation of ice crystal during freezing, thus maintaining cell integrity. After 2-3 hrs, the vials were moved from the freezing container into a plastic cryogenic storage box

and kept in the -80ºC freezer. the vials were stored at -130ºC in a liquid nitrogen tank for long-term storage.

2.2.4 Cells retrieval from -80ºC

The cells were retrieved from the -80ºC freezer into a 37ºC water bath as quickly as possible to reduce the possibility of cell damage. Following cell thawing, cell suspensions were mixed with 4 mL of plain medium supplemented with 100 unit/mL Penicillin-Streptomycin and 100 unit/mL Amphotericin-B. Afterwards. Cells were then pelleted down via centrifuging at 200 rcf for 5 min before being re-suspended in 4 mL of basal medium. Cells were then cultured in a tissue culture flask (based on the required density) and incubated at 37ºC, 5% CO_2 and ≥ 90% humidity. The medium was changed 24 hours after retrieval to remove dead cells and any possible cryogenic medium remnants.

2.3 Identifying cells' viability with fluorescent labelling

The cell population was labelled with the calcein AM green fluorescent dye, classified as a short-acting fluorescent marker to recognise living cells. This dye can cross the cellular membrane of the living cell by binding with calcium ions. However, the acetoxymethyl group hydrolyses intracellularly by the action of esterase enzymes, which converts the non-fluorescent form of calcein into a strongly green fluorescent molecule. Esterase enzyme is found in living cells only. Similarly, the green fluorescent chloromethyl derivatives of fluorescein diacetate (CMFDA) can enter the living cells and identify it. However, the latter marker can be used to monitor the cells' viability over an extended period (≥ 72 hr), with the advantage of multigenerational cell labelling.

In contrast, Ethidium homodimer-1 fluorescent dye is an impermeable molecule, with high affinity to DNA. Accordingly, this type of marker is used to detect dead cells due to the disruption of their cellular membrane.

According to the manufacturer's protocol, the staining solution was prepared by mixing 5 µl of calceinAM (Invitrogen, California, USA) and 20 µl ethidium for cell labelling with the fluorescent dye homodimer-1 (Invitrogen, California, USA) in 10 mL of plain α-MEM. The CMFDA was prepared by dissolving 50 µg of CellTracker™ Green CMFDA (Invitrogen, California, USA) in 10 µl of DMSO. The latter solution was diluted to a working concentration by mixing with 5 mL of plain α-MEM. Cells in monolayer or 3D

cell culture were washed, immersed in 1-2 mL of staining solution, and incubated in the dark for 45 min in tissue culture incubator. Afterwards, the staining solution was aspirated, with cells/construct immersed in a plain medium and incubated in the dark again for another 30 min to remove the staining solution's excess. The medium was changed once more, and cells were viewed with a Zeiss AXIO – Vert.A1 inverted fluorescent microscope (Oberkochen, Germany) at an excitation/emission of 495/515 nm for calcein AM, 528/617nm for ethidium homodimer-1, and 492/517 nm for CellTracker™ Green CMFDA,

2.4 Biochemical assays

2.4.1 Examining cells metabolic activity using AlamarBlue assay

This method was used to detect cell metabolic activity by detecting the reducing environment of intracellular fluid or cytoplasmic matrix (Cytosol). Resazurin is the active ingredient of AlamarBlue, a non-toxic substance, blue in colour and non-fluorescent. Living cells can reduce resazurin into resorufin, a red and fluorescent material. Thus, the fluorescence level indirectly reflects the volume of living cells (Rampersad, 2012).

For evaluation of cell metabolic activity, the cells were cultured in monolayer in 24-well plates as described previously in **2.2.2.** AlamarBlue (Generon, Slough, UK) was added at a ratio of 1/10 to medium volume in each vessel. Blanks were prepared by adding AlamarBlue reagent to the basal medium alone without cells to eliminate background fluorescence. Then, the plate was incubated in the dark in a cell culture incubator for at least 4 hours. A 100 µL sample of the mixture was transferred from each well into a 96-well plate with a flat bottom. Fluorescence was measured using a Varioskan Flash Multimode Microplate Reader – Model 3001, Thermo Fisher Scientific (Massachusetts, USA) at an excitation wavelength of 560 nm, and fluorescence emission of 590 nm. The final fluorescence value was calculated according to this equation:

$$Fluorescence\ value = fluorescence\ level\ of\ sample - fluorescence\ level\ of\ blank$$

Three technical replicates for each sample were prepared, with the average reading of the three replicates was used.

A standard curve was prepared to evaluate the corresponding level of fluorescence to the number of living cells. Cells were cultured in 24-well plates at different densities (according to each experiment), with fluorescence levels being recorded after 4 hours of incubation with AlamarBlue reagent.

2.4.2 Total DNA Quantification with PicoGreen Assay

Cells number could be measured indirectly by the quantification of the DNA contents (w/v). Quant-iT™ PicoGreen™ (Invitrogen, California, USA) is a specific and ultrasensitive fluorescent stain for nucleic acid that can detect as little as 25 pg/mL of double-stranded DNA (Singer *et al.*, 1997).

After 14 days of *in vitro* cells culture, the cells were washed gently twice with 1× PBS and lysed by mixing with 300 µl of 0.1% Triton X-100 (Thermo Fisher Scientific, Massachusetts, USA). The cell lysates were stored at -80^{o}C for at least 15 min. To increase the lysing process's efficiency, the mixture was subjected to three cycles of freezing-thawing, at -80^{o} C and 37^{o}C respectively, with continuous scraping in between. Cell lysates were mixed by continuous pipetting to ensure uniform mixing of contents. The same protocol was followed to prepare the cell lysates for the ALP assay (**2.3.3**).

Afterwards, a total volume of 100 µl was prepared by mixing 10 µl of cells lysate with 90 µl of 1× TE buffer. However, the blank included a 10 µl of 1× TE buffer instead of the cells' lysate.

The DNA standards were prepared by dissolving 10 mg of DNA acid sodium salt (Sigma-Aldrich, Missouri, USA) in 10 µl of 1× Tris-EDTA buffer (Thermo Fisher Scientific, Massachusetts, USA) and incubating at 37^{o}C for 60 min. Then, the DNA stock concentration of 10 mg/mL was diluted into many concentrations ranging from 1 ng/mL to 1 ml/mL (1 ng/mL, 10 ng/mL, 50 ng/mL, 100 ng/mL, 200 ng/mL, 500 ng/mL and 1 µg/mL). A Nanodrop spectrophotometer ND1000 (Thermo Fisher Scientific, Massachusetts, USA) was used to measure the prepared standards' DNA concentration at an absorbance wavelength of 260 nm (A260).

In a 96-well plate, a 100 µl of each of the blank, standards, and samples (cells lysate) were loaded in, with another 100 µl of PicoGreen® reagent (Quant-iT™ PicoGreen™ dsDNA Assay Kit, Invitrogen, California, USA) added to each well and mixed gently. The 96-well plate was incubated in the dark for 5 minutes at 37^{o}C. Three technical replicates were prepared for

all groups. The fluorometric changes were measured with Varioskan microplate reader at excitation/emission setting of 480/520 nm

The fluorometric blank reading was deducted from the readings of all samples, including the standards. The equation generated from the DNA standard curve was used to calculate the total volume of DNA for each well. The average of three readings for each sample was calculated.

2.4.3 Quantitative assessment of alkaline phosphatase activity

Alkaline phosphatase (ALP) was used as one of the early markers for cells osteogenic differentiation. Alkaline phosphatase can convert the colourless dephosphorylate 4-Nitrophenolphosphate (4-NPP) into yellow 4-Nitrophenyl (4-NP). Measuring this colourimetric change helps in assessing the ALP activity (Sabokbar *et al.*, 1994).

The assay buffer was prepared by mixing 2.875 mL of 70% NP-40 with 90 mL of dH_2O. Then, 60 µl of the latter was added to 10 ml of alkaline buffer solution, with a final 20 mL dH_2O was added and mixed. 4-Nitrophenol standard solution serial dilutions were prepared for the standards, ranging from 25 to 225 ng/mL. All the assay solutions were from Sigma-Aldrich (Missouri, USA).

The cell lysates were prepared as referred to in **2.3.2.** Samples were prepared by adding 10 µl of cell lysate into each well of a flat-bottom 96-well plate and mixed with 90 µl of 4-NPP substrate. 90 µL/well of the substrate was added to 10 µL/well of 0.1% Triton X to be used as a blank. Moreover, the standards included 100 µL/well of standards' solutions. All the samples, blanks and standards were prepared in the well-plate in triplicates. The 96-well plate was then incubated in the dark at 37ºC for about 30 minutes until a colour change was observed. The reaction was stopped by adding 100 µl/well of 1M NaOH (Thermo Fisher Scientific, Massachusetts, USA). The colourimetric changes were recorded by measuring the absorbance at 405 nm using a Varioskan microplate reader.

As this assay is time-dependent, the time from the beginning of the incubation until stopping the reaction was recorded. The generated standard curves were used in calculating the value of ALP level. The ALP activity (nM/hr/well) then calculated according to this equation:

$$Net\ ALP\ activity\ (mM/hours)$$

$$= \frac{\left(\frac{(mM\ of\ ALP\ \times 1000) \times total\ triton\ X - 100\ harvest\ volume)}{incubation\ time}\right)}{Assay\ volume}$$

The DNA content for each well was measured (see section **2.3.2**) and included to measure the ALP specific activity as follow:

$$ALP\ specific\ activity\ (mM/hours/\mu g\ DNA) = \frac{Total\ ALP\ per\ hour\ per\ well\ (nM)}{Total\ DNA\ content\ for\ the\ same\ well\ (\mu g)}$$

2.4.4 Recovery and quantification of calcium deposition with Alizarin red semi-quantitative assay

Alizarin red (AR) stain quantification assay is a semi-quantitive assay used to detect calcium deposits in monolayer cells culture. Generally, it is based on assessing the mineralisation by extracting of calcium at low pH, neutralising it with ammonium hydroxide and measuring the absorbance at 405 nm.

According to the manufacturer's protocol, monolayer culture cells were washed twice with 1× PBS and fixed with 4% formaldehyde for 15 min at RT. Afterwards, cells were gently washed with three changes of dH_2O. The cells were stained with 1 mL/well of 40 mM AR stain (ScienCell, California, USA), and kept for 20-30 min at RT with gentle shaking. The stain was removed with cells rewashed to remove the excess stain, then preserved in 200 µl/well of dH_2O. Cells in monolayer culture were imaged using an Olympus BX50 light microscope (Tokyo, Japan).

For the assay, the dH_2O was aspirated, and the cells were incubated in 200 µl/well of 10% acetic acid for 30 min with gentle shaking. A mixture of cells in acetic acid was collected by scraping and transferred into 1.5 mL Eppendorf tube; the contents were vortexed for 30 sec with Vortex-Genie 2 (Scientific Industries Inc, New York, USA). The mixture was then heated to 85°C for 10 minutes, followed by incubation on ice for 5 min to cool down. After centrifuging for 15 min at 200 rcf, 75 µL of 10% ammonium hydroxide add to neutralise the acid at low pH (4.1-4.5). All of the assay solutions were provided in the kit.

For the preparation of AR stain standards, 100 µl of 40 mM AR stain solution was mixed with 900 µl of standard stock solution to make a 1 mL of 4 mM AR stain working solution. Seven serial dilutions were prepared in 1.5 mL centrifuge tubes. The blank was including the standard working solution

without the AR stain. A triplicate of 50 µL/well for each of the samples, standards and blanks were aliquoted in a 96-well plate and measured at an absorbance of 405 nm with a Varioskan Flash Multimode microplate reader.

The blank reading was deducted from all samples and standards values. The total concentration of AR stain in the samples was then calculated using the equation generated from the AR stain standards curve.

2.4.5 Measuring genes expression using quantitative real-time polymerase chain reaction (rtPCR)

This method used to detect and measure the level of expression of genes of interest. It involved three main steps: RNA extraction and purification, preparation of complementary DNA (cDNA), and measuring the expression level with rtPCR assay.

2.4.5.1 RNA extraction and purification

RNeasy Mini kit from Qiagen (Hilden, Germany) was used for this step. According to the manufacturer's protocol, the cultured cells were washed with 1 mL of 1× PBS to ensure removal of the medium. The cell pellets were then harvested in RNase-free polypropylene centrifuge tubes after detaching the cells with trypsin/EDTA as described previously in **2.2.2.** Depending on the volume of cells within the pellet, cells lysed by mixing with either 300 or 600 µl/well of β-mercaptoethanol (β-ME) - RLT buffer (10 µl β-ME per 1 mL buffer RLT). The lysate was homogenised by adding the lysate into a QIAshredder homogeniser (Qiagen, Hilden, Germany) followed by centrifuging in an Eppendorf 5415D centrifuge (Hamburg, Germany) at 350 rcf for 2 min. Thus, a higher yield of RNA can be guaranteed.

The collected solution was then mixed with 1 volume (300 or 600 µl depending on the cells density) of 70% ethanol. This step is to enhance the selective binding of the RNA to the RNeasy membrane (silica-based membrane) of the spin column. A volume of 600 µl of the mixture was added into the spin column, attached to 2 mL collection tube, and centrifuged for 15 seconds at 350 rcf, with the flow-through discarded.

For on-column digestion of DNA contaminates, 80 µl DNase I incubation mix was prepared (10 µl DNase I stock solution mixed gently with 70 µl buffer RDD) aliquoted directly into RNeasy spin column membrane then incubated for 15 min at 20-30^{o}C. The RNeasy spin column was then treated with 350 µl buffer RW1 and centrifuged for another 15 seconds at 350 rcf.

Lastly, the membrane washed twice with 500 µl buffer RPE, each followed by centrifuging for 15 sec and 2 min respectively at 350 rcf, with the flow-throughs discarded. The RNA extract was collected from the membrane by adding 30 - 50 µl DNase/RNase-free dH_2O (Thermo Fisher Scientific, Massachusetts, USA) and centrifuging for 1 min at 350 rcf. A 1 µl aliquot of the extract was measured using a Nanodrop spectrophotometer ND1000 at an absorbance of 260 and 280 nm to assess the quality and quantity of collected RNA. The purity of RNA was measured according to the ratio of 260/280 nm, with a value > 1.8 and < 2.0 regarded as indicating the right level of purity. The final extract then stored at -80^{o}C until use.

2.4.5.2 Preparation of cDNA

High concentration samples of extracted RNA (see **2.3.5.1.)** were diluted with UltraPure DNase/RNase-Free dH_2O (Thermo Fisher Scientific, Massachusetts, USA) to a concentration of 200 ng/µl, which was used for making the cDNA.

The diluted RNA volume was treated with 1 µl the enzyme, 10 µl 10x buffer. Both are from High Capacity RNA-to-cDNA kit (Applied Biosystems, California, USA) the rest of the volume to 20 µl was completed with nuclease-free water. Using F. MJ Research PTC-100 Thermocycler (Thermo Fisher Scientific, Massachusetts, USA), the reaction was performed by incubation for 60 min at 37^{o}C, followed by another 5 min at 95^{o}C to ensure denaturation of the enzyme. The prepared cDNA then stored at -20^{o}C for the rtPCR step.

2.4.5.3 Quantitative rtPCR:

For rtPCR gene expression assay, TaqMan Gene Expression Assays kit (Applied Biosystems, California, USA) was used. All samples and controls were in triplicate and aliquoted in a semi-skirted PCR 96-well plate (Thermo Fisher Scientific, Massachusetts, USA). All expression levels of target genes were compared to Glyceraldehyde-3-phosphate (GAPDH) (Applied Biosystems, California, USA), which is used as a housekeeping gene during all rtPCR work.

The amplification reaction was performed by making a volume of 20 µl; this included 10 µl of gene expression master mix, 1 µl of TaqMan assay probe (both are from Applied Biosystems, California, USA), as well as 9 µl of prepared cDNA. Two kinds of negative controls were prepared; the first included the same mixture without a sample (non-template negative

control). The other did not contain any enzyme (RT-negative control). The well plate was sealed and centrifuged in a mini plate spinner MPS 1000™ (Labnet, New Jersey, USA) for 10 sec to ensure proper mixing. The amplification process was conducted in a Roche LC280 light cycler (Roche Applied Science, Penzberg, Germany) in three stages. These stages were: pre-incubation cycle at 95^{o}C for 10min, followed by 45 cycles of amplification at 95^{o}C for 10 sec, 60^{o}C for 30 sec and 72^{o}C for 1 sec. The final step involved cooling the temperature of the samples down to 40^{o}C. The value of the cycle threshold (Ct) was recorded, and the relative levels of genes expression were calculated using the $2^{-\Delta\Delta Ct}$ method (Livak and Schmittgen, 2001).

2.5 Histological and immunohistochemical examinations

2.5.1 Processing, paraffin embedding and sectioning of the 3D specimen

At the end of the related experiment, the 3D sample (scaffold or construct) was washed twice with 1× PBS to remove any remaining culture medium. The sample was then secured in a specimen processing cassette and fixed by immersing in 10% neutral buffered formalin (NBF) for at least 8 hours.

The Shandon Excelsior ES tissue processor (Thermo Fisher Scientific, Massachusetts, USA) was used for sample processing. The routine overnight processing cycle was used, which involved treating the sample with formaldehyde cycles, ethanol, xylene and hot melted wax, as presented in Table 2-3.

Table 2-3: Reagents and duration of the routine overnight cycle for histological processing of the 3D sample

Reagent	Cycle duration (hr)
Formaldehyde	1
Ethanol	1
Ethanol	1
Ethanol	1
Ethanol	1.5
Ethanol	1.5
Ethanol	1.5
Xylene	1
Xylene	1
Xylene	1.5
Wax	1.5
Wax	1.5
Wax	1.5

Following processing, the samples were embedded in paraffin wax and sectioned using a Leica Jung Biocut 2035 microtome (Leica Biosystems, Wetzlar, Germany) to produce 5 µm thick sections. The sections were then transferred into a 40^{o}C water bath, before being mounted on Apex superior adhesive slides (Leica Biosystems, Wetzlar, Germany). Afterwards, the mounted sections were dried on a hot plate for 15 minutes and incubated overnight at 37^{o}C in Gallenkamp vacuum oven (London, UK). This step enhances the staining process by drying the samples.

2.5.2 Clearing of sections (taking slides to water)

For histological staining, the sections were de-waxed by immersing in two 100% xylene changes for 5 minutes each, which were then cleared by immersing in two changes of 100% ethanol for 10 mins each, followed by washing in tap water for another 5 min.

2.5.3 Haematoxylin and Eosin (H&E) staining

For H&E staining, sections were stained with Harris' Haematoxylin (Surgipath, Linford Wood, UK) for 5 min. Excess stain was removed by gentle washing with running tap water. The stain was developed by immersing in Scott's tap water (Surgipath, Linford Wood, UK) for 1 min and cleared with running tab water. Slides were then dipped in aqueous eosin (Surgipath, Linford Wood, UK) for 1 min and cleared with tap water. Afterwards, sections were dehydrated with three ethanol changes (70%, 90% and 100%, respectively), before being cleared in two changes of 100% for 5 min each. Finally, the sections were mounted with a coverslip using Di-butyl-phthalate Polystyrene Xylene (DPX) non-aqueous mounting medium (Agar Scientific, Essex, UK).

In an H&E stained section, the nuclei are stained with a violet haematoxylin stain, while the pink eosin stain recognises the cytoplasm.

2.5.4 Van Gieson's stain

Collagen fibres were identified by staining the section with Van Gieson's stain (Dorn & Hart Microedge, Loxley, UK). First, the nuclei were stained with Mayer's haematoxylin (Thermo Fisher Scientific, Massachusetts, USA) for 5 min, with the extra stain then removed by gentle washing with running tap water. Van Gieson's solution was applied to the section and kept at RT for 5 min. Subsequently, the sections were immersed in 12% acetic acid to remove excess dye and differentiate the stain. Then, the sections were washed with tap water, cleared with 100% xylene before being mounted with DPX. Microscopic examination of stained section showed the collagen stained with red Van Gieson's stain, while the nuclei with the haematoxylin dark violet colour.

2.5.5 Von Kossa's stain for the detection of extracellular mineral deposition

This stain was used to detect cellular mineralisation. Basically, the reaction involves replacing the calcium ions that bind to the phosphate, with silver

ions. Thus, this method is considered as an indirect technique for the detection of calcium deposition.

Von Kossa stain kit from Atom Scientific (Cheshire, UK) was used for this staining method. Briefly, the sections were immersed in a 5% silver nitrate solution and exposed to bright sunlight (or a 60-watt lamp) for 60 min until deep brown deposits observed. After washing with three changes of dH_2O, 5% Sodium thiosulphate was applied to the section for 5 mins to remove unreacted silver. Sections were then rinsed with dH_2O before being counterstained with Neutral Red (0.5% Aqueous) solution applied for another 5 min. Afterwards, slides were washed, dehydrated, cleared and mounted, as described previously (**2.4.3**).

Viewing the section under the microscope reveals the mineral deposits' staining with dark brown colour, while the cytoplasm stained with pink colour.

2.5.6 Alkaline phosphatase stain for monolayer cells

Qualitative evaluation of alkaline phosphatase activity was performed by staining the cells in monolayer culture with ALP stain. Cells cultured in a 24-well plate were washed with 1 mL of 1× PBS and fixed with 98% Ethanol for 30 min at 4^{o}C in the dark. This step was followed by gentle washing with dH_2O. The G292 cells, human osteosarcoma cells (European collection of cell cultures, ECCAC, clone A141B1, passage 22), were cultured at the same cell density and culture environment as the hPDLCs to be used as a positive control.

10 mL of staining solution was prepared by mixing 9.6 mL dH_2O, 0.4 mL Naphthol AS-MX (Sigma-Aldrich, Missouri, USA), and 4.2 mg Fast violet B salt (Sigma-Aldrich, Missouri, USA) in a glass container covered with aluminium foil. Cells were incubated in 300 µl/ well of staining solution in the dark at 37^{o}C. The incubation period ranged from 30 to 60 min, depending on colour change in the positive control sample into a yellowish colour.

Following the incubation, the staining solution was aspirated, with cells being washed gently and kept in dH_2O. At this stage, the cells were ready for imaging.

2.5.7 Alizarin red stain for monolayer cells

Calcium deposition was detected directly by staining the monolayer cultured cells with AR stain. As described in **2.3.4**, cells were prepared and stained.

Briefly, a 1 mL of 40 mM AR stain was added to each well, with the whole 24-well plate being incubated for 20-30 min at RT with gentle shaking. Afterwards, the staining solution was removed, and cells washed again to remove excess stain. At this stage, cells were kept in 1 mL/well of dH_2O to be ready for microscopic imaging.

2.5.8 Immunohistochemical (IHC) staining

The expression of specific proteins of interest in both monolayer cell culture and processed sections of 3D samples was performed by IHC staining, which includes using specific primary and secondary antibodies.

For the monolayer cell culture, the cells were cultured either in 4- or 8-chambers cells culture slide (Falcon™, Loughborough, UK) for the required period according to each experiment. The cells were washed gently with 1× PBS and fixed with 4% NBF for at least 8 hr.

The 3D samples were prepared as described in **2.4.1**. and **2.4.2**. The slides containing the sections were positioned on cover plates in a Shandon™ Sequenza™ Slide Rack for Immunostaining (Thermo Fisher Scientific, Massachusetts, USA) with dH_2O being placed at the bottom of the rack to reduce the evaporation of the reagents and dryness of the sections. Such an orientation of the slide with the cover plate creates a capillary gap that will help distribute the reagents to cover all the section surface area. Also, it reduces the volume of used reagents. The endogenous peroxidase was blocked by incubating the sections for 5-10 min in 1 drop/slide of Dual Endogenous Enzyme Block (Dako-Envision, Glostrup, Denmark) by washing with 1× PBS.

Fixation of the samples with formalin can result in cross-linkage with the protein (antigen), heat-based antigen retrieval was used for some of the sections to disrupt this linkage and retrieval of proteins epitopes. Thus, it helps restore the protein's morphology and enhance antigen detection quality with IHC staining. This procedure is a simple, inexpensive, and effective technique. Sections were placed in a non-sealed, microwavable Coplin Jar and immersed in 1/10 Vector Antigen Unmasking Solution (citrate-based solution, pH 6.0) in dH_2O. Afterwards, the contents were heated to ~ 98^{o}C in a scientific microwave (850 W) and left to cool down to RT for 20 min. Increasing the temperature or the retrieval time could cause antigen over-retrieval, leading to a non-specific background staining and increasing the chances of sections dissociating from the slides. Slides were

replaced on cover plates and kept moisture with 1× PBS. For blocking non-specific binding, sections were incubated for 30 min in blocking serum.

Primary antibody was added to each slide, according to the optimised volume of each antibody. Simultaneously, the negative control section was kept in blocking serum, with all sections (experimental and control) incubated overnight at 4^{o}C. After gentle washing with two changes of 1× PBS, all sections, including the negative controls, were incubated in 1 drop of the secondary antibody for 30 min. The secondary antibody was cleared by washing with three changes of 1× PBS for 5 min each. The antibody activity was detected by incubating the sections in 100 µl/slide of 3,3'-diaminobenzidine (DAB) (Abcam, Cambridge, UK) for 10 min. This solution was prepared by mixing 20 µl of DAB+chromogen to 1 mL of DAB+substrate buffer). Presence of the protein of interest was detected as brown stained areas. The sections were washed with dH_2O and counterstained with H&E as described in **2.4.3.** Details of the blocking serums, primary and secondary antibodies used in this project, are listed in Table 2-4.

Table 2-4: Details of blocking serums, primary and secondary antibodies used for IHC staining

Target antigen	Blocking serum	Primary antibody	Secondary antibody
COL-1	1/5 Normal goat serum (Dako) in PBS	1:150 Mouse monoclonal to Collagen I (Abcam) in PBS. It reacts with Human.	100 µl/slide Labelled polymer-HRP Goat Anti-Rabbit and Goat Anti-Mouse (Dako)
OCN	1/5 Normal goat serum (Dako) in PBS	1/500 Mouse monoclonal osteocalcin (Abcam) in PBS. It reacts with Human.	100 µl/slide Labelled polymer-HRP Goat Anti-Rabbit and Goat Anti-Mouse (Dako)
OPN	1/5 Normal goat serum (Dako) in PBS	1/100 Rabbit polyclonal osteopontin (Abcam) in PBS. It reacts with Human.	100 µl/slide Labelled polymer-HRP Goat Anti-Rabbit and Goat Anti-Mouse (Dako)

2.6 Microscopic examination

2.6.1 Imaging of stained and fluorescent labelled samples

Stained sections were viewed and imaged in 2D using a coloured view Olympus BX50 (Tokyo, Japan) microscope supplemented by Nikon Digital Sight and Prior Optiscan II. Furthermore, fluorescently-labelled sections were examined with a Zeiss AXIO – Vert.A1, inverted fluorescent microscope (Oberkochen, Germany) supplemented with monochromic microscopy imaging equipment. ZEN 2 blue digital software (Carl Zeiss microscopy, Göttingen, Germany) was used to process and capture the images.

2.6.2 Scanning electron microscopy (SEM)

The SEM is an efficient tool used in tissue engineering and biomaterial studies to provide a visual dimension for assessing cell growth and scaffold structure. Many techniques for conducting this examination for biological tissue have been introduced. However, many of them are time-consuming and could affect cellular morphology by causing cells shrinkage (Jung *et al.*, 2010; Lee, J.T.Y. and Chow, 2012). Low temperature and variable-pressure-SEM is a specific technique that was investigated and suggested for biological tissues. It is based on the gradual cooling of the wet specimen to a low temperature (~ -25^{o}C) under a pressure of (85 Pa) to limit the specimen's water sublimation. Thus, minimising the structural damage of the sample and producing a cleared image, which is attributed to the better-obtained signal noise ratio (Talbot and White, 2013; Wassilkowska and Woźniakiewicz, 2015)

In the current project, the SEM was used to evaluate the cellular growth pattern and examine the scaffold structure. For this purpose, a Hitachi S3400N-VP SEM (Tokyo, Japan) was used at environmental, low vacuum, variable pressure mode.

At the end of the experiment, the scaffolds/constructs were transferred into a new 24-well plate and washed with two changes of 2 mL of 1X PBS to ensure removal of the culture medium. All samples were fixed with 10% NBF at RT for at least 8 hrs. Then, they were washed with two changes of 1X PBS to ensure removal of the fixative solution. Afterwards, the scaffold/construct was mounted on aluminium stubs of 10 mm diameter with both being placed in the Deben cooling stage at RT. Excess moisture was removed by gentle application of filter paper, before the mounted sample

was introduced to the SEM chamber that was then closed securely. The temperature was reduced gradually to -20^{o}C to avoid the development of ice crystals. Backscattering was measured at 20 Pa and a probe current of 50 A. Scaffold/construct images were captured at different magnifications at speed four, following the optimal working distance to enhance image resolution.

2.7 Statistical analysis

Unless mentioned otherwise, all samples, standards and blanks in this project were prepared in technical triplicate. GraphPad Prism version 7.00 (California, USA) and Microsoft Office Excel 2016 (Washington, USA), were used to analyse the data and present the results. The mean ± standard deviation (SD) was used for presenting the results.

Based on each experiment's data, the statistical difference between two groups was performed using the unpaired two−tailed t−test. In contrast, the difference among groups was measured either with one−way analysis of variance (ANOVA) with Tukey's post−test or two−way ANOVA with Sidak's post−test. The significance level was calculated at a *p*-value of ≤ 0.05. Table (2-5) explains the levels of significance according to the *p*-value.

Table 2-5: Codes of the significance level

Significance level	*p*-value	Code
Non-significant	> 0.05	Ns
Significant	≤ 0.05	*
More significant	≤ 0.01	**
Highly significant	≤ 0.001	***
Very highly significant	≤ 0.0001	****

Chapter Three: *In vitro* characterisation of hPDLCs

3.1 Introduction

The regeneration of periodontal tissue has been identified as one of the challenges in clinical dentistry; this can be attributed to the periodontium's unique anatomy and histology (Bosshardt and Sculean, 2009; Chen, F.-M. and Jin, 2010).

Tissue engineering has emerged as a promising approach in tissue regeneration, which could overcome the limitations of current treatment modalities (Izumi *et al.*, 2011; Iwata *et al.*, 2014). Cells are a central pillar in tissue engineering, as they represent the basic biological unit for any tissue (Paul, 1961; Bonassar and Vacanti, 1998; Muschler *et al.*, 2004). To date, many cells type has been investigated to be used for tissue engineering. In 1976, Fridenstein *et al.* presented mesenchymal stem cells as the clonal, plastic-adherent cells that can differentiate into many other cell's subtypes, especially osteogenic, adipogenic and chondrogenic cues. These cells were extensively investigated and applied in tissue engineering of different tissues and organs. Mesenchymal stem cells have been identified in various sites in the human body, with bone marrow suggested as the primary site for isolating these cells (Pittenger *et al.*, 1999; Baksh *et al.*, 2004; Bobis *et al.*, 2006; Marion and Mao, 2006). However, certain limitations are associated with the use of hBMSCs, mainly the high morbidity during the process of cell harvesting and the slow rate of proliferation. Because of that, other cell sources were investigated (Bianco *et al.*, 2001). Based on their embryonic origin from the neural crest-derived ectomesenchymal cells, hPDLCs were investigated as a possible source of mesenchymal stem cells (Kobayashi *et al.*, 2004; Ivanovski *et al.*, 2006; Nagatomo *et al.*, 2006; Mensing *et al.*, 2011).

Furthermore, these cells are developed from the dental follicle as are alveolar bone osteoblasts and cementoblasts (Nanci, 2017). Accordingly, PDLCs could be an alternative source for the isolation of progenitor cells that can be utilised for enhancing periodontal tissue regeneration (MacNeil and Somerman, 1999; Cho and Garant, 2000). Despite the presence of many studies that investigated this topic, there is a controversy regarding the methodology needed for identifying the multipotent MSCs in the hPDLCs population. The International Society for Cellular Therapy (ISCT) defined the minimum criteria to confirm multipotent MSCs within a primary cell population (Horwitz *et al.*, 2005; Dominici *et al.*, 2006). Based on that,

the current study attempts to characterise the primary hPDLCs isolated from extracted teeth based on the ISCT criteria, which includes cellular adhesion to plastic surface, immunophenotyping, and trilineage differentiation capacity.

3.2 Aim

To identify the *in vitro* multipotent MSCs characteristics of hPDLCs isolated from three different donors. Also, to evaluate these cells' quality, in terms of *in vitro* proliferation and differentiation potential, before their use in this project's next experiments.

3.3 Materials and methods

Following the isolation of hPDLCs, as described previously in **2.2.1.**, these cells were subjected to a series of *in vitro* examination to determine their characteristics.

3.3.1 Examining cellular morphology

The isolated hPDLCs of P (1) were cultured in a basal medium at a density of 1 x 10^4 cells/cm^2 in a 6-well plate and incubated at 37^{o}C, 5% CO_2 and ≥ 90% humidity. After 24 hr of monolayer culture, the cellular morphology was examined using the Olympus-CKX41 inverted light microscope.

3.3.2 Investigating the clonogenicity of hPDLCs and their adhesion capacity to vessel plastic surface

Colony-forming unit-Fibroblasts (CFU-F) assay is an extensively used method to identify the presence of multipotent mesenchymal stem cells within a primary cell population (Friedenstein, A. *et al.*, 1970; Dominici *et al.*, 2006; Pochampally, 2008). It is reliant on how MSCs can adhere to the culture vessel's plastic surface (Friedenstein, A. *et al.*, 1970; Prockop, 1997; Bobis *et al.*, 2006). Furthermore, when cultured at low density, these cells can form single-cell derived colonies (Castro-Malaspina *et al.*, 1980). Accordingly, this method was central in the current study to investigate these features within the isolated hPDLCs.

Briefly, the hPDLCs were cultured in sterile, 35 mm cells culture Petri dishes at a seeding density of 100 cell/35 mm. Three technical replicates (n=3) for each donor cell population were considered for this experiment. After ten days of monolayer culture in the basal medium, the medium was removed, with cells been washed gently twice with 3 mL of 1X PBS per Petri dish. Afterwards, 0.5% (w/v) crystal violet, dissolved in 100% methanol, was used to stain the cells for 10 mins at RT. The excess stain was aspirated, while the cells were washed with dH_2O. Afterwards, the cell colonies were viewed with an Olympus-BX50 bright field light microscope. Cell colonies of ≥ 50 cells were only counted. The number of colonies in each Petri dish was counted using Stuart™-SC6 colony counter (Staffordshire, UK), as shown in Figure 3-1.

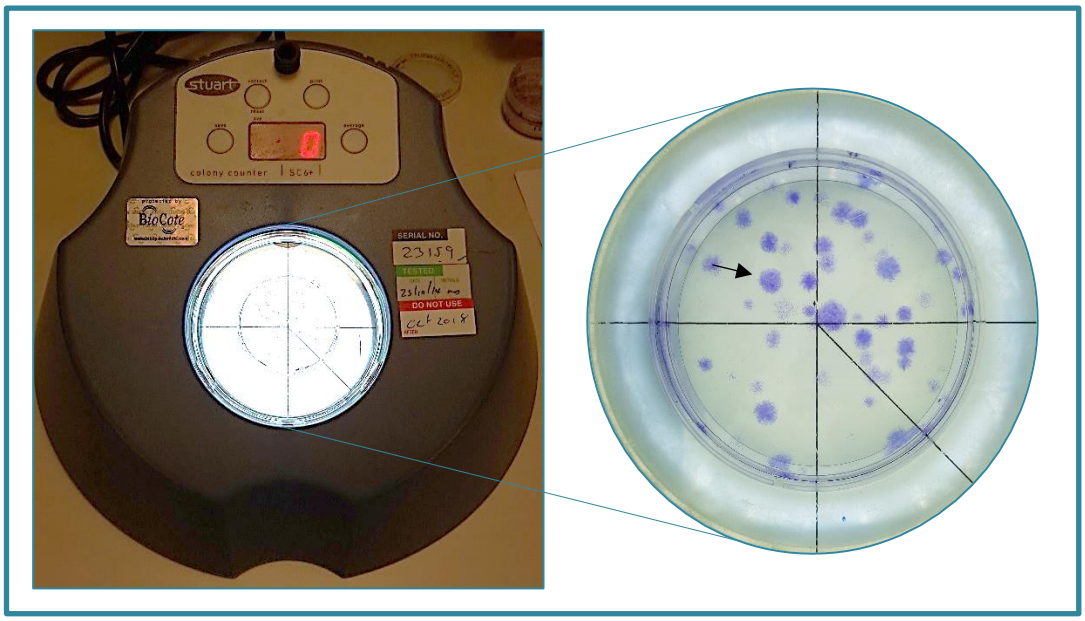

Figure 3-1: Stuart-SC6 digital colony counter used for visualisation and counting the cells' colonies. Cells colonies (black arrow) of ≥ 50 cells were recognised after ten days of culture in basal medium.

The CFU-F efficiency for each donor was calculated as follow:

$$CFU-F\ efficiency\ = \frac{number\ of\ formed\ colonies\ per\ Petri\ dish}{total\ number\ of cultured\ cells\ (100\ cells)} \times 100$$

The means ± SD for the replicates of each donor were also calculated

3.3.3 Immunophenotyping of hPDLCs

Flow cytometric analysis was used to identify the expression level of haemopoietic and mesenchymal stem cells markers in the isolated hPDLCs. Basically, this method depends on streaming the particles (cells) at a high velocity through a small diameter nozzle to obtain a single-cell stream. This stream is then subjected to laser light of different wavelengths, which scatters the light by the particles' action within it. Those particles are labelled with fluorescent-labelled antibodies that emit fluorescence when activated by the laser beams. Both the scattered and fluorescent light are detected by detectors that can transform the light signals into electrical signals. Accordingly, these electrical signals are collected and processed into data that reflect the examined particles' characteristics, including their size, shape and distribution within the sample (Johnson, 1992; Radcliff and Jaroszeski, 1998; Jaroszeski and Radcliff, 1999). Figure (3-2) illustrates the main components of the flow cytometry.

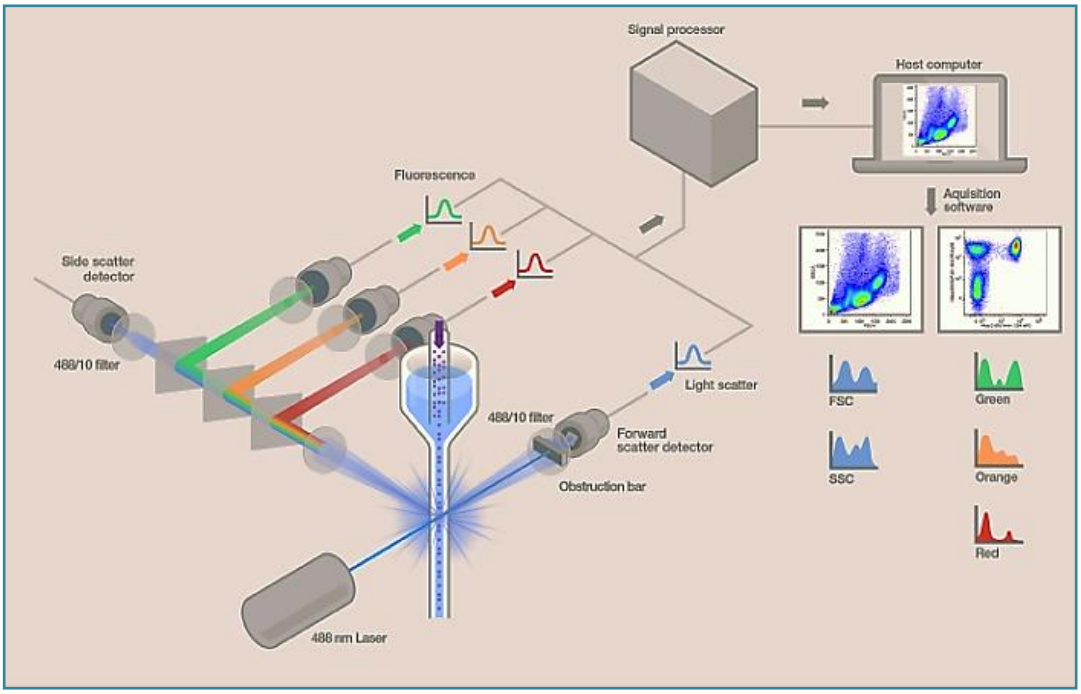

Figure 3-2: Main elements of the flow cytometer (ThermoFisher Scientific, 2017).

3.3.3.1 Optimising the concentration of haemopoietic and mesenchymal stem cells markers for hPDLCs

In the current study, hPDLCs, isolated from three different donors, were cultured and expanded as described previously in **2.2.2**. The culture medium was aspirated to prepare a single-cell suspension, and cells washed with 10 mL of 1× PBS. Then, cells were detached from the vessel surface by adding 5 mL of Trypsin/EDTA to each 150 cm^2 flask, followed by incubation (37^oC, 5% CO_2 and ≥ 90% humidity) for 5 mins. When the cells floated, Trypsin/EDTA action was neutralised by adding 10 mL of basal medium, with the mixture being centrifuged for 5 mins at 200 rcf to obtain the cell pellet. The cell pellet was subjected to another wash, this time with 5 mL of plain α-MEM medium and centrifuged again. Cells were re-suspended in a fresh 5 mL of plain α-MEM medium, counted and aliquoted into 5 mL of Falcon™ round-bottom polystyrene tubes at a density of $5x10^5$ cell/tube. This step is to reduce the chance of nozzles clogging due to high cells volume. To collect as many cells as possible in the form of a pellet, all Falcon tubes were centrifuged for 5 mins at 350 rcf. The medium was discarded and replaced by 1 mL/ tube of 1× PBS. This step was repeated twice to ensure removal of all medium. The cell suspension was kept at 4^oC to maintain the integrity of the cells. Finally, the pellets were suspended

individually with 70 µl of 1× PBS (4°C) and mixed thoroughly to obtain the required single cells suspensions.

The cell labelling process was begun by blocking the cells' fragment crystallisable (Fc) receptors to reduce the chances of non-specific antibodies binding that could result in a false-positive response. This step was performed by mixing the cells suspension with 5 µL/ tube of Fc blocker solution (Miltenyi Biotec, Bergisch Gladbach, Germany), followed by incubation for 10 mins at RT.

The fluorescent markers (see Table 3-1) used in this study were titrated to obtain the optimum concentration for the hPDLCs. Thus, minimising the risk of non-specific binding of the antibody that leads to false-positive results.

Five concentrations (2.5 µL, 5 µL, 10 µL, 15 µL, 20 µL) were tested for each of the markers. Stain Index method was used to determine the optimal concentration for each marker. Stain index defined as the ratio between the positive and negative cells populations divided by two times of standard deviation of the negative population, as presented in this equation:

$$Stain\ index = \frac{\mathrm{MFI\ (positive)} - \mathrm{MFI\ (negative)}}{2 \times SD}$$

Where MFI (positive) represents the mean of fluorescence intensity for positive cells population, MFI (negative) is the mean fluorescence intensity for the negative cell population, and SD is the standard deviation for the negative population (Muccio *et al.*, 2018).

Antibodies were added to each tube and incubated on ice for 20 mins in the dark to allow for enough time for the antigen-antibody reaction and reduce the chances of damaging the cells. This step was followed by gentle washing with 1 mL/tube of 1× PBS (4°C) to remove unconjugated antibodies. Finally, the cell suspension was centrifuged for 5 mins at 350 rcf. The cell pellet was then re-suspended in 300 µL/tube of 1× PBS (4°C). All samples were then transferred into the flow cytometry unit to measure the laser light scattering fluorescence using Beckman Coulter (California, USA) Cytoflex S Flow Cytometer with four excitation lasers and 13-colour emission detection capacity.

The gates (thresholds) of flow cytometry were determined based on analysing the auto-fluorescence level of the non-labelled sample. The first level gating was adjusted to include the intact cells bodies depending on the differences in particles' size. This point was achieved by plotting the

readings of side scattering against those of forwarding scattering. Furthermore, a second gate was set between the values of side scattering's width versus height to include a single-cell population of hPDLCs (Figure 3-3). A minimum of 10000 events was recorded for each tested sample. Post-acquisition data analysis for all labelled and non-labelled samples was performed using CytExpert 2.0 software (Beckman Coulter, California, USA).

3.3.3.2 Examining the expression levels of haemopoietic and mesenchymal stem cells markers for the hPDLCs

According to the cell markers optimisation experiment results, the optimal concentration for each antibody was determined. These concentrations were used for the second part of the immunophenotyping experiment, which includes labelling the hPDLCs with fluorescent markers to examine the MSCs characteristics of the isolated cells population by measuring expression levels of the markers.

Cells from three different donors were passaged, harvested as described in the previous section. Cells of each donor were aliquoted in several groups, as illustrated in the table (3-2). In this experiment, cell gating was performed using the fluorescence minus one (FMO) control method.

Table 3-1: Makers (antibodies) used for multicolour flow cytometry panel for characterisation of hPDLCs

Marker	Expression	Details
CD29	Mesenchymal stem cells, embryonic stem cells, fibroblasts (Pittenger *et al.*, 1999; Rojewski *et al.*, 2008).	• Monoclonal mouse anti-human antibody • Alexa Fluor® 488/519 nm • Biolegend® (California, USA)
CD34	Immature hematopoietic precursor cells and all hematopoietic colony-forming cells in the bone marrow and blood (Pittenger *et al.*, 1999; Müller *et al.*, 2006; Sotiropoulou *et al.*, 2006).	• Monoclonal mouse anti-human antibody • BUV 348/395 nm • BD Horizon™ (New Jersey, USA)
CD45	The plasma membrane of all hematopoietic cells, except erythrocytes and platelets (Stute *et al.*, 2004; Mareschi *et al.*, 2006).	• Monoclonal mouse anti-human antibody • Brilliant violet 405/785 nm • Biolegend®
CD73	Mesenchymal stem cells, follicular dendritic cells (Conget and Minguell, 1999; Rojewski *et al.*, 2008)	• Monoclonal mouse anti-human antibody • Brilliant violet 405/421 nm • Biolegend®
STRO-1	Bone marrow stromal cells and erythroid precursors (Simmons and Torok-Storb, 1991; Jones *et al.*, 2002).	• Monoclonal mouse anti-human antibody • Alexa Fluor 633/668 nm • Biolegend®

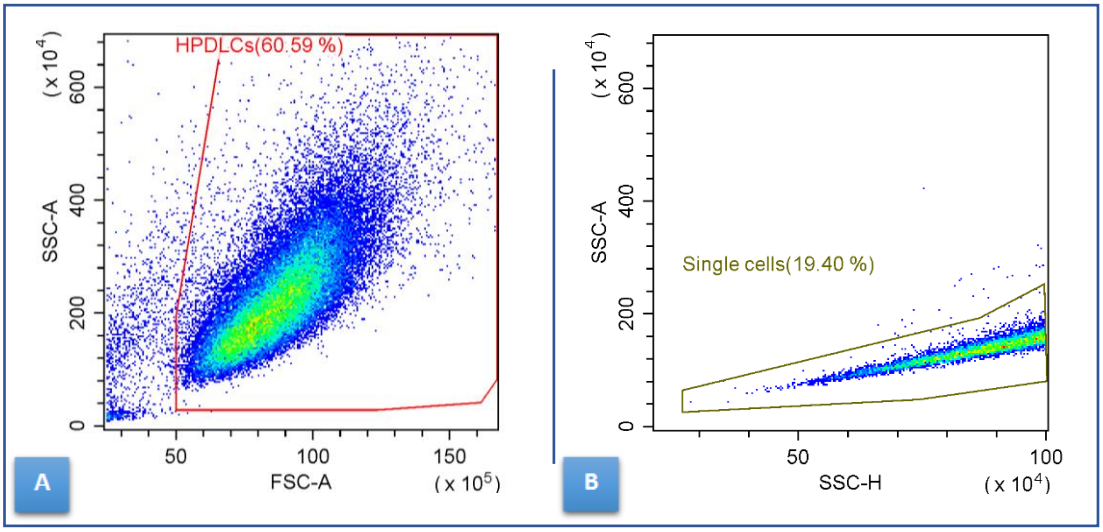

Figure 3-3: Gating strategy for the data of multicolour flow cytometry. A: first level gating was set by plotting side scattering against forward scattering, to determine the hPDLCs population. B: the second level of gating that set between side scatter area and height to define the single-cell population.

The technique involves labelling the cells with all markers except the one to be identified to be used as a specific negative control. Thus, presenting an indication of the effect of singles of other markers on the one of interest. As described in the previous experiment, the gate boundaries have been adjusted to include the intact cells bodies and single-cell population. A minimum of 10,000 events was recorded for each tested sample.

Since different markers have been used in this experiment, two detectors of close wavelength bands would be needed to detect the emitted signals (channels). To overcome this problem and to improve the detection sensitivity, a mathematical compensation was used. This involved using compensation beads (Comp beads, BD biosciences, New Jersey, USA), for multicolour flow cytometry. They are designed to provide a consistent, accurate, and simple-to-use tool to set compensation and reduce wasting the cell samples. Various groups of beads were prepared, with each group being labelled with only one of the markers used for this experiment. The expression level of each marker was measured by Beckman Coulter Cytoflex S, with the overlapping signal that slips over the next channel been subtracted using CytExpert 2.0 software. This compensation was applied for each marker for all tested groups.

Table 3-2: Panel design of multicolour flow cytometry for each donor

hPDLCs (per donor)	Compensation beads
Negative control (not stained)	**CD34** (BUV 348/395 nm)
Fully labelled sample (CD29, CD34, CD45, CD73 and STRO-1)	**CD29** (Alexa Fluor 488/519 nm)
FMO-CD29 (specific -ve control for CD29) labelled with CD34, CD45, CD73, STRO-1	**CD45** (Brilliant violet 405/785 nm)
FMO-CD34 (specific -ve control for CD34) labelled with CD29, CD45, CD73, STRO-1	**CD73** (Brilliant violet 405/421 nm)
FMO-CD45 (specific -ve control for CD45) labelled with CD29, CD34, CD73, STRO-1	**STRO-1** (Alexa Fluor 633/668 nm)
FMO-CD 73 (specific -ve control for CD73) labelled with CD29, CD34, CD45, STRO-1	
FMO-STRO-1 (specific -ve control for STRO-1) labelled with CD29, CD34, CD45, CD73	

3.3.4 Evaluation of hPDLCs multilineage differentiation potential

Evaluation multilineage differentiation capacity remains the gold standard method to identify the presence of MSCs. Basically, the cells must have the capacity to differentiate into at least three cell lineages (osteogenic, chondrogenic, and adipogenic) to be defined as MSCs (Dominici *et al.*, 2006). In this study, the isolated hPDLCs were examined for their *in vitro* multilineage differentiation capacity by inducing their differentiation into osteogenic, chondrogenic, and adipogenic cells.

3.3.4.1 Evaluation of osteogenic differentiation potential of hPDLCs

For inducing osteogenic differentiation, hPDLCs were cultured in StemMACS™ OsteoDiff human medium from Miltenyi Biotec (Bergisch Gladbach, Germany). This medium was proven to promote differentiation and further maturation of human MSCs into osteoblast cells (Elsaesser *et al.*, 2016; Pacini *et al.*, 2016). The manufacturer did not reveal the main components of this medium. However, the medium contains 100 unit/mL of P/S in each 100 mL StemMACS™ OsteoDiff Medium with phenol red.
Human PDLCs at P2 was detached, pelleted and counted to be cultured at a density of 3 x 10^4 cells/cm^2 in 24-well plates as described in **2.2.2**. Cells were divided into two groups, with each in triplicate (n=3). The first represents the control group's cultured in the basal medium, while the

experimental group cells were cultured in the osteoinductive medium. Four 24-well plates were prepared for each group in preparation for the next examinations. Two of the well plates were incubated for 14 days to evaluate the ALP activity. Whereas, the other two were kept for 21 days to evaluate the deposition of extracellular minerals. To identify the osteogenic markers using IHC staining, hPDLCs of the same passage (P2) for each of the donors were cultured in 4-chamber culture slides for 21 days (n=3). Medium for all samples was changed every three days.

Following 14 days of culture, cells were subjected to both qualitative and quantitative assessment of ALP activity performed with ALP staining and assay, respectively. For ALP staining, monolayered cells that cultured in 24-well plate were prepared and stained as described in **2.4.6**. The cell lysates were extracted from the second 24-well plate for ALP assay, as described in **2.3.3.** The ALP activity for the osteogenic group was statistically compared to that of the control group.

The process of osteogenic differentiation is accompanied by the expression of several proteins that contribute to this process; among those COL-1, OCN, and OPN are the most common (Marom *et al.*, 2005). Vimentin is a protein found in nonmuscle cells. It has been reported that it can inhibit the differentiation of osteoblasts (Lian *et al.*, 2009). Moreover, it has been linked to lower ALP levels, reduced bone protein expression as bone sialoprotein and OCN and decreased hard tissue mineralisation (Robinson-Bennett and Han, 2006; Li *et al.*, 2009). Accordingly, IHC staining was used to detect these markers' expression after 21 days of *in vitro* monolayer culture. Cells were washed, fixed and stained as described previously in **2.4.8.** A qualitative comparison was recorded for the expression of proteins in the control and osteogenic groups.

Likewise, Alizarin Red **(3.4.7)** and Von Kossa **(2.4.5)** staining methods were used to qualitatively evaluate the extent of extracellular mineral deposition (Ca^{+2} and phosphate) between the two groups (control vs osteogenic).

3.3.4.2 Evaluation of chondrogenic differentiation potential of hPDLCs

Another essential cell" lineage that MSCs can differentiate into is the chondrogenic one. For evaluating the potentiality of hPDLCs for chondrogenic differentiation, StemMACS™ ChondroDiff Medium (Miltenyi Biotec, Bergisch Gladbach, Germany) was used (Elsaesser *et al.*, 2016).

The ingredients of this medium were unknown as the manufacturer did not disclose it. According to the manufacturer protocol for chondrogenic differentiation, the cells should be cultured as a 3D pellet or aggregate structure rather than monolayer environment. This could be attributed to phenotypic changes, including a chondrocyte's morphology and function when being cultured in monolayer cell-vessel method (Estes and Guilak, 2011; Baker and Chen, 2012). Cells at P2 were washed, detached from the vessel, and counted to be cultured at a density of 2.5×10^5 cells/mL as described in **2.2.2.** One millilitre of cells suspension was transferred into 15 mL conical polypropylene tube and centrifuged for 5 mins at 200 rcf at RT, which helped in the formation of 3D spherical-like cells' pellet. The formed pellets were then cultured in 1 mL of either basal medium (control group), or StemMACS™ ChondroDiff Medium (experimental group). Medium was replaced regularly every three days for both groups.

Among the characteristic features of chondrocytes is the production of extracellular aggrecan, a large molecular weight proteoglycan. This protein is an integral part of cartilage formation and functioning (Frazer, A. *et al.*, 1994). After 21 days of *in vitro* 3D culture, both groups' pellets were harvested, washed and fixed in 10% NBF overnight. All samples were then subjected to tissue processing, embedding in paraffin wax, and sectioning as stated in **2.4.1.**

For histological examination, picrosirius red dye was used to detect collagen, while the Alcian blue stain was utilised to identify proteoglycan. Briefly, this staining method involves taking sections to water **(2.4.2.)**, staining with Wiegert's haematoxylin (Polysciences inc., Bergstraße, Germany) for 10 mins, and washing the excess of the stain with running tap water. Afterwards, sections were stained with 8GX Alcian Blue in acetic acid solution (TCS Biosciences, Buckinghamshire, UK) for 15 mins, followed by washing under running tap water for another 10 mins. For visualising the collagen, the sections were stained using the Picrosirius red staining (Sirius red staining kit, Polysciences inc., Bergstraße, Germany). This staining process was started with immersing in solution A (phospho-molybdic acid hydrate) for 3 minutes, followed by solution B (Picrosirius direct red stain) for 60 minutes, before final clearing with solution C (1 M hydrochloric acid) for 3 minutes. Finally, all sections were dehydrated with different concentrations of ethanol (70%, 90% and 100%, respectively) and mounted

with DPX, to be ready for imaging using Olympus-BX50 bright-field light microscope.

3.3.4.3 Evaluation of adipogenic differentiation potential of hPDLCs

StemMACS™ AdipoDiff Medium (Miltenyi Biotec, Bergisch Gladbach, Germany), was used to induce adipogenic differentiation of the isolated hPDLCs in monolayer culture. According to Pacini *et al.* (2016), this medium encourages differentiation MSCs into adipocyte and support their growth. The isolated hPDLCs were cultured in 4-chambers culture slides at a density of 2.5 $x10^4$ cell/cm^2. Then, cells were incubated (37^{o}C, 5% CO_2 and ≥ 90%) for 21 days, with the medium being changed every three days. This experiment included two groups; a control where cells were cultured in basal medium, and an experimental, including cells cultured in adipogenic induction medium.

Adipocytes are characterised by a round structure filled with lipid droplets, caused by the formation and accumulation of lipid. The droplets could be combined to form large vacuoles. This structure can be recognised by staining with the lipophilic stain as Oil Red O stain (Hausman, 1981).

A 0.5% (w/v) of Oil Red O (Newcomer Supply, Middleton, UK) stock solution in isopropanol was prepared. Afterwards, 6 mL of this solution was diluted by adding 4 mL of deionised water and filtered with a 0.22 µm filter to exclude large undissolved particles. Cells were washed gently with 1× PBS and fixed with 100% methanol for 5 mins at RT Afterwards, the fixation solution aspirated with cells being washed with two changes of deionised water. Cells were incubated with 500 µl/chamber of Oil Red O working solution, with gentle mixing using plate shaker for 20 mins at RT. Excess stain then removed, and cells were washed with and kept in deionised water. Cells of the two groups were imaged with Olympus-BX50 bright-field light microscope

3.4 Results

3.4.1 Morphology of isolated hPDLCs

Following 24 hrs of monolayer culture in the basal medium, the isolated hPDLCs population showed diversity in cellular morphology. The vast majority had a spindle, fibroblast-like shape with a central nucleus. Another cell type can be identified, which recognised by a cuboidal, polygonal, osteoblast-like shape with the short cytoplasmic process and a large oval nucleus, see Figure (3-4).

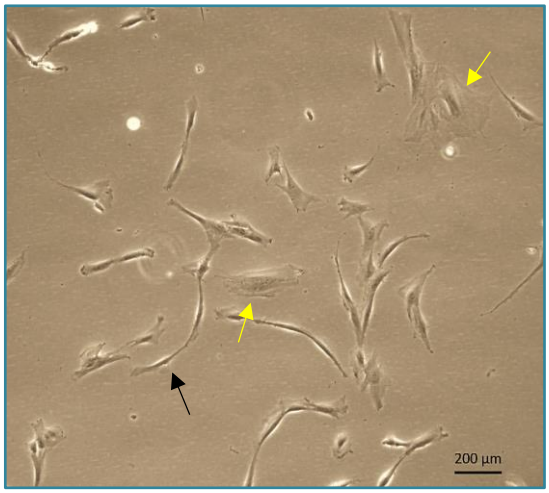

Figure 3-4: Microscope image of hPDLCs following 24 hr of monolayer culture in basal medium. Black arrow indicates cells with spindle, fibroblast-like shape, while cells referred to with yellow arrows showing a cuboidal, polygonal, osteoblast-like shape with a large oval nucleus.

3.4.2 The potential of hPDLCs to adhere to the plastic surface and their proliferative capacity

The CFU-F assay results demonstrated the potential of a subpopulation of the isolated hPDLCs to adhere to Petri dishes' untreated plastic surface when cultured in monolayer. Also, those cells were able to proliferate and form colonies of ≥ 50 cells each. These colonies were randomly distributed over the surface area of the culture vessel. The mean of formed colonies for the three donors was 42.22 ± 15.48 (Figure 3-5). Furthermore, the statistical analysis of the CFU-F assay's data revealed significant differences in the number of colonies between the first donor cells from one side and those of

second and third donors from the other side (Figure 3-6). However, no statistical difference was found between cells of second and third donors.

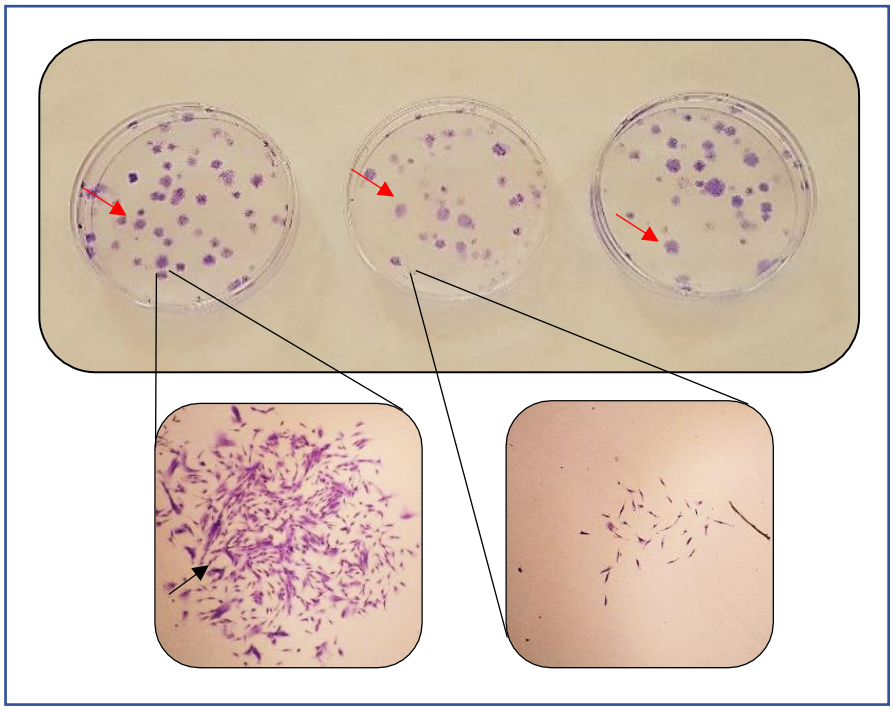

Figure 3-5: Macroscopic and microscopic (X10) overview of CFU-Fs for hPDLCs isolated from three donors. Cells were cultured in monolayer for ten days in basal medium. Colonies (red arrows) of ≥ 50 cells (black arrows) were only counted.

3.4.3 Immunophenotype of the hPDLCs

3.4.3.1 The optimal concentration of haemopoietic and mesenchymal stem cells markers for hPDLCs

The first step in the flow cytometry experiment included titration of markers' concentrations; this was the case for haemopoietic and mesenchymal stem cells markers. Statistical analysis of the flow cytometry data for each marker's five used concentrations revealed the optimum concentration for the hPDLCs; the results were calculated using stain index, which helps determine the relative brightness (light intensity) for each concentration.

There was no statistical difference in the value of stain index for hPDLCs labelled with different concentrations (2.5, 5, 10, 15, 20 µl/mL) of haemopoietic markers (CD34 and CD45). Accordingly, a concentration of 2.5 µl/mL of each of those two markers was dependant, as demonstrated in Figures (3-7/A) and (3-7/B).

The situation regarding mesenchymal stem cells markers (CD29, CD73 and STRO-1) was different. Cells labelled with 10 µL/mL of CD29 provided the

higher value of stain index than 2.5 and 5 µL/mL (Figure 3-7/C); this difference was highly significant (*P* <0.0001). However, the difference between the concentration of 10 µL/mL and those of 15 or 20 µL/mL was statically non-significant. Accordingly, the optimum concentration of CD29 for hPDLCs was 10 µL/mL. Moreover, the optimum concentration for CD73 was 15 µL/mL, as shown in Figure (3-7/D). There was a highly significant difference (*P* <0.0001) in the value of stain index between the concentration of 15 µL/mL and those of 2.5, 5, 10 or 20 µL/mL. However, between 10 and 20 µL/mL was statistically non-significant. Finally, the stain index values for STRO-1 revealed a non-significant difference in the brightness for cells labelled with any of the used concentrations (2.5, 5, 10, 15, 20 µL/mL) (Figure 3-7/E). Therefore, the minimum concentration (2.5 µL/mL) was dependent on reducing the waste of markers.

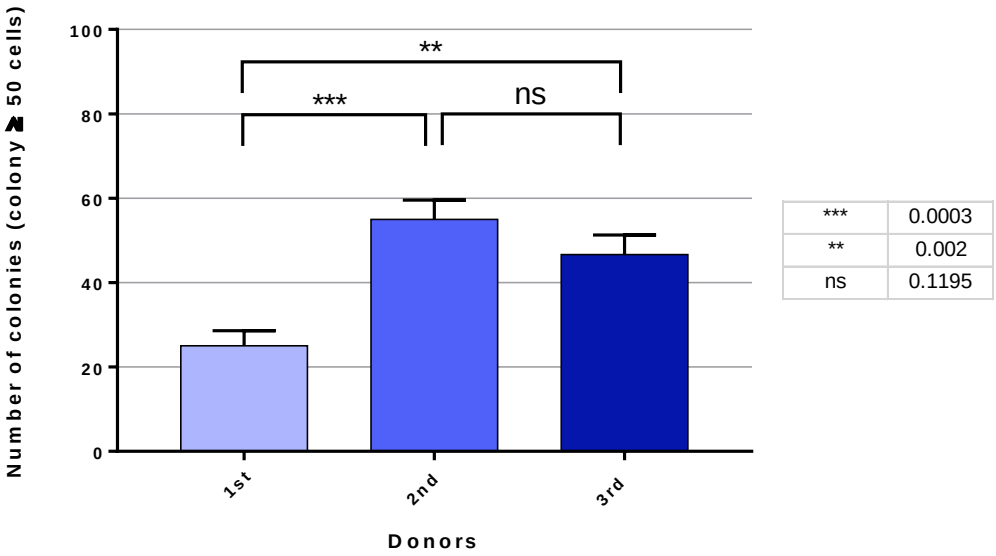

Figure 3-6: CFU-F assay for hPDLCs isolated from three different donors. Following 10 days of culture in basal medium, mean ± SD of colonies formed for each of the donor (n=3) cells were calculated. Data analysed using One-way ANOVA test (Tukey's multiple comparisons test), at *p*-value ≤ 0.05.

3.4.3.2 Expression levels of human haemopoietic and mesenchymal stem cells markers in hPDLCs

Following the optimisation of markers concentration, the phenotyping of the isolated hPDLCs was examined. This step was accomplished using multicolour flow cytometry, which helps estimate the percentage of cells' population that express the haemopoietic (CD34 and CD45) and mesenchymal stem cells markers (CD29, CD73 and STRO-1).

Statistical analysis of flow cytometry data showed that a mean of 0.73% of cells among the isolated cells population had expressed CD34. However, a mean of 28.73% of those cells had expressed CD45, as shown in Figure 3-8/A. Moreover, results demonstrated a variance in the expression of these two markers among three donors' cells. However, this variance was more obvious regarding the expression of CD45, as the expression percentage ranged from 2.24% to 71.18%. Whereas the percentage of cells expressed CD34 vary between 0.06% and 2.06% (Figure 3-8/B).

In contrast, a higher percentage of the isolated cells expressed CD29 and CD73 markers at 99.95% and 100%, respectively (Figure 3-8/A). Furthermore, the data in Figure 3-8/B revealed that the difference between the cells isolated from the three donors was minimum for both markers. Furthermore, STRO-1 marker was expressed in 1.05% of the examined cells populations. The difference between the three donors was evident, as the expression level ranged from 0.34% to 1.73%.

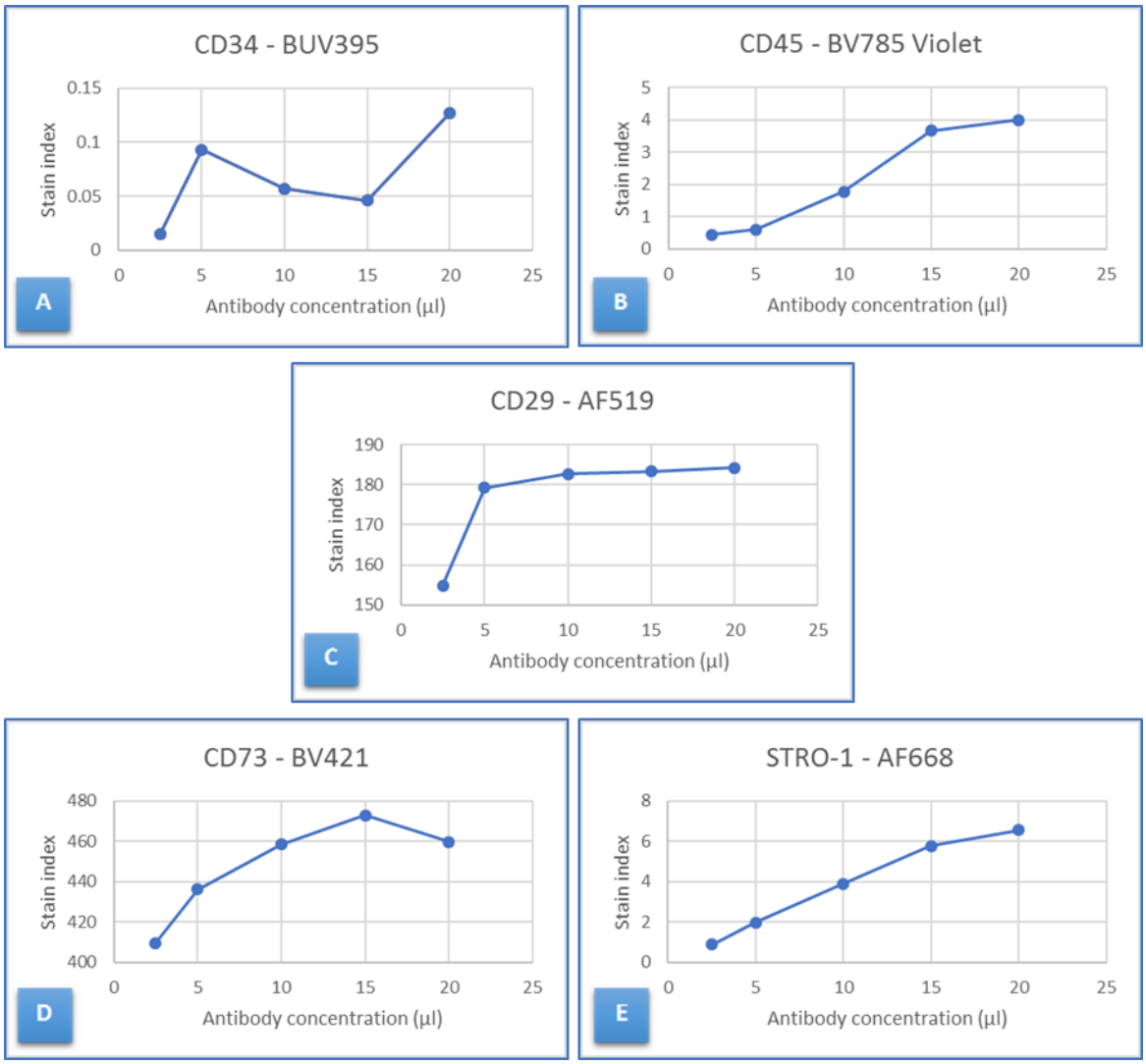

Figure 3-7: Results stain index for titration of haemopoietic and mesenchymal stem cells markers for hPDLCs. Five concentrations (2.5, 5, 10, 15, 20 µL) were used for each marker, CD34 (A), CD45 (B), CD29 (C), CD73 (D) and STRO-1 (E).

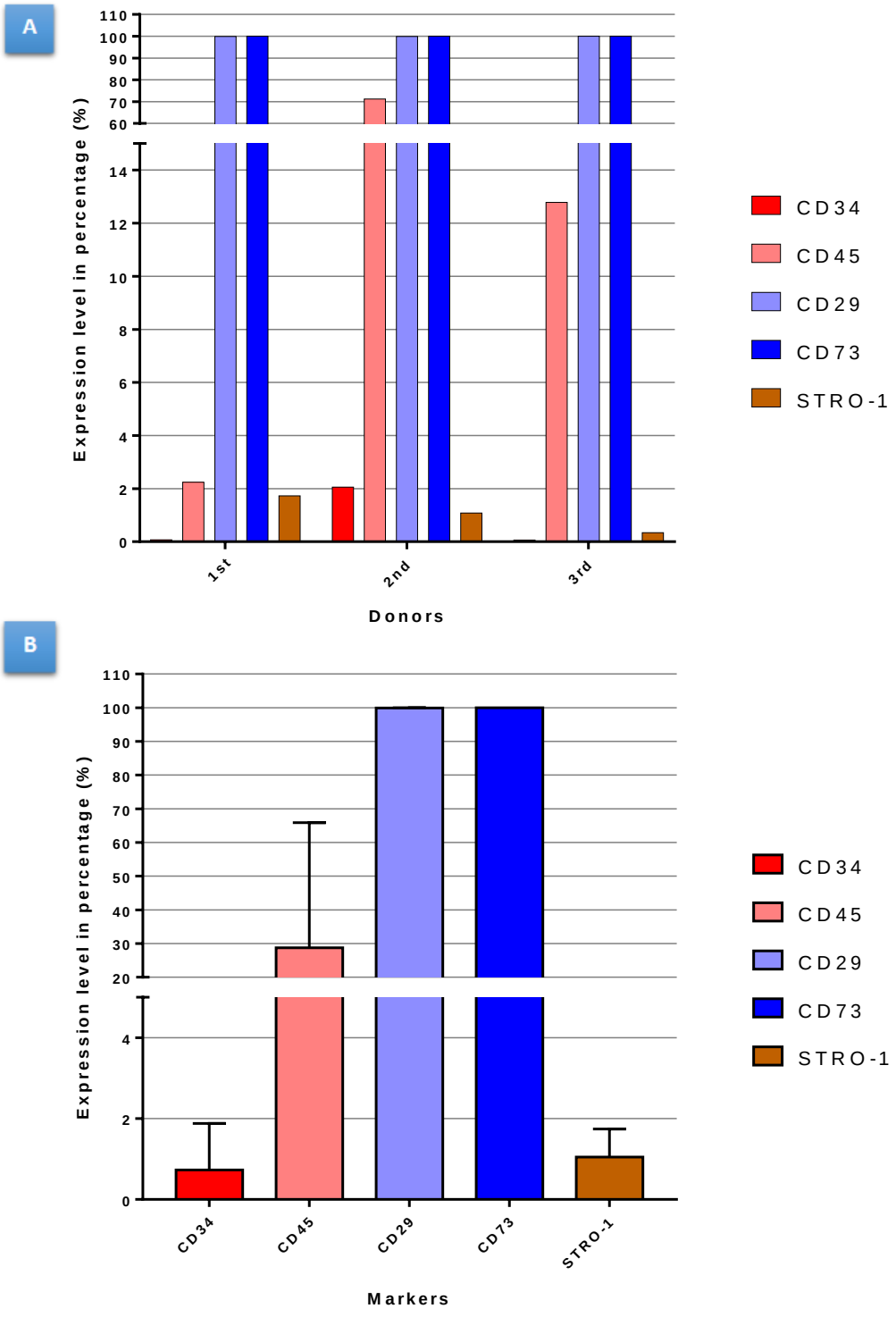

Figure 3-8: Flow cytometry immunophenotyping of hPDLCs population isolated from three different donors. A: levels of expression of haemopoietic and mesenchymal stem cells markers for hPDLCs for each donor. Cells of the three donors demonstrated high levels of CD29 and CD73, with low level of STRO-1. However, same cells barely expressed CD34 and relatively low levels of CD45. B: Mean ± SD of levels overall level of markers expression for the cells of the three donors.

3.4.4 Multilineage differentiation of hPDLCs

The isolated hPDLCs demonstrated the capacity for *in vitro* multilineage differentiation when induced with specific differentiation medium as presented below:

3.4.4.1 Induced osteogenic differentiation

Following seven days of monolayer culture in osteoinductive medium, more cells began to show morphological changes. The cell body ranged from cuboidal to polygonal shape, with fewer and shorter cytoplasmic processes and well-recognised central nucleus (Figure 3-9). In contrast, most control group cells, which are cultured in basal medium, retained their spindle, fibroblast-like shape. However, few cells in the control group showed different morphology with flat and full cell body and limited cytoplasmic processes (Figure 3-9).

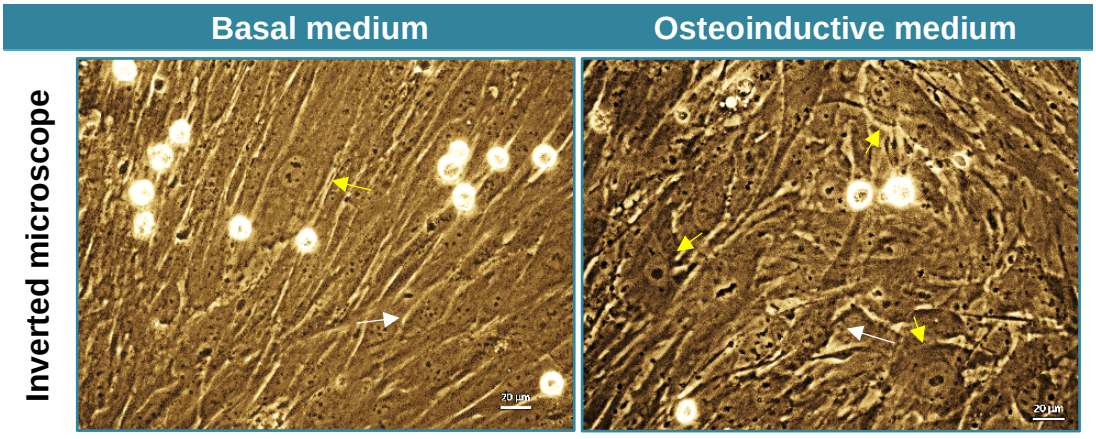

Figure 3-9: Comparison of change in cellular morphology of hPDLCs after inducing osteogenic differentiation. After seven days of monolayer culture of hPDLCs in either basal or osteoinductive medium, the cells in osteoinductive groups demonstrated a change in their morphology from the spindle, fibroblast-like shape (white arrows) into cuboidal, polygonal shape with shorter cytoplasmic processes (yellow arrows). In contrast, cells in the control group retain their spindle, fibroblast-like shape.

Furthermore, comparing the ALP stain results between the control and osteogenic group revealed a higher level of red ALP stain in the latter, as shown in Figure 3-10/A. The stain found within the cytoplasm adjacent to the cell membrane. Likewise, the stain was observed in the control group but to a lesser extent. These qualitative results were confirmed by the quantitative ALP assay results, which proved the difference between the two groups regarding the ALP activity. However, this difference was non-significant according to the results of the unpaired t-test (Figure 3-10/C). According to the results of the PicoGreen™ assay, the DNA content of osteogenic group was more than that of the control group, with no statistically significant difference between the two groups (Figure 3-10/B).

On the other hand, there was a variation in ALP stain results and specific ALP assay among the three donors' cells (Figure 3-11/A, 3-11/C). Statistical analysis revealed that this variation was significant between the third donor cells compared to those of the first and second donor. It was demonstrated that the cells isolated from the third donor have the highest level of ALP activity. In contrast, the third donor cells had the minimum amount of DNA content when evaluated along with the cells from other donors (Figure 3-11/B). However, the difference in the DNA contents among the cells of three donors was statistically non-significant.

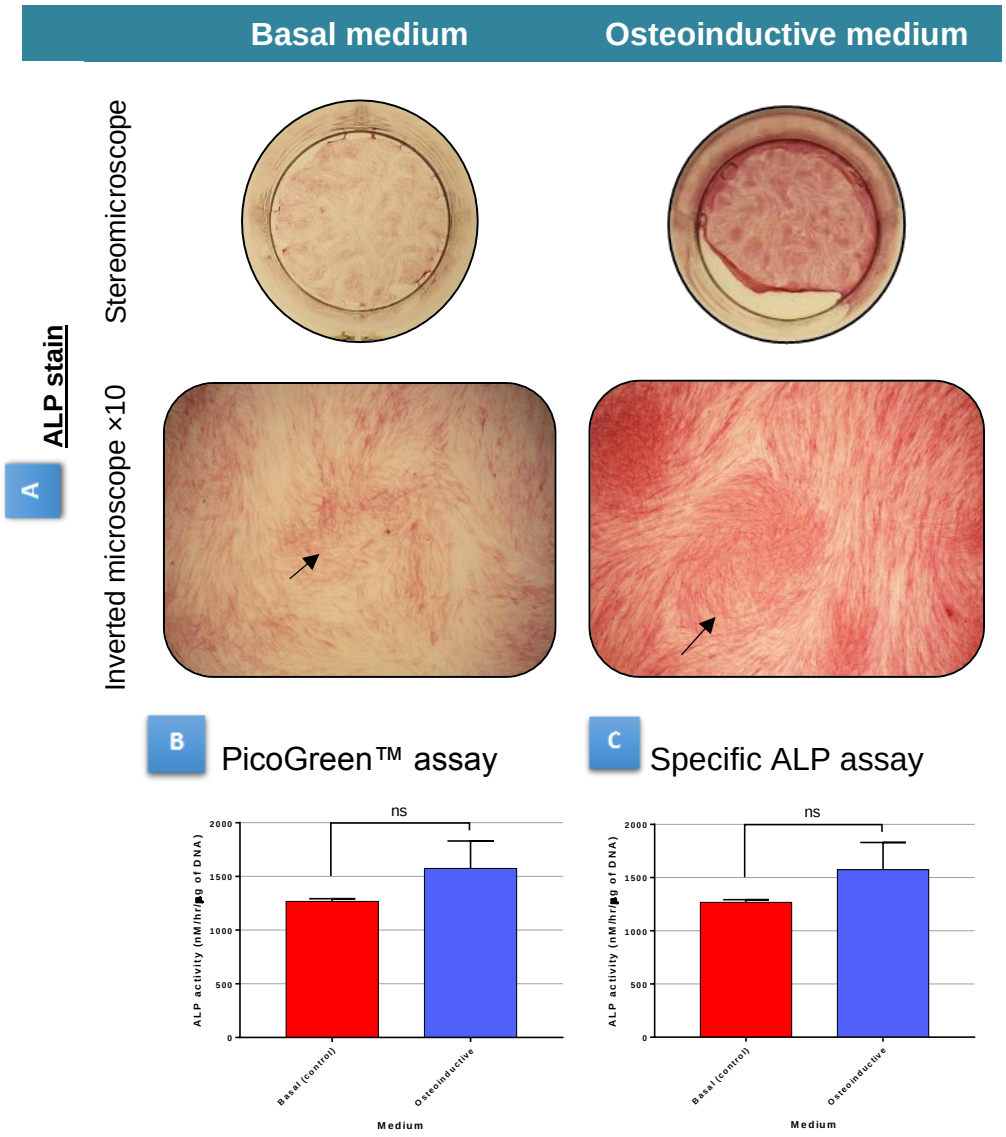

Figure 3-10: Qualitative and quantitative evaluation of ALP activity for hPDLCs in response to culture in the osteoinductive medium. hPDLCs monolayered samples (n=3) were cultured in either basal or osteoinductive medium for 14 days, then stained with ALP stain (red colour). Macroscopic and microscopic images of ALP stain showed a higher level of stain in the osteogenic group. Also, DNA contents (B) and specific ALP activity (C), were higher in the osteogenic group. However, statistical analysis, which performed using t-test with a *p*-value ≤ 0.05, revealed a non-significant difference between the two groups.

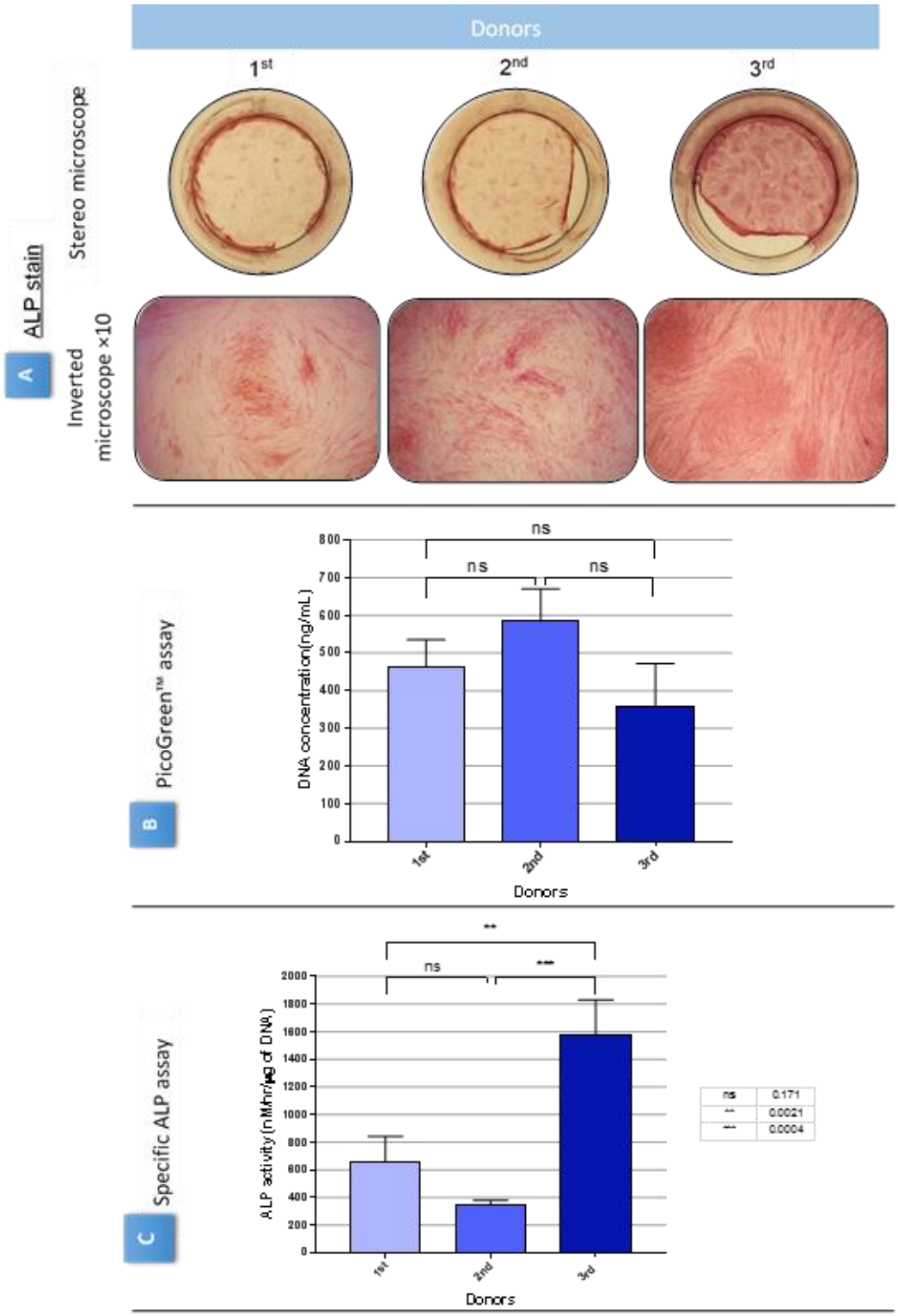

Figure 3-11: Effect of the donor variability on ALP activity for hPDLSCs cultured in osteoinductive medium. After 14 days of monolayered culture in osteoinductive medium, cells showed a variation in ALP stain (A) level among the donors. Similarly, the statistical analysis of both Picogreen™ (B) and specific ALP assays (C) revealed a difference in the DNA content and ALP activity between the three donors. Data were statistically analysed using one-way ANOVA and' Tukey's multiple comparisons test, with a *p*-value ≤ 0.05.

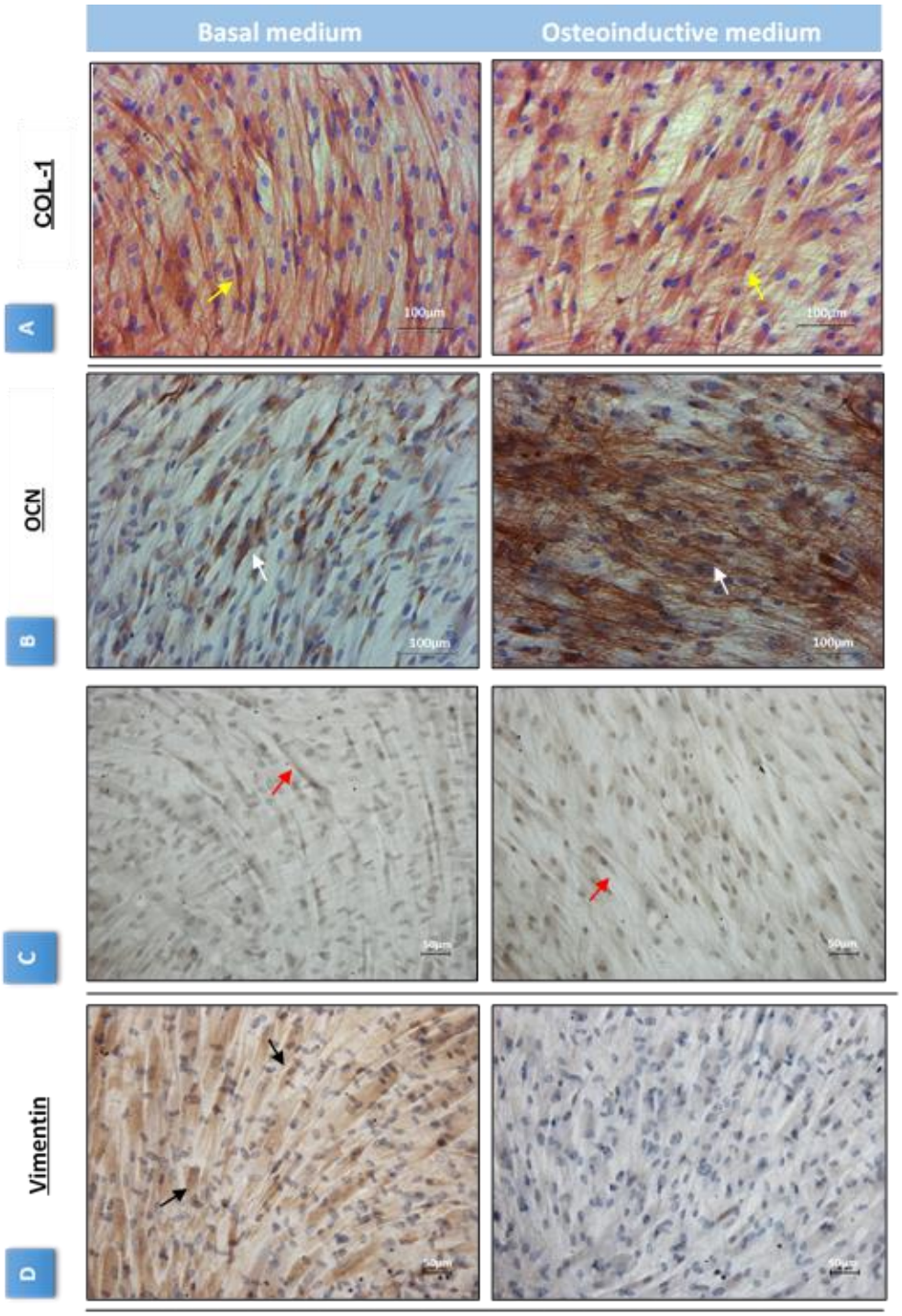

Figure 3-12: Immunohistochemical examination of the effect of osteoinductive medium on the expression of COL-1, OCN, OPN, and Vimentin. hPDLCs were cultured in monolayer either in basal (control) or osteoinductive medium (experimental). Proteins were recognised as brown coloured stains. Examining the sections revealed COL-1 and OPN at comparable levels in both groups, referred to with the yellow and red arrows respectively. However, the OCN was identified in a higher amount in the osteogenic group (white arrows). Vimentin was detected in the control group only (black arrows).

Following 21 days of monolayered culture, images of IHC staining showed the presence of collagenous and non-collagenous bone proteins, e.g. COL-1, OCN and OPN. Collagen type-1 was detected as brown stain distributed in the extracellular matrix in between the cells. The protein was equally expressed in both control and osteogenic groups. Moreover, cells presented as round to cuboidal-like shape, with a profoundly stained nucleus (Figure 3-12/A). Furthermore, the OCN was detected at a relatively higher level in the osteogenic group, where it identified as brown-coloured mesh scattered in between the cells, as demonstrated in Figure 3-12/B. Osteopontin is another bone protein that was investigated in this study. This protein was presented as a brown stain within the cytosol around the nucleus and the extracellular space between the cells (Figure 3-12/C). It has been observed in both groups at comparable levels. The IHC examination revealed expression of vimentin in the control group were cells cultured in basal medium. Interestingly, this protein was not detected in the osteogenic group, as shown in Figure 3-12.

Another essential feature of osteogenic differentiation is the deposition of extracellular minerals, including phosphate and calcium. Presence of these minerals was examined using VK and AR stains. Staining of monolayer cells sections with VK stain confirm the presence of phosphate deposition (indirectly the calcium) in the osteogenic group, which recognised as deeply stained, brown particles ranging in size from 3-36 µm. These particles were found in the extracellular space next to the cells. In contrast, the control group showed a limited number of these particles in a confined area (Figure 3-13/A).

Additionally, deposition of calcium was detected by AR stain for both groups. More areas in the osteogenic group were deeply stained with the red stain, which was distributed in an irregular pattern in the extracellular matrix. Such a stain was almost absent in the control group (Figure 3-13/B). The AR stain results were confirmed with those of AR quantification assay, which showed a highly significant difference in the level of stain between the two groups, as presented in Figure (3-13/C).

3.4.4.2 Induced chondrogenic differentiation

The chondrogenic group pellets appeared denser after 21 days of induced chondrogenic differentiation of hPDLCs in 3D culture compared to the control group's pellets. Histological examination of the chondrogenic group

pellets revealed a larger volume of compacted cells, with a capsule of thick bundles surrounding the entire pellet. Additionally, a fibrous mesh layer in a perichondrium-like structure, which was stained in green, was identified under the collagen bundles. These features were absent in the control group.

Moreover, cells cultured in chondrogenic medium showed a morphological change from the spindle, fibroblast-like shape into large, oval to the round shape, with a smooth outline. Those cells were located within lacunae. The intercellular spaces were filled with dense and long bundles of collagen fibres. In contrast, cells of control groups (basal medium) had small, round bodies, with an irregular surface and short processes. The intercellular space in the control group was larger; see Figure (3-14).

One observation of the differentiation between the two groups was the cellular attachment; most cells in the control group remained isolated with only a few connections, despite the long period (21 days) of *in vitro* culture in the basal medium. Also, there was no evidence of extracellular collagen or proteoglycan/aggrecan formation, which is an indicator of cartilage synthesis. In contrast, cells in the chondrogenic group showed the formation of collagen bundles that spread in between the cells and recognised by the red colour of the picrosirius red stain. Furthermore, evidence of aggrecan formation within the extracellular matrix was identified by staining with dark blue using the copper-containing Alcian blue dye, as shown in Figure (3-14).

3.4.4.3 Induced adipogenic differentiation

The adipogenic differentiation capacity of hPDLCs was examined after seven days of monolayer cell culture in the adipogenic medium. The cells began to show an increase in the cell body's overall size, with elongation of cytoplasmic processes. The intercellular space became wider with the aggregation of cells in small clusters. However, the cells in the control group retained their spindle, fibroblast-like shape. There was an increase in the cell number and a lack of intercellular spaces (Figure 3-15/A).

After 21 days of induced adipogenic differentiation, cells appeared as preadipocyte-like cells, with a large cell body with a prominent round nucleus and long cellular processes. Accumulation of intracellular lipid droplets was recognised after staining with Oil Red O-stained; these droplets were identified as clusters of the bright red beads-like structure

near the nucleus. No evidence of change in cellular morphology was observed in the cells of the control group. Cells kept the initial spindle-like shape with the centrally positioned nuclei. Furthermore, staining with Oil Red O stain did not reveal lipid droplets in those cells. These results are shown in Figure (3-15/B).

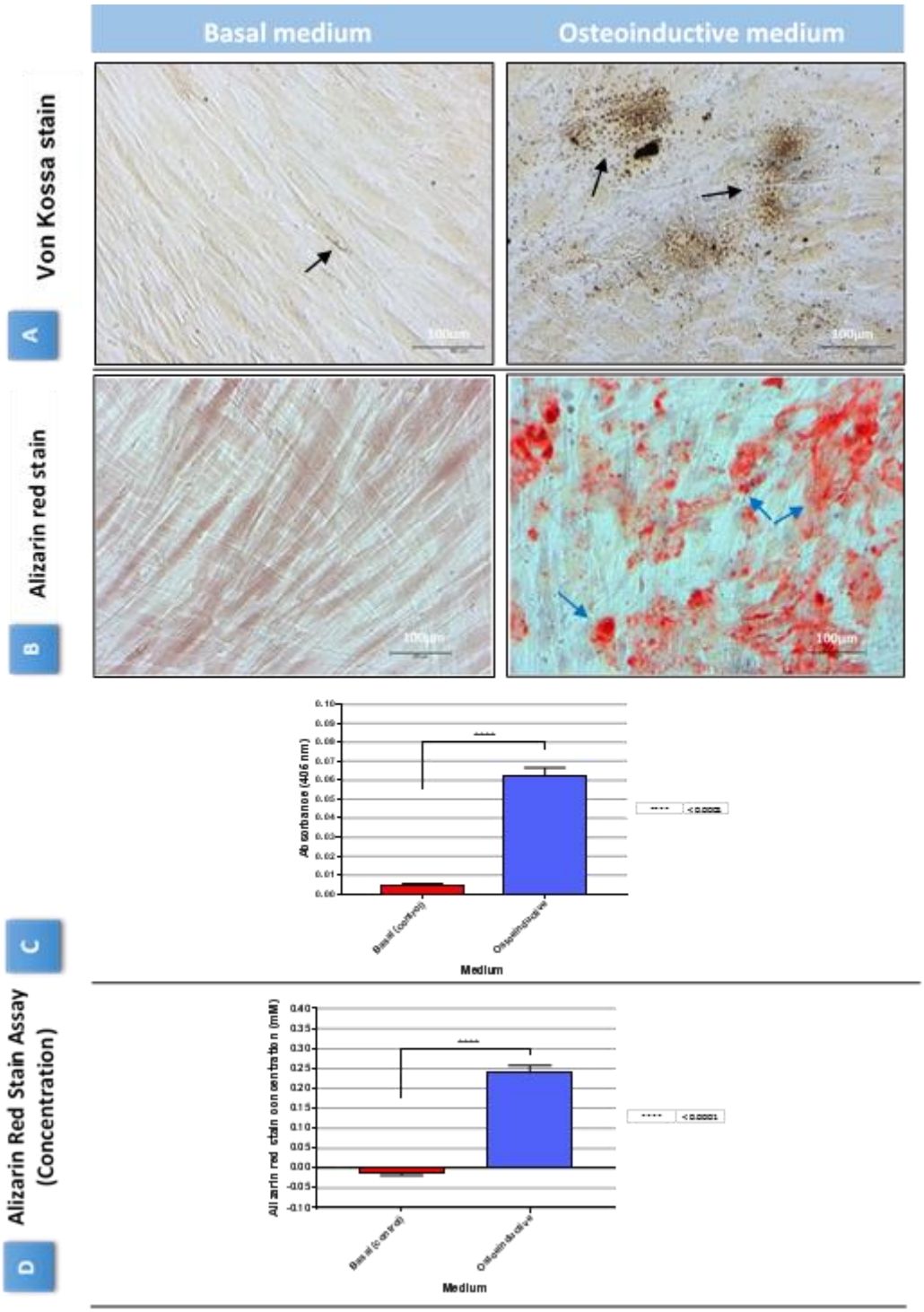

Figure 3-13: Effect of osteoinductive medium on extracellular mineralisation of hPDLCs. After 21 days of hPDLCs culture in osteoinductive medium, VK and AR stains were used to detect phosphate and calcium deposition, respectively (A and B). The Osteogenic group showed an increase in minerals deposition in comparison to the control group. The unpaired t-test for the level of absorbance (C) and concentration of AR stain (D) confirm a highly significant difference between the osteogenic and control groups.

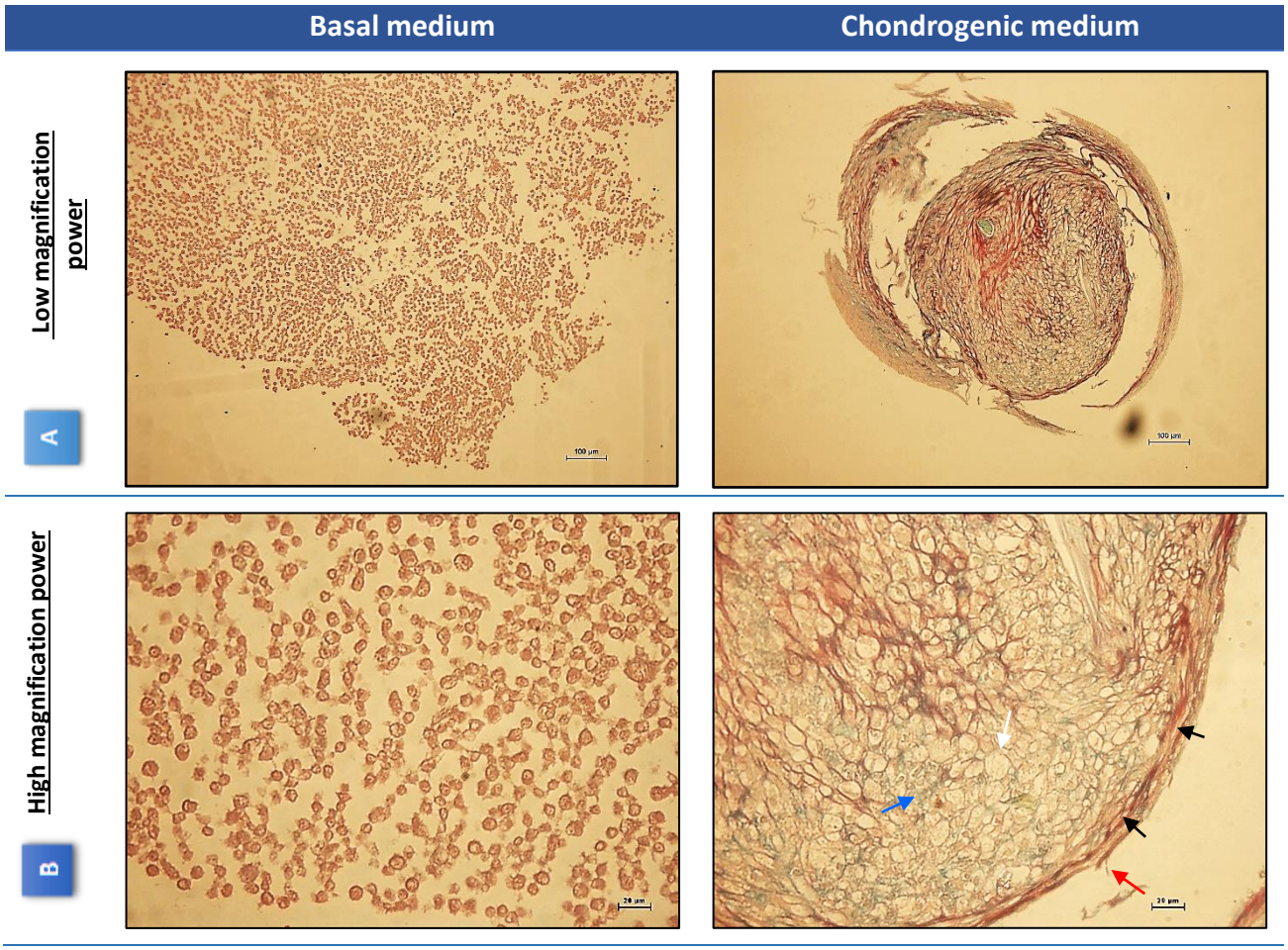

Figure 3-14: Effect of chondro-inductive medium on hPDLSCs. Cells were cultured in 3D pellet form for 21 days in either basal or chondrogenic medium. Staining of' pellets' sections with picrosirus red/Alcian blue stains revealed a change in the chondrogenic group's cellular morphology with oval to round cells captured inside a lacunae-like structure (white arrow). Intercellular spaces are filled with extracellular deposition of aggrecan recognised by Alcian blue stain (blue arrow). The pellet itself was surrounded by a dense bundle of collagen fibres (red arrow) superficial to a mesh of fibrous layer in a perichondrium-like structure (black arrow). Cells cultured in basal medium appeared as small, round cells with an irregular surface and short processes. The intercellular spaces were wide with few cellular attachments.

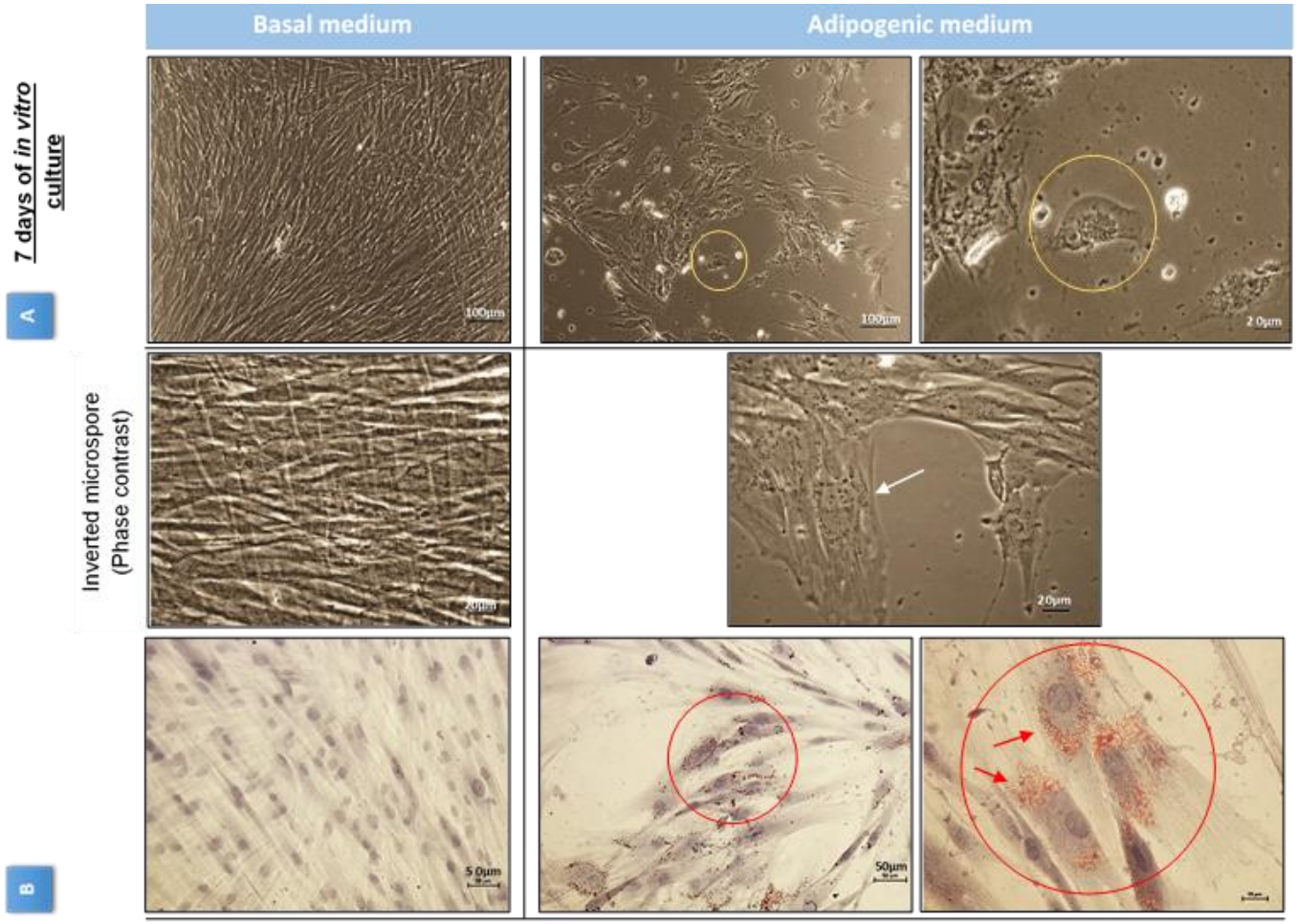

Figure 3-15: Adipogenic differentiation of hPDLCs. Evidence of adipogenic differentiation recognised after seven days (A) of *in vitro* monolayer culture in adipogenic medium, with a change in cellular morphology and intercellular space size. Following 21 days (B), the cellular changes become more evident as cells showed an increase in the size, with a prominent round nucleus and long cytoplasmic processes (white arrows). Moreover, Oil red O-stain revealed accumulation of intracellular lipid droplets next to the nucleus (red arrows). These changes were absent in the control group, as cells retain their original spindle, fibroblast-like shape, with tightly closed inter-cellular distance.

3.5 Discussion

Cells are the key players in the tissue regeneration process as they represent the basic building unit of the human body (Tribe *et al.*, 1975; Dienhart, 1979). This fact established the basis for tissue engineering and cellular therapy to provide an alternative approach for developing and enhancing tissue regeneration *in vitro* and *in vivo* (Muschler *et al.*, 2004; Vacanti, 2006; Glotzbach *et al.*, 2012). While many types of cells have been investigated for this purpose, multipotent stem cells were found to be the most suitable type due to their self-renewal and multilineage differentiation properties (Dominici *et al.*, 2006; Bobis *et al.*, 2006). These cells have been successfully isolated from many anatomical sites of the human body, including bone marrow, adipose tissue, umbilical cord in addition to the dental tissues (Bianco *et al.*, 2001; Gronthos *et al.*, 2002; Tepliashin *et al.*, 2005; Jo *et al.*, 2007; Diao *et al.*, 2009). With each of these sites having its advantages and disadvantages, periodontal ligament represents a promising source for this type of cells.

Many studies have tried to investigate the presence of multipotent mesenchymal stem cells within the hPDLSCs. However, most of these studies lacked a standardised methodology for cell identification; with limited attention being paid to the effect of donor variability on cells characteristics (Seo, B.-M. *et al.*, 2004b; Nagatomo *et al.*, 2006; Gay, I. *et al.*, 2007; Wang, L. *et al.*, 2011; Song *et al.*, 2012; Navabazam *et al.*, 2013; Zhu and Liang, 2015). However, the ISCT has suggested specific criteria in order to define cells as multipotent MSCs. These criteria include cellular adherence to the plastic surface of culture vessel, self-renewal, expression of MSCs markers, in addition to the cellular potential to differentiate *in vitro* into osteogenic, chondrogenic and adipogenic cells cues (Dominici *et al.*, 2006). Accordingly, the present study intended to overcome the previous limitations and investigated the characteristics of the isolated hPDLCs by following a systematic examination protocol. It was also an essential step in this project to evaluate the isolated cells' quality regarding their proliferation and differentiation capacities to prepare for the following experiments.

In the present study, the primary cells were isolated from third molar teeth. This type of tooth is the last to develop in the oral cavity, specifically post-natally (Nanci, 2017). Thus, it provides a source of periodontal tissue and increases the possibility of isolating cells less affected by ageing or disease

processes (Volponi *et al.*, 2010; Soheilifar *et al.*, 2016). Due to the lack of space and to reduce the complications of the malaligned eruption, third molars are frequently extracted in young adults, which increase the availability of these teeth for research purposes (Volponi *et al.*, 2010). The middle third of the root was the location from which PDL tissues were obtained. This location was recommended to reduce the contamination of the isolated tissue with other cells either from the gingival or apical tissues, which may have affected the study's result (Morsczeck *et al.*, 2005; Mrozik *et al.*, 2010).

The microscopic images for hPDLSCs in this study confirm the presence of a morphologically heterogeneous population. At least two different types of cells were recognised - dominant fibroblast-like cells and to a lesser extent, polygonal osteoblast-like cells. These findings are consistent with the histological features of human periodontal ligament tissue that consists of many cell types. i.e. fibroblast, osteoblasts, cementoblast, etc. (Nanci, 2017). Furthermore, this evidence agreed with previous studies investigating primary periodontal cells *in vitro* (Gronthos *et al.*, 2006; Song *et al.*, 2012; Navabazam *et al.*, 2013; Miletic *et al.*, 2014).

The biological behaviour of MSCs is directly affected by the interaction with the surrounding cells and matrix. This molecular-level interaction controls cellular activities, including their spreading, morphology, proliferation and differentiation (Salzig *et al.*, 2016; Roberts *et al.*, 2016; Mehanna, 2017). The CFU-F assay, described initially as fibroblastoid colony-forming cells, was one of the earliest physical methods used for identification of MSCs based on evaluation of two primary features, the adherence to the plastic surface and self-renewal capacity (Bradley *et al.*, 1969; Friedenstein, A. *et al.*, 1970; Pochampally, 2008). Friedenstein *et al.*, 1970 reported that cells isolated from bone marrow could adhere to the vessel polystyrene plastic surface, spread and proliferate from a single cell into a more massive cell colony. Using this assay makes it possible to estimate the ratio of adherent cells to the whole cultured cells population. The CFU-F assay results in the current study indicated a subpopulation within the primary hPDLCs that can adhere to the plastic surface and proliferate. Despite the variation in the initial seeding density of hPDLCs, these findings agreed with those of previous studies (Gay, I.C. *et al.*, 2007; Song *et al.*, 2012). Song *et al.*, 2012 reported an average of 51.4 ± 8.9 colonies following ten days of hPDLCs culture in standard condition. However, the seeding density was different

(50 cell/cm2). In another study, an average of 170 colonies was formed after the same period with an initial seeding density of 176 cell/cm^2. In the present study, a seeding density of 100 cells/35 mm (11 cell/cm^2), the lowest technically feasible, was dependent on performing the CFU-F assay. Reducing the cells seeding density minimises the bias due to false-positive results resulting from colonies forming from cells that migrated from close colonies rather than single precursor cells.

Despite the feasibility of the CFU-F assay in detecting the MSCs within primary cells, it cannot be used as the only method to detect and purify this subpopulation of cells. The reason behind that can be attributed to several points; first, it is not a sensitive method to distinguish between the MSCs and Haemopoietic stem cells as both can adhere to the plastic surface (Bradley *et al.*, 1969; Friedenstein, A.J. *et al.*, 1974); Secondly, it is a passage consuming method when purifying the cell subpopulations required (Mehanna, 2017). Accordingly, other methods are needed to confirm further the presence of MSCs, including phenotyping and trilineage differentiation.

One of the widely used cell identification and purification methods from a heterogenous cells population is immunological phenotyping. Basically, it depends on recognising and measuring specific cell surface and intracellular molecules (Mehanna, 2017). The ISCT has suggested this method for defining the MSCs and determining specific cells markers to be examined for that purpose (Dominici *et al.*, 2006). In this study, some of these markers were used to set the multicolour flow cytometry panel to identify the MSCs population in the isolated hPDLCs. Flow cytometry multicolour analysis used in this study helped assess each marker's percentage of expression for the whole cells population simultaneously (Baumgarth and Roederer, 2000). The ISCT also recommended this technique for the characterisation of MSCs (Dominici *et al.*, 2006).

Rojewski *et al.* (2008) suggested that expanded MSCs must be tested negative to CD34 for hematopoietic stem cells and CD45 for resting lymphocytes. In this study, the expression of CD34 ranged between 0.06% and 2.06%, which falls within limits of haematopoietic markers expression determined by the ISCT for the MSCs (≤ 2%). In contrast, CD45 was expressed at variable levels with an average of 28.73% ± 37.13, and the highest expression level of (71.18%) been recorded in one of the donors' cells population. CD45 is an essential regulator of signal transduction

pathways in immune cells, and It expressed in most of the haematopoietic cells, including lymphocytes (Thomas, 1989; Hermiston *et al.*, 2003). Accordingly, the higher level of CD45 expression in the current study could be attributed to the co-isolation and co-culture of such cells, e.g. lymphocyte, which reported to be found in the healthy periodontium (Amunulla *et al.*, 2008). On the other hand, Yeh *et al.* (2005) have reported the expression of CD45, one of the abundant and exclusive markers for haematopoietic cells, in MSCs isolated from the bone marrow of patients with haematological malignancy. Interestingly, the MSCs that expressed this marker have shown similar morphological features of the spindle, fibroblast-like cells of CD45 negative MSCs.

CD29 Is one of the adhesion molecules that proved to be expressed at a high level in MSCs at the early stage of culture (Rojewski *et al.*, 2008). However, the expression level of CD29 was passage related, as the marker expression was down-regulated following cell expansion and proliferation (Rojewski *et al.*, 2008). Additionally, CD73 is commonly used as a standard MSCs marker (Kolf *et al.*, 2007). Both markers were expressed at higher levels in the hPDLCs of the three donors in this study, 99.95% and 100% respectively. The same ranges of CD29 and CD73 were reported in previous studies that aimed to characterise the primary hPDLCs using phenotyping (Trubiani *et al.*, 2010; Zhang, J. *et al.*, 2012; Choi, S. *et al.*, 2013; Miletic *et al.*, 2014). Moreover, the current expressing levels fall within limits set by the ISCT for MSCs.

STRO-1 was recognised as a marker for MSCs and predominantly used to identify and sort MSCs (Simmons and Torok-Storb, 1991; Kolf *et al.*, 2007; Lin *et al.*, 2011). Xu *et al.* (2009) isolated hPDLCs from six donors' third molars (male and female subjects ranging between 16-25 years). It was found that 2.585% of the cells expressed STRO-1. To a relative level, in the current study, the percentage of hPDLCs that were positive for STRO-1 ranged between 0.34% - 1.73%. In contrast, higher levels of STRO-1 expression in hPDLCs were recorded by Zhang, J. *et al.* (2012) and Yang, H. *et al.* (2013), 14.4% and 16.6%, respectively. In both studies, the same concentration for all positive and negative MSCs markers was used. This point could directly affect the expression level for each of the markers by antibodies oversaturation, which turns into an increase in non-specific staining and reduction in the reading sensitivity and accordingly increases the bias (Cossarizza *et al.*, 2017).

Despite the advantages that flow cytometry phenotyping is offering for characterisation of MSCs, it still has several limitations regarding MSCs characterisation. To date, no specific markers were found for identification of mesenchymal stem cells, and a panel of several antibodies is commonly applied for most of the cells' characterisation studies. Add to that, the variation in the antibody's expression for cells from different donors or tissues is another crucial factor that could affect this method's results (Dominici *et al.*, 2006; Mehanna, 2017). Moreover, technical issues related to the technique itself that could have an impact on the validity of the results; including optimisation of markers concentration, gating, autofluorescence and fluorochrome combinations (Baumgarth and Roederer, 2000; Mehanna, 2017)

There is a general agreement in cellular therapy and tissue engineering that multilineage differentiation of cells is one of the main characteristics of MSCs (Pittenger *et al.*, 1999; Horwitz *et al.*, 2005; Dominici *et al.*, 2006). In the current study, the use of osteogenic medium induced osteogenic differentiation of hPDLCs as demonstrated in **3.4.4.1.** Several parameters were evaluated to confirm the osteogenic differentiation, e.g. cellular morphology, ALP activity, expression of specific bone markers, and an extracellular minerals deposition. There is an agreement on using these parameters to evaluate osteogenic differentiation (Marom *et al.*, 2005; Diao *et al.*, 2009; Bakopoulou *et al.*, 2011; Atari *et al.*, 2012). They give a clue regarding the early stage of cell transformation into osteogenic cells based on the expression of specific markers, i.e. ALP. Additionally, they provide evidence of the late stage of differentiation, such as mineral deposition, one of the osteoblast cells' functions (Nanci, 2017). The capacity of osteogenic differentiation demonstrated by hPDLCs in this study comes to confirm the findings of previous studies despite using a different type of inductive medium (Gay *et al.*, 2007; Ji *et al.*, 2013; Chen *et al.*, 2013).

Moreover, the hPDLCs showed signs of chondrogenic differentiation **(3.4.4.2.)** with a change in cellular morphology and lacune formation. Also, there was evidence of extracellular deposition of aggrecan. These signs were presented in many studies as proof of chondrogenic differentiation (Pittenger *et al.*, 1999; Gay *et al.*, 2007; Choi *et al.*, 2013). These findings agreed with that described previously by Miletic *et al.* (2014), Choi *et al.* (2013) and Xu *et al.* (2009). However, due to the time limitations, further

IHC examination is still required to identify the type of collagen formed and to confirm the previous findings (Barry *et al.*, 2001; Gay *et al.*, 2007).

Another important finding in the current study was the adipogenic differentiation of hPDLCs following their *in vitro* culture in adipogenic medium. The hPDLCs expressed the typical features of adipogenic transformation presented by Mor-Yossef Moldovan *et al.* (2019). These features can be summarised by an increase in the cells body accompanied by formation intracellular lipid droplet that can be detected with Oil red stain. Also, there was an increase in intercellular spaces. Some studies recorded this adipogenic transformation of hPDLCs, including Gay, I. *et al.* (2007) and Miletic *et al.* (2014). Collectively, it was confirmed that hPDLCs have the multilineage differentiation capacity of MSCs.

The hPDLCs of the three donors in this study have demonstrated the characteristics of MSCs defined by ISCT. However, there was a variation in the cellular proliferation, levels of surface markers expression and differentiation capacity between the different donors' cells. This variation could be linked to donor variability. Due to the limited availability of human tissue samples in the tissue bank, hPDLCs for this study were isolated from male and female donors. However, all donors' age group was within a relatively close range (19-25 years). Marchesan *et al.* (2011) suggested that several donor-related factors, e.g. donor age, smoking and certain pathological conditions, influence the *in vitro* behaviour of primary periodontal ligament cells.

Moreover, Siegel *et al.* (2013) confirm the difference in the growth rate of BMMSCs isolated from different sex donors. Also, they found that cellular activities were lowered in cells isolated from old-age donors. However, the cell differentiation capacity was not affected by either the donor age or gender. In this regard, Trivedi *et al.* (2019) refer to the importance of examining donor variability and characterise the isolated cells before their application in cell-based therapy. Although cells isolated from the bone marrow of different donors expressed the MSCs markers and differentiated into main cells lineage, they found that these cells showed various morphologies and different proliferation rates.

In contrast, Diomede *et al.* (2017) found a non-significant difference in the proliferation rate and level of expression of MSCs markers between hPDLCs isolated from healthy and multiple sclerosis patients. However, this

study did not investigate the effect of other donor-related factors such as age or gender. Accordingly, the evaluation of primary cells' quality, in terms of proliferation and differentiation capacity, is of great importance in tissue engineering and cell-based therapy. It could ensure the selection of the best donor based on cells performance. Also, it will help optimise culture condition according to the characteristics of each cells' population.

3.6 Conclusions

The current study's findings confirm the mesenchymal stromal characteristics of hPDLCs, including their potential to adhere to plastic surfaces, higher expression of mesenchymal stem cells markers with a limited expression of haemopoietic stem cells markers. It was also proved that hPDLCs could differentiate *in vitro* into osteogenic, chondrogenic and adipogenic cells lineages. However, these characteristics were found to vary among donors. Accordingly, it is crucial to evaluate the characteristics of primary hPDLCs before their use for research or therapeutic purpose.

Based on the current chapter's finding, the isolated hPDLCs can be described as hPDLSCs. Thus, the latter term will replace hPDLCs in the next chapters.

Chapter Four: Evaluation of biological efficacy of Bmf silk as a potential scaffold to support hPDLSCs proliferation and osteogenic differentiation

4.1 Introduction

Scaffolds are commonly used in tissue engineering and regenerative medicine to mimic the 3D tissue environment by establishing a skeleton for the adhesion and spreading of cells. Also, it plays a pivotal role by providing the essential mechanical and biochemical signalling that governs cellular activities, including proliferation and differentiation. The scaffold material must be chosen carefully based on specific criteria such as its biocompatibility, biodegradability, and mechanical characteristics, which could differ according to the regenerated tissue type. Other factors like the ease of preparation, castability and expense are also important.

For periodontal regeneration, many scaffold materials have been introduced and evaluated *in vitro*, *in vivo*, and clinically. However, due to the periodontium's complex biological nature, the ideal scaffold that could support the regeneration requirements for bone, cementum, and PDL simultaneously is still under research.

Bmf silk properties make it a good scaffold material option for the regeneration of many tissues such as bone, cartilage, ligament, and cornea. It is a natural polymer that is isolated from the cocoon of the mulberry silkworm. Besides its superior mechanical properties and adjustable degradability, in comparison to other natural polymers, it can be cast in different forms, e.g. porous foam, fibre and film.

Thus, Bmf silk presents a potential scaffold material for periodontal tissue regeneration. Unfortunately, a limited number of studies are available in this field. Also, most of the *in vitro* studies used Bmf silk in combination with other materials but not as a single component. The *in vivo* and periodontal clinical studies focused on investigating the use of silk material either as a film layer to guide the regeneration process or as a vehicle to deliver the antimicrobial agents, e.g. tetracycline.

Accordingly, the present study attempts to cover this gap by investigating Bmf silk material's biocompatibility in terms of immunogenicity and cytocompatibility. Additionally, to evaluate its role in supporting the growth of primary hPDLSCs both *in vitro* and *in vivo*.

4.2 Aim

The present chapter aims to evaluate the biological efficacy of 3D, porous, Bmf silk material when used as a scaffold to support the proliferation and osteogenic differentiation of primary hPDLSCs *in vitro* and *in vivo*.

4.3 Materials and methods

As shown in previous chapters, this section describes the materials and methods used in this chapter, each according to the related experiment. For the immunogenicity assay, the human THP-1 cell line was purchased from Sigma-Aldrich (Gillingham, UK). These cells were isolated from the peripheral blood of a one-year-old male with an acute monocytic leukaemia, and they have the morphology of monocyte. The hPDLSCs for the current experiments were isolated from healthy human teeth as described in **2.2.1**. Moreover, characterised, as demonstrated in **chapter four**. The culture media were supplied from Lonza (Slough, UK); while tissue culture reagents and supplements were all from Sigma-Aldrich (Gillingham, UK) unless otherwise stated. Corning (Flintshire, UK) vessels were used for cells culture.

4.3.1 Extraction of Bmf silk, 3D scaffold preparation, and scaffold sterilisation

Bombyx mori fibroin silk scaffolds were prepared by Dr John Hardy's team, a senior lecturer in materials chemistry at Department of Chemistry, and Materials Science Institute, Lancaster University. The extraction process briefly involved boiling Bombyx mori silkworm cocoons in an aqueous solution of Na_2CO_3 (0.02 M) for 20 min. Afterwards, the extract was washed thoroughly with distilled water; then silk fibroin was dissolved in LiBr (9.3 M) at 60^{o}C for 4 hrs. Following two days of dialysing, the aqueous solution was subjected to several rounds of centrifuging at 9000 rpm at 4^{o}C for 20 min each. The extracted silk fibroin solution (8 w/v%) was stored for several weeks at 4^{o}, before it being poured in glass Petri dishes (Falcon™, Loughborough, UK) filled with NaCl particles, of 425-500 µm in size. After 48 hrs of drying at RT, the construct immersed over two days in six changes of 2 L of water to remove the salt particles to have the porous structure of the scaffold. (Nazarov *et al.*, 2004; Rockwood *et al.*, 2011; Hardy, J.G. *et al.*, 2015). Scaffolds were cut into a cylindrical shape of around (4.5 mm × 3 mm) using a lyophilised biopsy punch and stored at RT.

Several sterilisation methods of silk materials have been investigated to determine their effect on the chemical, physical and mechanical properties of silk material itself, in addition to the biological effect on cells. However, the literature agrees that sterilisation of silk material with 70% ethanol could cause minor effects regarding structural, mechanical properties and cell

viability in comparison to other sterilisation methods such as autoclaving, exposure to ethylene oxide using dry heat (Siritientong *et al.*, 2011; Hattori *et al.*, 2012; Gil *et al.*, 2014; Hofmann *et al.*, 2014; Rnjak-Kovacina *et al.*, 2015). Accordingly, the prepared Bmf silk scaffolds were washed with sterile 1X PBS, then immersed for 30 mins in 70% of ethanol in 1X PBS at RT. Subsequently, the scaffold was washed with three changes of 1X PBS to remove any residuals and left to dry inside laminar flow hood. All sterile scaffolds were kept in secure, sterile, 15 mL polypropylene tubes (Falcon™, Loughborough, UK) and stored at 4^{o}C.

Dr Hardy performed many investigations to determine the physicochemical characteristics of the prepared Bmf silk scaffold, including porosity determination, swelling properties, mechanical properties under compressive loading, X-ray photoelectron spectroscopy (XPS), Fourier Transform infrared spectroscopy (FTIR), and *in vitro* degradation assay (Hardy, J.G. *et al.*, 2015). Thus, the current study focused more on examining the biological reaction of cells in response to this material.

4.3.2 Characterisation of the Bmf silk scaffold

4.3.2.1 Macroscopic inspection

The prepared Bmf silk scaffold's macroscopic appearance was inspected with a Leica TL4000 BFDF microscope supplemented by Leica KL1500 light source (Wetzlar, Germany). Images were recorded using Olympus C-7070 wide zoom camera (Tokyo, Japan). Scaffold's dimensions were measured using ImageJ 1.52a software with a physical ruler to calibrate the scale bar.

4.3.2.2 Examining microscopic scaffold structure with SEM

To examine the surface morphology and scaffold structure, a Hitachi S3400N-VP SEM (Tokyo, Japan) was used at environmental, low vacuum, variable pressure mode, as described previously in **2.5.2.**

4.3.3 Evaluation of the biocompatibility of Bmf silk scaffold

The biocompatibility of the prepared scaffold was evaluated through a series of investigations, including immunogenicity assays, metabolic activity assay, examining cells viability as well as osteogenic differentiation capacity as explained below:

4.3.3.1 Analysing the expression of inflammatory cytokine for THP-1 cells in response to their exposure to Bmf silk material using rtPCR

Tumour necrosis factor-α (TNF-α) and Interleukin-1β (IL-1β) are inflammatory cytokines that initiate and mediate the innate immune response and could activate adaptive immune system too (Strieter *et al.*, 1993; Beutler, 1999; Ott *et al.*, 2007). Measuring these markers' expression levels in the THP-1 cells, human monocyte cells could help determine certain materials' cytocompatibility (Schutte *et al.*, 2009; Bylski *et al.*, 2009; Wray *et al.*, 2011).

THP-1 cells were first thawed, transferred into 15 mL conical tube, and slowly mixed with 4 mL of RPMI-1640 medium (supplemented with 10% FBC, 200 mM L-Glutamine, and 100 unit/mL Penicillin-Streptomycin). Afterwards, the cells were centrifuged 150 rcf for 5 mins to have the cell pellet, followed by removing transfer medium and resuspension in fresh RPMI-1640 medium.

The THP-1 cell passage protocol involved counting the cells within the suspension to determine the required cell seeding density, which were then resuspended in RPMI-1640 medium and incubated in a T-175 flask at 37^{o}C; 5 % CO_2. The medium was exchanged every three days following the supplier protocol. The immunogenicity experiment included four groups, each prepared in triplicate, as demonstrated in Table 4-1.

All four groups were cultured in the same 24-well plate to normalise the environmental effect.

The first group included three wells; each contained 1 ml of THP-1 cells suspension at a density of 1.5 x 10^6 cell; while samples of the second group were prepared by dissolving the contents of phorbol 12-myristate 13-acetate (PMA) vail (Sigma-Aldrich, Gillingham, UK), a potent tumour promoter, in 1 mL of DMSO with gentle mixing. Then, 2 µL of this mixture was added to 200 µL of plain RMPI-1640 medium. Finally, 31 µL of latter was mixed with 1 mL of THP-1 cells suspension, at a density of 1.5 x 10^6 cell. Three samples of this preparation were prepared in 24-well plate.

To prepare samples of group three, 3D COL-1 scaffold was prepared by mixing a 331.1 µL of Bovine skin COL-1 gel stock (Sigma-Aldrich, Gillingham, UK) with 7.6 µl of sterile 1M NaOH plus 661.3 µl of plain RPMI-1640 medium to make a total volume of 1 mL. This volume was poured at

the bottom of three wells, with the entire 24-well plates then incubated in the tissue culture incubator to allow for gel to solidify.

The fourth group included sterile Bmf silk scaffolds incubated in the 10 % FBC RPMI-1640 medium at 4^{o}C overnight to enhance their surface modification. Then each of the three scaffolds was placed in an individual well. One millilitre of THP-1 cells suspension at a density of 1.5×10^{6} cells was added to each sample of group three and four. Medium for all groups was replaced every three days. To evaluate inflammatory cytokines expression, cells of all groups were harvested at days 1, 3, and 7.

Table 4-1: Experiment design for Bmf silk scaffolds immunogenicity assay

Code	Group	Scaffold	Clue	Timepoints	n
1	Monolayered THP-1 cells (alone)	None	Negative control for 2D culture	One day	3
				Three days	3
				Seven days	3
2	Monolayered THP-1 cells with PMA	None	Positive control for 2D culture	One day	3
				Three days	3
				Seven days	3
3	THP-1 cells in 3D culture	3D COL-1 gel (bovine skin)	Negative control for 3D culture	One day	3
				Three days	3
				Seven days	3
4	THP-1 cells in 3D culture	Bmf silk	Experimental	One day	3
				Three days	3
				Seven days	3

4.3.3.1.1 Cells harvesting

Cell suspensions were collected directly from every well and centrifuged at 350 rcf for 5 min to collect cell pellet at each time point. Then, each sample's contents were mixed with 1 mL of 1X PBS in Eppendorf tube and centrifuged again to ensure removal of culturing medium.

Other cells that remain attached to wells and scaffold surfaces were incubated in 300 µL of 1× PBS at 37°C / 5% CO_2 for 30 min to remove the excess medium. Following aspiration of the PBS, 300 µL of RLT/β-ME (prepared by mixing RLT buffer (Qiagen, Hilden, Germany) and β-Mercaptoethanol (Sigma-Aldrich, Gillingham, UK) in a ratio of 10:1) was added to each well and incubated at RT for 5 min to initiate cells lysis.

The volume of harvested cells was maximised by adding the contents collected in the first step (cells suspension) to one harvested in the second step (attached cells to the scaffold). This protocol was followed in groups three and four. Final volume for each sample was stored at -80^{o}C until samples of all periods are ready for the next step.

4.3.3.1.2 Extraction of RNA, cDNA preparation, and measuring levels of genes expression using qRT-PCR

The following steps were performed according to the procedures described previously in **2.3.5.** Briefly, the extracted RNA lysates were homogenised by allocating them into QIAshredder homogeniser (Qiagen, Hilden, Germany) followed by centrifuging for 2 min at 350 rcf to ensure the higher yield of RNA. The RNA extracts then mixed with 300 µl of 70% ethanol, with the final mixture run through several purifications steps to isolate 30 µl of pure RNA extract in DNase/RNase-free dH_2O.

The quality and quantity of collected RNA were measured by testing 1 µl of RNA extract for each sample using NanoDrop spectrophotometer ND1000. Purity was measured based on the ratio of absorbance 260/280 nm, with a value > 1.8 and < 2.0 regarded as the appropriate level of purity. The final extracts were then stored at -80^{o}C until the next treatment.

Preparation of cDNA includes dilution of high concentration RNA extracts with UltraPure DNase/RNase-Free Distilled water (Thermo Fisher Scientific, Loughborough, UK) to a concentration of 160 ng/µl. The final concentration was treated with 1 µl enzyme, 10 µl 10x buffer. Both are from High Capacity RNA-to-cDNA kit (Applied Biosystems, California, United States), with the

rest of the volume to 20 µl was completed with nuclease-free water. Using F. MJ Research PTC-100 Thermocycler, the reaction was conducted by incubation for 60 min at 37oC, followed by another 5 min at 95oC to ensure the enzyme's denaturation. The prepared cDNA then stored at -20^{o}C for the rtPCR step.

The last step involved preparing triplicates for all samples and controls, aliquoted in a semi-skirted PCR 96-well plate. All expression levels of target genes were compared to Glyceraldehyde 3-phosphate dehydrogenase (GAPDH), which is used as a housekeeping gene (Ragni *et al.*, 2013), while the specific primers were human IL-1β and human TNF-α.

The amplification reaction proceeded by making a volume of 20 µL; this includes 10 µL of gene expression master mix, 1 µL of TaqMan assay probe (Applied Biosystems, California, United States), as well as 9 µL of prepared cDNA. Two kinds of negative controls were prepared; the first includes the same mixture without a sample (non-template negative control), with the other, does not contain the enzyme (RT-negative control). The value of the cycle threshold (Ct) was recorded, and $^{\Delta\Delta}$Ct was calculated by normalising the $^{\Delta}$Ct of each sample to that of THP-1 cells control group of specific time point. Furthermore, the relative levels of genes expression were calculated using the $2^{-\Delta\Delta Ct}$ method (Livak and Schmittgen, 2001).

Two-way ANOVA test with the Dunnet test was dependent on statistically comparing the expression level of inflammatory cytokines between the three groups and the first group (control) at a *p*-value of ≤ 0.05.

4.3.3.2 Comparison of the efficiency of static and dynamic cells' seeding techniques

Ten sterile samples of Bmf silk material were divided into two groups and incubated in 3 ml of basal medium (supplemented with 10% FBS) for 24 hrs at 4^{o}C to modify the scaffold surface. Two seeding techniques were investigated; the static, where the pre-wet Bmf silk scaffold placed at the bottom of 15 mL sterile conical tube. Afterwards, 1 mL of cells suspension, at cells density of 4×10^{5} cells/cm^{2}, was slowly dispensed over the top surface of the scaffold. The dynamic technique involved placing the scaffold in a 1mL Eppendorf tube, where it immersed with 1 mL of cells suspension of same cells density (4×10^{5} cells/cm^{2}). The five Eppendorf tubes placed in MACSmix™ Tube Rotator (Figure 4-1), with rotation being activated at a speed of 12 rpm for 30-sec intervals followed by a 5-minute of pausing.

Figure 4-1: MACSmix™ Tube Rotator used for dynamic seeding of hPDLSCs on Bmf silk scaffold.

Samples of the two groups, static and dynamic seeding, were incubated for 24 hrs at 37ºC, 5% CO_2 to allow for the cells attachment and spreading over the scaffold surface.

The efficiency of seeding techniques was evaluated using: live/dead cell fluorescence labelling, the AlamarBlue metabolic activity assay in addition to manual counting of unattached cells.

Following 24 hrs of initial seeding, samples were transferred into a 24-well plate, where they were incubated in the dark for another 4 hrs in 1 mL/ scaffold/well of basal medium with 1:10 (v/v) of AlamarBlue reagent (Generon, Slough, UK). The assay then proceeded as described previously in **2.3.1.**

To count the unattached cells to the Bmf silk material, the cells adhering to the seeding vessel were detached using 0.5mL of a 0.25% trypsin/EDTA solution and re-suspended in the basal medium along with the remaining volume of cells seeding suspension. Those cells were manually counted as described in **2.2.2.** The efficiency of cell seeding for both techniques was calculated as follows:

$$Cell\ seeding\ efficiency\ (\%) = \frac{initial\ number\ of\ cells - unattached\ cells}{initial\ number\ of\ cells} \times 100$$

Data of both experiments were statistically analysed using Unpaired t-test with Welch's test at *p*-value ≤ 0.05.

Moreover, the viability of hPDLSCs attached to the Bmf silk scaffold was examined by labelling live and dead cells with fluorescent stains. The samples were stained with green-fluorescent calcein-AM and red-fluorescent ethidium homodimer-1 (Thermo Fisher Scientific, Loughborough, UK) and examined as described in **2.2.5.**

4.3.3.3 Evaluation of long-term viability of hPDLSCs in response to Bmf silk scaffold

4.3.3.3.1 Measuring the metabolic activity of hPDLSCs using the AlamarBlue assay

AlamarBlue metabolic activity assay was performed for samples dynamically seeded with hPDLSCs at days 1, 7 and 14. To perform the assay, the same protocol described in **2.3.1.** was followed.

4.3.3.3.2 Assessment of hPDLSCs viability using live/dead cells' fluorescent markers

Viability of hPDLSCs seeded on Bmf silk scaffold was investigated again following four weeks of initial seeding. Samples were labelled with both green-fluorescent calcein-AM and red-fluorescent ethidium homodimer-1 and examined as described previously in **2.2.5.**

4.3.4 Evaluation of hPDLSCs' behaviour *in vitro*, 3D, osteogenic culture condition

4.3.4.1 Preparation of hPDLSCs-Bmf silk constructs

Constructs of hPDLSCs-Bmf silk scaffold were prepared by seeding hPDLSCs dynamically as described previously in **4.3.3.2.** The constructs were incubated *in vitro* for four weeks in an osteo-inductive medium, with media being replaced every three days. Constructs were then subjected to several examinations at different time points to evaluate cells behaviour in the 3D environment.

4.3.4.2 Identification of cellular distribution using SEM

At the end of four weeks of *in vitro* culture, the constructs were transferred into a new 24-well plate and washed with two changes of 2 ml of 1X PBS to ensure removal of the medium. All samples were fixed overnight with 10% NBF at RT. Then, they were washed with two changes of 1X PBS to ensure removal of the fixative solution. The construct surfaces were examined by SEM as described previously in **4.3.2.2.** This examination helped in the

visualisation of the pattern of cells spreading and growth over the scaffold surface.

4.3.4.3 Histological and immunohistochemical examinations

Following four weeks of initial seeding, constructs were processed and sectioned as described previously in **2.4.1.** and **2.4.2.** The cellular growth on/in the scaffold surface was investigated by staining sample sections with Haematoxylin, Van Gieson's, and von Kossa's stains referred to in sections **2.4.3.** , **2.4.4.** and **2.4.5.**, respectively. Furthermore, the expression of COL-1, OCN and OPN markers were detected with immunohistochemical examination as described in **2.4.8.**

4.3.5 Evaluation of hPDLSCs behaviour *in vivo*, 3D, animal model

4.3.5.1 Preparation of hPDLSCs-Bmf silk constructs

To better understand the behaviour of hPDLSCs in a living animal model, constructs of hPDLSCs-Bmf silk scaffold (n=3) were prepared by dynamic cells seeding technique as described previously in **4.3.3.2.** The constructs were incubated in basal medium for five weeks *in vitro* to allow for the proliferation and distribution of hPDLSCs over Bmf silk scaffold surfaces.

The diffusion chambers (DCs) model was utilised for the *in vivo* work. This technique is based on placing the investigated cells/tissue sample inside a sterile chamber. This chamber allows for the passage of nutrients and growth factors from the host to the sample. However, it prevents the migration of the host's cells and tissues into the chamber space. Thus, it helps in providing the essential supplements for the survival of the sample, and permit for a long time *in vivo* evaluation of its behaviour without the need to intervene during the experiment period (Algire *et al.*, 1954; Osoba and Miller, 1964; Ashton *et al.*, 1984; Nakano *et al.*, 2009).

The EMD Millipore's Diffusion Chamber Kits (Darmstadt, Germany) used in this study, which includes clear Plexiglas® chamber's rings (without hole) in addition to the 13 mm, hydrophobic filter membrane with a pore size of 0.22 µm. Three rings were glued together with cyanoacrylate superglue to accommodate the prepared construct's size (Loctite, Farnell, UK). The first filter membrane was attached to the bottom of the chamber's rings with cyanoacrylate superglue again. After hardening of the glue, the whole

chamber was sterilised by exposure to the UV-C radiation of 254 nm wavelength for 15 min for each side (Meechan and Wilson, 2006).

Immediately before the surgical implantation in the animal model, the hPDLSCs-Bmf silk construct, which was incubated *in vitro* for five weeks, was transferred into the DC and immersed in 0.5 mL of plain medium. Finally, a second filter membrane was carefully glued to seal the DC contents (see Figure 4-2). All these steps were performed inside a laminar

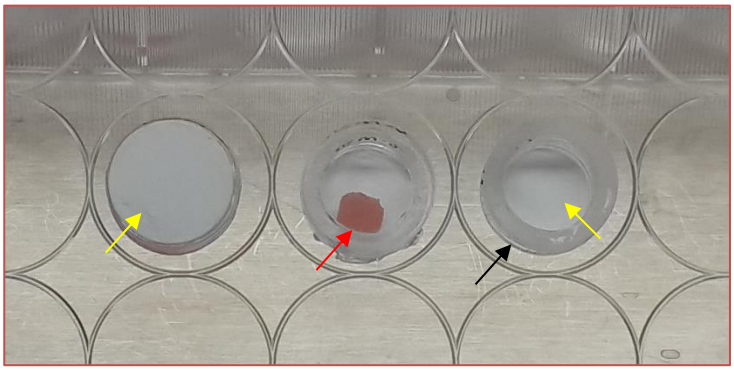

Figure 4-2: Diffusion chambers containing a hPDLSCs-Bmf silk construct. Chambers composed of three Plexiglas® rings glued together (black arrow), with both sides sealed with white, hydrophobic filter membrane (yellow arrows). Constructs (red arrow) were placed inside the chamber space and immersed in a basal medium.

flow hood to minimise the risk of contamination.

In the same way, the control group was prepared. However, instead of hPDLSCs-Bmf silk construct, an unseeded Bmf silk scaffold was placed in the DC space. Both groups were prepared in triplicate.

Chambers of the two groups were transferred within sterile, sealed 24-well plates to the surgical theatre in preparation for the implantation procedure.

4.3.5.2 Surgical implantation of DCs into CD-1 nude mice

In the present study, the *in vivo* work was performed by Mr Fahad Al-Dabbagh (personal licence number 37942) and Dr Xuebin Yang as a project holder (project licence number 70/8549). The University of Leeds Home Office granted the licences following training course for personal licence applicants for PIL categories A, B and C.

The CD-1 nude mice were the animal model of choice for the current study to exclude the possible adverse immunological effect on the constructs. The hPDLSCs were isolated from human species (Sharkey and Fogh, 1984;

Fidler, 1986). Three, male CD-1 mice of eight weeks age and 40g each (Figure 4-3/B) were utilised for this *in vivo* study.

The experimental design of the current study involved implantation of two DCs in each of the three mice. The first DC contained the hPDLSCs-Bmf silk construct, while the second (control) contained the unseeded Bmf silk scaffold. Both samples were implanted in the peritoneal space of the animal, each on a separate side.

The surgical procedure was started by anaesthetising each mouse inside an inhalation chamber (Figure 4-3/A) and administration of 100 % w/w of isoflurane (IsoFlo Zoetis, Leatherhead, UK) as a vapour supplied using a special vaporiser (Vet Tech Solutions Ltd, Congleton, UK). The initial dose of isoflurane was 5 L/min (Figure 5-3/C), which reduced to a maintenance dose of 2.5 L/min during the surgical procedure. The oxygen was supplied at a rate of 5 L/m throughout the procedure (Figure 4-3/D).

To access the mouse peritoneal space, a 1.5 cm incision was made using a surgical blade (size 15) at the midline of the animal ventral side. Then, the peritoneal space was approached using the surgical blade and artery forceps. Care was taken to avoid any damage to the surrounding and underlying tissues and organs. Afterwards, two DCs were inserted gently into the peritoneal space, with each one of them being on either side. The wound was then closed with absorbable coated 5/0 vicryl suture for the peritoneal wall, and non-absorbable 5/0 polyamide sutures for the abdominal skin (Miller Medical Supplies, Newport, UK). Surgical steps were illustrated in Figure (4-4). The mice were labelled by pinching their ear while they are anaesthetised. Intraperitoneal injection of 0.3 mg/mL of an analgesic (Vetergisic, CeVa, Amersham, UK) was administrated to each animal to reduce the possible post-operative pain.

Finally, the mice transferred to a pre-warmed chamber for the recovery, before being housed again in an Individually Ventilated Cage (IVC) system. The animals were monitored daily by the animal house technicians at the University of Leeds, and twice weekly by the operator for any possible postoperative complications.

At the end of this experiment (7^{th} week), the mice were sacrificed according to the Home Office approved Schedule 1 method. An incision was made at the same initial surgical site to extract the DCs. One of DC's filter membranes was removed, with samples being extracted and washed with

1X PBS. Afterwards, constructs were fixed overnight with 10% NBF at RT to prepare for the next examinations.

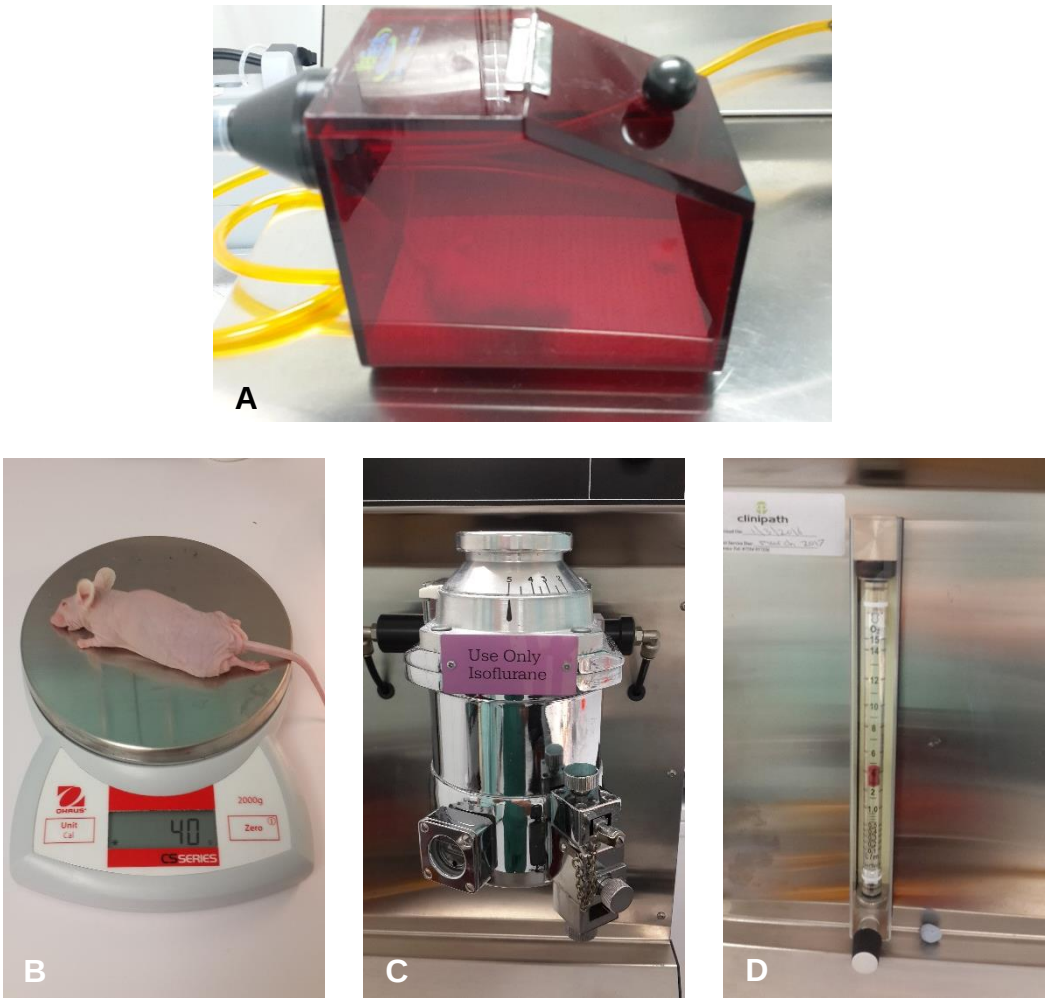

Figure 4-3: Equipment used for anaesthetising the CD-1 nude mice. A: An inhalation chamber for anaesthetising the animals through isoflurane inhalation B: an anesthetised CD-1 nude mouse being weighted (40 g). C: isoflurane vaporiser dispensing the induction dose of 5 L/m. D: Oxygen supplier set at a flow rate of 5 L/m.

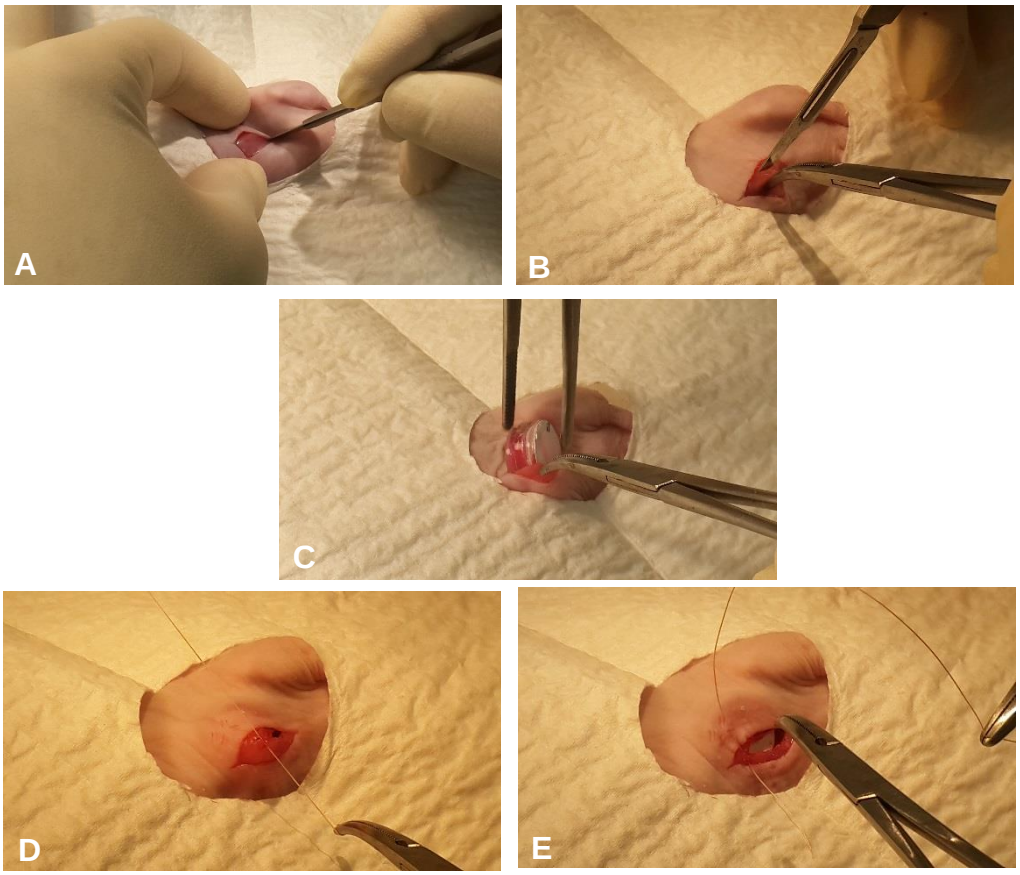

Figure 4-4: Surgical steps for implantation of diffusion chambers in the peritoneal space of CD-1 nude mice. A: Initial surgical incision at the midline of the animal ventral side. B: secondary incision to access the peritoneal space. C: Insertion of a diffusion chamber, which contains the construct. D: Closure of peritoneal space with absorbable coated 5/0 vicryl suture. E: Skin closure with non-absorbable 5/0 polyamide suture.

4.3.5.3 Identification of scaffold and constructs structures using SEM

Fixed samples were washed with two changes of 1X PBS to ensure removal of the fixative solution. The scaffolds and constructs were examined by SEM as described previously in **4.3.2.2.**

4.3.5.4 Histological examination

All extracted scaffolds and hPDLSCs-Bmf silk constructs were processed and sectioned as described previously in **2.4.1.** and **2.4.2.** The *in vivo* cellular growth was investigated by staining the sections with Haematoxylin, Van Gieson's stains referred to in sections **2.4.3.** and **2.4.4.**

4.4 Results

4.4.1 The macroscopic and microscopic structure of prepared Bmf silk scaffold

The prepared scaffold has a cylindrical shape of an average dimension of 4 mm × 3 mm. It was characterised by a rough, porous surface, as shown in Figure 4-5/A. SEM images presented more details about the scaffold topography, which demonstrated an irregular surface with many different size projections. The scaffold structure was composed of a large number of spherical-like empty spaces (pores) of an average diameter of 350 µm surrounded by the Bmf silk material. Furthermore, these pores' wall is connected by holes of different shapes and sizes with adjacent spaces. Bmf silk material forms an extensive frame surrounding the pores (Figure 4-5/B and 4-5/C).

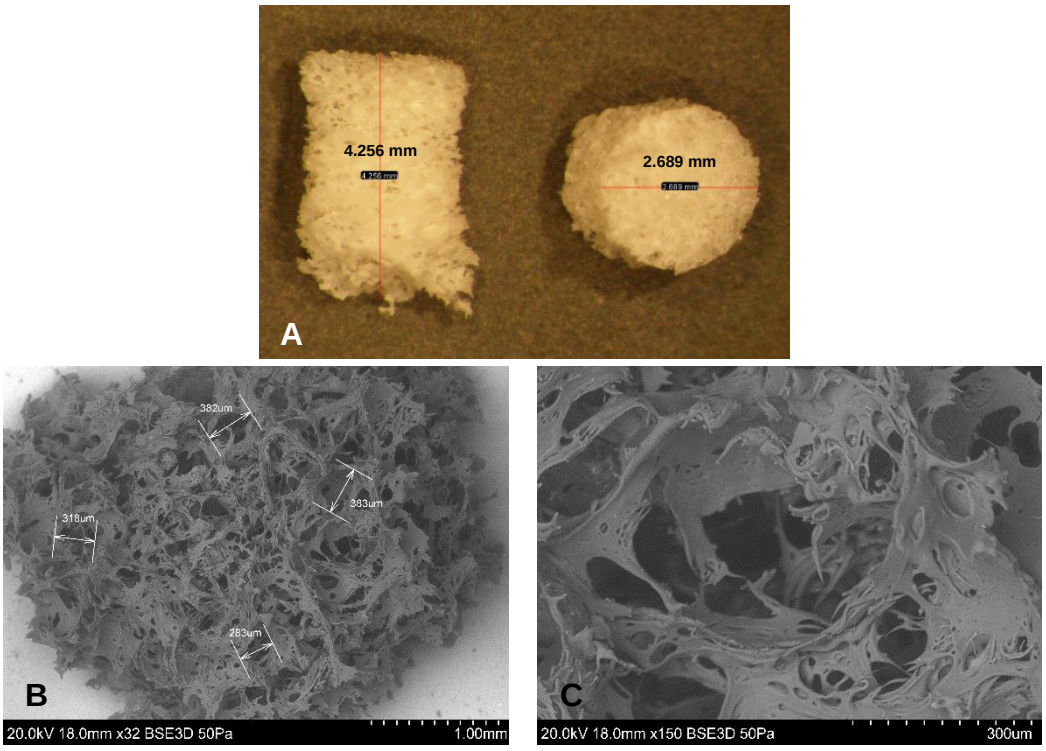

Figure 4-5: Surface morphology and architecture of Bmf silk scaffold. A: macroscopic structure of 3D, porous, cylindrical, Bmf silk scaffold (~ 4 mm x 3 mm). B: SEM image showing the porous structure of Bmf silk scaffold with pore size ranging between 283 -383 µm. C: SEM image demonstrating a single spherical-like space with many voids of different size in its wall, and many of micro spike-like projections.

4.4.2 Biocompatibility of Bmf silk scaffold

4.4.2.1 Inflammatory response of THP-1 cells against exposure to the Bmf silk material

After one day of THP-1 cell culture, the immunogenicity assay results revealed an increased TNF-α expression level in groups where THP-1 cells culture with PMA, 3D COL-1, and Bmf silk scaffold (2nd, 3rd and 4th group respectively). At this time point, the PMA group expressed a highly significant level (*p*-value = 0.0001) of TNF-α compared to the control group. The difference between COL-1 and Bmf silk scaffold groups from one side and monolayer control group from the other was statistically non-significant (*p*-value = 0.902 and 0.897 respectively), as shown in Figure 4-6/A.

On day three, the three groups (2nd, 3rd, and 4th) showed a reduction in the TNF-α levels. The statistical analysis revealed a non-significant difference between the three groups and control group (*p*-value = 0.990, 0.993 and 0.787), see Figure 4-6/A. Interestingly, cells exposed to Bmf silk scaffold expressed the lowest level compared to the other three groups, including the control one.

Similarly, on day seven, all groups kept the pattern of reduction in TNF-α expression levels. Again, with a non-significant difference between the three groups and the control group. The PMA group showed a further reduction, with the least expression among this group's three-time points. However, the Bmf silk scaffold induced a slight increase at day seven compared to the level expressed for the same group on day three (Figure 4-6/A).

It was essential to compare the response induced by 3D COL-1 and Bmf silk as both groups represent the reaction of THP-1 cells toward the 3D scaffold. The statistical comparison showed a non-significant difference between those two groups at the three-time points (*p*-value = >0.999, 0.205, 0.934 respectively). It was also evident that with time, the reaction toward

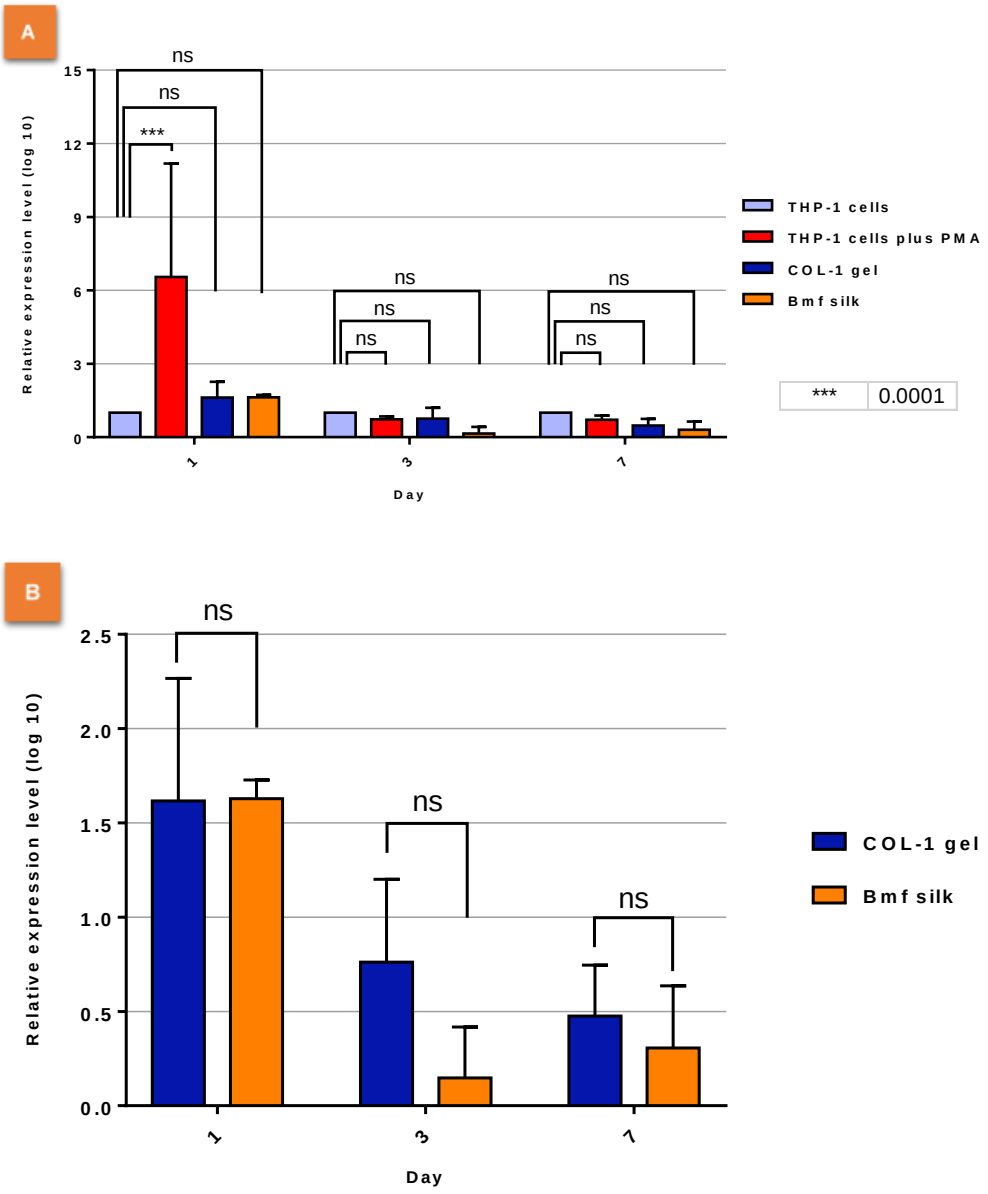

Figure 4-6: Relative expression levels of TNF-α for THP-1 cells against exposure to Bmf silk material. A: TNF-α levels among the four groups (1st : monolayered THP-1 cells, 2nd : THP-1 cells with PMA, 3rd : THP-1 cells with 3D COL-1 gel, 4th : THP-1 cells with Bmf silk material) measured at day 1, 3, and 7. B: Comparison of TNF-α levels for groups three and four at the three time points. Statistical analysis was performed with two-way ANOVA test with Dunnett test was used at *p*-value ≤ 0.05.

Bmf silk scaffold was becoming less, and it was less than that induced by COL-1 gel at days three and seven as shown in Figure (4-6/B).

The results of IL-1β expression were not far from those of TNF-α. At day one, all three groups, PMA, 3D COL-1, and Bmf silk, demonstrated the highest level during this experiment's three-time points. Again, the PMA

induced a highly significant IL-1β expression level compared to that of the control group (1st group), where *p*-value was 0.0001. In contrast, the effect induced by 3D COL-1 and Bmf silk was statistically non-significant compared to that of the control group (*p*-value = 0.999, 0.999 respectively).

On day three, the IL-1β levels for 2nd, 3rd and 4th groups showed a noticeable reduction. However, PMA still demonstrated the highest expression levels, which was statistically significant as *p*-value was 0.025. Interestingly, Bmf silk stimulated the minimum response among the four groups.

Day seven saw a slight increase in the response of THP-1 cells to PMA, which was significant in comparison to that of the control group (*p*-value =0.0012). Furthermore, 3D COL-1 showed a further reduction in the level of IL-1β that was the lowest during the entire experiment. There was a slight increase in the inflammatory response in IL-1β expression, against Bmf silk compared to day three. However, the difference between expression levels for 3D COL-1 and Bmf silk remains non-significant to that of the control group (Figure 4-7/A).

Comparing the results of 3D COL-1 and Bmf silk throughout the experiment's three-time points revealed a non-significant difference between the two groups. While the results were very close at day one between the two materials, the difference was clearly in favour of Bmf silk on day three. However, this pattern reversed on day seven as Bmf silk showed a slight increase in the expression level, which was higher than that of 3D COL-1 Figure (4-7/B).

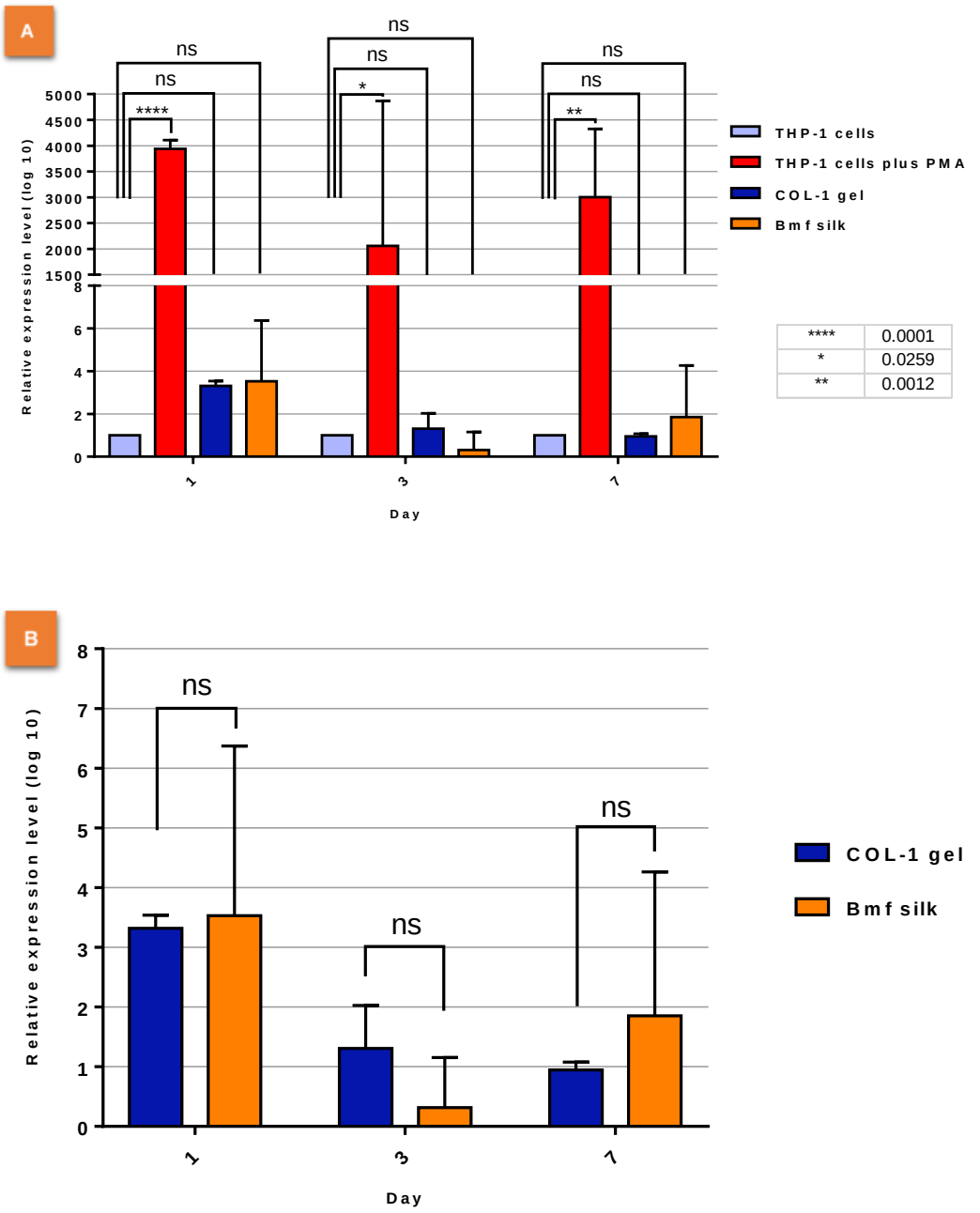

Figure 4-7: Relative expression levels of IL-1β for THP-1 cells against exposure to Bmf silk material. A: IL-1β levels among the four groups (1st : monolayered THP-1 cells, 2nd : THP-1 cells with PMA, 3rd : THP-1 cells with 3D COL-1 gel, 4th : THP-1 cells with Bmf silk material) measured at day 1, 3, and 7. B: Comparison of IL-1β levels for groups three and four at the three time points. Statistical analysis was performed with two-way ANOVA test with Dunnett test was used at p-value ≤ 0.05.

4.4.2.2 The efficiency of different cells' seeding techniques

Following the first 24 hrs of initial seeding, the efficiency of cells seeding techniques, static and dynamic, were evaluated using three different methods.

Comparison of cells' metabolic activity revealed a statistically significant difference between the two seeding techniques as *p*-value was 0.0005 (Figure 4-8). A higher rate of metabolic activity was observed in the samples where cells were seeded dynamically.

The difference between the two seeding techniques was not significant (p-value = 0.4085), in terms of the percentage of seeding efficiency based on counting unattached cells to the scaffolds. However, the mean of seeding efficiency for the dynamically seeded samples was higher than that of the statically seeding group (93.5% and 90.66% respectively) as demonstrated in Figure (4-9).

The fluorescent images demonstrated attachment and spreading of viable hPDLSCs over the scaffold surface in both groups after one day of initial seeding. Nevertheless, cells seeded by dynamic technique were more in number in comparison to those were seeded statically (Figure 4-10). Moreover, most of the cells in the dynamic samples were begin spreading at that point, with cells recognised by their flat cellular bodies and extended cytoplasmic processes. In contrast, many cells in the static seeding group were still showing a round morphology with less cytoplasmic processes. However, other cells showed evidence of the spreading over the Bmf silk scaffold (Figure 4-10).

Interestingly, cells in both groups demonstrated a circular pattern of distributions over the scaffolds, as shown in Figure (4-10). This pattern of distribution was corresponding to the morphology of the scaffold's pores. Furthermore, no dead cells were detected following the first 24 hrs of seeding in both groups.

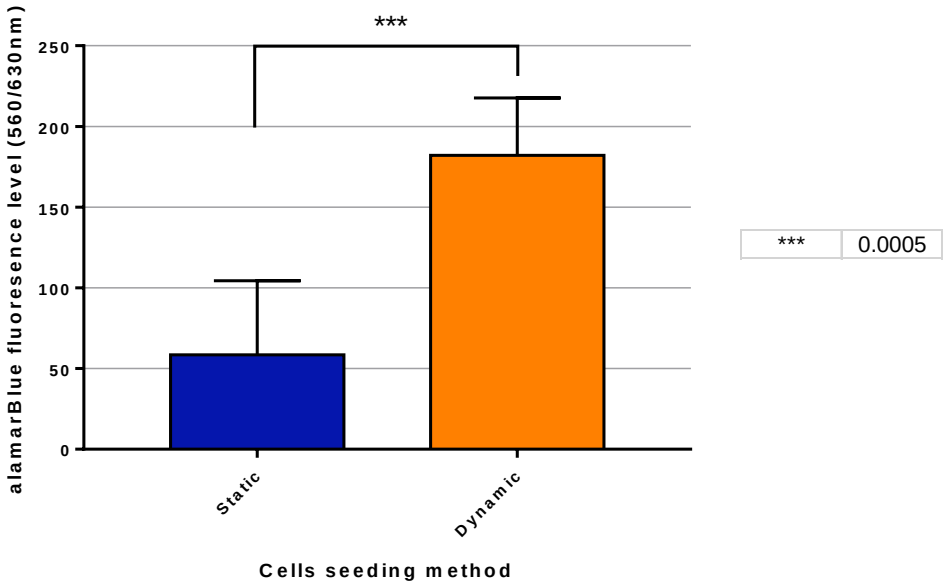

Figure 4-8: Effect of seeding technique (static/dynamic) on the metabolic activity of hPDLSCs measured with alamarBlue fluorescence assay. Results presented in mean ± SD of fluorescence levels for the two groups (n=3). Statistical analysis using Unpaired t test with Welch's correction showed a highly significant difference between the two groups.

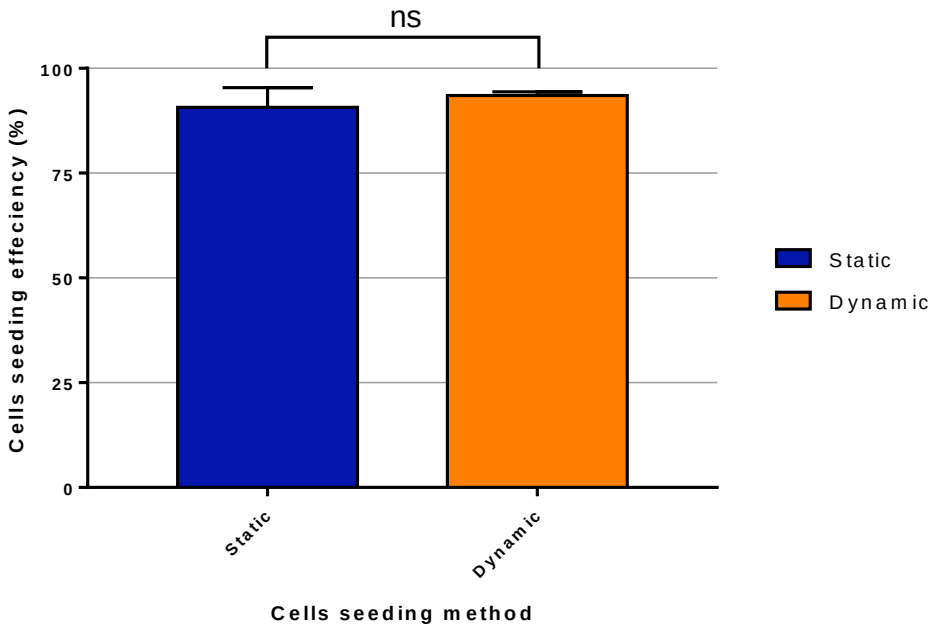

Figure 4-9: Comparison of cell seeding efficiency of static and dynamic seeding techniques following 24 hrs of seeding hPDLSCs. Results of Unpaired t-test with Welch's correction revealed a non-significant difference between the two techniques

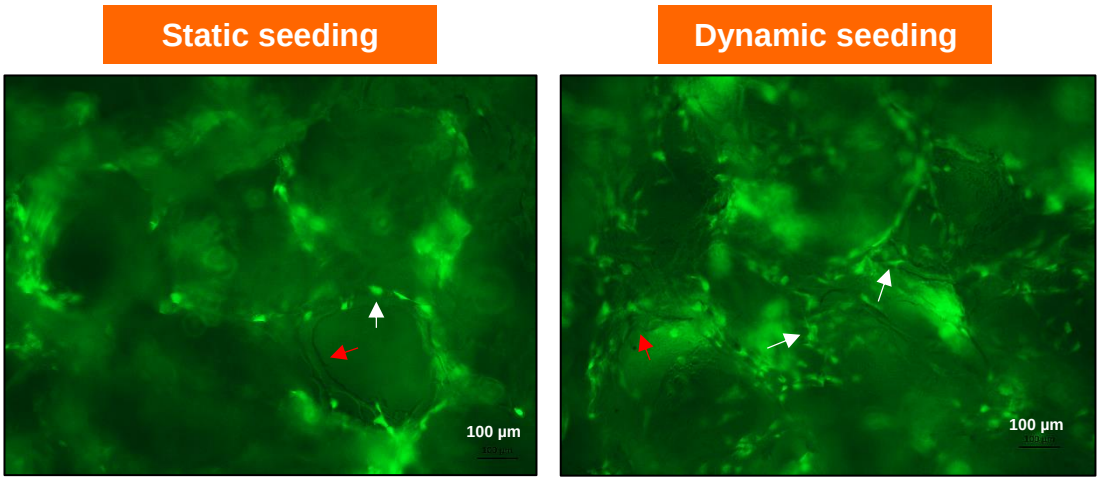

Figure 4-10: The effect of static and dynamic cells' seeding techniques on the viability of hPDLSCs seeded Bmf silk scaffold for 24 hrs. Cells were labelled with green-fluorescent calcein-AM to detect living cells (white arrows) and red-fluorescent ethidium homodimer-1 for dead cells. More living cells were recognised, spreading over the Bmf silk scaffold (red arrows) in the group were cells seeded dynamically. No dead cells were identified in both groups

4.4.2.3 The long-term viability of hPDLSCs in response to Bmf silk scaffold

During the first seven days, AlamarBlue assay results reflected an upregulation in the metabolic activity of hPDLSCs, which cultured in a 3D environment on Bmf silk scaffold. This increase was statistically significant between the first and seventh days (*p*-value = 0.001). However, on day fourteen, the metabolic activity slightly declined, but it was still higher in rate than that recorded at day one. The statistical analysis of results at day seven and fourteen revealed a non-significant difference in cells' metabolic activity.

Furthermore, fluorescent microscopy revealed a remarkable increase in the number of viable cells over four weeks. The cells continue growing over the external and internal surfaces of the scaffold and following its geometry. Additionally, an extensive mesh of cytoplasmic processes was formed and extended to cover a large Bmf scaffold area. Some of the pores of pores were entirely closed by the cells and their processes. However, pores with of larger diameter remain exposed, with cells growing on their internal wall only. A few dead cells were presented as a small, rounded, red-stained bodies that recognised at week four. These findings can be shown in Figure (4-11). Importantly, the Bmf silk scaffold demonstrated evidence of auto-

fluorescence that identified as dark red stain following the structure of the scaffold and showing through the distributed cells (Figure 4-11).

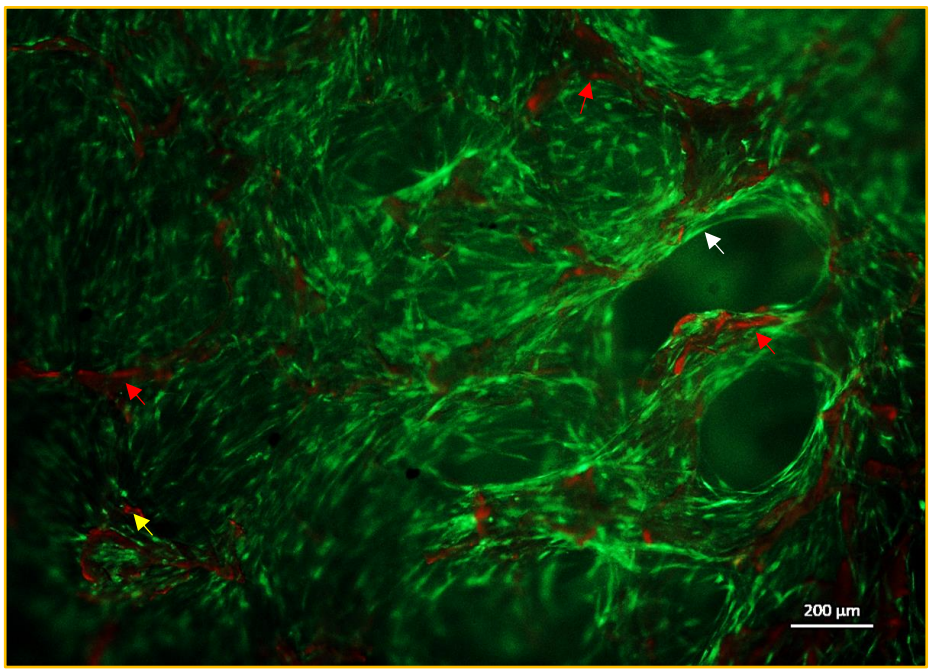

Figure 4-11: Long term evaluation of hPDLSCs viability following seeded on Bmf silk scaffold. At week 4, cells viability was investigated by labelling the cells with green-fluorescent calcein-AM and red-fluorescent ethidium homodimer-1 to detect living cells (white arrows) and dead cells (yellow arrows), respectively. Cells number showed increase with time, with more cells following the structural morphology of the Bmf silk scaffold in their distribution.

4.4.3 The *in vitro* behaviour of hPDLSCs in 3D, osteogenic culture condition

4.4.3.1 Cellular distribution and growth pattern identified by SEM

Following four weeks of *in vitro* culture of hPDLSCs in osteogenic condition and a 3D environment using Bmf silk scaffold, the SEM images showed cellular invasion of the scaffold structure. This invasion is characterised by cells' growth and forming a dense network of cellular processes, as demonstrated in Figure (4-12/A-C). The cells characterised by a polygonal or spindle-like morphology found attached to the scaffold's solid surface with several processes. These processes extended over a relatively long distance to bridge the scaffold structure gap (Figure 4-12/E-F). Despite the large diameter of scaffold pores (~ 350 µm) and the smaller size of the cell body (~ 50 µm). However, many of these pores were obturated by cellular

growth (Figure 4-13/C). Another exciting feature is the pattern of cells distribution; The cells followed a circular orientation around the orifices of large scaffold spherical spaces, while keep extending over their interior walls (Figure 4-12/D). Also, evidence of minerals-like deposits was detected on the scaffold surfaces next to cells. It presented as white particles of 1-5 µm in diameter (Figure 4-12/F).

4.4.3.2 Cellular growth and differentiation as identified by histological and immunohistochemical examinations

The histological examination of hPDLSCs-Bmf silk constructs cultures for four weeks *in vitro* in the osteogenic environment revealed cells' ingrowth into scaffold interstitial spaces. This growth combined by collagen mesh formation formed a layer enclosing the scaffold's outer surface and distributed in between the scaffold structure. However, this growth did not extend to the scaffold's full thickness and confined to 0.5 -1 mm from the outer scaffold surface (Figure 4-13/A). Also, extracellular, black deposits were detected by Von kossa stain in areas dense with cells, as shown in Figure (4-13/B).

Immunohistochemical staining confirms the type of formed collagen fibres as COL-1, which presented as deeply brown stained bundle extending along the scaffold's outer surface and as a mesh spreading to fill the spaces between the cells (Figure 4-13/D). However, the stain level gradually faded as travelled toward the core of the scaffold.

Furthermore, IHC examination presented evidence of osteogenic differentiation with detection of OCN and OPN. These two proteins were found at a detectable level at the construct's exterior surface, where cells are distributed (Figure 4-13/E-F). However, OCN presented at a relatively higher level than OPN and identified a deeper layer inside the scaffold scattered between the cells (Figure 4-13/E).

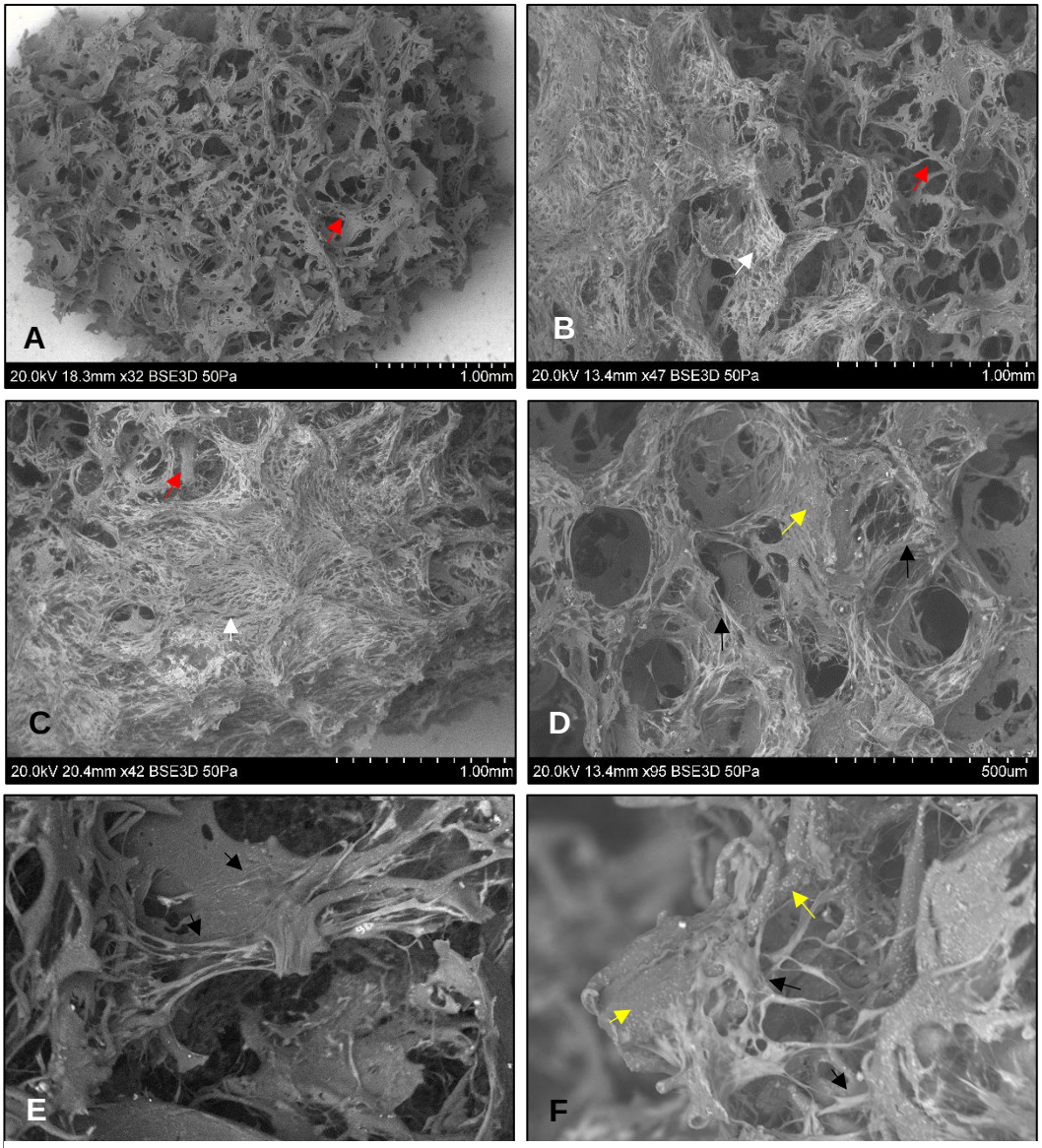

Figure 4-12: SEM evaluation of hPDLSCs growth over the Bmf silk scaffold following 4 weeks of *in vitro*, osteogenic culture. A: structure of unseeded Bmf silk scaffold (red arrows). B and C: hPDLSCs invading the surface of Bmf silk scaffold and establishing a dense network (white arrows). D: hPDLSCs (black arrow) following the circular morphology of spherical scaffold spaces and showing growth over scaffold walls. Also, evidence of extracellular mineral-like deposits (yellow arrows) on the surface of the scaffold can be identified. E and F: Highly magnified SEM images demonstrate the presence of polygonal and spindle-like cells (black arrow) attached to the surface of the scaffold with their process extending over the gaps. Mineral-like, white deposits (yellow arrows) were found distributed in between the cells and covering the scaffold surface.

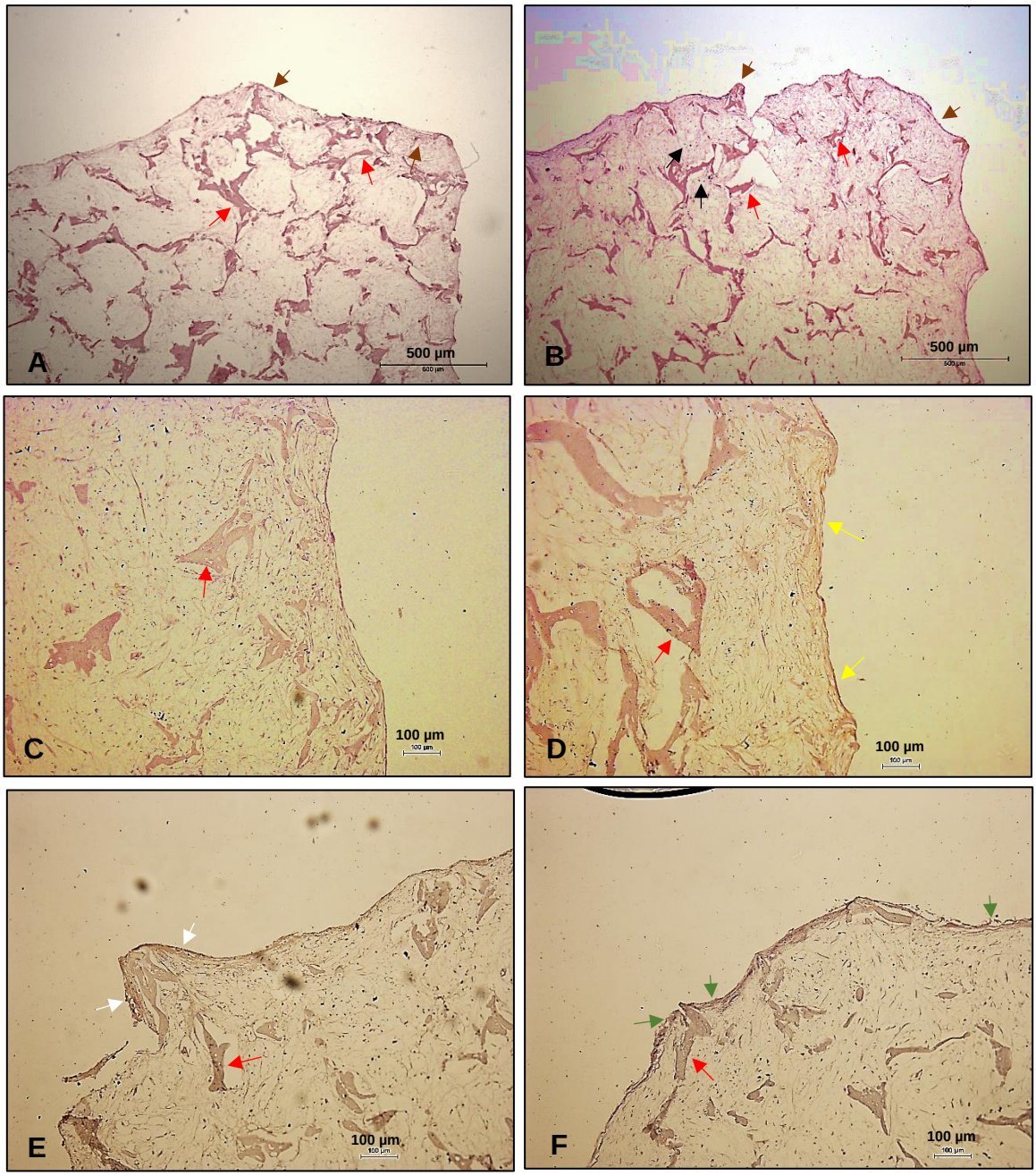

Figure 4-13: Histological and immunohistochemical examination of hPDLSCs seeded *in vitro* on Bmf silk scaffold for four weeks in an osteogenic condition. A: Section stained with Haematoxylin/Van Gieson's stains demonstrated hPDLSCs ingrowth with the formation of collagen mesh (red arrows) that distributed within the scaffold structure (black arrows). B: Von Kossa stained section revealed the presence of black coloured, extracellular mineral deposition (black arrow). C: Negative control for immunohistochemical staining. D, E and F: Immunohistochemical staining showed expression of COL-1 (yellow arrows), OCN (white arrows), and to a limited extent OPN (green arrows).

4.4.4 The behaviour of hPDLSCs *in vivo* 3D, an animal model

4.4.4.1 Macroscopic observations of DCs following seven weeks of intraperitoneal implantation

Macroscopic evaluation of the DCs for the control (cells free scaffold) and hPDLSCs-Bmf silk scaffold demonstrated a clear difference between the two samples. All DCs of the control group showed no evidence of host tissue invasion with blood-free surfaces, as illustrated in Figure (4-14/A). In contrast, the filter membranes of DCs of hPDLSCs-Bmf silk construct was fully covered by a dense layer of fibrovascular tissue. Furthermore, the DCs plastic rings were wrapped with a viscous coat of host fluids. However, upon uncovering the DC, no vascular or tissue invasion was observed inside the chamber. The construct was pale in colour with a smooth glossy surface and encapsulated by a white to a yellowish fibrous capsule. The construct was soaked in a clear fluid (Figure 4-14/B, C)

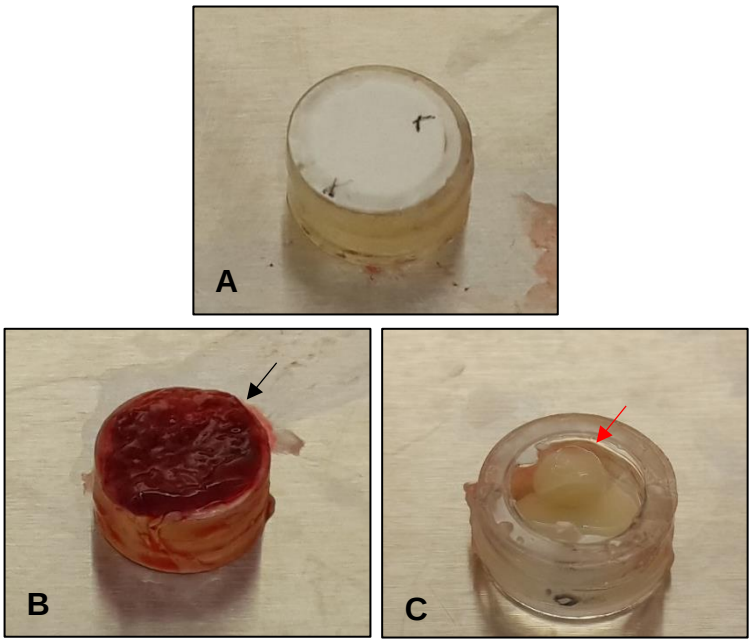

Figure 4-14: Macroscopic appearance of DCs following seven weeks of in vivo implantation in CD-1 nude mice. A: DCs containing cells-free Bmf silk scaffold (control). B: DCs containing hPDLSCs-Bmf silk construct, which demonstarted an invasion of DCs by host fibrovascular tissue. C: uncoverd DCs containing the hPDLSCs-Bmf silk construct that apprear encapsulated by a viscous layer, and contained in clear fuild.

4.4.4.2 Microscopic appearance of constructs as identified by SEM

The SEM images showed the difference between the two groups following seven weeks of intraperitoneal implantation.

A gelatinous layer partially covered the unseeded Bmf scaffolds with many bare areas of the scaffold. Also, no cells were detected in the control group samples, as demonstrated in Figure (4-15/A and 4-15/B). An exciting feature in the control samples was the increase in the scaffold interstitial spaces and signs of degradation in its structure (Figure 4-15/C).

Moreover, the hPDLSCs-Bmf silk constructs presented with another important feature. Here, the entire scaffold was encapsulated in a thick, dense capsule. In some areas, the capsule was composed of more than one-fold. A mesh-like structure was identified in many regions embedded within the wall of the capsule (Figure 4-15/D-E). Moreover, mineral-like deposits (~ 2-10 µm) were recognised attached to the scaffold surface. Cells-like bodies with many processes found laying over the scaffold surface, as seen in Figure (4-15/G).

4.4.4.3 *In vivo cellular growth based on histological findings*

After seven weeks of implantation in CD-1 nude mice, the histological comparison between the unseeded (control) and cells seeded Bmf silk scaffold revealed the absence of cellular activity in the first one. The scaffold material appeared separated in the control sample and lost the honey-comb structure that characterises porous Bmf silk scaffold (Figure 4-16/A and 4-16/B). Conversely, the hPDLSCs-Bmf silk constructs maintained the scaffold's initial structure with voids can still be seen. A remarkable feature was the construct's encapsulation by a thick layer of collagen bundles, as shown in Figure (4-16/C and 4-16/B). Cells with deep nucleus stain were recognised distributed in between the layers of this layer. However, the number of cells in the scaffold's core was limited, with most cells found in the superficial layer and capsule wall. A lightly stained collagenous mesh spread in-depth of the scaffold and filled its interstitial spaces (4-16/C and 4-16/B).

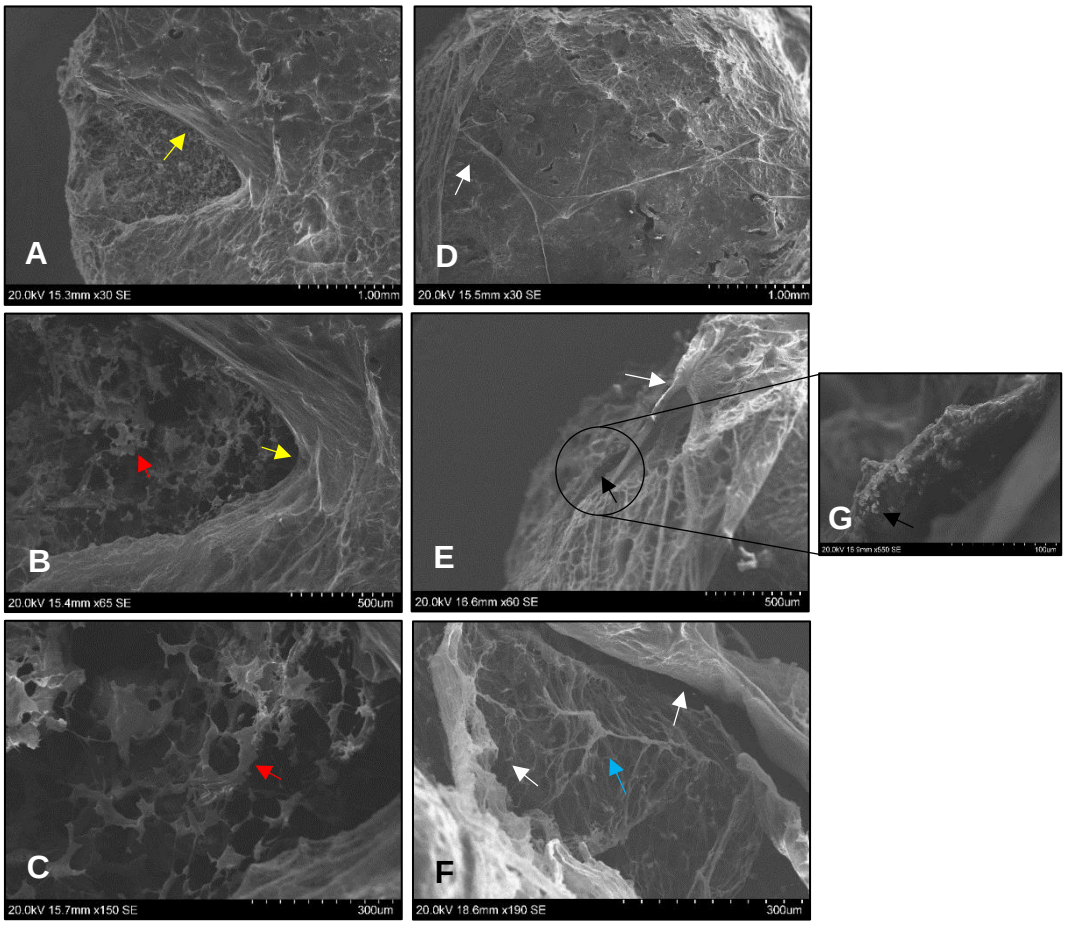

Figure 4-15: Microscopic appearance of unseeded and hPDLCSs seeded Bmf silk scaffolds following seven weeks of in vivo implantation in CD-1 nude mice. A-C: SEM images of unseeded Bmf silk scaffold (control) showing the structure of the scaffold (red arrows) covered partially by a layer (yellow arrows). D-F: SEM images of hPDLSCs-Bmf silk scaffold construct demonstrating its encapsulation by a dense, fibrous layer (white arrows). A mesh-like structure (blue arrow) was identified embedded within the capsule layer. G: Mineral-like deposits recognised in some areas of hPDLSCs-Bmf silk scaffold construct (black arrows).

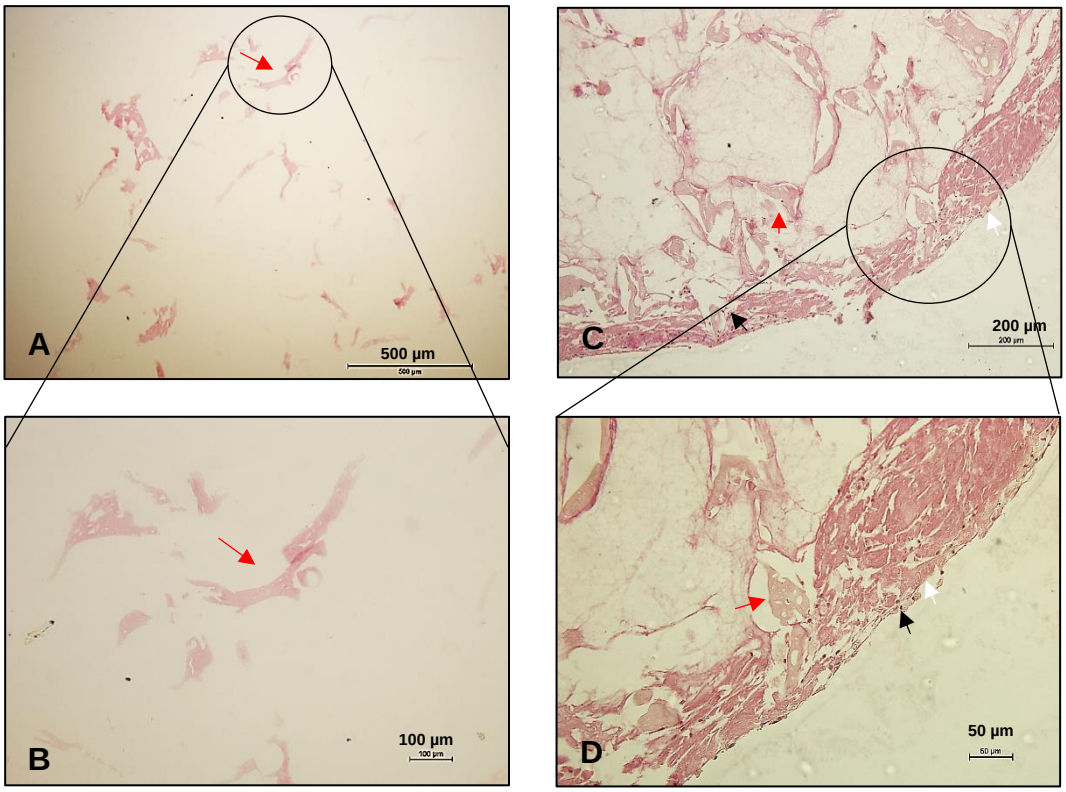

Figure 4-16: Histological evaluation of unseeded and hPDLSCs seeded Bmf silk scaffolds following seven weeks of *in vivo* implantation in CD-1 nude mice. A and B: Haematoxyline /Van Gieson stained section of unseeded Bmf silk scaffold (red arrows). C and D: Haematoxyline/Van Gieson stained sections of hPDLSCs-Bmf silk construct showing a thick collagenous wall (white arrows) of capsule enclosing the scaffold with cells (black arrows) distributed in between.

4.5 Discussion

Cells cultured in 2D monolayer can behave differently to the 3D environment of the normal tissue in the living organism (Baker and Chen, 2012; Duval *et al.*, 2017). Many factors can contribute to that reaction, as lack of 3D spatial orientation of the cell, which plays a critical role in transmitting the signal. Additionally, all the cells grown in the flat surface have similar access to the growth medium and their supplemented factors, and they will share the same proliferation and differentiation features. In contrast, 3D cell culture provides a better simulation for the living tissues' microenvironment (Edmondson *et al.*, 2014; Duval *et al.*, 2017; Kapałczyńska *et al.*, 2018). Moreover, it is possible with the 3D culture to combine various cells' types seeded on a different scaffold to produce a composite simulating that mimic the normal tissues (Almela *et al.*, 2016).

Many materials have been investigated for their characteristics to be used as a 3D scaffold in tissue engineering. Each of them has its pros and cons, e.g. Hydroxyapatite, bioceramic, nature and synthetic polymers (Kolos and Ruys, 2013; Chocholata *et al.*, 2019). In the current study, we decided to investigate the potential of using Bmf silk material as a scaffold for periodontal tissue regeneration. Silk is a natural polymer produced by many species. However, among those species, Bombyx mori silkworm was the most abundant source of silk for textile production, which has been used over thousands of years, because of the excellent quality and skin affinity of its silk fibres (Sutherland *et al.*, 2010; Rockwood *et al.*, 2011). Silk's fibre is composed of two major proteins, fibroin and sericin. It was found that the latter could cause an allergic reaction. Accordingly, more attention was given for fibroin protein due to its chemical composition and structure that proven to induce a negligible inflammatory response level (Zaoming *et al.*, 1996; Santin *et al.*, 1999).

Moreover, Silk-derived fibroin can be extracted and manipulated easily to use in many biomedical applications. This protein can be prepared and cast in various forms that fit many tissue engineering applications, e.g. fibres, 3D foams, films, tubes, and gels (McCool, 2011). Also, it has been proven that silk fibroin protein has a controllable, slow rate of degradation *in vivo*, which compensate the rate of natural tissues regeneration on the other side (Rockwood *et al.*, 2011). Add to that the economic factor, as silk is affordable for a reasonable cost due to the wide range cultivation of

silkworms for textile production (Cao and Wang, 2009; Sutherland *et al.*, 2010; Rockwood *et al.*, 2011; Melke *et al.*, 2016). These unique properties make it possible to use Bmf silk for many applications in the field of regenerative medicine, including dermal, corneal, vascular, cardiac, bone and tendon tissues regeneration. However, to the best of our knowledge, little evidence is available regarding its role in periodontal tissue regeneration, with most of the current data examining this role over a relatively short period (10-14 days).

This chapter tried to fill this gap by providing a long-term evaluation for the biocompatibility and feasibility of using Bmf silk material as a 3D scaffold for periodontal tissue regeneration. Based on the prepared Bmf silk scaffold structure, a comprehensive evaluation was performed to examine the immunological reaction of the human monocyte cell line (THP-1) toward Bmf silk scaffold. Additionally, the biological behaviour of hPDLSCs in response to this scaffold was assessed based on the cells' viability, metabolic activity, and differentiation capacity *in vitro*.

The immunogenicity assay conducted in this study aimed to analyse the levels of inflammatory cytokines (TNF-α and IL-1β) expressed by THP-1 Cells in response to their exposure to the Bmf silk material. Also, to compare these levels with negative and positive controls cultured in 2D (THP-1 cells, THP-1 with PMA) and 3D culture (COL-1 scaffold). The current results of immunogenicity assay indicated the initiation of immunological response upon exposure to Bmf silk scaffold. However, this response was comparable in its level to that induced by exposure of THP-1 cells to 3D COL-1 gel. Understanding the mechanism of host reaction against the foreign body is essential to explain the current results. The human immune reaction undergoes several stages in response to implantation of foreign material, the process that ends with either engraftment or rejection of the implant. This reaction is governed by many factors, including the type of material and its surface topography (Anderson *et al.*, 2008; Crupi *et al.*, 2015). Immediately after implanting a biomaterial inside the human body, a proteins layer begins to cover the implanted material. The characteristics of adsorbed proteins layer, e.g. type, concentration, and surface texture, are depending on the surface properties of biomaterial itself. Subsequently, the nature of this protein layer will determine the sequence of host immune reaction, as it will control the interaction and adhesion of inflammatory cells, this includes the key players in the inflammatory process, the monocyte and

macrophage cells (Anderson *et al.*, 2008; Crupi *et al.*, 2015). These cells produce the pro-inflammatory cytokines (TNF-α and IL-1β), which play a pivotal role in regulating cells proliferation, differentiation, and apoptosis and recruiting other inflammatory cells to act as immune response effector cells (Guo *et al.*, 2003; Parameswaran and Patial, 2010).

Moreover, these cytokines are an endogenous pyrogen that released in response to infections and stress (Arango Duque and Descoteaux, 2014). Due to its chemical structure, silk fibroin was a safe material in many biomedical applications. It was also proved by the US Food and Drug Administration in 1993 to be used as a biomaterial (Melke *et al.*, 2016).

Those results of cytocompatibility supported the results of immunogenicity assay. hPDLSCs were able to attach, proliferate and differentiate over the surface of Bmf silk scaffold. This effect can be attributed to the chemical and physical structure of prepared scaffold, which provides the surface that supports the cells attachment and spread (Minoura *et al.*, 1995; Mandal and Kundu, 2009).

According to Gotoh *et al.* (1998), the cellular attachment to the silk fibroin is due to the positively charged molecules near the C-terminal of silk fibroin hydrophilic regions. This charge attracted the negatively charged mammalian cells and enhanced their attachment.

The presence of pores is another factor that enhances cellular attachment and growth. Murphy *et al.* (2010) demonstrated that pore size of 325 mm of collagen-glycosaminoglycan induced more cell attachment and was associated with increased cell numbers. The 3D porous silk fibroin has been used for bone tissue regeneration. This porous structure simulates, to a certain extent, the structure of the bone which favour the cellular attachment, migration and proliferation. Also, it helps in clearing the metabolic waste via diffusion to the surrounding medium (Kim *et al.*, 2005; Choi *et al.*, 2018).

Despite that, other factors could affect the amount and nature of the cellular attachment to the scaffold material, including the seeding technique, i.e. static or dynamic, and surface modification of the scaffold surface. In the present study, seeding techniques' efficiency was evaluated based on comparing cellular viability and metabolic activity. The results indicated the advantage of dynamic seeding technique over the static one. However, the manual counting of unattached cells revealed a non-significant difference

between the two methods. This variation could be due to missing some cells that left in the culture vessel. Riesle and Van Blitterswijk (1999) found that dynamic seeding enhanced fibroblast cells' seeding efficiency on porous polyactive scaffold. The group seeded dynamically formed an abundant amount of extracellular matrix compared to the group seeded statistically.

The Bmf silk scaffold did not enhance hPDLSCs proliferation and metabolic activity only. Interestingly, it supported other cellular activities, including their osteogenic differentiation and extracellular minerals and matrix formation. Similar results were recorded by (Miyamoto *et al.*, 2013).

The results of *in vivo* study come to support those of *in vitro*. The hPDLSCs survived the *in vivo* incubation conditions with evidence of the formation of the abundance amount of collagenous extracellular matrix. However, further investigations are required to confirm the current findings.

4.6 Conclusion

Based on the current findings, it can be concluded that Bmf silk is a feasible option to be used as a scaffold to support the growth of hPDLSCs. This biomaterial's unique features can enhance the *in vitro* and the *in vivo* regeneration of periodontal tissues, e.g. bone and PDL.

Chapter Five: Development of a novel mechanical stimulation bioreactor to study the effect of cyclic compressive loading on the proliferation and differentiation of hPDLSCs

5.1 Introduction

Periodontium represents a unique joint that connects two different hard tissues, i.e. cementum and alveolar bone. This joint serves many roles, including applying applied masticatory forces to the tooth-investing bone (Wouter Beertsen, 1997). This function of periodontal tissue leads to another crucial contribution in the remodelling process of the surrounding bone and periodontal tissue itself; on top, it allows for physiological and orthodontic tooth movements (Ramfjord and Kohler, 1959; Shimomoto *et al.*, 2007). The sophisticated architecture design of this tissue and the cells' population found within the periodontal ligament are attributed to the periodontal joint (MacNeil and Somerman, 1999; Cho and Garant, 2000).

Tissue engineering of such multifunctional, dynamic organ requires enrolling in mechanical stimulation to mimic the physiological environment. It has been reported that lack of occlusal stimulation could lead to disuse atrophy of periodontium. The latter was featured by resorption of the alveolar bone crest, narrowing of periodontal ligament space, loss of normal S-shape orientation of fibres as well as deepening of periodontal pockets, which was accompanied with a slowly progressed gingival recession (Cohn, 1965; Levy and Mailland, 1980; Motokawa *et al.*, 2013).

Occlusal forces applied to periodontal tissue are complex, multidirectional, and ranging from 10 - 50 N. These forces, which recognised as either a compressive or shears forces, initiate compression and tension areas across different regions of the periodontium (Kikuchi *et al.*, 1997; Cordes *et al.*, 2012; Naveh *et al.*, 2012). Studying the periodontal mechanobiology is of great importance to understand the effect of such stimulation on the regeneration process; accordingly, it can be recruited and other tissue engineering elements, e.g. cells, scaffold, and growth factors, to enhance regeneration of periodontal tissues.

To achieve this aim, there was a need to carefully design a device that could replicate the oral environment, and mimic the mechanical forces applied on teeth. Many previous studies (De Araujo *et al.*, 2007; Berendsen *et al.*, 2009; Hu *et al.*, 2014; Chen, Y. *et al.*, 2015; DesRoches, 2016) have examined the effect of mechanical stimulation on periodontal cells by developing different designs of bioreactors. However, the complexity of periodontal biomechanics makes it challenging to replicate all aspects of applied forces in one model, including the compressive, shear, and tensile

stresses. The current chapter presents a novel mechanical loading bioreactor that could help study the effect of mechanical stimulation on hPDLCSs in a 3D setting *in vitro*. Also, it presents a preliminary study of the effect of cyclic compressive force on the *in vitro* behaviour of hPDLSCs seeded on the Bmf silk scaffold.

5.2 Aim

This study aimed to design, manufacture, and validate a novel bioreactor that could simulate some aspects of the physiological forces to which the periodontium is subjected, mainly the compressive and shear loading. Furthermore, to investigate *in vitro* the effect of cyclic compressive stimulation on the proliferation and differentiation of hPDLSCs in a 3D culture.

5.3 Materials and methods

All materials and methods used for experiments of the current study are described in this section.

5.3.1 Designing and manufacturing of a novel mechanical loading bioreactor for simulation the compressive and shear forces applied on periodontal tissue in the oral cavity

A novel mechanical loading bioreactor was designed and manufactured to simulate some aspects of the complex physiological forces to which the periodontium is subjected. This process runs through several stages, including designing, examining the biocompatibility of used materials, manufacturing, and validating the final product. The details of each stage are explained below.

5.3.1.1 Designing a mechanical loading bioreactor for *in vitro* tissue culture

For the purpose explained above, the SolidWorks software-2014 (Vélizy-Villacoublay, France) was used to design the bioreactor's different components. Furthermore, a simulation for the proposed modes of action was created to understand the mechanism of action better.

The bioreactor design included two main compartments. The first part has two electric motors along with their speed regulators, and gears. These items are contained inside an aluminium casing that can withstand the *in vitro* incubation environment's humidity and temperature.

The second part is detachable and designed with eight tissue culture chambers divided into two rows, as illustrated in Figure 5-1/A and 5-1/C. The chambers' unit is covered to permit the gas exchange to support the cells' culture conditions. Each chamber is supplemented with four aluminium holders. Two of these holders are fixed to the chamber's side and base, while the other two are attached to a stainless-steel bar by an adjustable joint. This orientation helps in applying compressive and shear loading in each chamber (Figure 5-1/B).

Two stainless bars are included in this bioreactor with each bar runs through the four chambers in a row. Thus, this design allows for studying the effect of two types of stimulation for two groups, each of four samples, simultaneously. The stainless bars play a vital role in transferring the

movement from the first part of the bioreactor to the second. They also transfer the motors' circular motion as a linear motion to the sample, Figure (5-1/C).

The linear displacement is controlled by a set of four stainless steel discs or different diameters (0.5mm, 1 mm, 1.5mm and 2 mm).

5.3.1.2 Evaluation biocompatibility of bioreactor material

Choosing the right material to manufacture the bioreactor was a crucial step, as it requires to be inert, easy to sterile, not to react with the used tissue culture medium and reagents, as well as to possess the property of withstanding the cells' incubation environment of 37^{o}C, 5 % CO_2, with ≥ 90% of humidity.

For these reasons, the metal bars were agreed to be prepared from stainless steel, while the scaffold holders to be made of aluminium. The recommended material for building the chambers unit that could meet the previous criteria was the acrylics polymethyl methacrylate (PMMA). It is a thermoplastic material that is optically transparent, unaffected by moisture, and offers a high strength-to-weight ratio. Also, it is unaffected by aqueous solutions of most detergents, acids, alkalies and laboratory chemicals. As described by the supplier, other properties of this material are listed in Table (5-1).

The material was supplied in a sheet form of different thickness (5 mm, and 60 mm) from Smiths metal centres LTS (Leeds, UK). These sheets can easily be drilled, engraved and finished with sharp carbide-tipped tools, with cut surfaces can be polished.

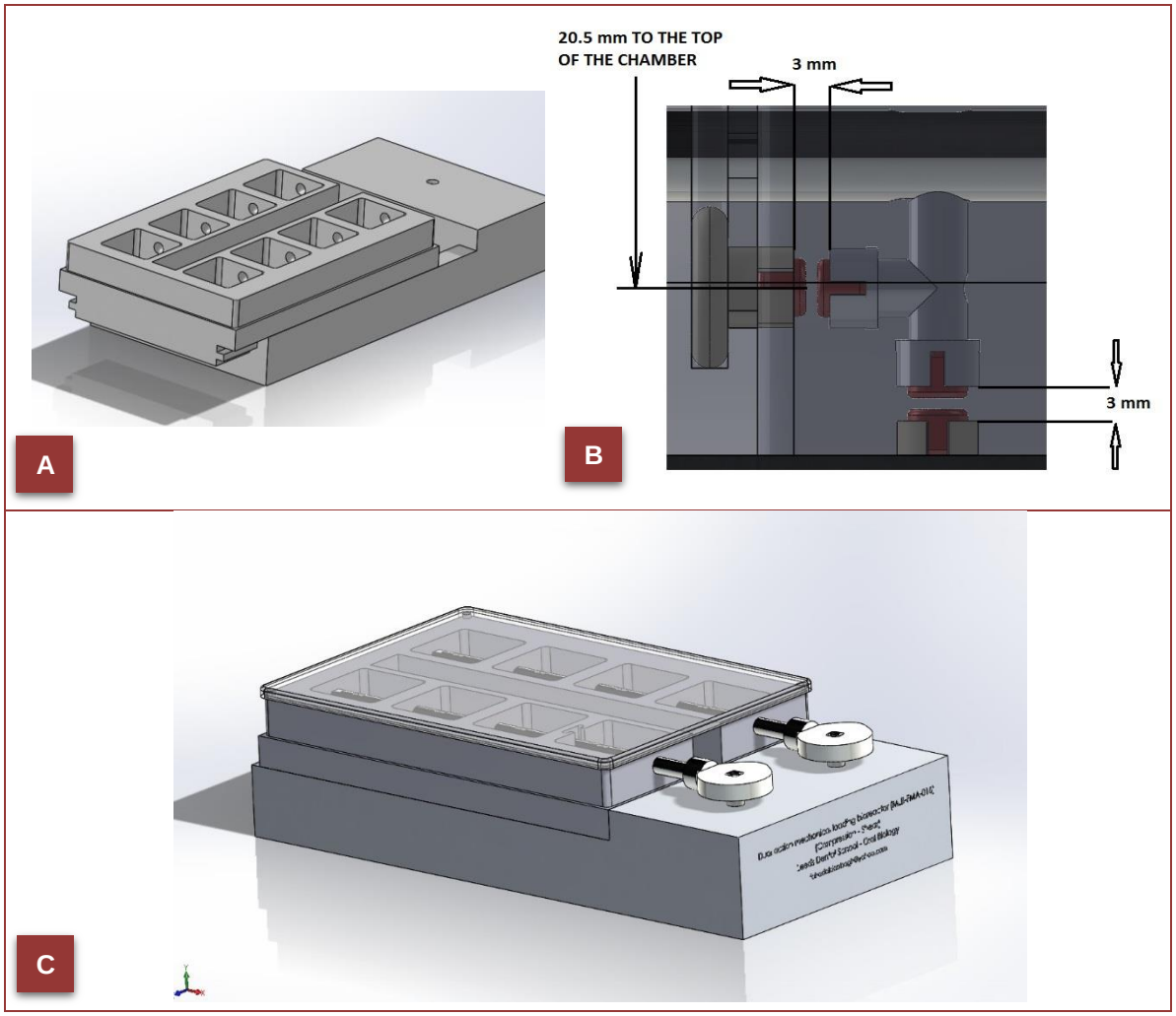

Figure 5-1: Design of dual-action (compression and shear forces), 8-chambers, mechanical loading bioreactor for *in vitro* tissue culture. The bioreactor includes two detachable compartments as shown in A. Each chamber contains two fixed scaffolds holders attached to the side and base of it and another two movable holders connected to a movable stainless-steel bar (B). Mode of activation for every four chambers in a row is controlled separately by two electric motors (C).

Table 5-1: Properties of Acrylics Polymethyl-Methacrylate according to the manufacturer

Thermal properties	
Coefficient of Thermal Expansion (x 10^5 in./in./°F)	5 - 9
Melting Temp (°C)	130-140
Max Operating Temp (°C)	65-93
Heat Deflection Temperature at264 (psi)	65-100
Mechanical properties	
Tensile Strength (psi)	8,000 - 11,000
Tensile Modulus (psi)	350,000 - 500,000
Tensile Elongation at break (%)	2
Flexural Strength (psi)	12,000 - 17,000
Flexural Modulus (psi)	350,000 - 500,000
Compressive Strength (psi)	11,000 - 19,000
Hardness Rockwell	M80 - M100
IZOD Notched Impact (ft-lb/in)	0.3
Other properties	
Good insulation properties	
UV resistant	
Low smoke emissions	
Good stiffness & abrasion resistance	
Clear / colourable - excellent clarity	
Low water absorption	
Good insulation properties	

To examine the biocompatibility of PMMA, more comprehensive tests were performed.

5.3.1.2.1 Analysing the expression of inflammatory cytokine of THP-1 cells in response to their exposure to acrylic PMMA material using rtPCR

The biocompatibility of acrylic PMMA materials was investigated by measuring the expression levels of inflammatory cytokines, i.e. TNF-α and IL-1β of THP-1 cell in response to their exposure to the material. Small blocks (5 × 5 × 5 mm) of acrylic PMMA sheet were prepared, washed 1× PBS, and sterilised by exposure to the UV-C radiation of 254 nm wavelength for 15 min for each side (Meechan and Wilson, 2006). Afterwards, the immunogenicity assay was performed as described previously in **4.3.3.1.**

The current immunogenicity experiment design includes four groups with triplicate for each, as demonstrated in Table (5-2). All four groups were

cultured in the same 24-well plate to normalise the effect of culturing environmental.

Table 5-2: Experiment design for acrylic PMMA immunogenicity assay

Code	Group	Scaffold	Clue	Timepoints	n
1	Monolayered THP-1 cells (alone)	None	Negative control for 2D environment	One day	3
				Three days	3
				Seven days	3
2	Monolayered THP-1 cells with PMA	None	Positive control for 2D environment	One day	3
				Three days	3
				Seven days	3
3	THP-1 cells in 3D culture	3D COL-1 gel (bovine skin)	Negative control for 3D environment	One day	3
				Three days	3
				Seven days	3
4	THP-1 cells in 3D culture	Acrylic PMMA blocks	Experimental	One day	3
				Three days	3
				Seven days	3

5.3.1.2.2 Assessment of cells viability using live/dead fluorescent markers

Sterile blocks of acrylic PMMA were incubated overnight at 4^{o}C in basal medium supplemented with 20 % FBS to modify the surface chemistry for enhancing cellular attachment. As described in **4.3.3.2.** the hPDLSCs (P2) were pelleted, resuspended, counted and dynamically seeded at a density of 2 × 10^5 Cell/block. Cells were examined after three and seven days for their viability by staining with both calcein-AM (green-fluorescent) and ethidium homodimer-1 (red-fluorescent) as described previously in **3.5.1.**

5.3.1.3 Manufacturing of mechanical loading bioreactor

Following the biocompatibility examination, the design of the bioreactor was transferred from paper to reality. The manufacturing process was accomplished in collaboration with Kirkstall precision engineering Ltd

(Leeds, UK), a specialised company in manufacturing precision components and assemblies for different industries.

The magnitude of force applied to the sample (cell-scaffold construct) was measured using a digital force gauge HF-50 by King Line (Guangdong, China). The probe of the gauge was attached to the distal end of the metal bar. Both the bioreactor and gauge were secured to avoid any displacement during the reading. Figure (5-2) shows the digital force gauge and the setting used for measuring the applied force.

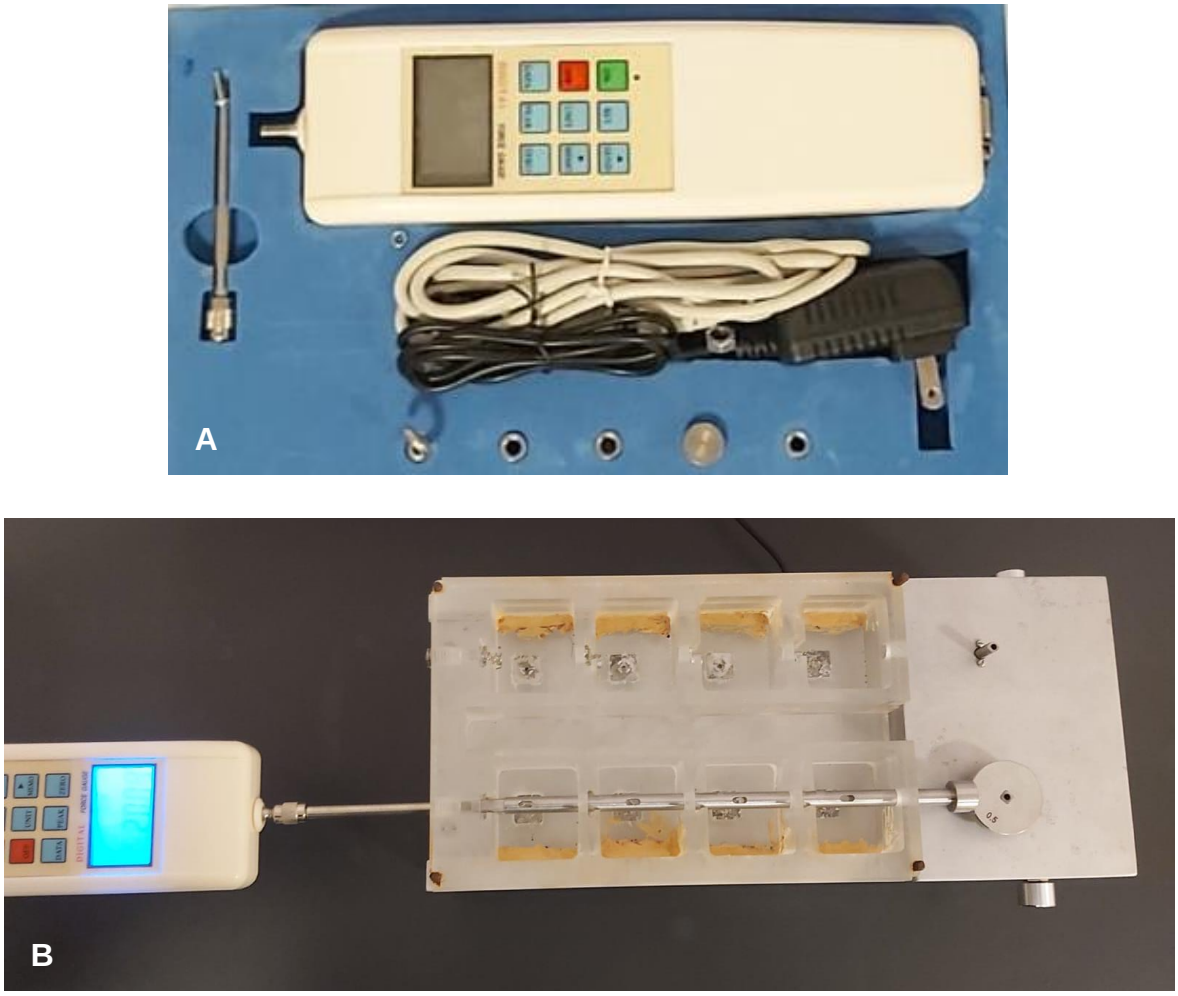

Figure 5-2: Digital force gauge HF-50 used for measuring the applied compressive force. A: the digital force gauge along with the probes and other accessories. B: the setting is used to measure the applied force by the electric motor via the horizontal metal bar.

5.3.2 Evaluation of the effect of cyclic compression force on hPDLSCs behaviour *in vitro*

Following the bioreactor's validation, a preliminary study was performed to investigate the impact of mechanical (compression) loading on the proliferation and differentiation of hPDLSCs *in vitro.*

Twelve constructs of Bmf silk 3D porous scaffolds seeded with hPDLSCs were prepared as described in **4.3.3.2.** Briefly, hPDLSCs (P2) were dynamically seeded on sterile silk scaffolds (~ 3 mm x 4 mm) at a 3 × 105 cell/scaffold density. The constructs were incubated in a 24-well plate in basal medium for two weeks to enhance cellular proliferation before being moved to the bioreactor.

Two groups were randomly aliquoted from the 12 constructs; in the first group (the control) the constructs were incubated without applying mechanical loading; while the second group was subjected to a cyclic compression force of 25 N, with 1.5 mm of linear displacement, for 15 min each time, twice daily over two weeks.

Each of the samples in this study consists of two Bmf silk-hPDLSCs constructs, with one of them attached to the fixed holder on the side of the chamber, and the other attached to the moveable holder screwed to the stainless-steel bar. Both parts placed in contact with no gap in between. The samples were immersed with 35 mL/chamber of basal medium, with the medium being changed every three days. Three replicates were considered for each of the two groups.

5.3.2.1 Investigating the effect of cyclic compression force on hPDLSCs viability

The viability of hPDLSCs in response to the applied compression force was evaluated by labelling the cells with fluorescent live/dead markers as described previously in **3.5.1.** Two-time points were determined for this evaluation; the first was performed following 24 hours of seeding the hPDLSCs on the scaffolds, which was performed to evaluate the level of cellular growth. However, the second one was followed by 28 days (14 days of stimulation), where the constructs were re-evaluated to compare the cellular viability between the two groups, the control as well as the mechanically stimulated constructs.

5.3.2.2 Measuring the metabolic activity of hPDLSCs in response to the applied compression force

The proliferation of hPDLSCs was assessed indirectly by measuring their metabolic activity. Following two weeks of incubation in the bioreactor, the samples were removed carefully from the holders into 24-well plates and incubated in fresh basal medium with AlamarBlue™ reagent (Thermo Fisher Scientific, Massachusetts, USA) being added in a ratio of 1:10 to the medium volume. The AlamarBlue™ assay was performed as referred to in **3.2.1.**

5.3.2.3 Examining the impact on compression force on the differentiation of hPDLSCs

5.3.2.3.1 Analysing the expression levels of osteogenic, cementogenic genes with rtPCR

The differentiation capacity of hPDLSCs (P2) was tested by analysing the osteogenic and cementogenic specific proteins' level of expression, including COL-1, OCN and CEMP. These markers could reflect the difference between the two groups regarding osteogenic and cementogenic differentiation.

After 14 days of culture in the basal medium in the bioreactor, all samples were subjected to the process of RNA extraction, in which they were washed with two changes of 1 × PBS to clear out the medium. Next, each sample incubated in 300 µL of RLT/β-ME for 30 min at room temperature to enhance cell lysis. The lysates were subjected processes of RNA extraction, cDNA preparation, and amplification reaction discussed before in 4.3.3.1 All expression levels of target genes (COL-1, OCN and CEMP) were compared Glyceraldehyde-3-phosphate (GAPDH), which is used as a housekeeping gene. The data were statistically analysed using unpaired t-test with Welch's test at p-value ≤ 0.05.

5.3.2.3.2 Histological examination

Although the 14 days period was not long enough for the samples to have evident histological changes, the histological examination was performed to investigate the interface between the two scaffolds in each sample. Moreover, to address the presence of any differences between the two study groups.

After 14 days of culture in the basal medium in the bioreactor, samples were fixed with 10% NBF to prepare for histological examination. As described in 2.4.1., sections were prepared, then stained with haematoxylin / Van Gieson stains as demonstrated in **2.4.3.** and **2.4.4.**, respectively.

5.4 Results

5.4.1 Features of the designed bioreactor

The manufactured bioreactor consisted of two parts; the first included two electric motors that provided the circular motion to stainless steel drop-like shaped adapters, as shown in Figure 5-3/A. The diameter of these adapter determines the amount of linear displacement. Four drop-like adapters were manufactured, which allow for displacement distance ranging between 0.5 mm to 2 mm (Figure 5-4). In addition to the motors and adapters, this part of the bioreactor also included two regulators to control each motor's speed individually. This feature enables the user to have two different frequency settings (speed) for two experimental groups simultaneously.

The second part is detachable and includes eight chambers arranged into two rows. Each row was supplied with a movable stainless-steel bar that runs horizontally through the four chambers and attached with four scaffold holders, one in each chamber. These two bars can move individually in a horizontal direction by the two motors' action (Figure 5-2/A). Thus, they convert the motors' circular motion into linear motion that transferred to the scaffold holders. The holder's attachment to the stainless-steel bar is adjustable, which allows for easy placement of scaffold. It also helps set the separation distance between the two scaffolds piece of the examined sample easily, see Figure (5-2/B).

The movable holder is supplied with two cup-like shape containers (3 mm in diameter) to accommodate two scaffolds simultaneously. One of them is oriented horizontally to examine the compression stimulation and the other positioned vertically to study the shear stimulation (see Figure 5-2/B).

The bioreactor can perform two modes of action on the cell-scaffold constructs, the compression and shear stimulation. These two modes simulate the mechanical loading that periodontium is exposed to in the oral cavity.

The bioreactor applies an average compressive force of 25 N as measured by the digital force gauge (Table 5-3).

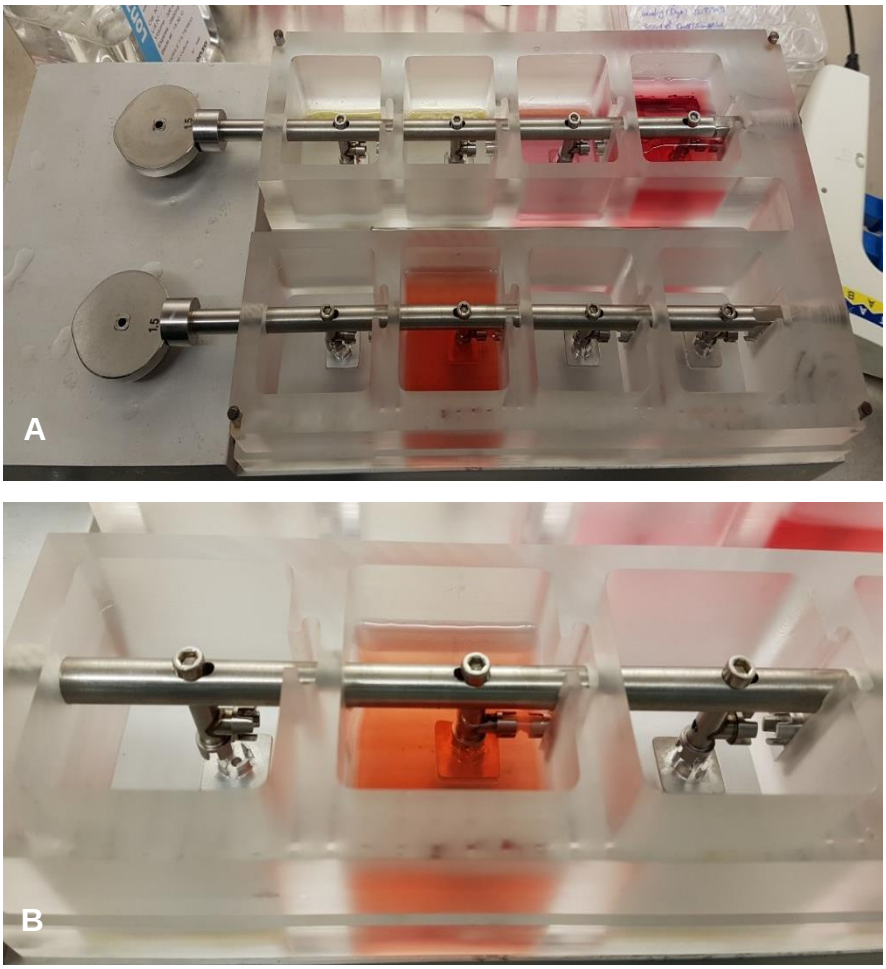

Figure 5-3: The novel mechanical loading bioreactor. Eight chambers of tissue culture with stainless steel bars running horizontally through them to apply the required forces (A). Each individual chamber contains two scaffold holders that fixed to the base and side of the chamber, while the other two movable holders attached to the movable stainless-steel bar (B).

Table 5-3: Compression forces applied on scaffold using the 1.5 mm metal disc. Force measured in N using a digital force gauge.

Reading	Compression force (N)
1	25.04
2	25.00
3	24.90
4	25.25
5	24.78

Figure 5-4: Drop-like adapters of the bioreactor. Metal adapters of four different diameters (0.5, 1, 1.5, and 2 mm) were prepared to control the displacement distance and the force magnitude that was applied on cells-scaffold constructs.

5.4.2 Biocompatibility of acrylic PMMA material

5.4.2.1 Effect of acrylic PMMA on expression inflammatory cytokines

In these experiments, the levels of pro-inflammatory cytokines (TNF-α and IL-1β) expressed by THP-1 cells were analysed in response to exposure to the acrylic PMMA block.

Compared to the control (1st) cell group cultured alone in a monolayer, the results of day one demonstrated a slight increase in TNF-α expression levels in groups where THP-1 cells cultured with either 3D COL-1 scaffold or acrylic PMMA blocks, 3rd and 4th groups, respectively. In contrast, THP-1 cells cultured with PMA (2nd) group expressed a higher level of TNF-α in comparison to the other groups, as demonstrated in Figure (5-5/A). This increase was statistically significant in comparison to the control group. At the same time, there was no statistically significant difference between the COL-1 and Acrylic PMMA block groups, as shown in Figure (5-5/B)

On day three, the TNF-α expression levels declined for the three groups (2nd, 3rd and 4th) in comparison to their levels on day one. Interestingly, the THP-1 cells cultured with PMA demonstrated the sharpest decline. There was no statistical difference between these three groups' results and the control at this stage (figure (5-5/A). Again, the difference between the COL-1 scaffold and acrylic PMMA block was non-significant, despite the lower level of TNF-α expressed in the acrylic PMMA block group, see Figure (5-5/B).

Following seven days of *in vitro* culture, the 2nd group maintained the same expression level, with 3rd group showed a further reduction in TNF-α level. However, there was a slight increase in the expression level of TNF-α in cells of the 4th group compared to results recorded at day three (Figure 5-5/A). Although the group of acrylic PMMA block showed a slight increase in TNF-α expression at day seven in comparison to COL-1 group, this increase was statistically non-significant (Figure 5-5/B)

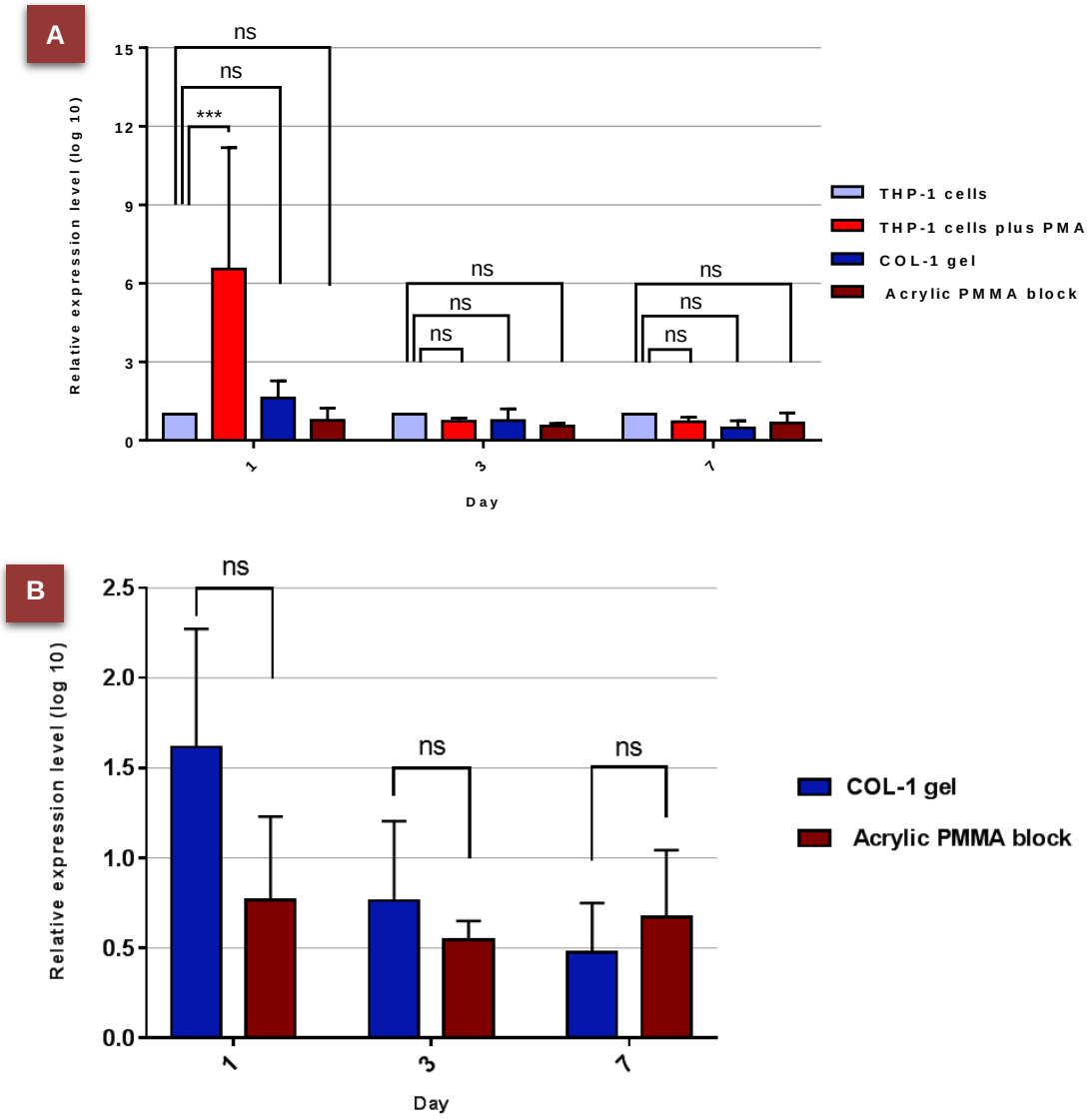

Figure 5-5: Analysis of relative expression levels of TNF-α for THP-1 cells against exposure to acrylic PMMA block. Four groups were examined, 1st: monolayered THP-1 cells, 2nd: THP-1 cells with PMA, 3rd: THP-1 cells with 3D COL-1 scaffold, 4th: THP-1 cells with acrylic PMMA block. Relative cytokine expression levels among the four groups were measured at day 1, 3, and 7 (A). Statistical comparison of TNF-α levels for 3rd and 4th were analysed at the three time points using two-way ANOVA test with Dunnett test was used at *p*-value ≤ 0.05 (B)

The levels of expression of IL-1β nearly followed the same pattern of TNF-α. At day one, the PMA group demonstrated a sharp increase in the IL-1β compared to the control group, which was statistically significant (Figure 5-6/A). The COL-1 group also showed a slight increase in the level of expression compared to the control group. However, there was no statistical difference between the results of this group and the control one. Interestingly, the acrylic PMMA block group induced the lowest level of IL-1β expression at this point, which was even lower than that of the control group, see Figure (5-6/A). A statistically significant difference was found between the COL-1 scaffold and acrylic PMMA block groups at day one (Figure 5-6/B).

On day three, the levels of IL-1β for 2nd and 3rd groups showed a reduction compared to the results of the same groups at day one. The 4th group begin to show an increased level of expression compared to the levels expressed at day one. However, the difference between the different groups and the control one was non-significant, except for the PMA, See Figure (5-6/A). There was no statistical difference regarding the expression levels of IL-1β between the COL-1 scaffold and acrylic PMMA block groups at this stage (Figure 5-6/B).

At day seven, further reduction in the expression of IL-1β was noticed in the group of COL-1 scaffold. In contrast, the PMA and acrylic PMMA block groups showed an increase in the levels of IL-1β compared to day three, see Figure (5-6/A). The level of IL-1β in PMA was significantly higher than that of the control group. However, for 3rd and 4th groups, the difference was non-significant. Comparing the COL-1 scaffold and acrylic PMMA block results revealed a non-significant difference between the two groups despite the latter's increased level of IL-1β.

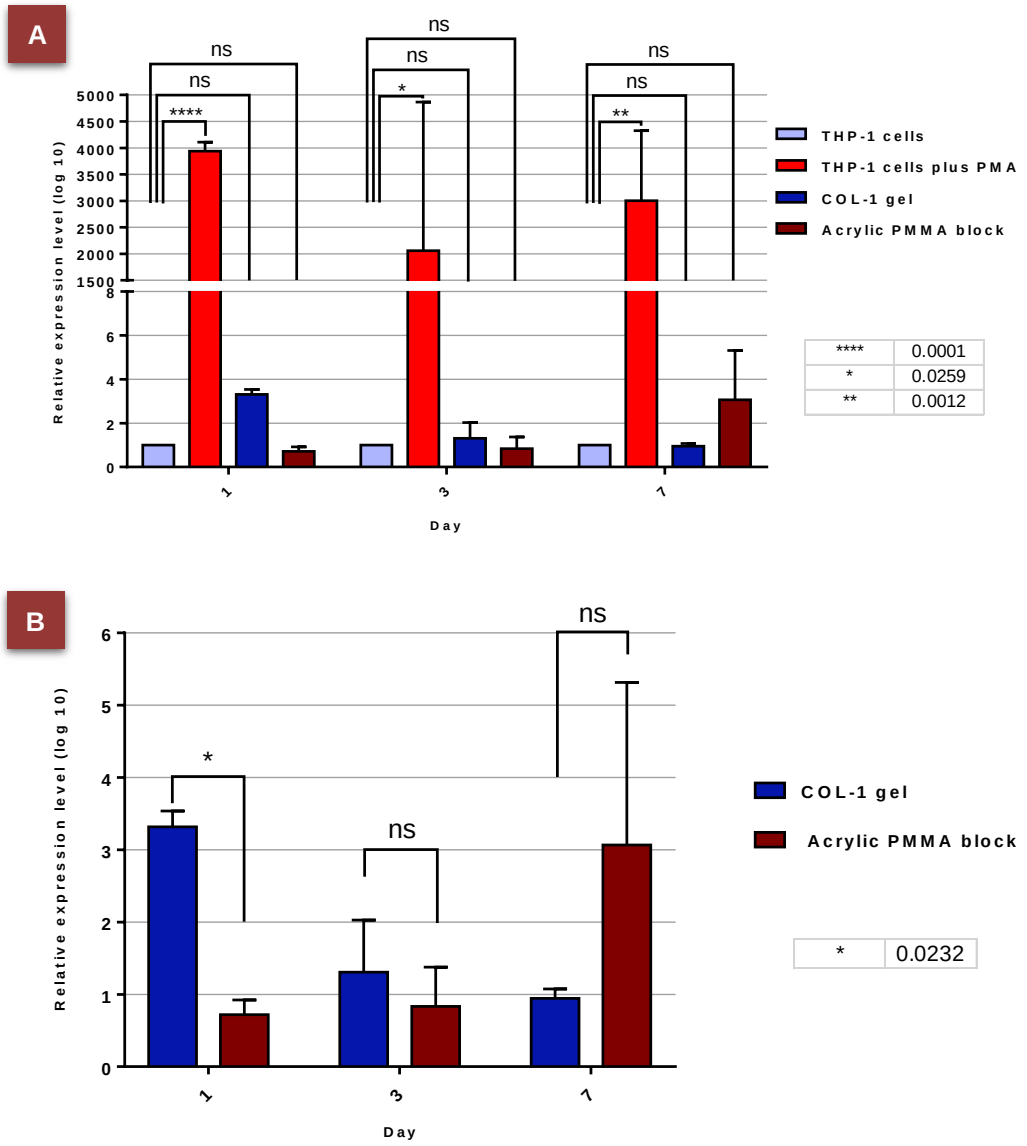

Figure 5-6: Relative expression levels of IL-1β for THP-1 cells against exposure to acrylic PMMA blocks. Four groups were set, 1st: monolayered THP-1 cells, 2nd: THP-1 cells with PMA, 3rd: THP-1 cells with COL-1 gel, 4th: THP-1 cells with acrylic PMMA block. Relative expression levels of IL-1β among the four groups were measured at day 1, 3, and 7 (A). Statistical results of two-way ANOVA test with Dunnett test was used at p-value ≤ 0.05 revealed a significant difference in the expression levels of IL-1β at day one between 3rd and 4th groups. However, this difference was not significant at day 3 and 7.

5.4.2.2 Qualitative analysis of cytotoxicity of acrylic PMMA

Following the first 24 hrs of *in vitro* culture, the fluorescent images of live/dead cells' markers for hPDLSCs seeded on acrylic PMMA blocks showed evidence of cells attachment and proliferation. The cells spread over the PMMA surface with their processed seen extending along the surface of the block. No dead cells were detected at this stage; see Figure (5-7).

At day seven, there was an increase in the number of living cells, with cells more packed against each other with close contact (Figure 5-7). Moreover, the living cells (green-fluorescent calcein-AM) dominated with few dead cells, stained with ethidium homodimer-1 red stain, see Figure (5-7). One interesting finding is that hPDLSCs followed a distinguished, band-like arrangement in their growth, which corresponds to the shape of grooves created by blades used to prepare the blocks (Figure 5-7).

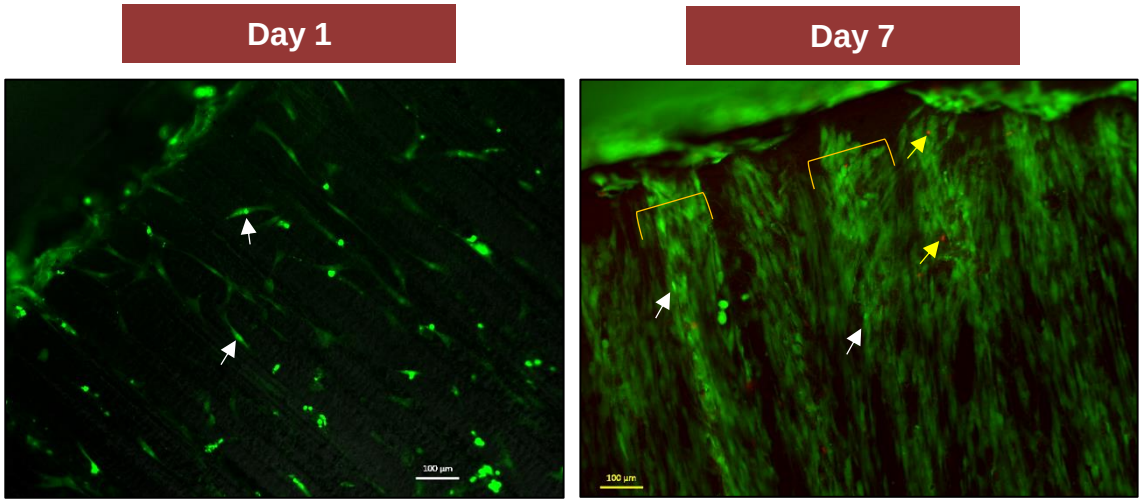

Figure 5-7: Fluorescent microscope images of live/dead cell markers for hPDLSCs seeded on acrylic PMMA block. Cells were cultured in basal medium, with cells' viability examined at day one and seven by labelling the cells with green-fluorescent calcein-AM and red-fluorescent ethidium homodimer-1 to detect living (white arrows) and dead cells (yellow arrows), respectively. An increase in the number of cells over the culture period was noticed, with living cells showing a band-like arrangement at day seven referred to with yellow brackets.

5.4.3 The behaviour of hPDLSCs in response to the compression forces

Cellular activity of hPDLSCs in response to the applied cyclic compressive force was compared to that of cells cultured unstimulated (control group). The comparison includes three aspects, the cells' viability, proliferation rate based on their metabolic activity, histological evaluation of constructs interfaces of each sample, in addition to the differentiation capacity of hPDLSCs by measuring the expression levels of early differentiation markers.

5.4.3.1 Effect of cyclic compression force on cellular viability of hPDLSCs

After 24 hours of seeding on Bmf silk scaffold, hPDLSCs found distributed over the entire surface of the Bmf silk scaffold and following the circular shape of its pores as demonstrated in Figure (5-8/A). No evidence was recorded for the presence of dead cells.

These findings were supported following 14 days of culturing hPDLSCs in the basal medium in the bioreactor. Fluorescent images of cells in both groups, Figures (5-8/B) and (5-8/C), showed an increase in their number. The cells subjected to the compressive stimulation appeared slightly at a higher density when compared to the unstimulated samples, as demonstrated in Figures (5-8/B) and (5-8/C). Also, few dead cells were recognised stained with red-fluorescent ethidium homodimer-1, see Figures (5-8/B).

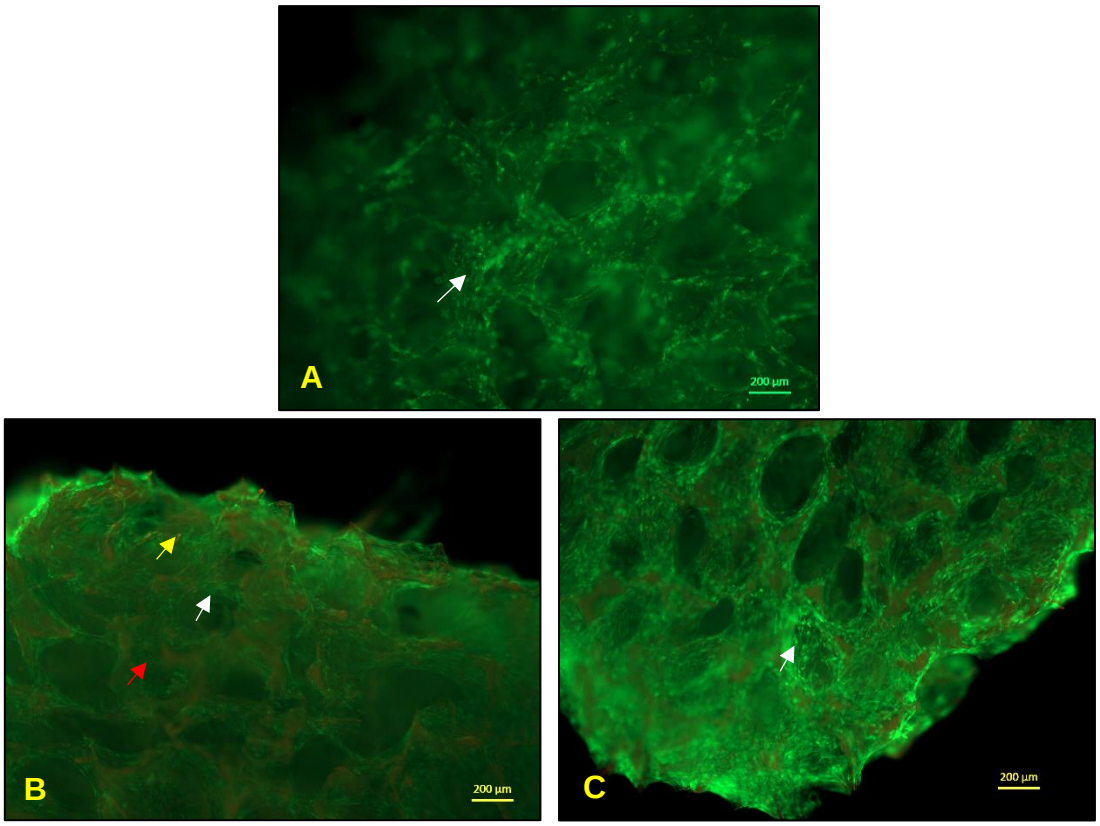

Figure 5-8: Fluorescent images of hPDLSCs, seeded on Bmf silk scaffold (red arrow), labelled with live/dead cell markers. Cells were cultured in basal medium with cellular viability examined following 24 hrs of initial seeding (A) by labelling the cells with green-fluorescent calcein-AM and red-fluorescent ethidium homodimer-1 to detect living (white arrows) and dead cells (red arrows), respectively. After 14 days of culture in either unstimulated (B) or stimulated with compressive loading (C), cellular viability was re-examined. Both groups' cells were distributed in a circular like-shape around the orifices of Bmf silk scaffold pores.

5.4.3.2 Influence of cyclic compression loading on the metabolic activity of hPDLSCs

AlamarBlue™ quantitative assay showed comparable results between the unstimulated and stimulated groups. The difference was statically non-significant (P>0.05), (Figure 5-9).

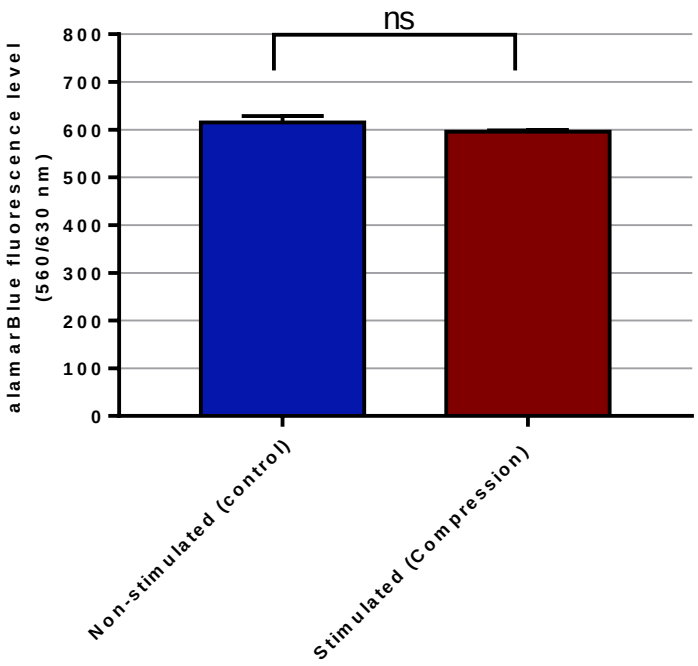

Figure 5-9: Effect of cyclic compression force on the metabolic activity of hPDLSCs measured with alamarBlue fluorescence assay (relative fluorescence units). Results represented by mean ± SD of fluorescence level for the two groups (n=3). Statistical analysis performed using unpaired t-test with Welch's test at *p*-value ≤ 0.05.

5.4.3.3 Proliferation and distribution of hPDLSCs in response to cyclic compressive stimulation as identified by histological examination

The constructs were subjected to histological examination after 14 days of *in vitro* culture in the basal medium either unstimulated or stimulated with cyclic compression force. The H/VG stained sections of the unstimulated (control) group revealed incomplete fusion between the two constructs of the sample, with few cells were recognised in the central part of the interface. However, an increased number of cells was evident at the interface's sides with no fusion between the constructs at the borders, as demonstrated in Figures (5-10/A) and (5-10/B).

In contrast, the samples of stimulated groups showed evidence of complete union between the two sample parts (constructs), see Figures (5-10/ C) and (5-10/D). Furthermore, the cells were found in a larger number at the interface's sides and in the central part of it.

Another important feature was the formation of collagen fibres, which presented as a mesh at the interface's sides. These collagen fibres were extended to the deep layers of the group's constructs subjected to the compressive stimulation. At the same time, they were confined to the sides in the control group.

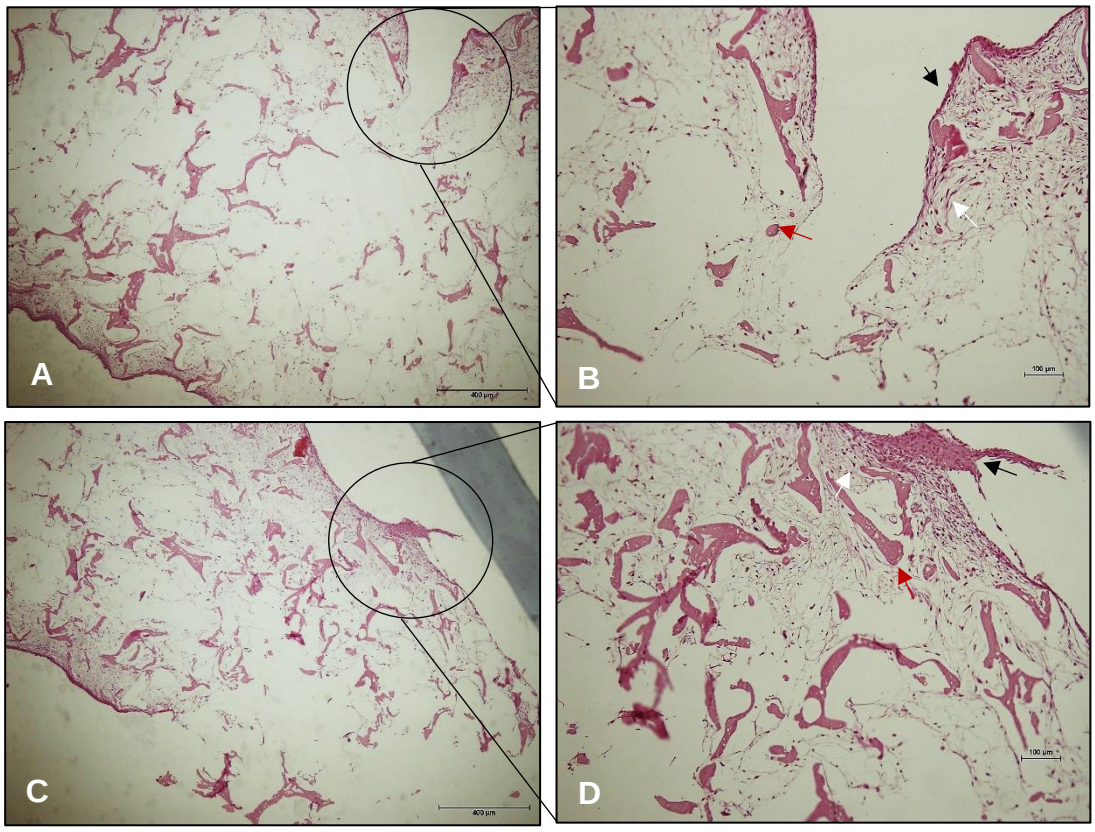

Figure 5-10: Histological comparison of the cellular growth at constructs interface in the unstimulated (control) and stimulated groups. Constructs' sections were stained with haematoxylin/ van Gieson stains to visualise the cells and collagen fibres (white and black arrows, respectively). In the control group, the cellular growth was recognised at both sides of the interface with few cells in the centre. In contrast, the gap between the two constructs was completely closed in the group exposed to the cyclic compression force, with a relatively higher volume of cellular growth in the centre and sides of the interface. The structure of the Bmf scaffold referred to in red arrows.

5.4.3.4 Differentiation capacity of hPDLSCs in response to the compressive stimulation

Results of relative genes expression immunogenicity assay revealed higher levels of expression of COL-1, OCN and CEMP in the cells exposed to the compression force. However, statistical analysis of these results revealed a non-significant difference between the two groups regarding the three genes' relative expression levels (Figure 5-11).

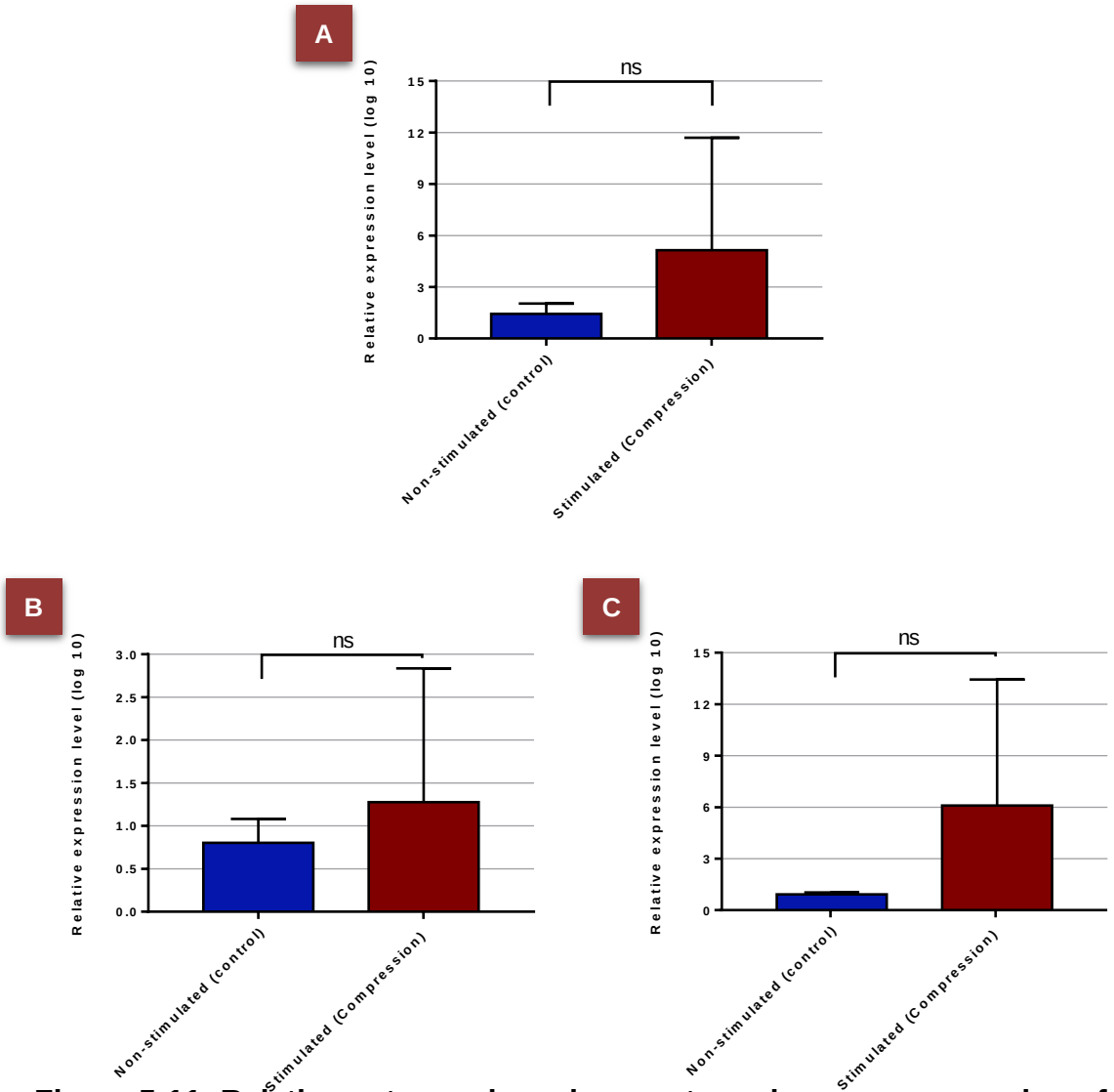

Figure 5-11: Relative osteogenic and cementogenic genes expression of hPDLSCs in response to cyclic compression stimulation. The cells exposed to cyclic compression stimulation showed increase in the expression of levels of COL-1 (A), OCN (B) and CEMP (C). However, statistical analysis revealed a non-significant difference between control and experimental groups. Statistical analysis performed using unpaired t-test at *p*-value ≤ 0.05.

5.5 Discussion

Understanding periodontal cells' behaviour in response to physiological and orthodontic mechanical loading is of great importance to improve the therapeutic approaches. In this part of the project, a novel, mechanical stimulation bioreactor was manufactured in an attempt to overcome the limitations of currently available models, i.e. the mode of force application, the number of tested samples. Also, it provides an affordable tool for studying the cells mechanobiology in 3D *in vitro* environment. This step was followed by a preliminary study to investigate the effect of applying a cyclic compressive stimulation on the behaviour of hPDLSCs *in vitro*. The following sections are discussing the present findings related to this part of the project.

5.5.1 The manufactured bioreactor: Unique design and useful features

The bioreactor was initially introduced in the early 80s to provide a safe and economical alternative to in vivo study and improve functional tissue regeneration outcomes. According to a report by Sladkova and de Peppo (2014), there are essential features that must be considered in designing a bioreactor for tissue engineering applications apart from manufacturing it from an inert, biocompatible material. Among those, it should support cultured cells' growth by providing essential supplements, e.g. oxygen and nutrients, and removal of biological waste. Another prominent feature is introducing an accurate mechanical stimulation that mimics the living organism's physiological environment. The bioreactor must also allow for an automatic and reproducible series of actions under full control Sladkova and de Peppo (2014). In the present study, a novel mechanical loading bioreactor has been designed and manufactured using biocompatible materials to allow the cells culture under various mechanical loading settings. The current bioreactor includes the essential components of bioreactors used for *in vitro* study to examine the effect of mechanical stimulation.

Sladkova and de Peppo (2014) described the requirement for a bioreactor, as it should contain electrical motors able to produce the required stimulation, a gears system that can transform the rotation motion of motors into linear forces applied directly to the cell-scaffold constructs, and culture chambers that could support the growth of the cells. The design of current

bioreactor includes a chambers unit that contains two separated rows of chambers for cells culture (four in every single row), the feature that could minimise the variation in the environment of cell culture between the samples of the same group. Furthermore, this configuration helps in examining four replicates of cell-scaffold constructs for each group simultaneously, which significantly reduces the experiment time and resources. The chamber unit's cover, made of PMMA cast acrylic, provides the required isolation from the surrounding atmosphere. However, gas exchange significantly impacts the behaviour and survival of cultured cells, especially the oxygen, which represent a singling and metabolic molecule (Martin *et al.*, 2004). The bioreactor's cover was designed to permit a narrow window that facilitates gas exchanges to support cells growth in a way similar to those of commercial cells culture vessels. As the cover is made from a transparent material, it enables direct monitoring of samples while being subjected to the mechanical loading; and it helps observe the changes in the culture medium during the cells' incubation period, e.g. changes in the colour of medium due to change in the pH.

Studying the cellular behaviour in response to physical loading requires a bioreactor with a capacity to produce such stimulation that simulates the physiological environment in both the form, rate and magnitude. This process should be achieved under a high degree of controllability over the stimulation parameters (Amrollahi *et al.*, 2017). With the current bioreactor, it became possible to study the influence of mechanical loading on tissue-engineered constructs within two different experimental groups simultaneously, with each group being subjected to different stimulation settings. These settings include the mode of loading, e.g. compressive, shear or unstimulated, the frequency of stimulation (stroke per minute), as well as the displacement distance (0.5 mm, 1 mm, 1.5 mm and 2 mm), which affects on the magnitude of applied forces and spreads the loading effect to the deep layers of the scaffold.

Ease of operation, sterilisability and reusability of components and consideration of unit size are other technical specifications that enhance the usefulness of the designed bioreactor. Consequently, the current bioreactor has features that expand the range of its application to study mechanical stimulation effects on cell behaviour *in vitro*.

5.5.2 Biocompatibility of bioreactor material

The manufactured bioreactor includes a cell-culture unit that was made of PMMA cast acrylic. This material has many medical and dental applications; among these are dental prosthesis, contact and intraocular lenses as well as its use as bone cement, filler, and fixation screws in orthopaedic (Cuffe *et al.*, 1978; Frazer, R.Q. *et al.*, 2005; Breusch and Malchau, 2005; Zheng *et al.*, 2011). This wide range of application is due to the properties of PMMA itself. It is an inert material with good physical and mechanical properties, including its excellent dimensional stability. It has a remarkable resistance to temperature variation, chemicals and body fluids. Furthermore, PMMA acrylic is transparent and able to transmit 92% of visible light similar to glass, with excellent clarity (Breusch and Malchau, 2005; Pawar, 2016); this is a crucial point to consider in building a bioreactor, as it enables direct monitoring of samples (Sladkova and de Peppo, 2014).

The immunogenicity test results revealed that PMMA acrylic block could induce the release of pro-inflammatory cytokines (TNF-α and IL-1β) at levels comparable to that induced by COL-1 scaffold at same time points. These findings indicate that PMMA material is a safe material to be used for bioreactor manufacturing.

The cast acrylic used for manufacturing the bioreactor chambers in this study is characterised by its unique features attributed to its production process. The process involves casting PMMA powder within glass mould, then a correct volume of methyl methacrylate (MMA) liquid added. The material then slowly polymerised by exposure to wet heat for up to twelve hours (heat-cured acrylic). The final product is a PMMA acrylic with the smooth, glassy surface. This heat-activated curing method reduces the amount of the residual MMA monomer, which is a volatile, cytotoxic material that can initiate a hypersensitivity reaction in humans (Dahl *et al.*, 1994; Leggat and Kedjarune, 2003). Moreover, among the various PMMA curing methods, e.g. heat-curing, light-curing or chemical-curing, it has been proven that heat-curing releases the lowest amount of residual monomer (Rose *et al.*, 2000).

In 1988, Baker *et al.* found that the release of residual MMA from the dental appliance is dependent on the length of the heat processing cycle. Whereas MMA was detected in the saliva of patients used acrylic denture cured for one hour only, no MMA was found in the saliva of those wearing dentures

cured for three hours. This study also recommended immersing the acrylic appliance in water for 24 hours to reduce monomer release. Tsuchiya *et al.* (1994) confirmed the previous result. They concluded that soaking the acrylic denture in hot water (50^{o}C) for one hour or in cold water for 24 hours minimises monomer's release by up to 75%, especially for self-cured acrylic. In this sense, it was concluded that the reduction in residual monomer could be attributed to two main mechanisms. First, it helps exclude oxygen, which inhibits the polymerisation of acrylic, enhancing the polymerisation process that consumes the remaining monomer. Secondly, it facilitates the surface monomer's leaching to the surrounding water (Basker *et al.*, 1989; Rose *et al.*, 2000).

Another critical factor to consider regarding the PMMA is the chemical structure of this material. PMMA acrylic composed of a repeated number of ($C_5O_2H_8$) formula with a methyl group, as shown in figure (5-10). Mariani *et al.* (2019) confirmed that this type of polymer, with a methyl group, expresses a neutral surface charge. Also, a hydrophobic surface permits selective interaction for CD8 T-lymphocyte (Chang *et al.*, 2009; Meeran, 2012; Khademi *et al.*, 2017). However, Fröhlich (2012) mentioned that hydrophobic surfaces of nanoparticles, like stearic acid-coated TiO_2 and nickel ferrite, could induce more cytotoxic reaction that noncoated particles.

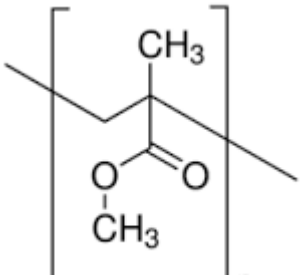

Figure 5-12: Chemical formula of PMMA

Immuno response can be affected by the surface charge of the implanted material. While positively charged surfaces can induce marked inflammatory reaction, negatively charged surfaces appeared to render the immune response via reducing the phagocytosis by antigen-presenting cells. On the other hand, it found that the positively charged gold nanoparticles are more cytotoxic than neutral particles (Fröhlich, 2012; Wen *et al.*, 2016).

These findings could explain the low level of immunogenicity induced by the cast, heat-cured acrylic used for manufacturing the bioreactor's cell culture unit in this study.

Cytotoxicity is one of the primary tests used for evaluation of biocompatibility of biomaterials. It depends on qualitative or quantitive monitoring of cell reactions upon contact with the examined material. This reaction to the toxic agents released from the material can be translated into deterioration in the cells bioactivities, including, cell adhesion, morphology, proliferation, metabolic activity, and cells death and lysis (Wang *et al.*, 2013; Li *et al.*, 2015).

In the present study, an examination of cytotoxicity was performed to validate the PMMA immunogenicity test finding. The cytotoxicity results signify that heat-cured PMMA acrylic supported the cellular attachment and spreading of hPDLSCs from the first 24-hour of seeding. Furthermore, the cells retained the normal spindle-like morphology and continued to proliferate over the culture period, with a limited number of dead cells. Based on these results, It becomes evident that hPDLCS similarly reacted to the PMMA material to other biocompatible scaffold material. (Papenburg *et al.*, 2010) stated that hydrophobicity, along with surface topography, could increase cell attachment.

Nevertheless, the current finding seems to contradict with the report by Ferrari *et al.* (2019). They concluded that material with a hydrophobic surface, like PMMA, could negatively interfere with cells attachment (Ferrari *et al.*, 2019). This fact was the reason behind many trials for modifying the PMMA surface as used in regenerative bone replacement (Patel *et al.*, 2006; Zheng *et al.*, 2011). In the current study, the cellular attachment of hPDLSCs over the PMMA surface could be attributed to PMMA blocks' treatment with a medium supplemented by 20% FBS. This step was performed to simulate the working environment of the bioreactor during mechanical stimulation. According to the literature, FBS surface treatment could enhance cellular attachment as it includes adhesive proteins, e.g. fibronectin and vitronectin (Hayman *et al.*, 1985; Warrener and Anderson, 2014; Raimondi *et al.*, 2016). Serum proteins adsorbed on the material surface, allowing for cells adhesion and subsequent cells proliferation (Weszl *et al.*, 2012; Shinto *et al.*, 2013).

The current findings necessitate careful decellularisation, cleaning and sterilisation of cells chambers after each experiment to ensure complete removal of cells/cellular remnants that could affect future tests results, involving the mechanical loading bioreactor.

The conclusions of PMMA biocompatibility study come in accordance with previous studies (Acosta-Torres *et al.*, 2012; Goiato *et al.*, 2015) that confirm the low toxicity of heat-cured PMMA acrylic. However, it is crucial to consider several factors while utilising this material for biological applications, including the polymerisation methods, removal of residual monomer, and surface treatment.

5.5.3 Effect of Compressive loading on the behaviour of hPDLSCs *in vitro*

The response of mechanical stimulation on periodontal cells was investigated both in 2D and 3D environments. Furthermore, several factors were set to define the outline for studies such as type of applied force, e.g. tensile, compressive, shear; mode of force application, i.e. static or intermittent; and force magnitude (Li *et al.*, 2019). Although, many studies used an *in vitro* model to investigate this topic. Limited data could be found in the literature regarding the role of compressive stress on the cell's behaviour. Most of those studies were reported to have many limitations related to the cells culturing environment and mode of force application (Li *et al.*, 2019). Accordingly, the current study was aiming to overcome these limitations by creating a model that could simulate the physiological pattern.

In this study, primary hPDLSCs were seeded on porous Bmf silk scaffolds to create 3D constructs. Subsequently, these constructs were combined in pairs with opposing surfaces, as an attempt to replicate the interface between two-component tissues of the periodontium. Given that this study's primary goal was to investigate the effect of mechanical stimulation on the behaviour of hPDLSCs, the developed bioreactor was utilised to apply an intermittent, compressive loading on the 3D constructs. Several cellular activities were monitored and compared to the unstimulated samples, including, cells viability, metabolic activity and differentiation capacity. Within the limitations of the current study, the findings confirm that mechanical stimulation affects the *in vitro* behaviour of hPDLSCs. It was found that cyclic, compressive stimulation could enhance cell proliferation

rate, improve the structure of ECM and induce hPDLSCs differentiation into osteogenic and cementogenic lineages.

Mechanical stimulation plays a critical role in development and regeneration of tissue. It defines the structural, cellular and physiological features of regenerated tissue. It has been introduced as the fourth element in tissue engineering in addition to cells, scaffold and growth factors. Also, it is believed that it could help improve the quality of constructed tissue to the level that mimics native ones (Berendsen *et al.*, 2009; Benhardt and Cosgriff-Hernandez, 2009; Goetzke *et al.*, 2018; Salinas *et al.*, 2018). Periodontal tissue is a dynamic organ that aids in accommodating and distributing forces applied to the teeth to prevent their damage along with other surrounding tissues (Howard *et al.*, 1998). Due to the complex nature of applied physiological forces, many studies tried to understand these forces' characteristics and the way that periodontal tissue responding to it (Rankovic *et al.*, 2019).

Based on the results of finite element studies, two main zones are defined across the surface of the periodontium; these involve tension zones where the tooth root move away from the investing alveolar bone applying tensile stress on periodontal tissue; and compression zones within which the root compresses against the alveolar bone (Cattaneo *et al.*, 2005; Matsunaga *et al.*, 2016; Li *et al.*, 2019). However, this software-based method cannot recognise and calculate the natural biological response (Garlet *et al.*, 2007; Poiate *et al.*, 2009).

While many previous studies investigated the role of tensile stress on periodontal cells, both in 2D and 3D *in vitro* environment, limited attention has been paid toward studying the effect of compression stress on these cells (Wang *et al.*, 2017; Manokawinchoke, Jeeranan *et al.*, 2019). Most of the compression studies were conducted on cells in 2D monolayered culture rather than 3D microenvironment. Thus, the cell's performance cannot be interpreted as a real reflection of normal biological events, as cell-cell and cell-extracellular matrix communication are significantly affected (Kang *et al.*, 2013; Yang, L. *et al.*, 2015; Goetzke *et al.*, 2018).

To the author's best knowledge, hydrogel-based scaffolds are mainly used in compression simulation studies (primarily rat tail COL-1). Although hydrogels have many advantages over other materials, they have drawbacks as a biomaterial used for tissue regeneration. Fine-tuning of

hydrogel viscoelasticity, stiffness, porosity and degradation rate is required to provide an optimum environment for cells spreading and migration with this scaffold material (Discher *et al.*, 2005; Dadsetan *et al.*, 2008; Patterson and Hubbell, 2010; McKinnon *et al.*, 2014). Also, widely used collagen-based scaffolds for mechanical loading studies are not the optimum choice for regenerating hard tissues due to its low mechanical properties and weak structure (Drury and Mooney, 2003; Lee *et al.*, 2007)

In this study, a 3D, porous scaffold made of a natural polymer material (Bmf silk) was chosen to culture and support hPDLSCs growth *in vitro*. This material was proven to support the regeneration of tendons, ligament, and bone tissues (Kuo *et al.*, 2010; Zhang *et al.*, 2014; Hardy *et al.*, 2016; Galateanu *et al.*, 2019). This could be attributed to its superior mechanical properties compared to other hydrogels. Additionally, it has many other vital characteristics, e.g. biocompatibility, favourable oxygen permeability, castability, and controllable degradation rates (Kuo *et al.*, 2010; Galateanu *et al.*, 2019).

Another critical factor to consider in mechanical stimulation studies is the loading force itself. This includes the method of load application, mode, frequency, and magnitude. Among many techniques that have been used for studying the effect of compressive force on cells, weight loading was the most widely used. Basically, it involves applying a specific weight load over the cells to be seeded in 2D or 3D culture. However, this approach can simulate orthodontic stress rather than the masticatory force (Kang *et al.*, 2013; Yang, L. *et al.*, 2015). Others methods include centrifuging (Wei *et al.*, 2008), low-intensity pulsed ultrasound stimulation (Lim *et al.*, 2013), hydrostatic pressure (Brown, 2000), mechanical vibration (Zhang, C. *et al.*, 2012). Most of these methods are applicable *in vitro,* mostly on monolayered cells culture rather than 3D constructs. Matsunaga *et al.*, (2016) suggested that exposing cells to loading in such a manner might be excessive, as the occlusion is a limited process that happens a few times during daily routine.

The developed bioreactor used in this study was able to direct a controlled compressive force (25N) to the 3D cells-scaffold construct in an intermittent mode at a frequency within the physiological limit. This approach represents the cyclic force applied to teeth and periodontium during mastication within certain limits. The magnitude of physiological occlusal force was estimated to range from tens to hundreds of Newtons (Thie and Lavigne, 2001; Bakke,

2006; Papadopoulou *et al.*, 2014). It was found that cyclic loading of the periodontal ligament allows for rest periods that help in improve homeostasis in the area by stimulating the release of FGF-2 and endothelial growth factor thus enhancing regeneration of periodontal tissue (Oppenheim, 1944; Manokawinchoke *et al.*, 2015; Ichioka *et al.*, 2016).

The period of the present study is another point of strength as most of previous periodontal mechanobiology studies were conducted over a brief period of hours to few days (Howard *et al.*, 1998; Nakao, K *et al.*, 2007; Berendsen *et al.*, 2009; Hacopian *et al.*, 2011; Jia *et al.*, 2020). During the fourteen days of the current experiment, several parameters were evaluated. Some of those parameters were monitored over a short phase, e.g. cells viability, while others required relatively a long time to be detected. This includes expression of early differentiation markers as well as the formation of ECM.

This study's force was applied for 15 minutes, twice a day to mimic the meals routine for most people. During this period, the mastication process could last for minutes, while the teeth being under thrust at intervals of a second or less (Picton, 1965; Van Driel *et al.*, 2000; Thie and Lavigne, 2001).

5.5.3.1 Viability and proliferation of hPDLSCs in response to cyclic compressive stimulation

Compared to cells-scaffold constructs that cultured unstimulated, those subjected to cyclic compression forces demonstrated an abundance of cells with the enhancement of their viability. The formed extracellular matrix was also denser and more organised with more cells growth that bridge the gap between the two constructs in each sample. These results are consistent with previous studies that support the positive effect of mechanical loading in enhancing the proliferation and remodelling of periodontal cells (Kang *et al.*, 2013; Ichioka *et al.*, 2016). In contrast, (Li, Y. *et al.*, 2013) concluded that the proliferation rate of hPDLCs was significantly inhibited in response to compression forces. However, in the latter study, compressive loading was applied in static mode for a prolonged time, i.e. 6, 24, and 72 hours rather than cyclic stimulation.

Goga *et al.* (2006) suggested that cells viability and apoptosis is force-dependant. Also, he stated that high magnitude mechanical stimulation could reduce the viability of the cells. When the amount of force exceeded

the tissue's physiological elastic limit, the consequences will be either microfractures or tissue degeneration (Henneman *et al.*, 2008). During load application, the ECM of periodontal tissue reacts by a change in its configuration, including alteration in collagen fibres' orientation, the main constituent. These events stimulate a cellular response that depends on the magnitude of stimuli. Subsequently, cells produce certain proteins and enzymes that govern the cellular processes and remodelling of ECM (Howard *et al.*, 1998; Krishnan, Vinod and Davidovitch, 2006; Masella and Meister, 2006; Krishnan, V and Davidovitch, 2009).

Several pathways were recognised to be responsible for controlling cells' response against mechanical loading, among those in the MAPK1 (mitogen-activated protein kinase 1). MAPK is involved in several cellular processes, including proliferation and differentiation (Reyes-Reyes *et al.*, 2001; Liedert *et al.*, 2006). In 2013, Kang *et al.* showed that MAPK signalling pathway was up regulated after two hours of applying a continuous compression load of 2.0 g/cm^2 on hPDLCs while being seeded in collagen gel. These facts support the findings of the current study.

5.5.3.2 Role of cyclic compressive stimulation in inducing differentiation of hPDLSCs

In the current study, the results of cellular differentiation in response to the cyclic compressive loading indicated that such stimulation could induce osteogenic and cementogenic differentiation of hPDLSCs. However, these results were not statistically significant, which could be attributed to the limited time of stimulation and the short period of the experiment.

The current findings support previous studies that demonstrated the positive effect of applying a mechanical stimulation within the physiological limits in inducing differentiation of hPDLCs *in vitro* (Liu, M. *et al.*, 2012; Liu, J. *et al.*, 2017; Ravichandran *et al.*, 2017). Jacobs *et al.* (2013) found that hPDL fibroblast cells showed an increase in ALP expression, OCN and OPN markers when exposed to a static mechanical strain of 5%. In another study, Zhang, L. *et al.* (2016) proved the increase in osteogenic differentiation of hPDLSCs following stimulation of hPDLSCs with static compression for 1 hour.

In contrast, Diercke *et al.* (2011), demonstrated that stressing same cells type with 30.3 g/cm^2 of static compressive force could induce a significant increase in Ephrin-A2 expression level. The ephrin-A2 ligand can activate

EphA2 receptors that play a role in inhibiting osteoblast cells' specific genes and enhancing the osteoclastic differentiation (Irie *et al.*, 2009). It is essential to state that previous studies investigated the effect of static loading rather than intermittent one, which is more representative of the orthodontic force but not the masticatory force. It has been suggested that intermittent loading rhythm is associated with more osteogenic differentiation activity than a single continuous dose of loading (Robling *et al.*, 2001). Moreover, a significant increase in the interleukin-6 was linked to the application of continuous compressive force, with a decrease in ALP expression (Lee, Y.H. *et al.*, 2007). In their review article, Chukkapalli and Lele (2018) referred to the conventional concept that links between the compressive loading and bone resorption, while attribute inducing bone formation to the tensile and shear forces.

Nevertheless, tissue reaction, including cellular differentiation, was directly related to the mode, magnitude and duration of the applied forces (Hacopian *et al.*, 2011; Goetzke *et al.*, 2018). In this context, Jia *et al.* (2020) confirmed the effect of force magnitude on the differentiation of hPDLSCs. It was found that applying cyclic hydrostatic pressure of 150 KPa can up-regulate the expression of inflammatory cytokines, including TNF-α, IL-1β, IL-6, IL-8, as well as pro-osteoclastic markers, e.g. RANKL.

Moreover, when 90 kPa of cyclic pressure was applied to the cells, there was a significant increase in the expression of COL-1 and osteogenic genes (ALP, RUNX2, OCN, OPN). The increase in the production of RANKL and a decrease in the viability of hPDLSCs has been associated with using excessive compressive force (Nakao, Kayoko *et al.*, 2007). RANKL/RANK and RANKL/OPG are among the signalling systems that determine cells' osteogenic activity. While binding RANKL ligand to the RANK receptor stimulates osteoclast maturation, OPG acts to prevent this reaction by binding to the RANKL itself; Thus, inhibiting the osteoclastogenesis (Theoleyre *et al.*, 2004).

A limited number of studies have investigated mechanical loading on cementogenic differentiation (Yu *et al.*, 2009; Wang, Liao *et al.*, 2016; Wu *et al.*, 2019). Result of the present study demonstrated an increase in the expression of CEMP1 in response to cyclic compressive loading; which could indicate the initiation of cementogenesis.

Several markers were used to recognise the cement formation, e.g. OCN, OPN, BSP. However, those markers are shared with other mineralised

tissue, i.e. bone. Thus, they cannot be specific enough to be dependant for monitoring the cementogenesis (Jin *et al.*, 2003; Komaki *et al.*, 2012; Bao *et al.*, 2014). Alvarez-Pérez *et al.* (2006) discovered a novel human cementum-derived protein (CP-23), which is also called CEMP1. This protein expressed in 98% of cementoblast and 15% of PDLCs cultured *in vitro.* Accordingly, this tissue-specific gene was used as a marker for cementum-related studies including the current one (Carmona-Rodríguez *et al.*, 2007; Diercke *et al.*, 2012; Barrera-Ortega *et al.*, 2017; Gauthier *et al.*, 2017; Dellavia *et al.*, 2019).

5.6 Conclusion

The novel mechanical stimulation bioreactor developed in the current study found to be a useful tool studying the effect of cyclic compressive and shear forces on the behaviour of 3D cells-scaffold constructs *in vitro*. This model provides the user with control over a wide range of essential parameters for studying the mechanobiology, including mode of action, frequency of application and displacement distance. Within the limitations of the mechanical loading experiment performed in this study, the results suggest that the *in vitro* proliferation and differentiation of hPDLSCs are affected by cyclic compression stimulation. These findings put the foundation for future studies to investigate the effect of frequency and mode of force on the regeneration of periodontal tissues *in vitro.* This step will help optimise the *in vitro* culture environment in an attempt to enhance the regeneration of periodontal tissue *in vitro*.

Chapter Six: Future work and conclusion

6.1 Future work

The findings of the current project form the basis for future studies to investigate the optimal culture environment to achieve the ultimate goal of enhancing periodontal regeneration both *in vitro* and *in vivo*. The future studies must investigate several points, including the factors affecting the characteristics of hPDLSCs as well as those related to scaffold material and mechanical stimulation and their role in the regeneration process.

The results illustrated in **Chapter 3** revealed presence of donor variability regarding the characteristics of isolated hPDLSCs, which can be attributed to many factors. This aspect might require further study to evaluate the effect of several donor-related factors on the properties of hPDLSCs. Such factors include donor age, gender, as well as the systemic medical status of the donor. Another point to be investigated is related to the site of isolation itself. In other words, to compare the characteristics of hPDLCs isolated from healthy or periodontally diseased sites, besides, the effect of tooth type, i.e. tooth number. This evaluation will help define the optimum source of cells before their isolation and implication for research or therapeutic purposes.

The current study has proven Bmf silk material's biocompatibility as a scaffold that can accommodate the proliferation and osteogenic differentiation of hPDLSCs. However, more in-depth studies are needed to evaluate the fibrogenic as well as the cementogenic proliferation and differentiation of those cells using the same scaffold. This evaluation should consider both *in vitro* and prolonged *in vivo* studies. This step will represent a milestone toward fabrication of multiphase, 3D composite that could accommodate the three periodontal tissues (bone, PDL and cementum) at the same time. The advance in 3D printing technology could be recruited to design each layer of this composite scaffold based on regenerated tissue properties.

Furthermore, it is useful to consider automating the bioreactor's current design with the digital technology era by introducing the computer-controlled

model. Accordingly, this improvement could help control the stimulation process's main parameters, e.g. frequency of stimulation and displacement distance. Also, to enable direct monitoring of cells culture's physicochemical environment for each of the chambers individually, this includes temperature, pH, and CO_2 levels.

It has been demonstrated in **Chapter 5** that compressive stimulation affects the proliferation and differentiation of hPDLSCs. However, further *in vitro* studies are required to confirm these findings and determine the role of stimulation parameters, including loading, frequency, and displacement distance. It is recommended that the evaluation process involve both qualitative and quantitative methods (biochemical assays, histological and immunohistological staining) to assess the cellular proliferation and differentiation accurately. Moreover, such studies must be performed over a relatively long period, i.e. up to 4 weeks, to provide representative results.

6.2 Conclusions

The transition of current research into a clinical application might require many years and massive efforts before becoming a reality. However, this project is another step toward optimising a protocol to enhance periodontal tissue regeneration, both *in vitro* and *in vivo*.

According to the current project findings, hPDLCs can be considered for periodontal cellular therapy and tissue regeneration *in vitro* and *in vivo*. They possess the characteristics of MSCs and can differentiate into several cells' lineages. However, these primary cells should be evaluated before they are applied for research or therapeutic purposes due to the donor variability that affects their characteristics.

On the other hand, Bmf silk is a potential scaffold material for periodontal tissue regeneration. The current results confirmed this material's biocompatibility and demonstrated its effect on supporting the attachment, proliferation and osteogenic differentiation of hPDLSCs, both *in vitro* and *in vivo*. The efficiency of this scaffold can be improved further with proper seeding technique and optimal cells seeding density.

Furthermore, mechanical stimulation plays a pivotal role in the development and regeneration of periodontium. Accordingly, it is essential to consider this factor in periodontal tissue regeneration. The manufactured mechanical stimulation bioreactor proved to be a useful tool for this purpose, with many features that enable control over the *in vitro* compressive/shear stimulation process of hPDLSCs. Moreover, cyclic compressive stimulation affects the proliferation rate, metabolic activity, and the differentiation capacity of hPDLSCs.

References

Acosta-Torres, L. S., I. Mendieta, R. E. Nuñez-Anita, M. Cajero-Juárez and V. M. Castaño (2012). Cytocompatible antifungal acrylic resin containing silver nanoparticles for dentures. International journal of nanomedicine 7: 4777.

Algire, G.H., Weaver, J.M. and Prehn, R.T. 1954. Growth of cells in vivo in diffusion chambers. I. Survival of homografts in immunized mice. Journal of the National Cancer Institute. 15(3), pp.493-507.

Almela, T., Brook, I.M. and Moharamzadeh, K. 2016. Development of three-dimensional tissue engineered bone-oral mucosal composite models. Journal of Materials Science: Materials in Medicine. 27(4), p65.

Al-Nasiry, S., Geusens, N., Hanssens, M., Luyten, C. and Pijnenborg, R., 2007. The use of Alamar Blue assay for quantitative analysis of viability, migration and invasion of choriocarcinoma cells. Human reproduction, 22(5), pp.1304-1309.

Alvarez-Pérez, M.A., Narayanan, S., Zeichner-David, M., Carmona, B.R. and Arzate, H. 2006. Molecular cloning, expression and immunolocalization of a novel human cementum-derived protein (CP-23). Bone. 38(3), pp.409-419.

Amrollahi, P., F. Moghadam and L. Tayebi 2017. Bioreactor design for oral and dental tissue engineering. Biomaterials for Oral and Dental Tissue Engineering, Elsevier: 193-204.

Amunulla, A., Venkatesan, R., Hemalatha Ramakrishnan, K., Sudarshan, S. and Talwar, A. 2008. Lymphocyte subpopulation in healthy and diseased gingival tissue. Journal of Indian Society of Periodontology. 12(2), p45.

Anderson, J. M. 2001. Biological responses to materials. Annual Review of Materials Research, 31(1), pp. 81-110.

Ashton, B., Eaglesom, C., Bab, I. and Owen, M. 1984. Distribution of fibroblastic colony-forming cells in rabbit bone marrow and assay of their osteogenic potential by an in vivo diffusion chamber method. Calcified tissue international. 36(1), pp.83-86.

Atala, A. and Yoo, J. 2009. Guest Editors Introduction, Methods. 47, pp.79 – 80.

Atari, M., Caballe-Serrano, J., Gil-Recio, C., Giner-Delgado, C., Martinez-Sarra, E., Garcia-Fernandez, D.A., Barajas, M., Hernandez-Alfaro, F., Ferres-Padro, E. and Giner-Tarrida, L. 2012. The enhancement of osteogenesis through the use of dental pulp pluripotent stem cells in 3D. Bone. 50(4), pp.930-941.

Baker, B.M. and Chen, C.S. 2012. Deconstructing the third dimension–how 3D culture microenvironments alter cellular cues. Journal of cell science. 125(13), pp.3015-3024.

Bakke, M. (2006). Bite Force and Occlusion. Seminars in Orthodontics 12(2): 120-126.

Bakopoulou, A., Leyhausen, G., Volk, J., Tsiftsoglou, A., Garefis, P., Koidis, P. and Geurtsen, W. 2011. Comparative analysis of in vitro osteo/odontogenic differentiation potential of human dental pulp stem cells (DPSCs) and stem cells from the apical papilla (SCAP). Arch Oral Biol. 56(7), pp.709-721.

Baksh, D., Song, L. and Tuan, R. 2004. Adult mesenchymal stem cells: characterization, differentiation, and application in cell and gene therapy. Journal of cellular and molecular medicine. 8(3), pp.301-316.

Bao, X., Liu, X., Zhang, Y., Cui, Y., Yao, J. and Hu, M. 2014. Strontium promotes cementoblasts differentiation through inhibiting sclerostin expression in vitro. Biomed Res Int. 2014, p487535.

Barrera-Ortega, C., Hoz-Rodríguez, L., Arzate, H., Fonseca-García, A., Pérez-Alvarez, J. and Rodil, S. 2017. Comparison of the osteogenic, adipogenic, chondrogenic and cementogenic differentiation potential of periodontal ligament cells cultured on different biomaterials. Materials Science and Engineering: C. 76, pp.1075-1084.

Barry, F., Boynton, R.E., Liu, B. and Murphy, J.M., 2001. Chondrogenic differentiation of mesenchymal stem cells from bone marrow: differentiation-dependent gene expression of matrix components. Experimental cell research. 268(2), pp.189-200.

Bascones, M. A. and Figuero, R. E. 2005. Periodontal diseases as bacterial infection. Avances en Periodoncia e Implantología Oral. 17(3), pp. 111 - 118.

Basker, R. M., J. Collier, I. Smith, K. D. Bartle, B. Frere and L. Wong 1989. Variation of residual monomer content of poly (methyl methacrylate) dental resins with time, and the influence of water immersion. Clinical Materials 4(2): 173-182.

Baumgarth, N. and Roederer, M. 2000. A practical approach to multicolor flow cytometry for immunophenotyping. Journal of immunological methods. 243(1-2), pp.77-97.

Beertsen, W., McCulloch, C.A. and Sodek, J. 1997. The periodontal ligament: a unique, multifunctional connective tissue. Periodontology 2000. 13(1), pp.20-40.

Benatti, B. et al. 2007. Physiological features of periodontal regeneration and approaches for periodontal tissue engineering utilizing periodontal ligament cells. Journal of bioscience and bioengineering, 103(1), pp.1 - 6.

Benhardt, H.A. and Cosgriff-Hernandez, E.M. 2009. The role of mechanical loading in ligament tissue engineering. Tissue Engineering Part B: Reviews. 15(4), pp.467-475.

Berendsen, A. D., T. H. Smit, F. Walboomers, V. Everts, J. A. Jansen and A. L. J. J. Bronckers (2009). Three-Dimensional Loading Model for Periodontal Ligament Regeneration In vitro. TISSUE ENGINEERING: Part C 15(4).

Berendsen, A.D., Smit, T.H., Walboomers, F., Everts, V., Jansen, J.A. and Bronckers, A.L.J.J. 2009. Three-Dimensional Loading Model for Periodontal Ligament Regeneration In Vitro. TISSUE ENGINEERING: Part C. 15(4).

Berkovitz, B. 1990. The structure of the periodontal ligament: an update. The European Journal of Orthodontics. 12(1), pp.51-76.

Beutler, B.A. 1999. The role of tumor necrosis factor in health and disease. The journal of rheumatology. Supplement. 57, pp.16-21.

Bhattacharjee, P., Kundu, B., Naskar, D., Kim, H.-W., Maiti, T.K., Bhattacharya, et al., 2017. Silk scaffolds in bone tissue engineering: An overview. Acta biomaterialia. 63, pp.1-17.

Bianco, P., Riminucci, M., Gronthos, S. and Robey, P.G. 2001. Bone marrow stromal stem cells: nature, biology, and potential applications. Stem cells. 19(3), pp.180-192.

Bini, E., Knight, D.P. and Kaplan, D.L. 2004. Mapping domain structures in silks from insects and spiders related to protein assembly. Journal of molecular biology. 335(1), pp.27-40.

Bird, S., Zou, J., Wang, T., Munday, B., Cunningham, C. and Secombes, C.J., 2002. Evolution of interleukin-1β. Cytokine & growth factor reviews, 13(6), pp.483-502.Bobis, S., Jarocha, D. and Majka, M. 2006. Mesenchymal stem cells: characteristics and clinical applications. Folia histochemica et cytobiologica. 44(4), pp.215-230.

Bonassar, L.J. and Vacanti, C.A. 1998. Tissue engineering: the first decade and beyond. Journal of cellular biochemistry. 72(S30–31), pp.297-303.

Bornstein, MM et al. 2009. Properties of barrier membranes. In: Buser, D. ed. 20 Years of Guided Bone Regeneration in Implant Dentistry. 2nd ed. Chicago, IL: Quintessenz. pp. 47– 69.

Bose, S. et al. 2012. Recent advances in bone tissue engineering scaffolds. Trends in Biotechnology. 30(10), pp. 546 - 547.

Bosshardt, D.D. and Sculean, A. 2009. Does periodontal tissue regeneration really work? Periodontology 2000. 51(1), pp.208-219.

Boyko, G. et al. 1981. Formation of new periodontal ligament by periodontal ligament cells implanted in vivo after culture in vitro. A preliminary study of transplanted roots in the dog. Journal of Periodontal Research. 16, pp.73 – 88.

Bradley, T., Metcalf, D., Sumner, M. and Stanley, R. 1969. Characteristics of in vitro colony formation by cells from haemopoietic tissues. In vitro. 4(1), pp.22-35.

Bray, L. J., et al. 2013. Incorporation of exogenous RGD peptide and inter-species blending as strategies for enhancing human corneal limbal epithelial cell growth on Bombyx mori silk fibroin membranes. Journal of functional biomaterials, 4(2), pp. 74-88.

Breusch, S. and H. Malchau 2005. The well-cemented total hip arthroplasty, Springer.

Brown, T.D., 2000. Techniques for mechanical stimulation of cells in vitro: a review. Journal of biomechanics, 33(1), pp.3-14.

Bylski, D., Wedemeyer, C., Xu, J., Sterner, T., Löer, F. and von Knoch, M. 2009. Alumina ceramic particles, in comparison with titanium particles, hardly affect the expression of RANK-, TNF-α-, and OPG-mRNA in the THP-1 human monocytic cell line. Journal of Biomedical Materials Research Part A: An Official Journal of The Society for Biomaterials, The Japanese Society for Biomaterials, and The Australian Society for Biomaterials and the Korean Society for Biomaterials. 89(3), pp.707-716.

Cao, Y. and Wang, B. 2009. Biodegradation of silk biomaterials. International journal of molecular sciences. 10(4), pp.1514-1524.

Cardona, M. A. et al. 1992. TNF and IL-1 generation by human monocytes in response to biomaterials. Journal of biomedical materials research, 26(7), pp. 851-859.

Carmona-Rodríguez, B., Álvarez-Pérez, M.A., Narayanan, A.S., Zeichner-David, M., Reyes-Gasga, J., Molina-Guarneros, J., et al., 2007. Human Cementum Protein 1 induces expression of bone and cementum proteins by human gingival fibroblasts. Biochemical and biophysical research communications. 358(3), pp.763-769.

Castro-Malaspina, H., Gay, R.E., Resnick, G., Kapoor, N., Meyers, P., Chiarieri, D., et al., 1980. Characterization of human bone marrow fibroblast colony-forming cells (CFU-F) and their progeny. Blood. 56(2), pp.289-301.

Caton, J. and Zander, HA. 1976. Osseous repair of an infrabony pocket without new attachment of connective tissue. Journal of clinical periodontology. 3, pp.54–58.

Cattaneo, P., Dalstra, M. and Melsen, B. 2005. The finite element method: a tool to study orthodontic tooth movement. Journal of dental research. 84(5), pp.428-433.

Chan, B. P. and Leong, K. W. 2008. Scaffolding in tissue engineering: general approaches and tissue-specific considerations. European spine journal, 17(4), pp. 467-479.

Chang, D.T., Colton, E., Matsuda, T. and Anderson, J.M. 2009. Lymphocyte adhesion and interactions with biomaterial adherent

macrophages and foreign body giant cells. Journal of Biomedical Materials Research Part A: An Official Journal of The Society for Biomaterials, The Japanese Society for Biomaterials, and The Australian Society for Biomaterials and the Korean Society for Biomaterials. 91(4), pp.1210-1220.

Chang, G., et al. 2007. Porous silk scaffolds can be used for tissue engineering annulus fibrosus. European Spine Journal, 16(11), pp. 1848-1857.

Chen, F. and Jin, Y. 2010. Periodontal tissue engineering and regeneration: current approaches and expanding opportunities. Tissue engineering: part B. 16(2), pp. 219 – 255.

Chen, K., Xiong, H., Huang, Y. and Liu, C. 2013. Comparative analysis of in vitro periodontal characteristics of stem cells from apical papilla (SCAP) and periodontal ligament stem cells (PDLSCs). Arch Oral Biol. 58(8), pp.997-1006.

Chen, Y., A. Mohammed, M. Oubaidin, C. A. Evans, X. Zhou, X. Luan, and T. G. Diekwisch (2015). Cyclic stretch and compression forces alter microRNA-29 expression of human periodontal ligament cells. Gene 566(1): 13-17.

Chen, Y.J., Jeng, J.H., Chang, H.H., Huang, M.Y., Tsai, F.F. and Jane Yao, C.C. 2013. Differential regulation of collagen, lysyl oxidase and MMP-2 in human periodontal ligament cells by low-and high-level mechanical stretching. Journal of periodontal research. 48(4), pp.466-474.

Chesnutt, B. M., et al. 2009. Composite chitosan/nano-hydroxyapatite scaffolds induce osteocalcin production by osteoblasts in vitro and support bone formation in vivo. Tissue Engineering Part A, 15(9), pp. 2571-2579.

Cho, M.I. and Garant, P.R. 2000. Development and general structure of the periodontium. Periodontology 2000. 24(1), pp.9-27.

Chocholata, P., Kulda, V. and Babuska, V. 2019. Fabrication of scaffolds for bone-tissue regeneration. Materials. 12(4), p568.

Choi, J.H., Kim, D.K., Song, J.E., Oliveira, J.M., Reis, R.L. and Khang, G. 2018. Silk fibroin-based scaffold for bone tissue engineering. Novel Biomaterials for Regenerative Medicine. Springer, pp.371-387.

Choi, S., Cho, T.J., Kwon, S.K., Lee, G. and Cho, J. 2013. Chondrogenesis of periodontal ligament stem cells by transforming growth factor-beta3 and bone morphogenetic protein-6 in a normal healthy impacted third molar. Int J Oral Sci. 5(1), pp.7-13.

Christopher, A. et al., 2000. Role of physical forces in regulating the form and function of the periodontal ligament. Periodontology 2000. 24, pp. 56–72

Chukkapalli, S. S. and T. P. Lele (2018). Periodontal cell mechanotransduction. Open biology 8(9): 180053.

Clarke, B., 2008. Normal bone anatomy and physiology. Clinical journal of the American Society of Nephrology, 3(3), S131-S139.

Cohn, S. 1965. Disuse atrophy of the periodontium in mice. Archives of oral biology 10(6): 909-919.

Conget, P.A. and Minguell, J.J. 1999. Phenotypical and functional properties of human bone marrow mesenchymal progenitor cells. Journal of cellular physiology. 181(1), pp.67-73.

Cordes, V., Lüpke, M., Gardemin, M., Seifert, H. and Staszyk, C. 2012. Periodontal biomechanics: finite element simulations of closing stroke and power stroke in equine cheek teeth. BMC veterinary research. 8(1), p60.

Cortellini, P. and Bowers, GM. 1995. Periodontal regeneration of intrabony defects: an evidence-based treatment approach. International journals of periodontics and restorative dentistry. 15, pp.128 – 145.

Cossarizza, A., Chang, H.D., Radbruch, A., Akdis, M., Andrä, I., Annunziato, F., Bacher, P., Barnaba, V., Battistini, L. and Bauer, W.M. 2017. Guidelines for the use of flow cytometry and cell sorting in immunological studies. European journal of immunology. 47(10), pp.1584-1797.

Craig, C. L., and Riekel, C. 2002. Comparative architecture of silks, fibrous proteins and their encoding genes in insects and spiders. Comparative Biochemistry and Physiology Part B: Biochemistry and Molecular Biology, 133(4), pp. 493-507.

Cuffe, P. M., A. R. LeBoeuf and E. A. Travnicek (1978). Material for the fabrication of artificial intraocular lenses and hard contact lenses, Google Patents.

Dadsetan, M., Hefferan, T.E., Szatkowski, J.P., Mishra, P.K., Macura, S.I., Lu, L. and Yaszemski, M.J. 2008. Effect of hydrogel porosity on marrow stromal cell phenotypic expression. Biomaterials. 29(14), pp.2193-2202.

Dahl, O. E., L. J. Garvik and T. Lyberg (1994). Toxic effects of methylmethacrylate monomer on leukocytes and endothelial cells in vitro. Acta Orthopaedica Scandinavica 65(2): 147-153.

Daniel, J. 2014. Essentials of oral histology and embryology: a clinical approach. 4th ed. USA: Elsevier. pp:136-137.

Darby, I. 2011. Periodontal materials. Australian Dental Journal. 56(1), p.113.

De Araujo, R., Oba, Y. and Moriyama, K. 2007. Identification of genes related to mechanical stress in human periodontal ligament cells using microarray analysis. Journal of periodontal research. 42(1), pp.15-22.

Dellavia, C., Canciani, E., Rasperini, G., Pagni, G., Malvezzi, M. and Pellegrini, G. 2019. CEMP-1 Levels in Periodontal Wound Fluid during the Early Phase of Healing: Prospective Clinical Trial. Mediators of inflammation. 2019.

Dennison, D.K., Vallone, D.R., Pinero, G.J., Rittman, B. and Caffesse, R.G., 1994. Differential effect of TGF-β1 and PDGF on proliferation of periodontal ligament cells and gingival fibroblasts. Journal of Periodontology, 65(7), pp.641-648.

DesRoches, M. 2016. The Effect of Mechanical Vibration on Human PDL Cell Differentiation and Response to Inflammation.

Diao, Y., Ma, Q., Cui, F. and Zhong, Y. 2009. Human umbilical cord mesenchymal stem cells: osteogenesis in vivo as seed cells for bone tissue engineering. J Biomed Mater Res A. 91(1), pp.123-131.

Dienhart, C.M. 1979. Basic human anatomy and physiology. Saunders.

Diercke, K., König, A., Kohl, A., Lux, C. and Erber, R. 2012. Human primary cementoblasts respond to combined IL-1β stimulation and

compression with an impaired BSP and CEMP-1 expression. European Journal of cell biology. 91(5), pp.402-412.

Diercke, K., Sen, S., Kohl, A., Lux, C. and Erber, R. 2011. Compression-dependent up-regulation of ephrin-A2 in PDL fibroblasts attenuates osteogenesis. Journal of dental research. 90(9), pp.1108-1115.

Dinarello, C. A. 2009. Immunological and inflammatory functions of the interleukin-1 family. Annual review of immunology, 27, pp. 519-550.

Diomede, F., Rajan, T.S., D'Aurora, M., Bramanti, P., Merciaro, I., Marchisio, M., Gatta, V., Mazzon, E. and Trubiani, O. 2017. Stemness characteristics of periodontal ligament stem cells from donors and multiple sclerosis patients: A comparative study. Stem Cells International.

Discher, D. E., P. Janmey and Y.-l. Wang 2005. Tissue cells feel and respond to the stiffness of their substrate. Science 310(5751): 1139-1143.

Dominici, M., Le Blanc, K., Mueller, I., Slaper-Cortenbach, I., Marini, F., Krause, D., et al., 2006. Minimal criteria for defining multipotent mesenchymal stromal cells. The International Society for Cellular Therapy position statement. Cytotherapy. 8(4), pp.315-317.

Drury, J. L. and D. J. Mooney 2003. Hydrogels for tissue engineering: scaffold design variables and applications. Biomaterials 24(24): 4337-4351.

Du, N., et al. 2011. Structural Origin of the Strain-Hardening of Spider Silk. Advanced Functional Materials, 21(4), pp. 772-778.

Duan, X. et al. 2011. Application of induced pluripotent stem (iPS) cells in periodontal tissue regeneration. Journal of Cellular Physiology. 226, pp.150-157.

Duval, K., Grover, H., Han, L.-H., Mou, Y., Pegoraro, A.F., Fredberg, J., et al., 2017. Modeling physiological events in 2D vs 3D cell culture. Physiology. 32(4), pp.266-277.

Edmondson, R., Broglie, J.J., Adcock, A.F. and Yang, L. 2014. Three-dimensional cell culture systems and their applications in drug discovery and cell-based biosensors. Assay and drug development technologies. 12(4), pp.207-218.

Elsaesser, A.F., Schwarz, S., Joos, H., Körber, L., Brenner, R.E. and Rotter, N. 2016. Characterization of a migrative subpopulation of adult human nasoseptal chondrocytes with progenitor cell features and their potential for in vivo cartilage regeneration strategies. Cell & bioscience. 6(1), p11.

Estes, B.T. and Guilak, F. 2011. Three-dimensional culture systems to induce chondrogenesis of adipose-derived stem cells. Adipose-Derived Stem Cells. Springer, pp.201-217.

Etienne, O., Schneider, A., Kluge, J.A., Bellemin-Laponnaz, C., Polidori, C., Leisk, G.G., Kaplan, D.L., Garlick, JA and Egles, C. 2009. Soft tissue augmentation using silk gels: an in vitro and in vivo study. Journal of periodontology. 80(11), pp.1852-1858.

Ferrari, M., Cirisano, F. and Morán, M.C., 2019. Mammalian cell behavior on hydrophobic substrates: influence of surface properties. Colloids and Interfaces. 3(2), p48.

Fidler, I.J., 1986. Rationale and methods for the use of nude mice to study the biology and therapy of human cancer metastasis. Cancer and Metastasis Reviews. 5(1), pp.29-49.

Frazer, A., Bunning, R.A., Thavarajah, M., Seid, J.M. and Russell, R.G.G. 1994. Studies on type II collagen and aggrecan production in human articular chondrocytes in vitro and effects of transforming growth factor-β and interleukin-1β. Osteoarthritis and cartilage. 2(4), pp.235-245.

Frazer, R. Q., R. T. Byron, P. B. Osborne and K. P. West 2005. PMMA: an essential material in medicine and dentistry. Journal of long-term effects of medical implants 15(6).

Friedenstein, A., Chailakhjan, R. and Lalykina, K. 1970. The development of fibroblast colonies in monolayer cultures of guinea-pig bone marrow and spleen cells. Cell Proliferation. 3(4), pp.393-403.

Friedenstein, A.J., Chailakhyan, R.K., Latsinik, N.V., Panasyuk, A.F. and Keiliss-Borok, I.V. 1974. Stromal cells responsible for transferring the microenvironment of the hemopoietic tissues: cloning in vitro and retransplantation in vivo. Transplantation. 17(4), pp.331-340.

Friedenstein, A.J., Gorskaja, J. and Kulagina, N. 1976. Fibroblast precursors in normal and irradiated mouse hematopoietic organs. Experimental hematology. 4(5), pp.267-274.

Fröhlich, E., 2012. The role of surface charge in cellular uptake and cytotoxicity of medical nanoparticles. International journal of nanomedicine. 7, p5577.

Fromigue, O., Marie, P.J. and Lomri, A., 1998. Bone morphogenetic protein-2 and transforming growth factor-β2 interact to modulate human bone marrow stromal cell proliferation and differentiation. Journal of cellular biochemistry, 68(4), pp.411-426.

Fujii, S., Maeda, H., Tomokiyo, A., Monnouchi, S., Hori, K., Wada, N. and Akamine, A., 2010. Effects of TGF-β1 on the proliferation and differentiation of human periodontal ligament cells and a human periodontal ligament stem/progenitor cell line. Cell and tissue research, 342(2), pp.233-242.

Galateanu, B., A. Hudita, C. Zaharia, M.-C. Bunea, E. Vasile, M.-R. Buga , et al., 2019. Silk-Based Hydrogels for Biomedical Applications. Polymers and Polymeric Composites: A Reference Series: 1791-1817.

Garlet, T.P., Coelho, U., Silva, J.S. and Garlet, G.P. 2007. Cytokine expression pattern in compression and tension sides of the periodontal ligament during orthodontic tooth movement in humans. European journal of oral sciences. 115(5), pp.355-362.

Gauthier, P., Yu, Z., Tran, Q.T., Zhu, X. and Huang, G.T.-J. 2017. Cementogenic genes in human periodontal ligament stem cells are downregulated in response to osteogenic stimulation while upregulated by vitamin C treatment. Cell and tissue research. 368(1), pp.79-92.

Gay, I.C., Chen, S. and MacDougall, M., 2007. Isolation and characterization of multipotent human periodontal ligament stem cells. Orthodontics & craniofacial research, 10(3), pp.149-160.

Ge, S., Zhao, N., Wang, L., Liu, H. and Yang, P., 2013. Effects of hydroxyapatite nanostructure on channel surface of porcine acellular dermal matrix scaffold on cell viability and osteogenic differentiation of human periodontal ligament stem cells. International journal of nanomedicine, 8, p.1887.

Geão, C., Costa-Pinto, A.R., Cunha-Reis, C., Ribeiro, V.P., Vieira, S., Oliveira, J.M., Reis, R.L. and Oliveira, A.L. 2019. Thermal annealed silk fibroin membranes for periodontal guided tissue regeneration. Journal of Materials Science: Materials in Medicine. 30(2), p27.

Giannobile, W. et al. 1996. Comparative effects of platelet derived growth factor-BB and insulin-like growth factor-I, individually and in combination, on periodontal regeneration in Macaca fascicularis. Journal of Periodontal Research. 31, pp. 301-312.

Gil, E.S., Park, S.H., Hu, X., Cebe, P. and Kaplan, D.L. 2014. Impact of Sterilization on the Enzymatic Degradation and Mechanical Properties of Silk Biomaterials. Macromolecular bioscience. 14(2), pp.257-269.

Glotzbach, J.P., Wong, V.W., Levi, B., Longaker, M.T. and Gurtner, G.C. 2012. Delivery strategies for stem cell-based therapy. Journal of Healthcare Engineering. 3.

Goetzke, R., Sechi, A., De Laporte, L., Neuss, S. and Wagner, W. 2018. Why the impact of mechanical stimuli on stem cells remains a challenge. Cellular and Molecular Life Sciences. 75(18), pp.3297-3312.

Goga, Y., Chiba, M., Shimizu, Y. and Mitani, H. 2006. Compressive force induces osteoblast apoptosis via caspase-8. Journal of dental research. 85(3), pp.240-244.

Goiato, M.C., Freitas, E. and Sonego, M. 2015. Acrylic Resin Cytotoxicity for Denture Base--Literature Review. Advances in clinical and experimental medicine: official organ Wroclaw Medical University. 24(4), pp.679-686.

Gotoh, Y., Tsukada, M. and Minoura, N. 1998. Effect of the chemical modification of the arginyl residue in Bombyx mori silk fibroin on the attachment and growth of fibroblast cells. Journal of Biomedical Materials Research: An Official Journal of The Society for Biomaterials, The Japanese Society for Biomaterials, and the Australian Society for Biomaterials. 39(3), pp.351-357.

Gronthos, S., Brahim, J., Li, W., Fisher, L.W., Cherman, N., Boyde, A., DenBesten, P., Robey, P.G. and Shi, S. 2002. Stem Cell Properties of Human Dental Pulp Stem Cells. Journal of Dental Research. 81(8), pp.531-535.

Grzesik, WJ. et al., 1998. Normal human cementum-derived cells: isolation, clonal expansion, and in vitro and in vivo characterization. Journal of bone and mineral research. 13, pp., 1547 – 1554.

Guo, J. et al. 2013. Human periodontal ligament cells reaction on a novel hydroxyapatite-collagen scaffold. Dental Traumatology. 29, pp. 103-109.

Hacopian, N., Nik, T.H., Ghahremani, M.H., Rahimi, H.R. and Ostad, S.N. 2011. Effects of continuous and interrupted forces on gene transcription in periodontal ligament cells in vitro. Acta Medica Iranica. pp.643-649.

Han, P., Wu, C., Chang, J. and Xiao, Y., 2012. The cementogenic differentiation of periodontal ligament cells via the activation of Wnt/β-catenin signalling pathway by Li+ ions released from bioactive scaffolds. Biomaterials, 33(27), pp.6370-6379.

Hardy, J., Torres-Rendon, J., Leal-Egaña, A., Walther, A., Schlaad, H., Cölfen, H. and Scheibel, T. 2016. Biomineralization of engineered spider silk protein-based composite materials for bone tissue engineering. Materials. 9(7), p560.

Hardy, J.G., Geissler, S.A., Aguilar Jr, D., Villancio-Wolter, M.K., Mouser, D.J., Sukhavasi, R.C., Cornelison, R.C., Tien, L.W., Preda, R.C. and Hayden, R.S. 2015. Instructive Conductive 3D Silk Foam-Based Bone Tissue Scaffolds Enable Electrical Stimulation of Stem Cells for Enhanced Osteogenic Differentiation. Macromolecular bioscience. 15(11), pp.1490-1496.

Hardy, J.G., Römer, L.M. and Scheibel, T.R. 2008. Polymeric materials based on silk proteins. Polymer. 49(20), pp.4309-4327.

Hassell, T.M., 1993. Tissues and cells of the periodontium. Periodontology 2000. 3(1), pp.9-38.

Hattori, S., Terada, D., Bintang, A.B., Honda, T., Yoshikawa, C., Teramoto, H., Kameda, T., Yasushi, T. and Kobayashi, H. 2012. Influence of sterilisations on silk protein-based materials. Bioinspired, Biomimetic and Nanobiomaterials. 1(3), pp.195-199.

Hausman, G., 1981. Techniques for studying adipocytes. Stain technology. 56(3), pp.149-154.

Hayman, E.G., Pierschbacher, M.D., Suzuki, S. and Ruoslahti, E. 1985. Vitronectin—a major cell attachment-promoting protein in fetal bovine serum. Experimental cell research. 160(2), pp.245-258.

He, Y., Macarak, E.J., Korostoff, J.M. and Howard, P.S. 2004. Compression and tension: differential effects on matrix accumulation by periodontal ligament fibroblasts in vitro. Connective tissue research. 45(1), pp.28-39.

Henneman, S., J. Von den Hoff and J. Maltha 2008. Mechanobiology of tooth movement. The European Journal of Orthodontics 30(3): 299-306.

Hermiston, M.L., Xu, Z. and Weiss, A. 2003. CD45: a critical regulator of signaling thresholds in immune cells. Annual review of immunology. 21(1), pp.107-137.

Hess, K., Ushmorov, A., Fiedler, J., Brenner, R.E. and Wirth, T., 2009. TNFα promotes osteogenic differentiation of human mesenchymal stem cells by triggering the NF-κB signaling pathway. Bone, 45(2), pp.367-376.

Hofmann, S., Stok, K.S., Kohler, T., Meinel, A.J. and Müller, R. 2014. Effect of sterilization on structural and material properties of 3-D silk fibroin scaffolds. Acta biomaterialia. 10(1), pp.308-317.

Horwitz, E., Le Blanc, K., Dominici, M., Mueller, I., Slaper-Cortenbach, I., Marini, F.C., Deans, R., Krause, D. and Keating, A. 2005. Clarification of the nomenclature for MSC: The International Society for Cellular Therapy position statement. Cytotherapy. 7(5), pp.393-395.

Howard, P. S., U. Kucich, R. Taliwal and J. M. Korostoff 1998. Mechanical forces alter extracellular matrix synthesis by human periodontal ligament fibroblasts. Journal of periodontal research 33(8): 500-508.

Hu, B., Zhang, Y., Zhou, J., Li, J., Deng, F., Wang, Z. and Song, J., 2014. Low-intensity pulsed ultrasound stimulation facilitates osteogenic differentiation of human periodontal ligament cells. PLoS One, 9(4), p.e95168.

Hu, Y., Zhang, Q., You, R., Wang, L. and Li, M. 2012. The relationship between secondary structure and biodegradation behavior of silk fibroin scaffolds. Advances in Materials Science and Engineering. 2012.

Huang, GT et al. 2009. Mesenchymal stem cells derived from dental tissues vs. those from other sources: their biology and role in regenerative medicine. Journal of Dental Research. 88(9), pp. 792-806.

Huang, L., Meng, Y., Ren, A., Han, X., Bai, D. and Bao, L. 2009. Response of cementoblast-like cells to mechanical tensile or compressive stress at physiological levels in vitro. Molecular biology reports. 36(7), p1741.

Hung, C. et al. 2011. A comparison between adipose tissue and dental pulp as sources of MSCs for tooth regeneration. Biomaterials. 32, pp., 6995 - 7005.

Hutmacher, D. W. and Cool, S. 2007. Concepts of scaffold-based tissue engineering: the rationale to use solid free-form fabrication techniques. Journal of Cellular and Molecular Medicine. 11(4), pp. 654-669.

Hutton, D. L., et al., 2014. Tumor necrosis factor improves vascularization in osteogenic grafts engineered with human adipose-derived stem/stromal cells. PLOS One, e107199.

Hwang, W.-J., Jeong, S.-n., Kim, Y.-S., Pi, S.-H., You, H.-K., Chung, C.-p. and Shin, H.-S. 2009. Clinical study of guided bone regeneration of extracted socket with PLA/PGA membrane and silk fibroin membrane. The Journal of the Korean Academy of Periodontology. 39(2), pp.129-138.

Ichioka, H., Yamamoto, T., Yamamoto, K., Honjo, K.-i., Adachi, T., Oseko, F., et al., 2016. Biomechanical force induces the growth factor production in human periodontal ligament-derived cells. Odontology. 104(1), pp.27-34.

Irie, N., Takada, Y., Watanabe, Y., Matsuzaki, Y., Naruse, C., Asano, M., et al. . 2009. Bidirectional signaling through ephrinA2-EphA2 enhances osteoclastogenesis and suppresses osteoblastogenesis. Journal of Biological Chemistry. 284(21), pp.14637-14644.

Ishikawa, I., Iwata, T., Washio, K., Okano, T., Nagasawa, T., Iwasaki, K. et al., 2009. Cell sheet engineering and other novel cell-based approaches to periodontal regeneration. Periodontology 2000, 51(1), pp.220-238.

Ivanovski, S., 2009. Periodontal Regeneration. Australian Dental Journal. 54, pp. S118–S128.

Ivanovski, S., Gronthos, S., Shi, S. and Bartold, P.M. 2006. Stem cells in the periodontal ligament. Oral Dis. 12(4), pp.358-363.

Iwata, T., Yamato, M., Ishikawa, I., Ando, T. and Okano, T. 2014. Tissue engineering in periodontal tissue. The Anatomical Record. 297(1), pp.16-25.

Izumi, Y., Aoki, A., Yamada, Y., Kobayashi, H., Iwata, T., Akizuki, T., et al., 2011. Current and future periodontal tissue engineering. Periodontology 2000. 56(1), pp.166-187.

Jacobs, C., Grimm, S., Ziebart, T., Walter, C. and Wehrbein, H. 2013. Osteogenic differentiation of periodontal fibroblasts is dependent on the strength of mechanical strain. Arch Oral Biol. 58(7), pp.896-904.

Jan Lindhe, N.P.L., Thorkild Karrin. 2008. Clinical Periodontology and Implant Dentistry. 5th Ed. ed. Oxford, UK: Blackwell Munksgaard.

Janssens, K. et al. 2005. Transforming growth factor-beta1 to the bone. Endocrine Reviews. 26, pp. 743 - 74.

Jaroszeski, M.J. and Radcliff, G. 1999. Fundamentals of flow cytometry. Molecular biotechnology. 11(1), pp.37-53.

Jeffcoat, M. K. et al. 2014. Impact of periodontal therapy on general health: evidence from insurance data for five systemic conditions. American Journal of Preventive Medicine. 47, 166-174.

Ji, J., Sun, W., Wang, W., Munyombwe, T. and Yang, X.B., 2014. The effect of mechanical loading on osteogenesis of human dental pulp stromal cells in a novel in vitro model. Cell and tissue research, 358(1), pp.123-133.

Ji, K., Liu, Y., Lu, W., Yang, F., Yu, J., Wang, X., et al., 2013. Periodontal tissue engineering with stem cells from the periodontal ligament of human retained deciduous teeth. J Periodontal Res. 48(1), pp.105-116.

Jia, R., Yi, Y., Liu, J., Pei, D., Hu, B., Hao, H., et al., 2020. Cyclic compression emerged dual effects on the osteogenic and osteoclastic status of LPS-induced inflammatory human periodontal ligament cells according to loading force. BMC Oral Health. 20(1), pp.1-11.

Jin, Q.-M., Zhao, M., Webb, S.A., Berry, J.E., Somerman, M.J. and Giannobile, W.V. 2003. Cementum engineering with three-dimensional polymer scaffolds. Journal of Biomedical materials research. 67(A).

Jin, S.-H., Kweon, H., Park, J.-B. and Kim, C.-H. 2014. The effects of tetracycline-loaded silk fibroin membrane on proliferation and osteogenic potential of mesenchymal stem cells. Journal of Surgical Research. 192(2), pp.e1-e9.

Jo, Y.Y., Lee, H.J., Kook, S.Y., Choung, H.W., Park, J.Y., Chung, J.H., et al., 2007. Isolation and characterization of postnatal stem cells from human dental tissues. Tissue Eng. 13(4), pp.767-773.

Johnson, K., 1992. Basics of flow cytometry. Clinical laboratory science: journal of the American Society for Medical Technology. 5(1), pp.22-24.

Jones, E.A., Kinsey, S.E., English, A., Jones, R.A., Straszynski, L., Meredith, et al., 2002. Isolation and characterization of bone marrow multipotential mesenchymal progenitor cells. Arthritis & Rheumatism. 46(12), pp.3349-3360.

Jørgensen, N.R., Henriksen, Z., Sørensen, O.H. and Civitelli, R., 2004. Dexamethasone, BMP-2, and 1, 25-dihydroxyvitamin D enhance a more differentiated osteoblast phenotype: validation of an in vitro model for human bone marrow-derived primary osteoblasts. Steroids, 69(4), pp.219-226.

Jung, S.W., Joo, H.M., Park, J.S. and Lee, J.H. 2010. Development of a rapid and effective method for preparing delicate dinoflagellates for scanning electron microscopy. Journal of applied phycology. 22(3), pp.313-317.

Kang, K.L., Lee, S.W., Ahn, Y.S., Kim, S.H. and Kang, Y.G. 2013. Bioinformatic analysis of responsive genes in two-dimension and three-dimension cultured human periodontal ligament cells subjected to compressive stress. Journal of periodontal research. 48(1), pp.87-97.

Kapałczyńska, M., Kolenda, T., Przybyła, W., Zajączkowska, M., Teresiak, A., Filas, V., et al., 2018. 2D and 3D cell cultures–a comparison of different types of cancer cell cultures. Archives of medical science: AMS. 14(4), p910.

Karring, T. et al. 1993. Development of the biological concept of guided tissue regeneration – animal and human studies. Periodontology 2000. 1(1), pp. 26–35.

Karring, T. et al. 2003. Regenerative periodontal therapy. In: Lindhe J, Karring T, Lang NP, eds. Clinical Periodontology and Implant Dentistry. 4th ed. Oxford, UK: Blackwell Munksgaard. 650–704.

Kearns, V., MacIntosh, A., Crawford, A. and Hatton, P. 2008. Silk-based biomaterials for tissue engineering. Topics in tissue engineering. 4, pp.1-19.

Khademi, M., Wang, W., Reitinger, W. and Barz, D.P., 2017. Zeta Potential of Poly (methyl methacrylate)(PMMA) in Contact with Aqueous Electrolyte–Surfactant Solutions. Langmuir. 33(40), pp.10473-10482.

Kikuchi, M., Korioth, T. and Hannam, A. 1997. The association among occlusal contacts, clenching effort, and bite force distribution in man. Journal of dental research. 76(6), pp.1316-1325.

Kim, H.H., Kim, M.K., Lee, K.H., Park, Y.H. and Um, I.C. 2015. Effects of different Bombyx mori silkworm varieties on the structural characteristics and properties of silk. International journal of biological macromolecules. 79, pp.943-951.

Kim, K.-H., Jeong, L., Park, H.-N., Shin, S.-Y., Park, W.-H., Lee, S.-C, et al., 2005. Biological efficacy of silk fibroin nanofiber membranes for guided bone regeneration. Journal of biotechnology. 120(3), pp.327-339.

Kim, S.G., Kim, S.G., Viechnicki, B., Kim, S. and Nah, H.D., 2011. Engineering of a periodontal ligament construct: cell and fibre alignment induced by shear stress. Journal of clinical periodontology, 38(12), pp.1130-1136.

King, G. N., and Hughes, F. J., 2001. Bone morphogenetic protein-2 stimulates cell recruitment and cementogenesis during early wound healing. Journal of clinical periodontology, 28(5), pp. 465-475.

King, G.N., King, N. and Hughes, F.J., 1998. Effect of two delivery systems for recombinant human bone morphogenetic protein-2 on periodontal regeneration in vivo. Journal of periodontal research, 33(3), pp.226-236.

King, G.N., King, N., Cruchley, A.T., Wozney, J.M. and Hughes, F.J., 1997. Recombinant human bone morphogenetic protein-2 promotes wound healing in rat periodontal fenestration defects. Journal of dental research, 76(8), pp.1460-1470.

Kitamura, M., Akamatsu, M., Machigashira, M., Hara, Y., Sakagami, R., Hirofuji, T., et al., 2011. FGF-2 stimulates periodontal regeneration: results of a multi-center randomized clinical trial. Journal of dental research, 90(1), pp.35-40.

Kitamura, M., Nakashima, K., Kowashi, Y., Fujii, T., Shimauchi, H., Sasano, T., et al.,2008. Periodontal tissue regeneration using fibroblast growth factor-2: randomized controlled phase II clinical trial. PloS one, 3(7), p.e2611.

Kobayashi, E., Kuremoto, K.-I., Matsuno, T., Tabata, Y., Eto, K., Shimizu, Y., et al., 2004. In Situ Tissue Engineering of Periodontal Tissues by Seeding with Periodontal Ligament-Derived Cells. TISSUE ENGINEERING. 10(3/4).

Kolf, C.M., Cho, E. and Tuan, R.S. 2007. Mesenchymal stromal cells: biology of adult mesenchymal stem cells: regulation of niche, self-renewal and differentiation. Arthritis research & therapy. 9(1), p204.

Kolos, E. and Ruys, A., 2013. Biomimetic scaffold materials used in tissue engineering. J Biomim Biomater Tissue Eng 18: e101.

Komaki, M., Iwasaki, K., Arzate, H., Narayanan, A.S., Izumi, Y. and Morita, I. 2012. Cementum protein 1 (CEMP1) induces a cementoblastic phenotype and reduces osteoblastic differentiation in periodontal ligament cells. Journal of cellular physiology. 227(2), pp.649-657.

Kosaka, T., Ono, T., Yoshimuta, Y., Kida, M., Kikui, M., Nokubi, T., et al., 2014. The effect of periodontal status and occlusal support on masticatory performance: the Suita study. Journal of Clinical Periodontology, 41(5), pp.497-503.

Krishnan, V. and Davidovitch, Z., 2009. On a path to unfolding the biological mechanisms of orthodontic tooth movement. Journal of dental research. 88(7), pp.597-608.

Krishnan, V. and Davidovitch, Z.e. 2006. Cellular, molecular, and tissue-level reactions to orthodontic force. American Journal of Orthodontics and Dentofacial Orthopedics. 129(4), pp.469. e461-469. E432.

Krishnan, V. and Z. Davidovitch 2009. On a path to unfolding the biological mechanisms of orthodontic tooth movement. Journal of dental research 88(7): 597-608.

Kuboyama, N., Kiba, H., Arai, K., Uchida, R., Tanimoto, Y., Bhawal, U.K., et al., 2013. Silk fibroin-based scaffolds for bone regeneration. Journal of Biomedical Materials Research Part B: Applied Biomaterials, 101(2), pp.295-302.

Kumar, A., Mukhtar-Un-Nisar, S. and Zia, A., 2011. Tissue Engineering-The promise of regenerative dentistry. Biol Med, 3(2), pp.108-113.

Kuo, C.K., Marturano, J.E. and Tuan, R.S. 2010. Novel strategies in tendon and ligament tissue engineering: Advanced biomaterials and regeneration motifs. Sports Med Arthrosc Rehabil Ther Technol. 2, p20.

Lang, H., Schiiler, N., Arnhold, S., Nolden, R. and Mertens, T., 1995. Formation of differentiated tissues in vivo by periodontal cell populations cultured in vitro. Journal of dental research, 74(5), pp.1219-1225.

Lang, N.P. and Karring, T. eds., 2003. Clinical periodontology and implant dentistry (Vol. 4, pp. 650-754). Copenhagen: Blackwell Munksgaard.

Langer, R. and Vacanti, JP. 1993. Tissue engineering. science. 260:pp. 920-926.

Lee, J.T.Y. and Chow, K.L. 2012. SEM sample preparation for cells on 3D scaffolds by freeze-drying and HMDS. Scanning. 34(1), pp.12-25.

Lee, Y.H., Nahm, D.S., Jung, Y.K., Choi, J.Y., Kim, S.G., Cho, M., et al.,2007. Differential gene expression of periodontal ligament cells after loading of static compressive force. Journal of periodontology. 78(3), pp.446-452.

Leggat, P. A. and U. Kedjarune 2003. Toxicity of methyl methacrylate in dentistry. International dental journal 53(3): 126-131.

Lekic, P. and McCulloch, CA. 1996. Periodontal ligament cell population: the central role of fibroblasts in creating a unique tissue. The anatomical record. 245, pp. 327 – 341.

Levy, G. G. and M. L. Mailland 1980. Histologic study of the effects of occlusal hypofunction following antagonist tooth extraction in the rat. Journal of periodontology 51(7): 393-399.

Lewis, R. 1996. Unraveling the weave of spider silk. Bioscience. 46(9), pp.636-638.

Li, L., Han, M., Li, S., Wang, L. and Xu, Y. 2013. Cyclic tensile stress during physiological occlusal force enhances osteogenic differentiation of human periodontal ligament cells via ERK1/2-Elk1 MAPK pathway. DNA and cell biology. 32(9), pp.488-497.

Li, L., Han, M., Li, S., Wang, L. and Xu, Y., 2013. Cyclic tensile stress during physiological occlusal force enhances osteogenic differentiation of human periodontal ligament cells via ERK1/2-Elk1 MAPK pathway. DNA and cell biology, 32(9), pp.488-497.

Li, L., Han, M.X., Li, S., Xu, Y. and Wang, L. 2014. Hypoxia regulates the proliferation and osteogenic differentiation of human periodontal ligament cells under cyclic tensile stress via mitogen-activated protein kinase pathways. J Periodontol. 85(3), pp.498-508.

Li, M., Zhang, C. and Yang, Y. 2019. Effects of mechanical forces on osteogenesis and osteoclastogenesis in human periodontal ligament fibroblasts: A systematic review of in vitro studies. Bone & joint research. 8(1), pp.19-31.

Li, W., Zhou, J. and Xu, Y., 2015. Study of the in vitro cytotoxicity testing of medical devices. Biomedical reports. 3(5), pp.617-620.

Li, X., Kolltveit, K.M., Tronstad, L. and Olsen, I., 2000. Systemic diseases caused by oral infection. Clinical microbiology reviews, 13(4), pp.547-558.

Li, Y., Li, M., Tan, L., Huang, S., Zhao, L., Tang, T., et al.,2013. Analysis of time-course gene expression profiles of a periodontal ligament tissue model under compression. Archives of oral biology. 58(5), pp.511-522.

Li, Y., Li, M., Tan, L., Huang, S., Zhao, L., and Tang, T. 2013. Analysis of time-course gene expression profiles of a periodontal ligament tissue model under compression. Archives of oral biology. 58(5), pp.511-522.

Lian, N., Wang, W., Li, L., Elefteriou, F. and Yang, X. 2009. Vimentin inhibits ATF4-mediated osteocalcin transcription and osteoblast differentiation. Journal of biological chemistry. 284(44), pp.30518-30525.

Liedert, A., D. Kaspar, R. Blakytny, L. Claes and A. Ignatius 2006. Signal transduction pathways involved in mechanotransduction in bone cells. Biochemical and biophysical research communications 349(1): 1-5.

Lim, K., Kim, J., Seonwoo, H., Park, S.H., Choung, P.H. and Chung, J.H. 2013. In vitro effects of low-intensity pulsed ultrasound stimulation on the osteogenic differentiation of human alveolar bone-derived mesenchymal stem cells for tooth tissue engineering. Biomed Res Int. 2013, p269724.

Lin, G., Liu, G., Banie, L., Wang, G., Ning, H., Lue, T.F., et al.,2011. Tissue distribution of mesenchymal stem cell marker Stro-1. Stem cells and development. 20(10), pp.1747-1752.

Lin, N.H., Gronthos, S. and Bartold, P.M., 2008. Stem cells and periodontal regeneration. Australian dental journal, 53(2), pp.108-121.

Liu, J., Li, Q., Liu, S., Gao, J., Qin, W., Song, Y., et al.,2017. Periodontal ligament stem cells in the periodontitis microenvironment are sensitive to static mechanical strain. Stem cells international.

Liu, M., J. Dai, Y. Lin, L. Yang, H. Dong, Y. Li, et al., 2012. Effect of the cyclic stretch on the expression of osteogenesis genes in human periodontal ligament cells. Gene 491(2): 187-193.

Liu, X. and Zhang, K.-Q. 2014. Silk fiber—molecular formation mechanism, structure-property relationship and advanced applications. Oligomerisation of Chemical and Biological Compounds. 3.

Livak, K.J. and Schmittgen, T.D. 2001. Analysis of relative gene expression data using real-time quantitative PCR and the 2− ΔΔCT method. Methods. 25(4), pp.402-408.

Lu, Z., Wang, G., Dunstan, C.R. and Zreiqat, H., 2012. Short-term exposure to tumor necrosis factor-alpha enables human osteoblasts to direct adipose tissue-derived mesenchymal stem cells into osteogenic differentiation. Stem cells and development, 21(13), pp.2420-2429.

Luppen, C.A., Smith, E., Spevak, L., Boskey, A.L. and Frenkel, B., 2003. Bone morphogenetic protein-2 restores mineralization in glucocorticoid-inhibited MC3T3-E1 osteoblast cultures. Journal of Bone and Mineral Research, 18(7), pp.1186-1197.

Lynch, S.E., Williams, R.C., Poison, A.M., Howell, T.H., Reddy, M.S., Zappa, U.E., et al.,1989. A combination of platelet-derived and insulin-like growth factors enhances periodontal regeneration. Journal of Clinical Periodontology, 16(8), pp.545-548.

Machtei, EE. and Schallhorn, RG. 1995. Successful regeneration of mandibular Class II furcation defects: an evidence-based treatment approach. International journals of periodontics and restorative dentistry. 15, pp. 146 – 167.

MacNeil, R. L. and M. J. Somerman, 1999. Development and regeneration of the periodontium: parallels and contrasts. Periodontology 2000 19(1): 8-20.

Mailhot, J.M., Schuster, G.S., Garnick, J.J., Hanes, P.J., Lapp, C.A. and Lewis, J.B., 1995. Human periodontal ligament and gingival fibroblast response to TGF-β1 stimulation. Journal of clinical periodontology, 22(9), pp.679-685.

Mandal, B.B. and Kundu, S.C. 2009. Cell proliferation and migration in silk fibroin 3D scaffolds. Biomaterials. 30(15), pp.2956-2965.

Manokawinchoke, J., Limjeerajarus, N., Limjeerajarus, C., Sastravaha, P., Everts, V. and Pavasant, P. 2015. Mechanical force–induced TGFB1 increases expression of SOST/POSTN by hPDL cells. Journal of dental research. 94(7), pp.983-989.

Manokawinchoke, J., Pavasant, P., Sawangmake, C., Limjeerajarus, N., Limjeerajarus, C.N., Egusa, H., et al., 2019. Intermittent compressive force promotes osteogenic differentiation in human periodontal ligament cells by regulating the transforming growth factor-β pathway. Cell death & disease. 10(10), pp.1-21.

Marchesan, J.T., Scanlon, C.S., Soehren, S., Matsuo, M. and Kapila, Y.L. 2011. Implications of cultured periodontal ligament cells for the clinical and experimental setting: a review. Archives of oral biology. 56(10), pp.933-943.

Mareschi, K., Ferrero, I., Rustichelli, D., Aschero, S., Gammaitoni, L., Aglietta, et al., 2006. Expansion of mesenchymal stem cells isolated from pediatric and adult donor bone marrow. Journal of cellular biochemistry. 97(4), pp.744-754.

Marion, N.W. and Mao, J.J. 2006. Mesenchymal stem cells and tissue engineering. Methods in enzymology. 420, pp.339-361.

Marom, R., Shur, I., Solomon, R. and Benayahu, D. 2005. Characterization of adhesion and differentiation markers of osteogenic marrow stromal cells. Journal of cellular physiology. 202(1), pp.41-48.

Martin, I., D. Wendt and M. Heberer, 2004. The role of bioreactors in tissue engineering. TRENDS in Biotechnology 22(2): 80-86.

Masella, R. S. and M. Meister 2006. Current concepts in the biology of orthodontic tooth movement. American Journal of Orthodontics and Dentofacial Orthopedics 129(4): 458-468.

Matsunaga, K., C. Ito, K. Nakakogawa, A. Sugiuchi, R. Sako, M. Furusawa and T. Muramatsu 2016. Response to light compressive force in human cementoblasts in vitro. Biomedical Research 37(5): 293-298.

McCool, J., 2011. Silk Fibroin-Based Scaffolds for Tissue Engineering Applications.

McGuire, M.K., Scheyer, E.T., Nevins, M.L., Neiva, R., Cochran, D.L., Mellonig, J.T., Giannobile, W.V. and Bates, D., 2011. Living cellular construct for increasing the width of keratinized gingiva: Results from a randomized, within-patient, controlled trial. Journal of Periodontology, 82(10), pp.1414-1423.

McKinnon, D. D., D. W. Domaille, J. N. Cha and K. S. Anseth 2014. Biophysically defined and cytocompatible covalently adaptable networks as viscoelastic 3D cell culture systems. Advanced Materials 26(6): 865-872.

Meechan, P. J. and C. Wilson 2006. Use of ultraviolet lights in biological safety cabinets: A contrarian view. Applied Biosafety 11(4): 222-227.

Meeran, N.A. 2012. Biological response at the cellular level within the periodontal ligament on application of orthodontic force–An update. Journal of orthodontic science. 1(1), p2.

Mehanna, R., 2017. Physical versus Immunological Purification of Mesenchymal Stem Cells. Mesenchymal Stem Cells-Isolation, Characterization and Applications.

Meinel, L., Hofmann, S., Karageorgiou, V., Kirker-Head, C., McCool, J., Gronowicz, G., et al., 2005. The inflammatory responses to silk films in vitro and in vivo. Biomaterials. 26(2), pp.147-155.

Melke, J., Midha, S., Ghosh, S., Ito, K. and Hofmann, S. 2016. Silk fibroin as biomaterial for bone tissue engineering. Acta biomaterialia. 31, pp.1-16.

Mensing, N., Gasse, H., Hambruch, N., Haeger, J.D., Pfarrer, C. and Staszyk, C. 2011. Isolation and characterization of multipotent mesenchymal stromal cells from the gingiva and the periodontal ligament of the horse. BMC Vet Res. 7, p42.

Mieszawska, A.J., Llamas, J.G., Vaiana, C.A., Kadakia, M.P., Naik, R.R. and Kaplan, D.L. 2011. Clay enriched silk biomaterials for bone formation. Acta biomaterialia. 7(8), pp.3036-3041.

Miletic, M., Mojsilovic, S., Okic-Djordjevic, I., Kukolj, T., Jaukovic, A., Santibacez, J.F., Jovcic, G., et al.,2014. Mesenchymal stem cells isolated from human periodontal ligament. Archives of Biological Sciences. 66(1), pp.261-271.

Minoura, N., Aiba, S.-I., Higuchi, M., Gotoh, Y., Tsukada, M. and Imai, Y. 1995. Attachment and growth of fibroblast cells on silk fibroin. Biochemical and biophysical research communications. 208(2), pp.511-516.

Minoura, N., Tsukada, M. and Nagura, M. 1990. Physico-chemical properties of silk fibroin membrane as a biomaterial. Biomaterials. 11(6), pp.430-434.

Miyamoto, S., Koyanagi, R., Nakazawa, Y., Nagano, A., Abiko, Y., Inada, M., et al., 2013. Bombyx mori silk fibroin scaffolds for bone regeneration studied by bone differentiation experiment. Journal of bioscience and bioengineering. 115(5), pp.575-578.

Monnouchi, S., Maeda, H., Yuda, A., Hamano, S., Wada, N., Tomokiyo, A., et al., 2015. Mechanical induction of interleukin-11 regulates osteoblastic/cementoblastic differentiation of human periodontal

ligament stem/progenitor cells. Journal of periodontal research. 50(2), pp.231-239.

Morsczeck, C., Götz, W., Schierholz, J., Zeilhofer, F., Kühn, U., Möhl, C., et al., 2005. Isolation of precursor cells (PCs) from human dental follicle of wisdom teeth. Matrix Biology. 24(2), pp.155-165.

Mor-Yossef Moldovan, L., Lustig, M., Naftaly, A., Mardamshina, M., Geiger, T., Gefen, A., et al.,2019. Cell shape alteration during adipogenesis is associated with coordinated matrix cues. Journal of cellular physiology. 234(4), pp.3850-3863.

Motokawa, M., A. Terao, E. I. Karadeniz, M. Kaku, T. Kawata, Y. Matsuda, et al., 2013. Effects of long-term occlusal hypofunction and its recovery on the morphogenesis of molar roots and the periodontium in rats. Angle Orthod 83(4): 597-604.

Mrozik, K., Gronthos, S., Shi, S. and Bartold, P.M. 2010. A method to isolate, purify, and characterise human periodontal ligament stem cells. Oral biology. Springer, pp.269-284.

Muccio, V., Saraci, E., Gilestro, M., Oddolo, D., Ruggeri, M., Caltagirone, S., et al., 2018. Relevance of sample preparation for flow cytometry. International journal of laboratory hematology. 40(2), pp.152-158.

Müller, I., Kordowich, S., Holzwarth, C., Spano, C., Isensee, G., Staiber, A., et al., 2006. Animal serum-free culture conditions for isolation and expansion of multipotent mesenchymal stromal cells from human BM. Cytotherapy. 8(5), pp.437-444.

Murphy, C.M., Haugh, M.G. and O'brien, F.J. 2010. The effect of mean pore size on cell attachment, proliferation and migration in collagen–glycosaminoglycan scaffolds for bone tissue engineering. Biomaterials. 31(3), pp.461-466.

Muschler, G.F., Nakamoto, C. and Griffith, L.G. 2004. Engineering principles of clinical cell-based tissue engineering. JBJS. 86(7), pp.1541-1558.

Nagatomo, K., Komaki, M., Sekiya, I., Sakaguchi, Y., Noguchi, K., Oda, S., et al., 2006. Stem cell properties of human periodontal ligament cells. Journal of periodontal research. 41(4), pp.303-310.

Nakano, K., Hayashi, T., Kawai, H., Takei, Y., Sato, Y., Ando, K., et al., 2009. Cell culture in vivo by means of diffusion chamber system. Dental materials journal. 28(4), pp.382-387.

Nakao, K., Goto, T., Gunjigake, K., Konoo, T., Kobayashi, S. and Yamaguchi, K. 2007. Intermittent force induces high RANKL expression in human periodontal ligament cells. Journal of dental research. 86(7), pp.623-628.

Nakao, K., T. Goto, K. Gunjigake, T. Konoo, S. Kobayashi and K. Yamaguchi 2007. Neuropeptides modulate RANKL and OPG expression in human periodontal ligament cells. Orthodontic Waves 66(2): 33-40.

Nanci, A. 2017. Ten Cate's Oral Histology-E-Book: Development, Structure, and Function. Elsevier Health Sciences.

Navabazam, A.R., Nodoshan, F.S., Sheikhha, M.H., Miresmaeili, S.M., Soleimani, M. and Fesahat, F. 2013. Characterization of mesenchymal stem cells from human dental pulp, preapical follicle and periodontal ligament. Iran J Reprod Med. 11(3).

Naveh, G.R., Chattah, N.L.-T., Zaslansky, P., Shahar, R. and Weiner, S. 2012. Tooth–PDL–bone complex: response to compressive loads encountered during mastication–a review. Archives of oral biology. 57(12), pp.1575-1584.

Nazarov, R., Jin, H.-J. and Kaplan, D.L. 2004. Porous 3-D scaffolds from regenerated silk fibroin. Biomacromolecules. 5(3), pp.718-726.

Newman, M.G., Takei, H.H. and Klokkevold, P.R., 2012. Carranza’s Clinical Periodontology 11th Ed, vol.

Ohshima, S., Komatsu, K., Yamane, A. and Chiba, M. 1991. Prolonged effects of hypofunction on the mechanical strength of the periodontal ligament in rat mandibular molars. Archives of oral biology. 36(12), pp.905-911.

Oppenheim, A., 1944. A possibility for physiologic orthodontic movement. American journal of orthodontics and oral surgery 30(6): 277-328.

Osoba, D. and Miller, J., 1964. The lymphoid tissues and immune responses of neonatally thymectomized mice bearing thymus tissue in

millipore diffusion chambers. Journal of Experimental Medicine. 119(1), pp.177-194.

Ott, L.W., Resing, K.A., Sizemore, A.W., Heyen, J.W., Cocklin, R.R., Pedrick, N.M., Woods, H.C., Chen, J.Y., Goebl, M.G. and Witzmann, F.A. 2007. Tumor necrosis factor-α-and interleukin-1-induced cellular responses: Coupling proteomic and genomic information. Journal of proteome research. 6(6), pp.2176-2185.

Pacini, S., Barachini, S., Montali, M., Carnicelli, V., Fazzi, R., Parchi, P. et al., 2016. Mesangiogenic progenitor cells derived from one novel CD64brightCD31brightCD14neg population in human adult bone marrow. Stem cells and development. 25(9), pp.661-673.

Papadopoulou, A., Iliadi, A., Eliades, T. and Kletsas, D. 2016. Early responses of human periodontal ligament fibroblasts to cyclic and static mechanical stretching. European journal of orthodontics. 39(3), pp.258-263.

Papadopoulou, K., Keilig, L., Eliades, T., Krause, R., Jager, A. and Bourauel, C. 2014. The time-dependent biomechanical behaviour of the periodontal ligament--an in vitro experimental study in minipig mandibular two-rooted premolars. Eur J Orthod. 36(1), pp.9-15.

Papenburg, B. J., E. D. Rodrigues, M. Wessling and D. Stamatialis, 2010. Insights into the role of material surface topography and wettability on cell-material interactions. Soft Matter 6(18): 4377-4388.

Patel, S., R. G. Thakar, J. Wong, S. D. McLeod and S. Li, 2006. Control of cell adhesion on poly (methyl methacrylate). Biomaterials 27(14): 2890-2897.

Patterson, J. and Hubbell, J.A., 2010. Enhanced proteolytic degradation of molecularly engineered PEG hydrogels in response to MMP-1 and MMP-2. Biomaterials. 31(30), pp.7836-7845.

Paul, J., 1961. Cell and tissue culture. Academic Medicine. 36(5), p557.

Pawar, E., 2016. A review article on acrylic PMMA. IOSR J. Mech. Civ. Eng. e-ISSN 13(2): 1-04.

Picton, D., 1965. On the part played by the socket in tooth support. Archives of Oral Biology 10(6): 945-955.

Pittenger, M.F., Mackay, A.M., Beck, S.C., Jaiswal, R.K., Douglas, R., Mosca, J.D., et al., 1999. Multilineage potential of adult human mesenchymal stem cells. Science. 284(5411), pp.143-147.

Pochampally, R., 2008. Colony forming unit assays for MSCs. Mesenchymal Stem Cells. Springer, pp.83-91.

Poiate, I. A. V. P., A. B. de Vasconcellos, R. B. de Santana and E. Poiate Jr (2009). Three-dimensional stress distribution in the human periodontal ligament in masticatory, parafunctional, and trauma loads: finite element analysis. Journal of periodontology 80(11): 1859-1867.

Prockop, D.J., 1997. Marrow stromal cells as stem cells for nonhematopoietic tissues. Science. 276(5309), pp.71-74.

Qi, Y., Wang, H., Wei, K., Yang, Y., Zheng, R.-Y., Kim, I. and Zhang, K.-Q. 2017. A review of structure construction of silk fibroin biomaterials from single structures to multi-level structures. International journal of molecular sciences. 18(3), p237.

Radcliff, G. and Jaroszeski, M.J., 1998. Basics of flow cytometry. Flow Cytometry Protocols. Springer, pp.1-24.

Ragni, E., Vigano, M., Rebulla, P., Giordano, R. and Lazzari, L. 2013. What is beyond aq RT-PCR study on mesenchymal stem cell differentiation properties: how to choose the most reliable housekeeping genes. Journal of Cellular and Molecular Medicine. 17(1), pp.168-180.

Raif el, M. 2008. Effect of cyclic tensile load on the regulation of the expression of matrix metalloproteases (MMPs -1, -3) and structural components in synovial cells. J Cell Mol Med. 12(6A), pp.2439-2448.

Raimondi, M. T., S. Bertoldi, S. Caddeo, S. Farè, C. Arrigoni and M. Moretti (2016). The effect of polyurethane scaffold surface treatments on the adhesion of chondrocytes subjected to interstitial perfusion culture. Tissue engineering and regenerative medicine 13(4): 364-374.

Ramfjord, S.P. and Kohler, C.A. 1959. Periodontal reaction to functional occlusal stress.

Rampersad, S.N., 2012. Multiple applications of Alamar Blue as an indicator of metabolic function and cellular health in cell viability bioassays. Sensors. 12(9), pp.12347-12360.

Rankovic, M.J., Docheva, D., Wichelhaus, A. and Baumert, U. 2019. Effect of static compressive force on in vitro cultured PDL fibroblasts: monitoring of viability and gene expression over 6 days. Clinical oral investigations. pp.1-15.

Ravichandran, A., J. Lim, M. S. K. Chong, F. Wen, Y. Liu, Y. T. Pillay, J. K. et al., 2017. In vitro, cyclic compressive loads potentiate early osteogenic events in engineered bone tissue. Journal of Biomedical Materials Research Part B: Applied Biomaterials 105(8): 2366-2375.

Reyes-Reyes, M., Mora, N., Zentella, A. and Rosales, C. 2001. Phosphatidylinositol 3-kinase mediates integrin-dependent NF-(κ) B and MAPK activation through separate signaling pathways. Journal of Cell Science. 114(8), pp.1579-1589.

Riesle, J. and Van Blitterswijk, C. 1999. Static and dynamic fibroblast seeding and cultivation in porous PEO/PBT scaffolds. Journal of Materials Science: Materials in Medicine. 10(12), pp.773-777.

Rnjak-Kovacina, J., DesRochers, T.M., Burke, K.A. and Kaplan, D.L. 2015. The effect of sterilization on silk fibroin biomaterial properties. Macromolecular bioscience. 15(6), pp.861-874.

Roberts, J.N., Sahoo, J.K., McNamara, L.E., Burgess, K.V., Yang, J., Alakpa, E.V., et al., 2016. Dynamic surfaces for the study of mesenchymal stem cell growth through adhesion regulation. ACS nano. 10(7), pp.6667-6679.

Robling, A. G., D. B. Burr and C. H. Turner, 2001. Recovery periods restore mechanosensitivity to dynamically loaded bone. Journal of Experimental Biology 204(19): 3389-3399.

Rockwood, D.N., Preda, R.C., Yücel, T., Wang, X., Lovett, M.L. and Kaplan, D.L. 2011. Materials fabrication from Bombyx mori silk fibroin. Nature protocols. 6(10), p1612.

Rodríguez-Lozano, F., García-Bernal, D., Aznar-Cervantes, S., Ros-Roca, M., Algueró, M., Atucha, N., Lozano-García, A., Moraleda, J. and Cenis, J. 2014. Effects of composite films of silk fibroin and graphene oxide on the proliferation, cell viability and mesenchymal phenotype of periodontal ligament stem cells. Journal of Materials Science: Materials in Medicine. 25(12), pp.2731-2741.

Rojewski, M.T., Weber, B.M. and Schrezenmeier, H. 2008. Phenotypic characterization of mesenchymal stem cells from various tissues. Transfusion Medicine and Hemotherapy. 35(3), pp.168-184.

Rose, E.C., Bumann, J., Jonas, I.E. and Kappert, H.F. 2000. Contribution to the biological assessment of orthodontic acrylic materials measurement of their residual monomer output and cytotoxicity. Journal of Orofacial Orthopedics/Fortschritte der Kieferorthopädie. 61(4), pp.246-257.

Rylev, M. and Kilian, M., 2008. Prevalence and distribution of principal periodontal pathogens worldwide. J Clin Periodontol. 35(8 Suppl), pp.346-361.

Sabokbar, A., Millett, P., Myer, B. and Rushton, N. 1994. A rapid, quantitative assay for measuring alkaline phosphatase activity in osteoblastic cells in vitro. Bone and mineral. 27(1), pp.57-67.

Salinas, E. Y., J. C. Hu and K. Athanasiou, 2018. A guide for using mechanical stimulation to enhance tissue-engineered articular cartilage properties. Tissue Engineering Part B: Reviews 24(5): 345-358.

Salzig, D., Leber, J., Merkewitz, K., Lange, M.C., Köster, N. and Czermak, P. 2016. Attachment, growth, and detachment of human mesenchymal stem cells in a chemically defined medium. Stem cells international. 2016.

Santin, M., Motta, A., Freddi, G. and Cannas, M. 1999. In vitro evaluation of the inflammatory potential of the silk fibroin. Journal of Biomedical Materials Research: An Official Journal of The Society for Biomaterials, The Japanese Society for Biomaterials, and The Australian Society for Biomaterials and the Korean Society for Biomaterials. 46(3), pp.382-389.

Schutte, R.J., Parisi-Amon, A. and Reichert, W.M. 2009. Cytokine profiling using monocytes/macrophages cultured on common biomaterials with a range of surface chemistries. Journal of Biomedical Materials Research Part A: An Official Journal of The Society for Biomaterials, The Japanese Society for Biomaterials, and The Australian Society for Biomaterials and the Korean Society for Biomaterials. 88(1), pp.128-139.

Seo, B.-M., Miura, M., Gronthos, S., Mark Bartold, P., Batouli, S., Brahim, J., et al.,. 2004b. Investigation of multipotent postnatal stem cells from human periodontal ligament. The Lancet. 364(9429), pp.149-155.

Seo, B.M., Miura, M., Sonoyama, W., Coppe, C., Stanyon, R. and Shi, S. 2005. Recovery of Stem Cells from Cryopreserved Periodontal Ligament. Journal of Dental Research. 84(10), pp.907-912.

Sharkey, F.E. and Fogh, J. 1984. Considerations in the use of nude mice for cancer research. Cancer and Metastasis Reviews. 3(4), pp.341-360.

Shen, T., Qiu, L., Chang, H., Yang, Y., Jian, C., Xiong, J., et al., 2014. Cyclic tension promotes osteogenic differentiation in human periodontal ligament stem cells. International Journal of Clinical and Experimental Pathology. 7(11), p7872.

Shimomoto, Y., C. Chung, Y. Iwasaki-Hayashi, T. Muramoto and K. Soma 2007. Effects of occlusal stimuli on alveolar/jaw bone formation. Journal of dental research 86(1): 47-51.

Shinto, H., Hirata, T., Fukasawa, T., Fujii, S., Maeda, H., Okada, M., et al., 2013. Effect of interfacial serum proteins on melanoma cell adhesion to biodegradable poly (l-lactic acid) microspheres coated with hydroxyapatite. Colloids and Surfaces B: Biointerfaces. 108, pp.8-15.

Siegel, G., Kluba, T., Hermanutz-Klein, U., Bieback, K., Northoff, H. and Schäfer, R. 2013. Phenotype, donor age and gender affect function of human bone marrow-derived mesenchymal stromal cells. BMC medicine. 11(1), p146.

Simmons, P.J. and Torok-Storb, B. 1991. Identification of stromal cell precursors in human bone marrow by a novel monoclonal antibody, STRO-1.

Singer, V.L., Jones, L.J., Yue, S.T. and Haugland, R.P. 1997. Characterisation of PicoGreen reagent and development of a fluorescence-based solution assay for double-stranded DNA quantitation. Analytical biochemistry. 249(2), pp.228-238.

Siritientong, T., Srichana, T. and Aramwit, P. 2011. The effect of sterilization methods on the physical properties of silk sericin scaffolds. Aaps PharmSciTech. 12(2), pp.771-781.

Sladkova, M. and de Peppo, G., 2014. Bioreactor systems for human bone tissue engineering. Processes. 2(2), pp.494-525.

Soheilifar, S., Amiri, I., Bidgoli, M. and Hedayatipanah, M. 2016. Comparison of periodontal ligament stem cells isolated from the periodontium of healthy teeth and periodontitis-affected teeth. Journal of dentistry (Tehran, Iran). 13(4), p271.

Song, J.S., Kim, S.O., Kim, S.H., Choi, H.J., Son, H.K., Jung, H.S., et al., 2012. In vitro and in vivo characteristics of stem cells derived from the periodontal ligament of human deciduous and permanent teeth. Tissue Eng Part A. 18(19-20), pp.2040-2051.

Sotiropoulou, P.A., Perez, S.A., Salagianni, M., Baxevanis, C.N. and Papamichail, M. 2006. Characterization of the optimal culture conditions for clinical scale production of human mesenchymal stem cells. Stem cells. 24(2), pp.462-471.

Strieter, R.M., Kunkel, S.L. and Bone, R.C. 1993. Role of tumor necrosis factor-alpha in disease states and inflammation. Critical care medicine. 21(10 Suppl), pp.S447-463.

Stute, N., Holtz, K., Bubenheim, M., Lange, C., Blake, F. and Zander, A.R. 2004. Autologous serum for isolation and expansion of human mesenchymal stem cells for clinical use. Experimental hematology. 32(12), pp.1212-1225.

Sutherland, T.D., Young, J.H., Weisman, S., Hayashi, C.Y. and Merritt, D.J. 2010. Insect silk: one name, many materials. Annual review of entomology. 55, pp.171-188.

Taddei, P., Arai, T., Boschi, A., Monti, P., Tsukada, M. and Freddi, G. 2006. In vitro study of the proteolytic degradation of Antheraea pernyi silk fibroin. Biomacromolecules. 7(1), pp.259-267.

Talal, A., Ghuman, M. and Hughes, F.J. 2010. Periodontal regeneration: a challenge for the tissue engineer? Proceedings of the Institution of Mechanical Engineers, Part H: Journal of Engineering in Medicine. 224(12), pp.1345-1358.

Talbot, M.J. and White, R.G. 2013. Cell surface and cell outline imaging in plant tissues using the backscattered electron detector in a variable pressure scanning electron microscope. Plant methods. 9(1), p40.

Tang, N., Zhao, Z., Zhang, L., Yu, Q., Li, J., Xu, Z. and Li, X. 2012. Up-regulated osteogenic transcription factors during early response of human periodontal ligament stem cells to cyclic tensile strain. Arch Med Sci. 8(3), pp.422-430.

Tepliashin, A., Korzhikova, S., Sharifullina, S., Chupikova, N., Rostovskaia, M. and Savchenkova, I. 2005. Characteristics of human mesenchymal stem cells isolated from bone marrow and adipose tissue. Tsitologiia. 47(2), pp.130-135.

Tepliashin, A., Korzhikova, S., Sharifullina, S., Chupikova, N., Rostovskaia, M, Savchenkova, I., et al.,2004. The molecular triad OPG/RANK/RANKL: involvement in the orchestration of pathophysiological bone remodeling. Cytokine & growth factor reviews. 15(6), pp.457-475.

ThermoFisher scientific 2017, United Kingdom, accessed 1st November 2018, https://www.thermofisher.com/uk/en/home/life-science/cell-analysis/cell-analysis-learning-center/molecular-probes-school-of-fluorescence/flow-cytometry-basics/flow-cytometry-fundamentals/how-flow-cytometer-works.htmL.

Thie, N. and G. J. Lavigne 2001. Bruxism and orofacial movements during sleep. Dental, clinics of North America 45(4): 657.

Thomas, M.L., 1989. The leukocyte common antigen family. Annual review of immunology. 7(1), pp.339-369.

Tribe, M.A., Eraut, M.R. and Snook, R.K. 1975. Basic Biology Course Unit 1: Volume 2, Electron Microscopy and Cell Structure. CUP Archive.

Trivedi, A., Miyazawa, B., Gibb, S., Valanoski, K., Vivona, L., Lin, M., Potter, D., Stone, M., Norris, P.J. and Murphy, J. 2019. Bone marrow donor selection and characterization of MSCs is critical for pre-clinical and clinical cell dose production. Journal of translational medicine. 17(1), p128.

Trubiani, O., Zalzal, S.F., Paganelli, R., Marchisio, M., Giancola, R., Pizzicannella, J., et al., 2010. Expression profile of the embryonic markers Nanog, OCT-4, SSEA-1, SSEA-4, and frizzled-9 receptor in human periodontal ligament mesenchymal stem cells. Journal of cellular physiology. 225(1), pp.123-131.

Trulsson, M., 2006. Sensory-motor function of human periodontal mechanoreceptors. J Oral Rehabil. 33(4), pp.262-273.

Uebersax, L., Hagenmüller, H., Hofmann, S., Gruenblatt, E., Müller, R., Vunjaknovakovic, G., et al., 2006. Effect of scaffold design on bone morphology in vitro. Tissue engineering. 12(12), pp.3417-3429.

Usumi-Fujita, R., Hosomichi, J., Ono, N., Shibutani, N., Kaneko, S., Shimizu, Y. and Ono, T. 2013. Occlusal hypofunction causes periodontal atrophy and VEGF/VEGFR inhibition in tooth movement. Angle Orthod. 83(1), pp.48-56.

Vacanti, C.A., 2006. History of Tissue Engineering and A Glimpse Into Its Future. Tissue engineering. 12(5).

Van Driel, W., Van Leeuwen, E., Von den Hoff, J., Maltha, J. and Kuijpers-Jagtman, A. 2000. Time-dependent mechanical behaviour of the periodontal ligament. Proceedings of the Institution of Mechanical Engineers, Part H: Journal of Engineering in Medicine. 214(5), pp.497-504.

Vera-Sánchez, M., Aznar-Cervantes, S., Jover, E., Garcia-Bernal, D., Onate-Sánchez, R.E., Hernández-Romero, D., Moraleda, J.M., Collado-González, M., Rodríguez-Lozano, F.J. and Cenis, J.L. 2016. Silk-fibroin and graphene oxide composites promote human periodontal ligament stem cell spontaneous differentiation into osteo/cementoblast-like cells. Stem cells and development. 25(22), pp.1742-1754.

Volkov, V., Ferreira, A.V. and Cavaco-Paulo, A. 2015. On the Routines of Wild-Type Silk Fibroin Processing Toward Silk-Inspired Materials: A Review. Macromolecular Materials and Engineering. 300(12), pp.1199-1216.

Volponi, A.A., Pang, Y. and Sharpe, P.T. 2010. Stem cell-based biological tooth repair and regeneration. Trends in cell biology. 20(12), pp.715-722.

Wada, S., Kanzaki, H., Narimiya, T. and Nakamura, Y. 2017. Novel device for application of continuous mechanical tensile strain to mammalian cells. Biology open. 6(4), pp.518-524.

Wang, D., Wang, H., Gao, F., Wang, K. and Dong, F. 2017. ClC-3 Promotes Osteogenic Differentiation in MC3T3-E1 Cell After Dynamic Compression. Journal of cellular biochemistry. 118(6), pp.1606-1613.

Wang, L., Hu, H., Cheng, Y., Chen, J., Bao, C., Zou, S., et al., 2016. Screening the expression changes in microRNAs and their target genes in mature cementoblasts stimulated with cyclic tensile stress. International journal of molecular sciences. 17(12), p2024.

Wang, L., Shen, H., Zheng, W., Tang, L., Yang, Z., Gao, Y., et al., 2011. Characterization of stem cells from alveolar periodontal ligament. Tissue Eng Part A. 17(7-8), pp.1015-1026.

Wang, M. O., J. M. Etheridge, J. A. Thompson, C. E. Vorwald, D. Dean and J. P. Fisher 2013. Evaluation of the in vitro cytotoxicity of cross-linked biomaterials. Biomacromolecules 14(5): 1321-1329.

Wang, Y., Rudym, D.D., Walsh, A., Abrahamsen, L., Kim, H.-J., Kim, H.S., et al., 2008. In vivo degradation of three-dimensional silk fibroin scaffolds. Biomaterials. 29(24-25), pp.3415-3428.

Warrener, M. and C. R. Anderson, 2014. Cellular adhesion and protein adsorption to P (MEO 2 MA-co-OEGMA) polymer substrates. 2014 40th Annual Northeast Bioengineering Conference (NEBEC), IEEE.

Wassilkowska, A. and Woźniakiewicz, T., 2015. Application of Peltier cooling device in a variable-pressure SEM. In: Solid State Phenomena: Trans Tech Publ, pp.139-144.

Wei, F., C. Wang, G. Zhou, D. Liu, X. Zhang, Y. Zhao et al., 2008. The effect of centrifugal force on the mRNA and protein levels of ATF4 in cultured human periodontal ligament fibroblasts. Archives of oral biology 53(1): 35-43.

Wei, F., Liu, D., Feng, C., Zhang, F., Yang, S., Hu, Y., et al., 2015. microRNA-21 mediates stretch-induced osteogenic differentiation in human periodontal ligament stem cells. Stem cells and development. 24(3), pp.312-319.

Wen, Y., A. Waltman, H. Han and J. H. Collier 2016. Switching the immunogenicity of peptide assemblies using surface properties. Acs Nano 10(10): 9274-9286.

Weszl, M., Skaliczki, G., Cselenyák, A., Kiss, L., Major, T., Schandl, K., et al., 2012. Freeze-dried human serum albumin improves the adherence and proliferation of mesenchymal stem cells on mineralized human bone allografts. Journal of Orthopaedic Research. 30(3), pp.489-496.

Woloszyk, A., Buschmann, J., Waschkies, C., Stadlinger, B. and Mitsiadis, T.A. 2016. Human dental pulp stem cells and gingival fibroblasts seeded into silk fibroin scaffolds have the same ability in attracting vessels. Frontiers in physiology. 7, p140.

Wouter Beertsen, C. A. G. M. A. J. S. 1997. The periodontal ligament: a unique, multifunctional connective tissue. Periodontology 2000 13.

Wray, L.S., Hu, X., Gallego, J., Georgakoudi, I., Omenetto, F.G., Schmidt, D. et al., 2011. Effect of processing on silk-based biomaterials: Reproducibility and biocompatibility. Journal of Biomedical Materials Research Part B: Applied Biomaterials. 99(1), pp.89-101.

Wu, Y., Ou, Y., Liao, C., Liang, S. and Wang, Y. 2019. High-throughput sequencing analysis of the expression profile of microRNAs and target genes in mechanical force-induced osteoblastic/cementoblastic differentiation of human periodontal ligament cells. American journal of translational research. 11(6), p3398.

Xu, J., Wang, W., Kapila, Y., Lotz, J. and Kapila, S. 2009. Multiple differentiation capacity of STRO-1+/CD146+ PDL mesenchymal progenitor cells. Stem cells and development. 18(3), pp.487-496.

Yang, C., Lee, J.S., Jung, U.W., Seo, Y.K., Park, J.K. and Choi, S.H. 2013. Periodontal regeneration with nano-hyroxyapatite-coated silk scaffolds in dogs. J Periodontal Implant Sci. 43(6), pp.315-322.

Yang, H., Gao, L.N., An, Y., Hu, C.H., Jin, F., Zhou, J., et al., 2013. Comparison of mesenchymal stem cells derived from gingival tissue and periodontal ligament in different incubation conditions. Biomaterials. 34(29), pp.7033-7047.

Yang, L., Yang, Y., Wang, S., Li, Y. and Zhao, Z. 2015. In vitro mechanical loading models for periodontal ligament cells: from two-dimensional to three-dimensional models. Archives of oral biology. 60(3), pp.416-424.

Yeh, S.-P., Chang, J., Lin, C., Lo, W., Lee, C., Lin, C.-Y., et al., 2005. Mesenchymal stem cells can be easily isolated from bone marrow of patients with various haematological malignancies but the surface

antigens expression may be changed after prolonged ex vivo culture. Leukemia. 19(8), pp.1505-1507.

Yu, H., Ren, Y., Sandham, A., Ren, A., Huang, L. and Bai, D. 2009. Mechanical tensile stress effects on the expression of bone sialoprotein in bovine cementoblasts. The Angle Orthodontist. 79(2), pp.346-352.

Zaoming, W., Codina, R., Fernandez-Caldas, E. and Lockey, R. 1996. Partial characterization of the silk allergens in mulberry silk extract. Journal of investigational allergology & clinical immunology. 6(4), pp.237-241.

Zhang, C., Li, J., Zhang, L., Zhou, Y., Hou, W., Quan, H., et al.,2012. Effects of mechanical vibration on proliferation and osteogenic differentiation of human periodontal ligament stem cells. Archives of oral biology. 57(10), pp.1395-1407.

Zhang, J., An, Y., Gao, L.-N., Zhang, Y.-J., Jin, Y. and Chen, F.-M. 2012. The effect of aging on the pluripotential capacity and regenerative potential of human periodontal ligament stem cells. Biomaterials. 33(29), pp.6974-6986.

Zhang, L., Liu, W., Zhao, J., Ma, X., Shen, L., Zhang, Y., et al., 2016. Mechanical stress regulates osteogenic differentiation and RANKL/OPG ratio in periodontal ligament stem cells by the Wnt/β-catenin pathway. Biochimica et Biophysica Acta (BBA)-General Subjects. 1860(10), pp.2211-2219.

Zhang, W., C. Zhu, D. Ye, L. Xu, X. Zhang, Q. Wu, X. Zhang, et al., 2014. Porous silk scaffolds for delivery of growth factors and stem cells to enhance bone regeneration. PloS one 9(7): e102371.

Zheng, J., Q. Su, C. Wang, G. Cheng, R. Zhu, J. Shi, et al., 2011. Synthesis and biological evaluation of PMMA/MMT nanocomposite as denture base material. Journal of Materials Science: Materials in Medicine 22(4): 1063-1071.

Zhou, C.-Z., Confalonieri, F., Medina, N., Zivanovic, Y., Esnault, C., and Yang, T., 2000. Fine organisation of Bombyx mori fibroin heavy chain gene. Nucleic acids research. 28(12), pp.2413-2419.

Zhu, W. and Liang, M., 2015. Periodontal ligament stem cells: current status, concerns, and future prospects. Stem cells international.

2015.Cohn, S. 1965. Disuse atrophy of the periodontium in mice. Archives of oral biology. 10(6), pp.909-919.